PARTICLE DYNAMICS IN VERTICAL PNEUMATIC TRANSPORT AND THEIR APPLICATION TO THE TRANSPORT REDUCTION OF NICKEL OXIDE WITH HYDROGEN

by

J.R. ROACH, B.E. (Hons.)

of the

Department of Chemical Engineering

A THESIS

Submitted for the Degree of Doctor of Philosophy

in the

Faculty of Engineering of the University of Adelaide

August 1965

TABLE OF CONTENTS

Page

Page

Page

Page

Page

Page

Page

Page

Page

LIST OF APPENDICES

LIST OF TABLES

LIST OF FIGURES

SUMMARY

The dynamics of particles in vertical pneumatic transport have been examined both theoretically and experimentally with particular reference to the acceleration zone. A theoretical model has been proposed in which the mean particle velocity is related to the observed pressure drop in the system. The model was tested with a series of experiments using three different sizes of glass spheres (diam. range 1.15 to .64 mm) and one size of steel spheres (1.0 mm diam.) transported with air. The results of the analysis are presented in a form that can be used to determine particle residence times in a vertical pipe from pressure drop measurements. In particular the model can be used to estimate particle residence times in transport system in which a chemical reaction occurs between the transporting gas and the entrained solids.

Three size ranges of sintered nickel monoxide (viz. 35/42, 42/48, 48/60 Tyler screen mesh) have been reduced in both a fixed bed (temp. range 300 -425°C) and in a transport reactor (temp. range 500-700°C). The kinetics of the reduction for the two cases are expressed quantitatively and compared. The results showed that the reaction rates observed for the reduction in the transport reactor were much faster than those predicted by extrapolation of the fixed bed kinetic data. The marked increase in reaction rate is attributed to a change in reaction mechanism associated with the mode of chemisorption of the hydrogen on the nickel monoxide surface.

The work indicated that both low particle residence times and high reaction temperatures can be controlled quite closely in the transport reactor. It is shown that the transport reactor is particularly suitable for carrying out chemical reactions between a gas and a particulate solid when high reaction temperatures can be used to produce fast reaction rates.

I hereby certify that this Thesis contains no material which has been accepted for the award of any other Degree or Diploma in any University and that, to the best of my knowledge and belief, this thesis contains no material previously published or written by another person except when due reference is made in the text of this thesis.

J. R. ROACH

ACKNOWLEDGEMENTS

The author wishes to thank Dr. R.V. Culver who supervised this project and Professor R.W.F. Tait for helpful advice during the investigation.

Thanks are also due to the workshop staff of the Chemical Engineering Department for their assistance and cooperation during the construction of the apparatuses and to Mr. J. Sickert for his assistance with the experimental work on the hydrogen reduction of nickel monoxide.

In addition the author is indebted to the Broken Hill Associated Smelters Ltd. and to Albright and Wilson Ltd. for financial assistance.

The International Nickel Company (Mond) Ltd. kindly donated the nickel monoxide used in the research.

1 INTRODUCTION

1. INTRODUCTION

This thesis, "Particle dynamics in vertical pneumatic transport and their application to the transport reduction of nickel oxide with hydrogen", describes an investigation to assess the suitability of the dilute fluidized phase as a suitable means for carrying out a chemical reaction between a gas and a finely divided solid. The reduction of NiO with H_2 was chosen for the study because it is a relatively fast reaction, the reaction products were not likely to stick or scale in the reactor, and at equilibrium the system has only four components, viz. H_2, NiO, Ni, H_2O.

Now in most reactors used for reactions between fine solid particles and a gas stream two problems are usually encountered: first, the problem of materials handling, and second, the problem of achieving adequate gas solids contact in the reaction zone. A significant contributory factor to both these problems is the tendency of the solid particles to segregate due to the action of gravitational forces. Three general methods exist for carrying out gas-solid reactions, viz. reactions in fixed beds, reactions in fluidized beds, and reactions in the dilute fluidized phase. Fixed bed reactors, including reactors with slowly moving beds such as the blast furnace, are usually suited to coarse materials, which permit the reacting gases to be circulated through the solid bed with a low gas pressure drop and uniform gas solid contact. However, fine particles are not suited to this type of treatment and often an additional sintering or agglomerating process is required to make such material suitable for fixed bed treatment. On the other hand the fluidized bed and the dilute fluidized phase can be used for the treatment of fine particles, the fluid drag forces on the particles being used to counteract the tendency of the particles to segregate under the action of gravitational forces.

For the purpose of this thesis the transport reactor is defined as a dilute fluidized phase reactor in which there is upward co-current flow of the gas and the dispersed solid phase. For fine particles this type of reactor has several operational advantages, the materials handling problem is overcome with the well established techniques of pneumatic conveying, the residence time of the particles in the reaction zone can be closely controlled by regulating the gas flow rate, and the temperature of the reaction zone can be controlled by controlling the gas temperature. Because vertical pneumatic transport with solids velocities below 0.5 ft/sec tends to be unstable, the transport reactor is only suitable for relatively fast reactions. However, if fast

reaction rates can be obtained with the use of high temperatures, the transport reactor provides a means of obtaining controllable low residence times which are not readily achieved in a fluidized or fixed bed reactor.
In addition to the points discussed above, the use of a transport reactor for reacting gases and fine solids is not indicated in the following instances:

(i) if sticking or scaling of the solid material is anticipated,

(ii) if the particles leaving the reactor are so fine that their recovery from the gas stream is difficult, or

(iii) if it is desired to use the heat of reaction to provide the temperatures necessary to initiate and maintain the reaction.

The objectives of the investigation undertaken for this thesis were:

(i) to carry out experimental and theoretical analyses of particle dynamics in vertical pneumatic transport with particular reference to low average particle velocities, with a view to applying these results to the estimation of particle residence times in a transport reactor,

(ii) to study experimentally the fixed bed reduction of several size ranges of N_iO particles with H_2, and to derive a characteristic chemical rate equation for the reaction, and

(iii) to build and operate an apparatus to investigate the transport reduction of samples of the N_iO used in investigation (ii) and to assess the results using any relevant information obtained from investigations (i) and (ii).

The thesis is presented in three main parts corresponding to these three objectives. Introductory remarks preface each of these sections and each section has a separate literature review, discussion of results, and conclusions.

2 PARTICLE DYNAMICS IN VERTICAL PNEUMATIC TRANSPORT

2.1 Introduction

This section of the thesis is concerned with the development of a relationship which may be used for the determination of actual average particle velocities (actual as distinct from theoretical) in vertical pneumatic transport systems. Following the discussion of the literature a relationship which relates the actual average particle velocity to the observed pressure drop between two reference points is derived. The investigation which is both theoretical and experimental is aimed at establishing the following relationships:

(i) the relationship between the observed average particle velocity and the average gas velocity,

(ii) the relationship between the observed average particle velocity and the calculated average theoretical velocity, and

(iii) the relationship between the observed pressure drop and the actual and theoretical particle velocities; the result of this analysis is a momentum balance.

Sections (ii) and (iii) refer to theoretical solids velocities which may be calculated provided that both the gas velocity and the terminal velocity of the solid particles are known. Since the particle terminal velocity under actual transport conditions is not reliably calculable a method of estimating the terminal velocity from observed pressure drop measurements is proposed.

The experimental work is confined to the transport of small glass and steel spheres in a short vertical tube.

2.2 Literature Review

2.2.1 Turbulent flow in pipes

The following discussion is a brief summary of the main aspects of the fluid mechanics of turbulent fluid flow in pipes, based largely on the writings of HINZE (19), PRANDTL (20), and SCHLICHTING (21).

Turbulent flow and velocity fluctuation

Turbulent flow is said to exist in a pipe when secondary velocity fluctuations can be observed in directions other than along the axis of the cylinder formed by the pipe wall. Since the velocity in any direction of turbulent flow is continuously fluctuating, it is usually represented by a vector having both steady and fluctuating components. If U represents the instantaneous velocity at any point, then

$$U = \bar{U} + u \qquad .....(2.1)$$

where U = instantaneous velocity,

$\bar{U}$ = time average point velocity,

and u = the fluctuating component of U; by definition $\bar{u} = 0$.

The intensity of turbulence

The intensity of turbulence is usually denoted by the R.M.S. value of u which is

$$\sqrt{\overline{u^2}}$$

The relative turbulence intensity is then defined by

$$\sqrt{\overline{u^2}} \;/\; \overline{U}$$

Three cylindrical coordinates are generally used to define the field of turbulence; viz. axial, radial and azimuthal.

A value of the fluctuating velocity component can be measured in each of these three directions (mutually at right angles). The components are:

$$\left.\begin{aligned} U_x &= \overline{U}_x + u_x \quad \text{(axial)}, \\ U_r &= \overline{U}_r + u_r \quad \text{(radial)}, \\ \text{and} \quad U_\phi &= \overline{U}_\phi + u_\phi \quad \text{(azimuthal)}. \end{aligned}\right] \quad \ldots\ldots (2.2)$$

For pipe flow $\overline{U}_r$ and $\overline{U}_\phi$ are both zero, in this case the turbulence intensities are usually expressed relative to $\bar{U}_x$.

Values of relative intensities in fully developed turbulent pipe flow are reported by LAUFER (17) and SANDBORN (18). SANDBORN (18) states that the axial turbulence intensity at the centre of the pipe can be represented by an empirical relation:

$$\left[\sqrt{\overline{u_x^2}} \,/\, \bar{U}_x \right]_{r=0} = 0.144\, Re^{-0.146} \quad .....(2.3)$$

The scale of turbulence

The scale of turbulence will only be briefly discussed as its specification involves mathematical and statistical procedures beyond the scope of the present work. Broadly, turbulent eddies consist of zones in the fluid which vary continuously in size and translational speed. These eddies are in a fluctuating state of generation by instabilities in the flow and of dissipation by viscous shear forces. The statistical techniques used to specify the scale of turbulence are correlations between the magnitudes of the fluctuating velocity components, the displacement in time or distance being the factor used to relate the pairs (or sometimes triple correlations) of velocity values correlated. The correlation based on linear displacement is referred to as the Eulerian scale of turbulence and the correlation based on time displacement is called the Lagrangian scale of turbulence. A detailed discussion of these correlations and practical methods of measurement is given by HINZE (19).

The time average point velocity ($\bar{U}_x$) in turbulent pipe flow

The time average point velocity ($\bar{U}_x$) varies across the pipe, being a maximum at the centre and zero at the pipe wall. A power law provides a very good approximation for this distribution if an accurate knowledge of the distribution in the boundary layer is not required. HINZE (22) gives the following equation:

$$(\bar{U}_x)_r = (\bar{U}_x)_{max.}(1-\frac{2r}{D})^{1/n} \qquad \ldots\ldots (2.4)$$

where $(\bar{U}_x)_r$ = time average axial point velocity,

r = radial distance of the reference point from the pipe centre,

D = pipe diameter,

and $1/n$ is some $f(\lambda)$, where λ is a dimensionless friction factor defined by eqn. (2.8).

For $\lambda<0.1$, the functional relationship simplifies to $1/n = \sqrt{\lambda}$.

The relationship between the maximum axial velocity and the average mass flow velocity

The maximum axial velocity, $(\bar{U}_x)_{max.}$, occurs at pipe centre and $V_{av.}$ is defined by the equation:

$$(V_{av.})(A_c)(\rho_{av.}) = M \qquad \text{......} (2.5)$$

where $V_{av.}$ = average mass flow velocity,

A_c = area of cross section of the pipe,

and $\rho_{av.}$ = average fluid density.

In terms of $\bar{U}_x$, M is defined by the equation:

$$M = \rho_{av.} \int_{r=0}^{D/2} \int_{\phi=0}^{2\pi} (\bar{U}_x).r.dr.d\phi \qquad \text{......} (2.6)$$

Substituting the value of $\bar{U}_x$ from eqn. (2.4) yields the result [SCHLICHTING (23)] :

$$\frac{V_{av.}}{(\bar{U}_x)_{max.}} = \frac{2n^2}{(2n+1)(n+1)} \qquad \text{......} (2.7)$$

SCHLICHTING (23) evaluates this ratio for five values of n, these are reproduced in TABLE 2.1.

TABLE 2.1. Ratio of mean to maximum velocity in turbulent pipe flow, after SCHLICHTING (23)

n	6	7	8	9	10
$\frac{V_{av.}}{(\bar{U}_x)_{max.}}$	0.791	0.817	0.837	0.852	0.865

Pressure drop in turbulent pipe flow

The equation for pressure drop in turbulent pipe flow is generally written [SCHLICHTING (24)] :

$$\frac{dP}{dL} = \frac{-\lambda}{D} \; \frac{\rho V_{av.}^{2}}{2\, g_c} \qquad \text{...... (2.8)}$$

where $\frac{dP}{dL}$ = pressure gradient along the pipe,

D = pipe diameter,

ρ = fluid density,

$V_{av.}$ = average mass flow velocity,

and λ = dimensionless friction factor.

SCHLICHTING (24) gives the following equation for estimating λ for smooth pipes where $3{,}500 < Re < 100{,}000$:

$$\lambda = 0.3164\ (Re)^{-0.25} \qquad \text{...... (2.9)}$$

and also another relation (25):

$$\frac{1}{\sqrt{\lambda}} = 2.0 \log_{10} (Re.\sqrt{\lambda}) - 0.8 \qquad \text{...... (2.10)}$$

which is valid for

$$2.8 < \log_{10} (Re.\sqrt{\lambda}) < 5.4$$

2.2.2 The nature of fluid drag

Drag is the force exerted on a body submerged in a fluid when the fluid moves relative to the body. The mechanism of drag forces can be considered in two sections. The first section is the total viscous flow (Stoke's Law) regime and the second is the regime where a true 'boundary layer' exists. Viscous flow or 'creeping motion' [PRANDTL (26)] does not normally occur in pneumatic transport. When a true boundary layer exists the total drag force on a submerged body can be reduced to two components [SCHLICHTING (27)]. The first component is skin friction or viscous drag and is equal to the integral of all shear forces taken over the surface of the body. The second component is form or pressure drag; this is equal to the integral of all normal forces taken over the surface of the body. Hence

total (or profile) drag = form (or pressure) drag + skin friction (or viscous) drag ...... (2.11)

For simple body profiles the skin friction can be calculated from boundary layer theory. However, even in simple cases, the form drag must be estimated with the aid of empirical methods.

Drag normally depends on the following factors: shape and orientation of the body, the relative velocity between the body and the fluid, and the physical properties of the fluid. Because these physical phenomena are associated in a complex manner to produce the drag force, information on drag is usually represented by empirical relationships. However, the basic concepts of the theory are often used qualitatively to explain measured results.

2.2.3 The variation of particle drag with the particle Reynolds number

The Stoke's Law region is not considered in this discussion, hence it is assumed that a true boundary layer exists on the particle surface. It is customary to employ the following empirical equation when calculating drag forces [PRANDTL (28)], viz.

$$F_D = (C_D \cdot A_p \cdot \rho_f \cdot V_R^2)/2 \cdot g_c \qquad \ldots\ldots (2.12)$$

where F_D = total drag force,

C_D = dimensionless drag coefficient,

A_p = projected area of the particle in the direction of relative motion,

ρ_f = fluid density,

and V_R = relative velocity between the particle and the fluid.

It can be shown by dimensional analysis, and confirmed by experiment [SCHLICHTING (29)], that C_D is a function of the particle Reynolds number, viz.

$$C_D = f\,(Re_p) \qquad \ldots\ldots (2.13)$$

where the particle Reynolds number is defined by the relation

$$Re_p = \frac{d \cdot V_R \cdot \rho_f}{\mu} \qquad \ldots\ldots (2.14)$$

where d = particle diameter and μ is the fluid viscosity.

2.2.4 The functional relationship between the drag coefficient (C_D) and the particle Reynolds number (Re_p) for spheres

Because of the complexity of the processes involved in fluid drag on a sphere, the functional relationship is usually represented graphically, not analytically. A typical representation is a plot of C_D vs. Re_p with logarithmic scales. The data used in this thesis are those of LAPPLE (31); they are reproduced in TABLE 2.2 and plotted in FIGURE 2.1. These data were obtained for spherical bodies in a laminar or quiescent fluid. The shape of the curve suggests that as the particle Reynolds number is increased, the physical processes which combine to cause the drag change their relative contributions. This has been discussed in detail by TOROBIN and GAUVIN (32). Neglecting the Stoke's Law range, the curve is normally divided into three regions for comment [TOROBIN and GAUVIN (32)] :

(i) Region (a), corresponding to $0.5 < Re_p < 500$,

(ii) Region (b), corresponding to $500 \leq Re_p < 200{,}000$,

and (iii) Region (c), corresponding to $200{,}000 \leq Re_p$.

Region (a) $0.5 < Re_p < 500$

A true laminar boundary layer starts to form

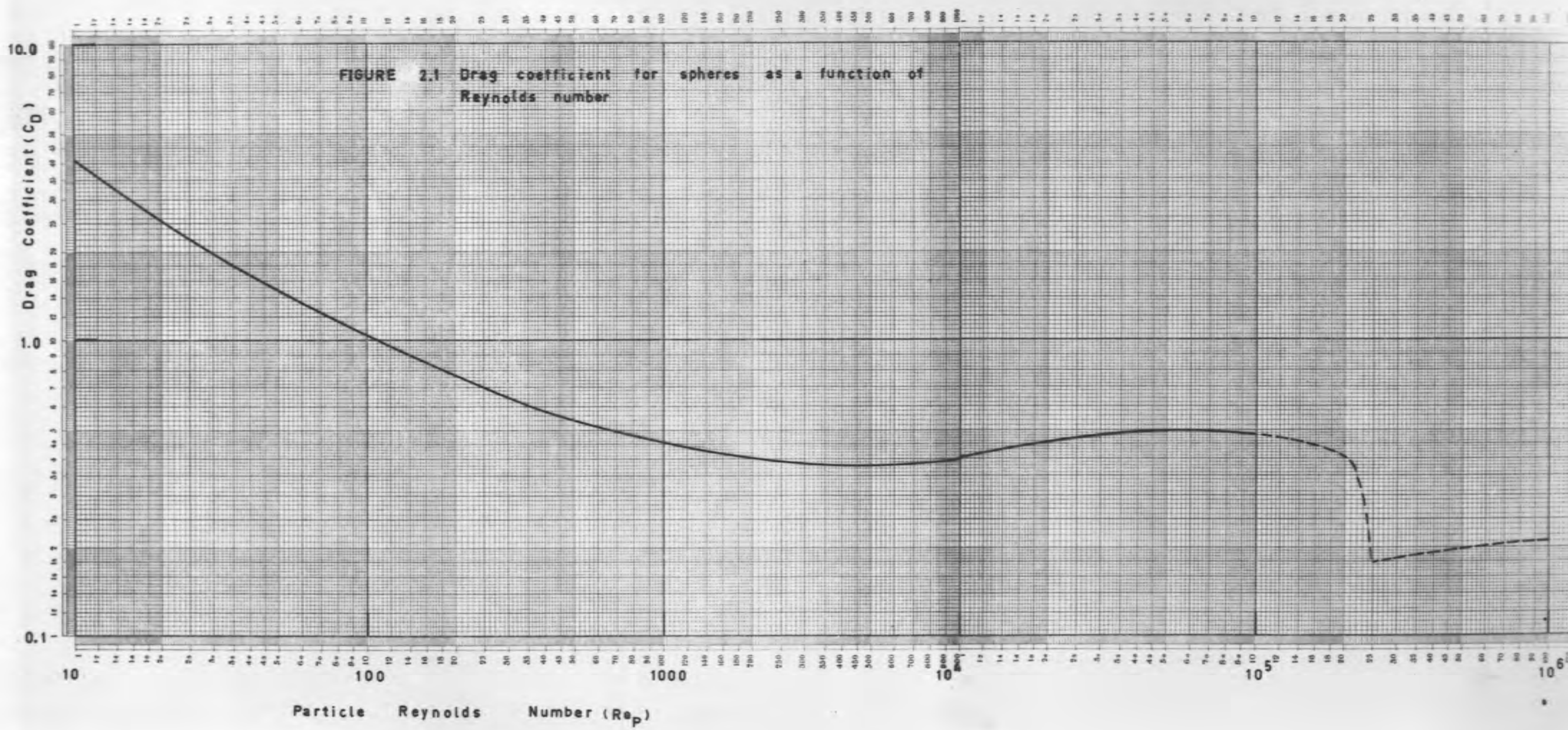

FIGURE 2.1 Drag coefficient for spheres as a function of Reynolds number

at the lower limit, $Re_p = 0.5$. As Re_p is increased the boundary layer starts to separate and forms a symmetrical vortex behind the sphere. The drag in this region consists of skin friction and form drag.

Region (b) $500 \leq Re_p < 200,000$

At a particle Reynolds number in the vicinity of 500 (sometimes referred to as the lower critical Reynolds number, NEMENYI (33)), the vortex behind the sphere becomes unstable. Elements of the vortex break off and form a wake behind the sphere. The flow in the boundary layer is still laminar, however, the drag consists mostly of form drag. It is apparent from FIGURE 2.1 that the value of C_D in the region $2,000 < Re_p < 200,000$ is approximately constant and in the vicinity of 0.44. This is sometimes referred to as the Newton's Law range [COULSON and RICHARDSON (34)] :

$$F_D = 0.22 \left[\frac{\rho_f V_R^2}{g_c}\right]\left[\frac{\pi d^2}{4}\right] \qquad \text{..... (2.15)}$$

Region (c) $200,000 \leq Re_p$

The flow in the boundary layer starts to become turbulent in the vicinity of $Re_p = 200,000$. At some value of Re_p as it approaches 300,000 the circle of separation of the boundary layer on the sphere moves from just upstream of the maximum profile section to slightly to the rear of this section, [COULSON and RICHARDSON (35)]. This causes a reduction in the area of the wake. Since form drag is primarily determined by the kinetic energy in the eddies of the wake [PRANDTL (36)], a decrease in the size of the wake should lower the drag. The value of Re_p at which this sharp decrease occurs is known as the upper critical Reynolds number. This critical Reynolds number is usually taken as the value of Re_p at which the drag coefficient (C_D) is equal to 0.3 [TAYLOR (39)].

TABLE 2.2 Values of the drag coefficient for spherical particles, after LAPPLE (31)

Particle Drag Coefficient C_D	Particle Reynolds No. $Re_p = \frac{dV_R \rho_f}{\mu}$
4.1	10.0
1.5	50.0
1.07	100.0
0.55	500.0
0.46	1000
.385	5000
.405	10000
.49	50000
.48	100000

2.2.5 The functional relationship between the drag coefficient and the particle Reynolds number for non-spherical particles

The factors which influence the drag on spheres also apply to other solid bodies. Complex profiles and possible variations in orientation render these irregularly shaped bodies even less amenable to theoretical treatment than spheres. As with spheres, the drag coefficient relationship can be represented by a plot of C_D vs. Re_p. ROUSE (42) gives drag data for various solids of revolution.

In sedimentation, elutriation, or pneumatic transport, particles can have almost random orientation in the fluid stream. In such cases average values of the drag coefficient can be obtained and plotted against the value of the particle Reynolds number based on the average screen size [BROWN (43)]. These results are specific, for the particular measurements made. BROWN (43) also discusses a more general alternative approach based on the sphericity of a particle, by definition:

sphericity = surface area of a sphere having the same volume as particle/surface area of particle

The particle Reynolds number is then based on the diameter of a sphere having the same volume as the particle. Values of the drag coefficient may be plotted against the particle Reynolds number with sphericity as a parameter. However, unless the particle shape is regular, the sphericity is difficult to determine.

2.2.6 The effect of free stream turbulence on the particle drag coefficient

The drag relationships for spheres in quiescent or laminar fluids were discussed in section 2.2.4; in this section possible effects of free stream turbulence are considered. (So far, in this discussion an upper and lower critical Reynolds number have been referred to; in all future discussion, however, the term critical Reynolds number will refer to the upper critical Reynolds number for the particle.)

TOROBIN and GAUVIN (37) quote the results of HOERNER (38), which indicated qualitatively that increased turbulence levels lowered the critical Reynolds number. TAYLOR (39) also observed this effect and was of the opinion that the stream turbulence acted in such a way as prematurely to induce turbulent flow in the boundary layer. Turbulent flow in the boundary layer increases the stability of the layer and moves the point of separation further from the front stagnation point which reduces the wake area and lowers the drag force.

TAYLOR (39) deduced theoretically that both the intensity and scale of turbulence influenced the drag. Both high intensities of turbulence and a small scale of turbulence relative to the body diameter should lower the critical Reynolds number. The functional relationship deduced was

$$(Re_p)_{crit.} = f\left[\sqrt{\bar{u}_x^2}/V_R \,,\, \left(\frac{d}{L_s}\right)^{1/5} \right]$$

where L_s is the scale of turbulence. TAYLOR (39) assumed that L_s would be the same order of size as the grid or mesh spacing generating the turbulence.

ZIJNEN (41) deduced from pressure measurements that the form drag for a cylinder was slightly increased by stream turbulence at sub-critical Reynolds numbers. Presumably the free stream turbulence modified the wake in such a way as to increase the drag. Since the drag mechanism for a cylinder is in many ways similar to that for a sphere it may be reasonably inferred that the form drag for a sphere would also be slightly increased by stream turbulence at sub-critical Reynolds numbers.

The literature reviewed contained no analytical expression for the functional relationship between C_D, Re_p and the turbulence parameters, however, there is evidence to suggest that the qualitative effect of turbulence is to lower the critical Reynolds number and also to moderately increase the drag force in the sub-critical region (39)(41) .

2.2.7 Determination of drag coefficients in vertical co-current (pneumatic transport) gas-solid flow systems

The drag coefficient is an important parameter in the theoretical analysis of gas solids transport systems. So far the discussion of fluid drag on solid bodies has been confined to freely falling solid bodies in a quiescent fluid or to fixed bodies in a wind tunnel. However, pneumatic transport involves the co-current flow of gas and freely entrained solids, the fluid stream in most practical cases being turbulent. Additional factors to be taken into account are (i) the effect of the fluid velocity distribution (resulting in large gradient in the axial velocity near the pipe wall, section 2.2.1) and (ii) the possible close proximity of particles in multiparticle suspensions, both of which may modify the particle drag coefficients. The two main methods used to determine particle drag coefficients in free suspension are, first the measurement of the 'support velocity' of a particle and second the study of particle trajectories. The 'support velocity' is the fluid velocity required just to suspend a particle in a vertical fluid stream.

The 'support velocity' technique

WILHELM and VALENTINE (44) used the support velocity technique to obtain drag data for single particles over the experimental range $1,400 < Re_p < 30,000$. The observed values of the apparent drag coefficient (C_D) were higher than those recorded for a laminar or quiescent environment by a factor of 1.4.

On the other hand MILLER and McINALLY (45) compared free falling velocities of coal particles in water over a wide range of sizes with the upward velocity required to suspend these particles. The respective support velocities were from 10 to 40 per cent greater than the free falling velocities. For the relatively fine particles, where a 40 per cent deviation was observed, the particle Reynolds number was of the order of 25, i.e. within the region where 'creeping motion' (Stoke's Law) could still contribute to the drag. It was claimed (45) that the reduction in the apparent drag coefficient may have been caused by turbulent conditions in the apparatus reducing the viscous drag.

The apparently contradictory findings of WILHELM and VALENTINE (44) and MILLER and McINALLY (45) with regard to the effect of fluid turbulence on the 'support velocity' (and hence the apparent drag coefficient), may possibly be resolved by considering the effect of a probable particle wake modification in the first instance where $1,400 < Re_p < 30,000$, and, in the second instance the probable lowering of the 'creeping' resistance where the Re_p is approximately equal to 25. Unfortunately insufficient experimental details were given to enable a more critical appraisal to be made, particularly with regard to the possible effects of the axial fluid velocity distributions in the apparatuses.

WHETTON and BROADHURST (46) attempted to measure the support velocity for pneumatically conveyed underground stowage material. The apparatus used was a vertical 6.0 in dia. pipe with a perspex window. They reported that it was not possible to hold a particle stationary for more than a fraction of a second. This difficulty was probably due to the fluid velocity gradient existing in the vertical pipe (section 2.2.1). With regard to this point GARNER and KENDRICK (47), while studying mass transfer from drops, found that the essential gas stream characteristics for floating a particle were a symmetrical velocity distribution across the working section with a minimum at the axis, and a decreasing axial velocity in the direction of flow attained with a tapered section.

TOROBIN and GAUVIN (37) on the other hand claim that the results of these floating velocity measurements cannot be directly applied to particles moving co-currently with the stream. Two objections are raised; first, that the fluid velocity in the pipe would be the same as the relative velocity between the particle and the fluid, and second for fine particles, it would be difficult to obtain turbulent fluid conditions and still have particle Reynolds numbers in the Stoke's Law region. These are valid objections but they are specific, probably due to the writers' (37) special interest in the effects of turbulence, and they do not apply to all practical ranges of pneumatic transport.

Particle trajectory measurements

TOROBIN and GAUVIN (48) measured particle drag coefficients by analysing single particle trajectories in a vertical wind tunnel which they describe in reference (49). Particular attention was paid to the control of fluid velocity distribution and the turbulence parameters. They obtained distance-time data for single particles using a radioactive tracer technique. They also extended the theoretical analysis of TAYLOR (39) and derived the equation:

$$(Re_p)_{crit.} \times \left[\sqrt{\bar{u}_x^2} \,/\, V_R \right] = \text{const.}$$

The experimental results indicated that the free stream turbulence first caused a moderate increase in the drag coefficient, (thus agreeing with the observations of ZIJNEN (41) and WILHELM and VALENTINE (44) for sub-critical Reynolds numbers), which was then followed by a sharp decrease which indicated that the critical Reynolds number had been attained. TOROBIN and GAUVIN (48) found that the relation between the critical Reynolds number and the turbulence intensity parameter for their system was defined by the equation:

$$(Re_p)_{crit.} \times \left[\sqrt{\bar{u}_x^2} / V_R \right] = 45 \qquad \ldots\ldots (2.16)$$

The scale of turbulence and the particle acceleration apparently had no effect on the particle drag coefficient.

2.2.8 Some general characteristics of a vertical pneumatic transport system

Conditions necessary for transport

Vertical pneumatic transport involves the lifting of a dispersed solid phase with a gas stream constrained in a riser, momentum being transferred from the gas stream to the solid particles. FIGURE 2.2 shows a schematic diagram of a vertical pneumatic transport system. To lift the particles it is necessary for the fluid drag force (F_D), (defined by equation (2.12)), on the individual particles to be greater than the particle weight. The relative velocity between the fluid and the particle at which the drag force equals the particle weight is called the terminal velocity of the particle. In an ideal system, if the gas velocity is greater than the terminal velocity, the force exerted on the particles by the gas stream accelerates them towards an upper velocity limit, given by the equation:

$$V_P = (V_G - V_T) \qquad ..... (2.17)$$

where V_P = vertical particle velocity,

V_T = particle terminal velocity,

and V_G = vertical gas velocity.

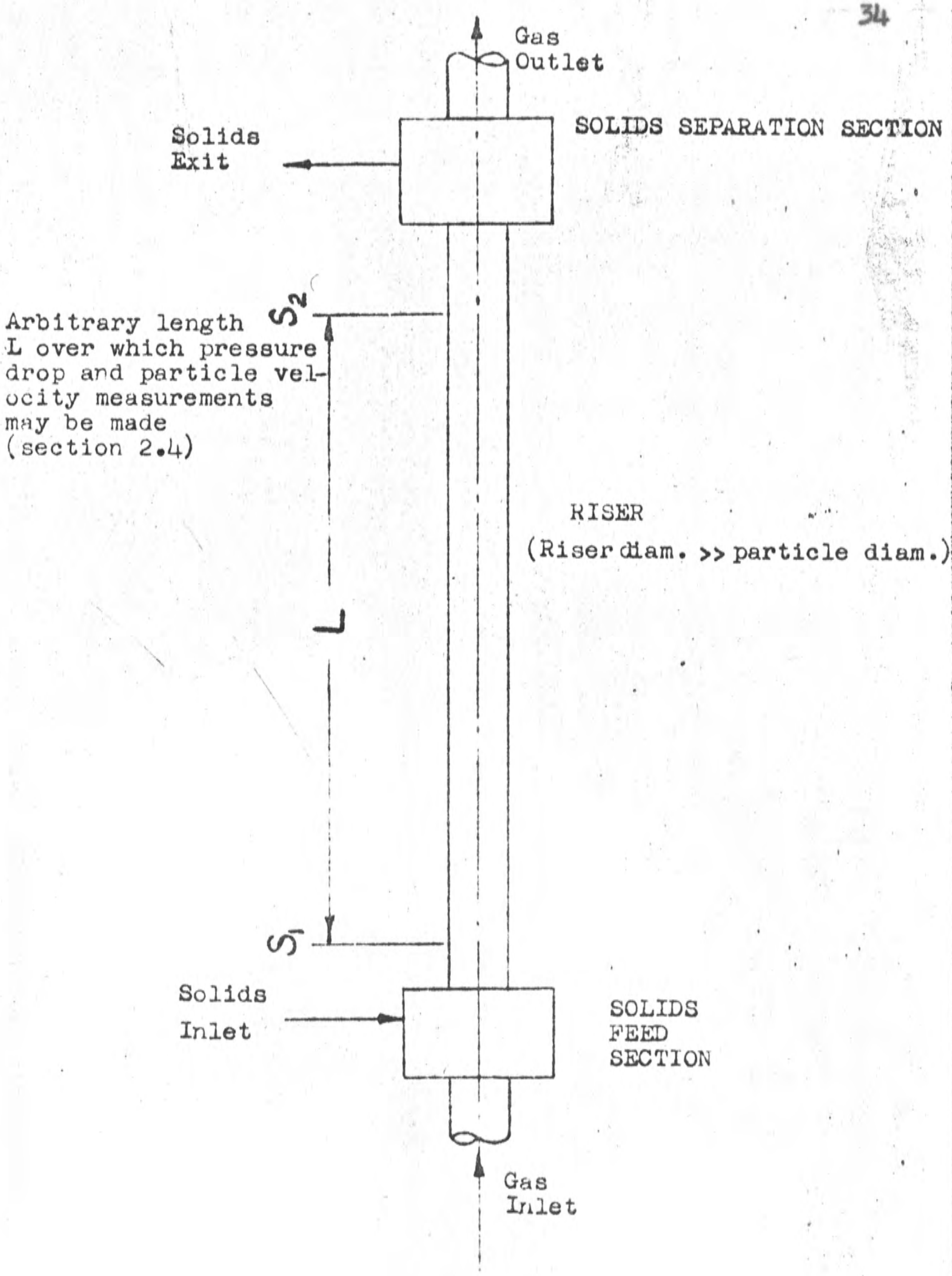

FIGURE 2.2 Schematic diagram of a vertical pneumatic transport system

(Because of the relatively high percentage of voids usually encountered in pneumatic transport systems, the gas velocity used in calculations is taken as the 'superficial gas velocity', i.e. it is assumed that no solids are present and the velocity is based on the cross sectional area of the riser.)

In practice the upper particle velocity limit (eqn. (2.17)) is not reached because of friction losses resulting from inter-particle and particle pipe-wall collisions. As $V_G \rightarrow V_T$ the system becomes unstable and what is termed 'slug' flow occurs. At some critical point the velocity represented by the difference between V_G and V_T is no longer sufficient to overcome the friction losses and to lift the particles. The particles collect near the bottom of the riser and form a 'slug'; due to the close proximity of the particles, the drag coefficients are increased and the 'slug' of particles is lifted, sometimes violently, up the almost empty riser. A photograph of slug flow is shown in FIGURE 2.3. LEWIS et al (56) noticed that the value of the gas velocity at which this instability occurred depended on the solids feed rate.

Solids hold-up

The solids hold-up (weight of dispersed solids

FIGURE 2.3 Photograph of slug flow in vertical pneumatic transport

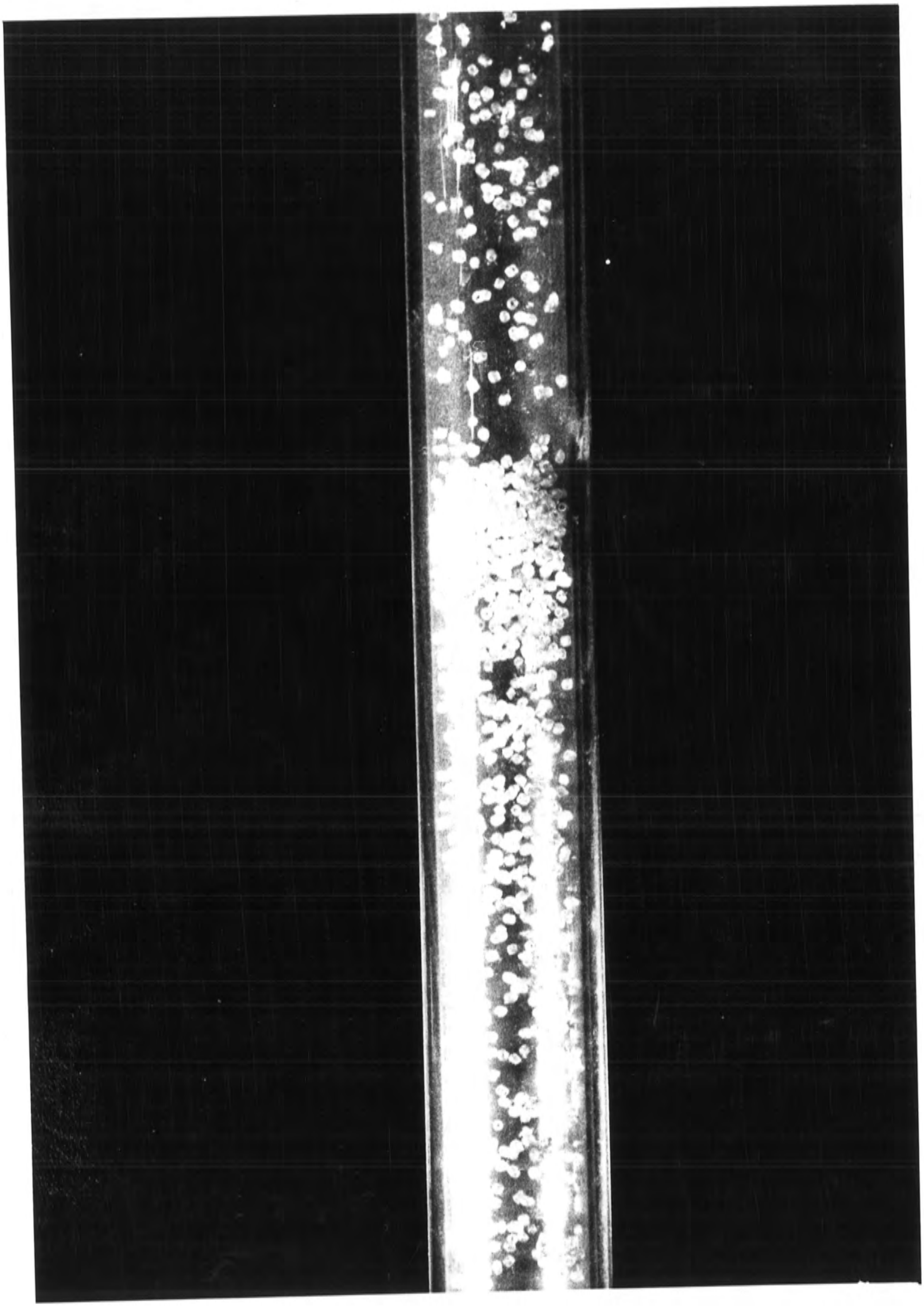

in the riser) depends on the solids feed rate and on the average vertical solids velocity. For a given riser length the hold-up is defined by the equation:

$$H = (W_s \times L) / \bar{V}_p \qquad \text{..... (2.18)}$$

where H = solids hold-up,

W_s = solids feed rate,

L = riser length,

and $\bar{V}_p$ = average vertical particle velocity in the riser.

Void space in the riser

The void space ratio or voidage in the riser is the fraction of the riser volume not occupied by solids. The analytical expression for defining the void space is:

$$\epsilon = 1.0 - \left[\frac{H}{\rho_s} \cdot \frac{4}{\pi D^2 L} \right] \qquad \text{..... (2.19)}$$

where ϵ = voidage,

and ρ_s = solids density.

LEVA (53) describes the gas-solids system in pneumatic transport as the dilute fluidized phase, since the voidage is usually in excess of 90 per cent. The results of

ZENZ (54) indicate that a value of ϵ =0.98 is the minimum possible for stability in a system of dense particles.

Characteristic pressure drop relationship

The presence of solids in the riser increases the pressure drop over the riser length above that resulting from the gas flow alone. The solids hold-up, particle acceleration, particle friction and gas friction all contribute to the total pressure drop. A typical plot of pressure drop vs. gas velocity is seen in FIGURE 2.4, [ZENZ (54)]. This diagram also shows the dependence of the slugging point on the solids feed rate.

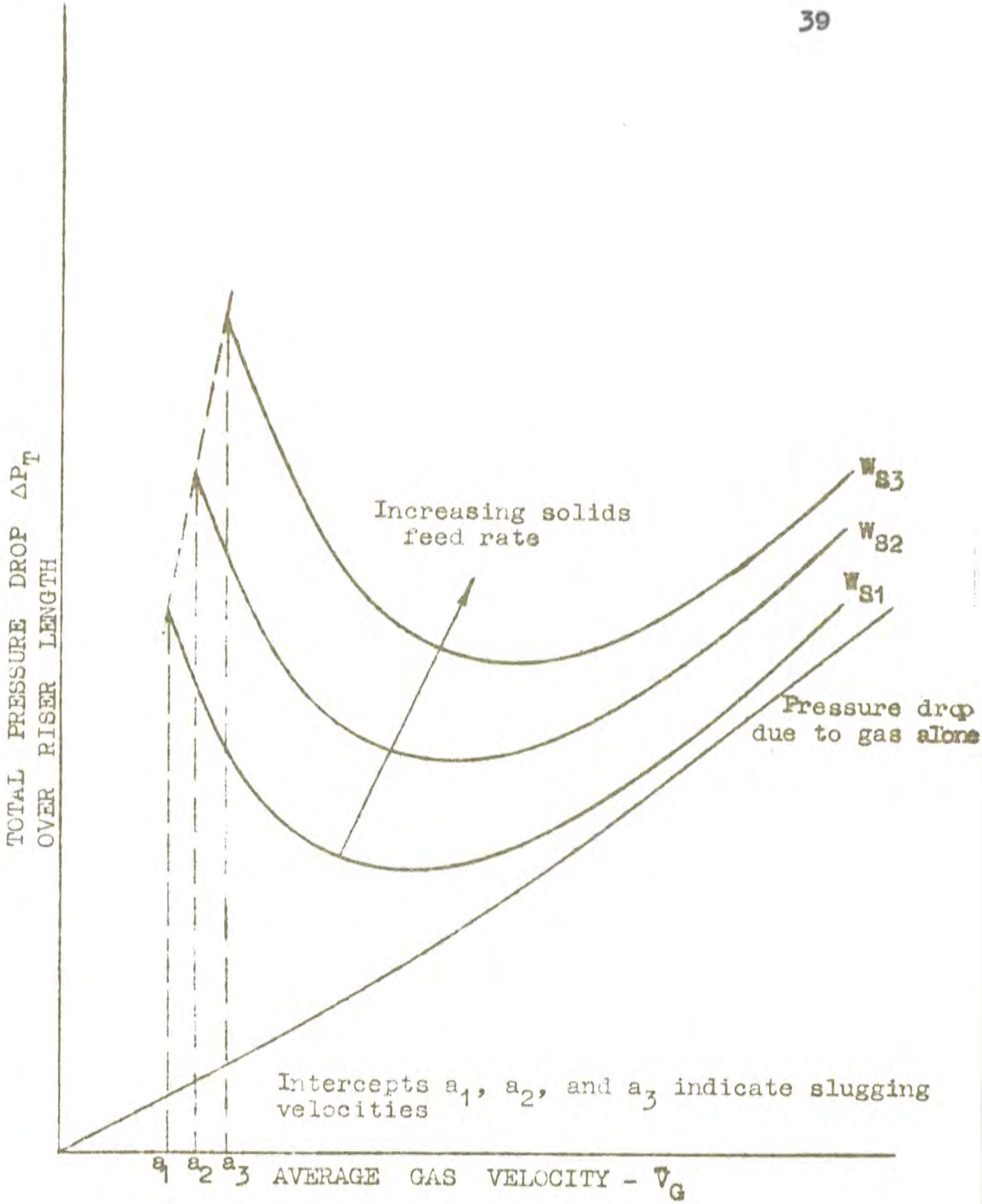

FIGURE 2.4 Typical total pressure drop vs. average gas velocity plot for pneumatic transport with solids feed rate as a parameter, (ZENZ (54))

2.2.9 Average particle velocities and particle trajectories in pneumatic transport

The average particle velocity

The average particle velocity in a section of a riser can be determined by measuring the solids hold-up in that section for a given feed rate and using equation (2.18) in the form:

$$\bar{V}_P = \frac{W_s L}{H} \qquad .....(2.20)$$

CRAMP and PRIESTLEY (55), LEWIS et al (56) and HARIU and MOLSTAD (57) measured average particle velocities in vertical pneumatic transport systems. The solids hold-up was measured by trapping the solids in a section of the riser (length L) with fast closing valves. None of these writers [(55), (56) and (57)] attempted to derive the functional relationship between $\bar{V}_P$ and $\bar{V}_G$, the average gas velocity. This functional relationship is of particular interest because it is hoped to apply the results of the particle dynamics work to residence time estimates in the study of chemical reactions in transport. LEWIS et al (56) presented corresponding values of $\bar{V}_G$ and V_{slip}, where

$$V_{slip} = \bar{V}_G - \bar{V}_P \qquad .....(2.21)$$

In their opinion the slip velocity was essentially independent of the gas velocity and the solids feed rate.

It was decided to re-analyse the data in references (55) and (56) in an attempt to obtain some indication of the nature of the functional relationship between $\bar{V}_P$ and $\bar{V}_G$. The work of HARIU and MOLSTAD (57) is of related interest but is primarily concerned with the pressure drop in vertical pneumatic transport. Since only three levels of gas velocity were used their results are not included in this detailed discussion.

Corresponding values of $\bar{V}_P$ and $\bar{V}_G$ obtained by CRAMP and PRIESTLEY (55) and LEWIS et al (56) are reproduced in TABLES 2.3 and 2.4 respectively. LEWIS et al (56) referred to V_{slip} and $\bar{V}_G$, hence values of $\bar{V}_P$ in TABLE 2.4 have been computed from $\bar{V}_P = (\bar{V}_G - V_{slip})$. These data are plotted in FIGURES 2.5 and 2.6 respectively. In view of the conclusion of LEWIS et al (56) that the solids feed rate does not significantly effect the slip velocity, solid feed rate is not considered as a parameter in FIGURES 2.5 and 2.6. When plotted these data indicated that a linear relationship exists between $\bar{V}_P$ and $\bar{V}_G$. Linear regressions were calculated using the data of TABLES 2.3 and 2.4 and the results of the regression appear in TABLE 2.5; the regression lines are drawn in FIGURES 2.5 and 2.6.

TABLE 2.3

Average solids velocity measurements for pneumatic transport of grain [CRAMP and PRIESTLEY (55)]

Experiment No	Solids feed rate g/sec	$\bar{V}_G$ Mean air velocity m/sec	$\bar{V}_P$ Mean grain velocity m/sec
1	380	10	1.5
2	350	11	2.5
3	710	13	3.2
4	900	14	5.2
5	1590	14	6.1
6	1260	14	6.0
7	1530	15	5.3
8	510	16	6.7
9	1290	16	8.7
10	760	18	7.1
11	850	18	7.1
12	1250	19	10.1
13	1320	19	9.4
14	1180	20	10.2

TABLE 2.4

Average solids velocity measurements for the pneumatic transport of fine glass spheres [LEWIS et al. (56)]

Run C6			Run C7			Run C8		
D_P = 0.004 in			D_P = 0.0016 in			D_P = 0.0112 in		
$\overline{V}_G$	V_{slip}	$\overline{V}_P$	$\overline{V}_G$	V_{slip}	$\overline{V}_P$	$\overline{V}_G$	V_{slip}	$\overline{V}_P$
ft/sec	ft/sec	ft/sec	ft/sec	ft/sec	ft/sec	ft/sec	ft/sec	ft/sec
13.6	4.43	9.17	3.92	1.98	1.94	9.67	7.91	1.76
10.8	3.80	7.00	5.50	2.49	3.01	9.26	7.95	1.31
8.11	3.86	4.25	6.85	2.84	4.01	8.84	7.69	1.15
5.51	3.88	1.63	4.11	2.18	1.93	8.24	7.63	0.61
7.90	4.60	3.30	5.80	3.02	2.78	8.01	7.72	0.29
7.87	4.60	3.27	6.55	2.84	3.71	8.16	7.79	0.37
7.55	4.60	2.95	6.99	2.73	4.26	7.57	7.28	0.29
7.08	5.00	2.08	6.95	2.24	4.71	13.42	8.06	5.36
5.58	4.90	0.68	5,99	2.07	3.92	10.88	8.18	2.70
5.11	3.70	1.41	6.09	3.48	2.61	8.41	7.70	0.71
7.01	4.20	2.81	8.29	3.03	5.26			
5.48	4.30	1.18						
5.56	4.30	1.26						

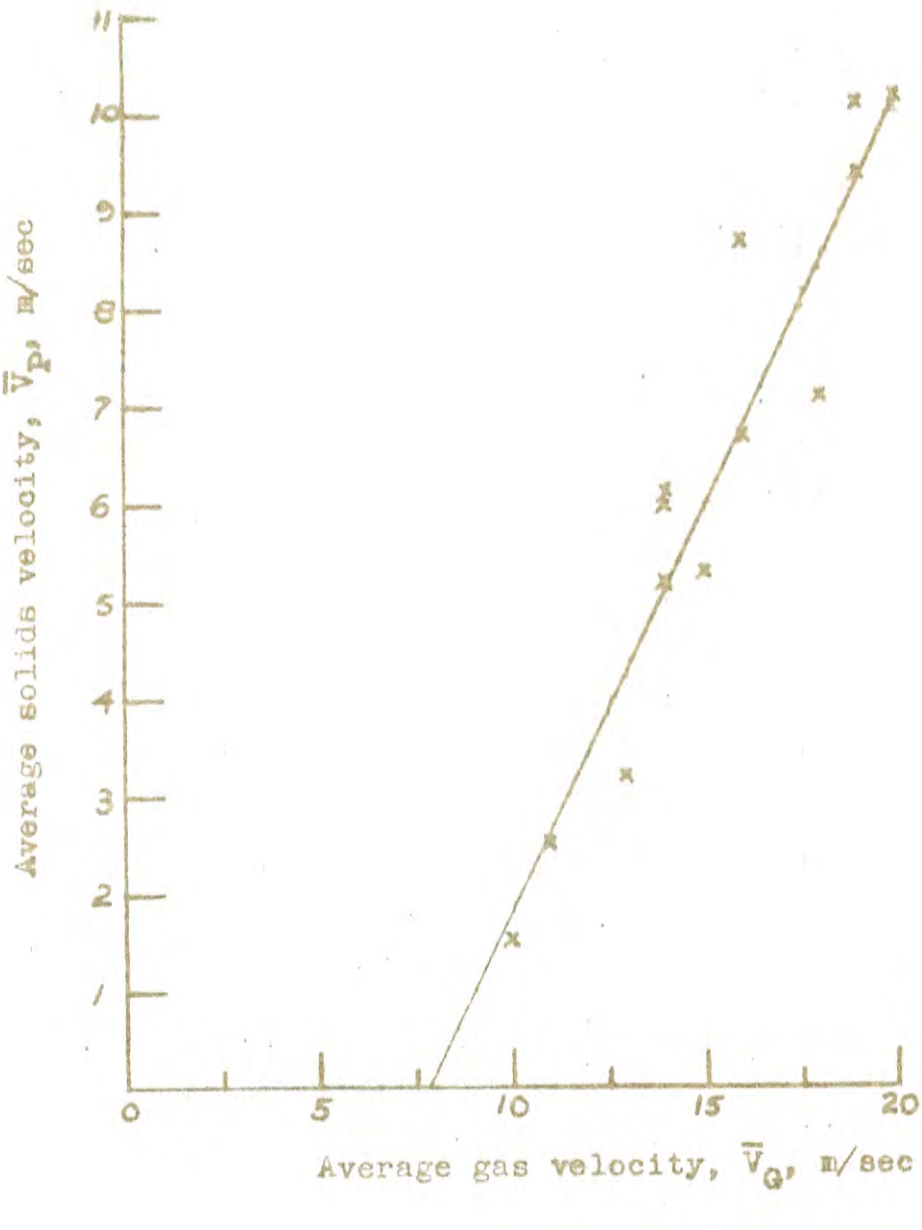

FIGURE 2.5 Plot of $\overline{V}_P$ vs. $\overline{V}_G$ for the data of CRAMP and PRIESTLEY (55)

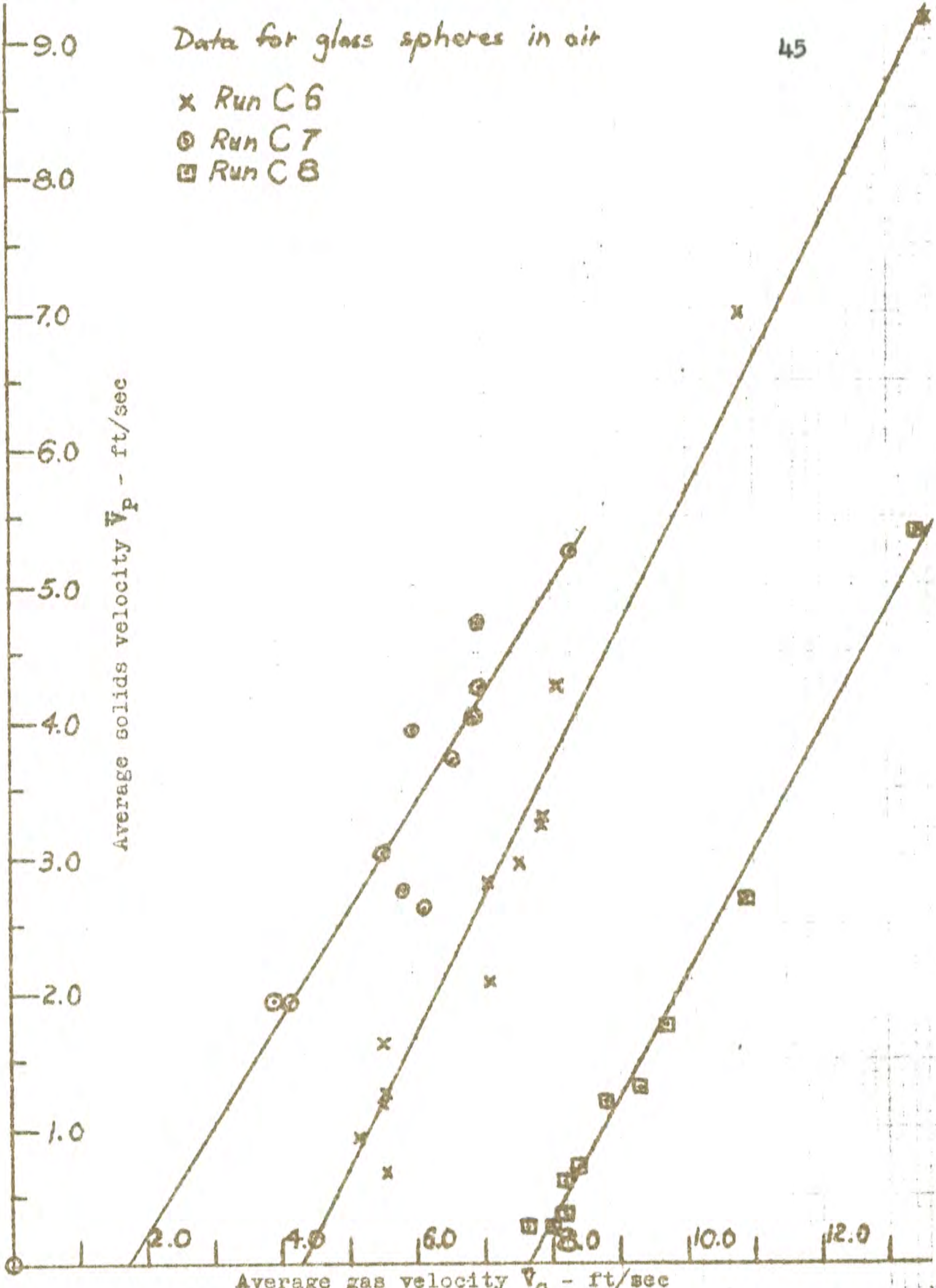

FIGURE 2.6 Plot of $\overline{V}_P$ vs. $\overline{V}_G$ for the data of LEWIS et al (56)

TABLE 2.5 Linear regression results for the particle velocity data of the data of CRAMP and PRIESTLEY (55) and LEWIS et al (56)

Source of data	Regression equation $\bar{V}_P = \alpha \bar{V}_G$ + const.		Standard error estimate
	α (slope)	const. — intercept on V_P axis	
Ref. (55) Wheat grains	0.831	-6.51	0.971
Ref. (56) Run C6 glass spheres D_p=0.004 in	1.000	-4.32	0.439
Ref. (56) Run C7 glass spheres D_p=0.0016 in	0.82	-1.42	0.422
Ref. (56) Run C8 glass spheres D_p=0.0112 in	0.890	-6.78	0.173

The regression data of LEWIS et al (56) in TABLE 2.5 show that the regression lines have different slopes for the three particle sizes. However, in view of the scatter of the data and the fact that the variation in slope is not related to the particle diameter, the difference in the slopes is probably not significant and the mean value of the slopes (α) is probably a reasonable estimate of the true slope. This means that an expression, incorporating the value of the mean slope, viz., $\alpha = 0.897$, can be written for the glass spheres:

$$\bar{V}_P = 0.897 . \bar{V}_G + \text{const.} \qquad ..... (2.22)$$

the constant apparently being some function of the particle diameter.

Similarly for the data of CRAMP and PRIESTLEY (55):

$$\bar{V}_P = 0.831 . \bar{V}_G + (-6.531) \qquad ..... (2.23)$$

Differences in the dimensions of the apparatuses and the characteristics of the solids being transported, make direct comparison between the results of CRAMP and PRIESTLEY (55) and LEWIS et al (56) difficult, due to probable effects of particle acceleration and particle wall friction. However, the form of the functional relationship in both cases is similar, viz.

$$\bar{V}_P = \alpha\bar{V}_G + \text{const.} \qquad ..... (2.24)$$

If this is so, and if $\alpha \neq 1$, the conclusion of LEWIS et al (56) that the slip velocity, $(\bar{V}_G - \bar{V}_P)$, is independent of the gas velocity appears to be unfounded since:

$$V_{slip} = (\bar{V}_G - \bar{V}_P) = (1 - a)\bar{V}_G - \text{const.}$$

In a real system it is reasonable to expect $a<1$ as the effects of particle acceleration and particle wall friction should increase with increasing average solids velocity. However, equation (2.24) is empirical and the scant data are not really sufficient to confirm the general validity of the equation. In addition the measurements of CRAMP and PRIESTLEY (55) and LEWIS et al (56) are not sufficiently precise to reveal any slight curvature.

It is of interest to consider the ratio of the intercept of the plot of $\bar{V}_P$ vs. $\bar{V}_G$ (FIGURES 2.5 and 2.6) on the horizontal $\bar{V}_G$ axis (i.e. - const./a eqn. 2.24) to the estimated terminal velocity of the particles being transported; at this point the apparent average particle velocity is zero and the gas velocity would be expected just to support the particle weight. Corrected intercepts for the data shown in FIGURE 2.6 are computed from a line of mean slope 0.897 drawn through the centres of gravity of the three sets of points. The estimates of the respective terminal velocities, the corrected intercepts and the intercept: terminal velocity ratios are shown in TABLE 2.6 together with similar data (no correction) for wheat grains from CRAMP and PRIESTLEY (55).

TABLE 2.6 Summary of intercept:terminal velocity ratio data calculated from the experimental results of CRAMP and PRIESTLEY (55) and LEWIS et al (56)

Data source	Intercept on $\bar{V}_G$ axis (corrected intercept for Ref.(56))	Terminal velocity estimate	Ratio intercept: terminal velocity	Calculated particle Reynolds number
Ref. (56) Run C7 glass spheres D_p=0.0016 in	2.15 ft/sec	0.4** ft/sec	5.48	0.34
Ref. (56) Run C6 glass spheres D_p=0.004 in	3.88 ft/sec	1.8** ft/sec	2.16	3.8
Ref. (56) Run C8 glass spheres D_p=0.0112 in	7.58 ft/sec	7.0** ft/sec	1.08	42
Ref. (55) wheat grains	7.74 m/sec	7.52* m/sec	1.03	-

Note:

(i) (**) these values were calculated from the standard drag relationship for spheres by LEWIS et al (56), and

(ii) (*) this value was obtained from the experimental data of CRAMP (58).

No direct conclusions regarding any fundamental mechanism can be made from the scant data in TABLE 2.6. However, it appears that the intercept:terminal velocity ratio is relatively high for very fine particles and approaches unity for large particles. LEWIS et al (56) observed this trend in a different form when they plotted the ratio of the calculated slip velocity:predicted slip velocity vs. particle diameter. This increase in the required minimum transport velocity may be due to the influence of fluid turbulence on the drag mechanism of the particles, since the fine particles are well within the 'creeping motion' (Stoke's Law) range. In section 2.2.7 it was noted that MILLER and McINNALLY (45) observed a similar effect with fine coal particles suspended in water, which was attributed to fluid turbulence. If this intercept:terminal velocity ratio is regarded as a modification of the particle drag coefficient, it should be some function of the particle Reynolds number. The results calculated from the data of LEWIS et al (56) from TABLE 2.6 are plotted in FIGURE 2.7 as the log of the intercept: terminal velocity ratio vs. log (Re_p) together with the point corresponding to an intercept:terminal velocity ratio of 1.4 and an Re_p of 25 calculated from the data of MILLER and McINNALLY (45). While it would be speculative to form any conclusion from the scant data shown in

FIGURE 2.7, the graph does suggest that some functional relationship exists relating the intercept:terminal velocity ratio and the particle Reynolds number, at least for $Re_p < 50$.

If the fluid turbulence in the riser contributes to these deviations from the classical drag relationship, transporting fluid Reynolds number for the riser should be considered in any further analysis. It is of interest to note that ZENZ (54) warns that standard drag relationships should be used with caution for fine particles in large pipes.

The intercept should not be regarded as a measure of the 'choking' or 'slug flow' velocity, as this velocity has been shown to depend on the solids feed rate, LEWIS et al (56).

TRIPURANENI et al (59) investigated the average solids velocity but reported their results as an empirical correlation for $(1-\epsilon)$, which is related to $\bar{V}_P$ by equations (2.20) and (2.21). However, the empirical approach adopted and the wide scatter of their data render the paper of little use for direct prediction of the average particle velocity.

Particle trajectories

In an ideal system with uniform gas velocity

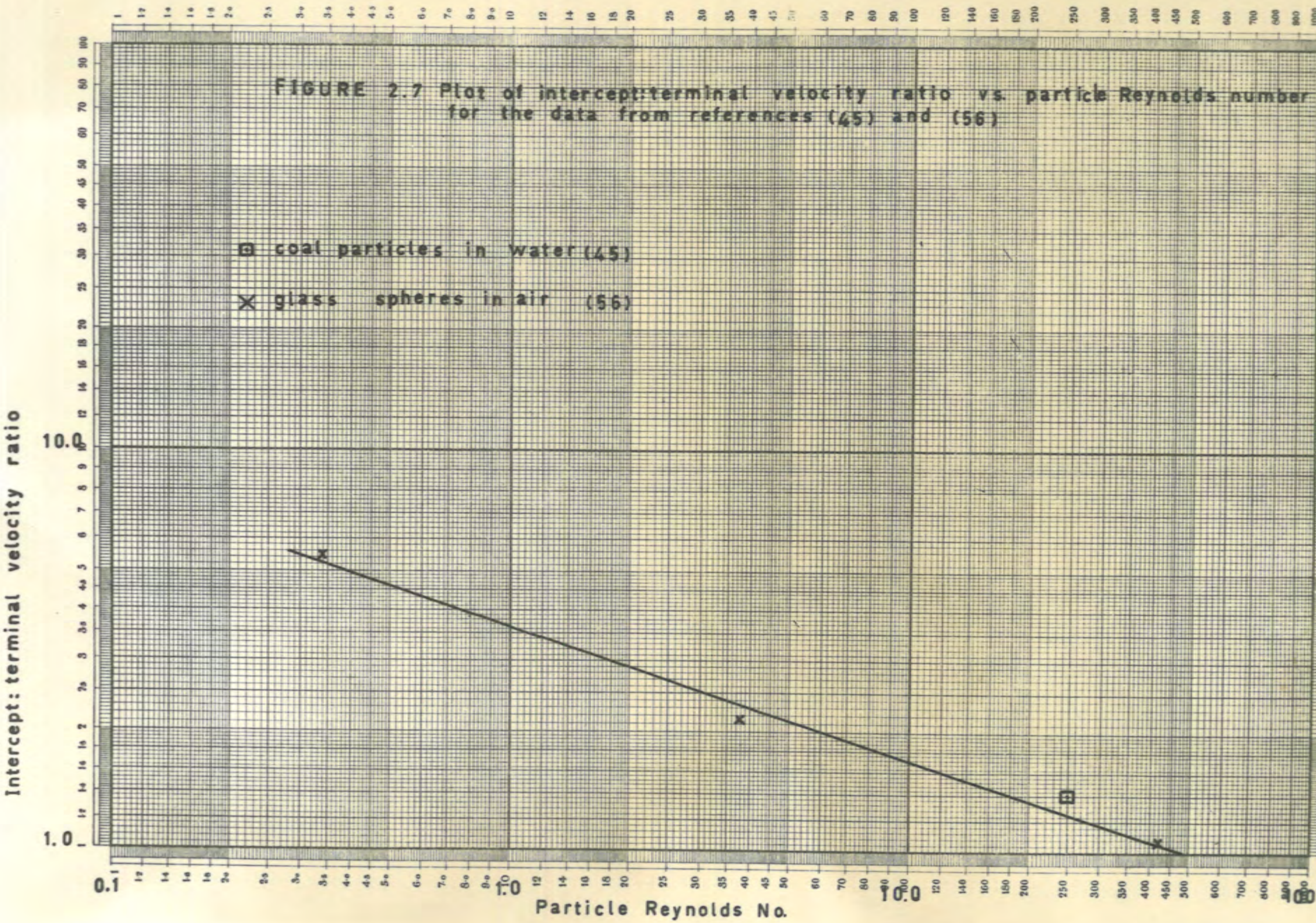

FIGURE 2.7 Plot of intercept:terminal velocity ratio vs. particle Reynolds number for the data from references (45) and (56)

across the riser section, the particle trajectory may be calculated by making the following assumptions, [CRAMP and PRIESTLEY (55)], viz.

(i) the gas velocity remains constant along the riser length,

(ii) the drag coefficient and the gas density remain constant along the riser length,

(iii) the space occupied by the solids is negligible,

and (iv) the solids friction is negligible.

The force balance on a particle may be written (assuming $g/g_c = 1.0$):

$$F_D - m\left(1 - \frac{\rho_f}{\rho_s}\right) = \frac{m}{g} \cdot \frac{d\,V_P}{dt} \qquad \text{..... (2.25)}$$

i.e. drag force - effective particle weight = (mass x acceleration)/g

where m = mass of the particle

ρ_s = density of the particle,

and t = time.

Since, in pneumatic transport, ρ_s is usually significantly greater than ρ_f, considering assumption (ii), equation (2.25) reduces to:

$$C_D \cdot A_p \cdot ({}^{\rho_f}/_{2g})(V_G - V_P)^2 - m = ({}^m/_g) \cdot \frac{d\ V_P}{dt}$$

..... (2.26)

In this ideal equation, when the acceleration transient has finished,

$$\frac{d\ V_P}{dt} = 0 \quad \text{and} \quad (V_G - V_P) = V_T$$

where V_T = particle terminal velocity. Hence, equation (2.26) becomes

$$C_D \cdot A_p \cdot ({}^{\rho f}/_{2g}) \cdot V_T^2 - m = 0$$

so equation (2.26) can be written:

$$\frac{m}{V_T{}^2} \ (V_G - V_P)^2 - m = ({}^m/_g) \cdot \frac{d\ V_P}{dt} \qquad \text{..... (2.27)}$$

Both CRAMP and PRIESTLEY (55) and JENNINGS (60) have published solutions for this equation, but do not show the derivation of the solutions. The solutions published by JENNINGS (60) are in parametric form, viz.:

(i) $$S = ({}^{V_T}/_{2g}) \left[(V_G - V_T) \ln \frac{(V_G - V_T)}{(V_G - V_T - V_P)} - (V_G + V_T) \ln \frac{(V_G + V_T)}{(V_G + V_T - V_P)} \right] \qquad \text{..... (2.28)}$$

and (ii)

$$t = (^{V_T}/_{2g}) \left[\ln \frac{(V_G - V_T)}{(V_G - V_T - V_P)} - \ln \frac{(V_G + V_T)}{(V_G + V_T - V_P)} \right]$$

..... (2.29)

where S is the distance the particle travels in time t.

It is also possible to obtain a solution for S = f(t), however, the resulting expression is transcendental and it is not possible to obtain explicitly t = f(s).

HARIU and MOLSTAD (57) considered the effect of including frictional forces in the particle trajectory equation. They assumed the frictional force acting on a suspension (wall shear force) could be represented by a Fanning type of friction equation:

$$\text{i.e. wall shear force} = \left[\frac{4\ f_s\ \rho d_s\ V_P^2}{2g\ D} \right] \cdot \left[\frac{\pi D^2}{4} \right] \cdot dL$$

where ρd_s = dispersed solids density, i.e. the mass of solid per unit volume of space. Hence, for a single particle:

$$\text{wall shear force} = (m.2.f_s.V_P^2)/(D.g)$$

where f_s is the solids friction factor. Hence, the force balance may be written:

Drag force - particle weight - wall shear force = inertia force

and the differential equation for the particle trajectory becomes:

$$\frac{d\,V_P}{dt} = \frac{3}{4}\left(\rho_f/\rho_s\right)\frac{(V_G-V_P)^2}{d}\cdot C_D - g - \frac{2\,f_s\,V_P^2}{D}$$

..... (2.30)

This equation can be integrated numerically or graphically.

The solids friction factor, f_s, will depend on the physical characteristics of the solid conveyed, the roughness of the riser wall, and possibly on the actual solids velocity. Because of the difficulty of determining f_s in a system where acceleration occurs, equation (2.30) is only useful for systems where the transient effects have stabilized (i.e. $\frac{d\,V_P}{dt} = 0$) or are negligible.

Now this thesis is particularly concerned with average particle velocities in a system where acceleration must be considered. It may be possible to account for the solids friction effect by determining the functional relationship between a theoretical average particle velocity calculated from equations (2.28) and (2.29) and the actual measured average particle velocity in the system. For acceleration in a frictionless zone, between points 1 and 2, the average theoretical velocity is given by the equation:

$$(\bar{V}_P)_{Theoretical} = \frac{(s_2 - s_1)}{(t_2 - t_1)} \qquad \ldots\ldots (2.31)$$

and the actual measured average particle velocity is given by the equation:

$$(\bar{V}_P)_{Actual} = \frac{W_s \times L}{H} \qquad \ldots\ldots (2.20)$$

where L, the riser length, is equal to $(s_2 - s_1)$.

One of the assumptions made in deriving equations (2.28) and (2.29) was that the drag coefficient remained constant over the interval s_1 to s_2.

2.2.10 The pressure drop in vertical pneumatic transport

One of the objectives of this part of the work is to examine the relationship that exists between the average particle velocity and the pressure drop in vertical pneumatic transport with a view to predicting average particle velocities from pressure drop measurements. This section (2.2.10) is therefore concerned primarily with the theoretical aspects of this pressure drop.

The pressure drop in vertical pneumatic transport was mentioned briefly in section 2.2.8 and a set of typical pressure drop curves is shown in FIGURE 2.4. CRAMP (58) and CRAMP and PRIESTLEY (55) recognised that the rate of change of momentum in a riser is equal to the sum of the forces acting on the gas and on the particles. Neglecting the *pressure difference due to the height of the air column, (the atmospheric lapse rate is approx. 0.012 in H_2O/ft at sea level), the forces acting on the particles and the gas were assumed to be:

(i) the wall shear force between the gas and the riser,

---

* Note: MEHTA et al (64) point out that this pressure drop is not detectable if the pressure measurements are made with a manometer with lead lines containing the same fluid.

(ii) the weight of the solids in the riser,

and (iii) the wall shear force between the particles and the riser.

CRAMP (58) and CRAMP and PRIESTLEY (55) showed that the forces resulting from gas acceleration were negligible but neglected to consider the effect of particle acceleration. JENNINGS (60) formed similar conclusions to the writers (58) and (55) but also recognised the need to include particle acceleration in the momentum equation. VOGT and WHITE (61) produced an empirical correlation for the total pressure drop in a riser, but included the effect of the weight of solids in the riser on total pressure drop in a Fanning friction factor. The part of the Fanning friction factor in this case which accounted for the weight of solids in the riser would be analogous to the drag coefficient.

HARIU and MOLSTAD (57) initially assumed that the total pressure drop would be independent of particle acceleration effects, but an analysis of their results indicated that the pressure drop due to particle acceleration should have been included in their analysis. Their final expression for the total pressure drop components was:

$$\Delta P_T = \Delta P_G + \Delta P_H + \Delta P_{SF} + \Delta P_{SA} \qquad \ldots\ldots (2.32)$$

where ΔP_T = total pressure drop,

ΔP_G = pressure drop due to gas-wall shear force,

ΔP_H = pressure drop due to solids hold-up,

ΔP_{SF} = pressure drop due to solids-wall shear force,

and ΔP_{SA} = pressure drop due to solids acceleration.

The pressure drops due to the height of the air column and gas acceleration were considered negligible.

At this stage it is possible to explain the shape of the characteristic pressure drop curves in FIGURE 2.4. The contributing factors to the total pressure drop are contained in equation (2.32). The gas pressure drop will increase with gas velocity; for a fixed solids mass flow rate the pressure drops due to solids friction (ΔP_{SF}) and solids acceleration (ΔP_{SA}) will increase with solids velocity. On the other hand the pressure drop due to solids hold-up (ΔP_H) will, for a given solids mass flow rate, decrease with increasing solids velocity since:

$$\Delta P_H = \frac{H}{A_c} = \frac{W_s \cdot L}{A_c \cdot \bar{V}_p} \qquad \ldots\ldots (2.33)$$

As $\bar{V}_p$ can be represented by a function:

$$\bar{V}_P = \alpha \bar{V}_G + \text{const.} \qquad \ldots\ldots (2.24)$$

the term $\Delta P_H \rightarrow$ zero as $\bar{V}_G \rightarrow \infty$; it then follows that $\Delta P_T \rightarrow (\Delta P_G + \Delta P_{SF} + \Delta P_{SA})$ as $\bar{V}_G \rightarrow \infty$.

The terms ΔP_H, ΔP_{SF} and ΔP_{SA} are proportional to the solids feed rate. Equation (2.33) indicates that ΔP_H is directly proportional to feed rate while a momentum balance shows that ΔP_{SF} and ΔP_{SA} are proportional to the solids mass flow rate, (i.e. the feed rate). The solids friction term, ΔP_{SF}, has been represented by a Fanning type equation by HARIU and MOLSTAD (57), BARTH (62) and STEMERDING (63). For ΔP_G to be independent of solids velocity and solids feed rate, it must be assumed that the gas-wall shear forces are not effected by the presence of solid particles, which should be a valid assumption at low solids concentrations [HARIU and MOLSTAD (57)]. The position of the minimum of the curves shown in FIGURE 2.4 will depend on the relative contributions of the terms ΔP_G, ΔP_{SF} and ΔP_{SA} to the total pressure drop.

HARIU and MOLSTAD (57) derived the following expression for the solids pressure gradient:

$$\frac{dP_{solids}}{dL} = \frac{W_s}{A_c}\left[\frac{1}{V_P} + \frac{2\, f_s\, V_P}{g.D} + \frac{d\, V_P}{dt} \cdot \frac{1}{g\, V_P}\right]$$

..... (2.36)

by making two assumptions, viz.:

(i) $\Delta P_{solids} = \Delta P_T - \Delta P_G$ ..... (2.34)

and (ii) $\Delta P_{SF} = \frac{2\, f_s\, V_P}{g.D} \cdot \frac{W_s}{A_c} \cdot \Delta L$ ..... (2.35)

i.e. $\frac{dP_{solids}}{dL} = \frac{d\, P_H}{dL} + \frac{d\, P_{SF}}{dL} + \frac{d\, P_{SA}}{dL}$

..... (2.37)

However, they had difficulty in obtaining reproducible values of f_s using a graphical technique for integrating equation (2.36).

STEMERDING (63) simplified a momentum balance derived by HINZE (65) for a dispersed two phase flow system. He neglected gas friction and turbulence effects and obtained an equation of the form:

$\Delta P_{solids} = \Delta P_H + \Delta P_{SF} + \Delta P_{SA}$ ..... (2.38)

which is an integrated form of the equation derived by

HARIU and MOLSTAD (57). For the discussion of the paper by STEMERDING (63), the original nomenclature will be used for convenience:

D = riser diameter,

g = gravitational acceleration,

G_s = solids mass velocity (mass per unit time per unit area),

L = length of riser,

L_e = length of acceleration zone,

ΔP = riser pressure drop (absolute units),

u_s = true solids velocity,

$u_{s\infty}$ = equilibrium solids velocity,

U_g = superficial gas velocity,

z = vertical distance from riser entrance,

$\bar{\alpha}$ = volumetric solids fraction,

$\bar{\gamma}$ = average segregation factor defined by:

$$\int_0^L \bar{\alpha} \cdot dz = \frac{G_s(L + \bar{\gamma} L_e)}{\rho_s \cdot u_{s\infty}} ,$$

λ^*_s = apparent solids friction factor,

ρ_s = solids density,

and σ_{ws} = solids-wall shear stress (absolute units).

The integral form of the momentum balance is:

$$\Delta P = P_0 - P_L = \rho_s g \int_0^L \bar{\alpha}\, dz + {}^4/_D \int_0^L \sigma_{ws} . dz + (G_s \bar{u}_s)_{z=L}$$

..... (2.39)

with the boundary condition $\bar{u}_s = 0$ at $z = 0$.

STEMERDING (63) divides the riser into two sections for the analysis, viz.:

(i) the section $z = 0$ to L_e in which particle acceleration occurs,

and (ii) the section $z = L_e$ to L, the remainder of the riser length, where for a given gas velocity the particle velocity has reached an equilibrium value of $u_{s\infty}$.

Substituting $\sigma_{ws} = \frac{1}{8} \lambda^*_s G_s u_{s\infty}$ (a form of the Fanning friction equation) and evaluating the integrals in equation (2.39) gives:

$$\Delta P = \frac{g G_s}{u_{s\infty}} (L + \bar{\gamma} L_e) + \frac{1}{2} \lambda^* G_s u_{s\infty} . \frac{L}{D} + G_s . u_{s\infty}$$

..... (2.40)

The advantage of using $u_{s\infty}$ now becomes apparent as it is common to all the terms on the R.H.S. of equation (2.40). The use of $u_{s\infty}$ also removes the necessity for tedious graphical integration, a problem encountered by HARIU and MOLSTAD (57).

The next assumption made by STEMERDING (63) is:

$$h = \frac{U_g}{u_{s\infty}} \qquad \text{..... (2.41)}$$

so that equation (2.40) can be rearranged in the dimensionless form:

$$S^{*} = \frac{\Delta P . U_g}{G_s . g . L} = h\left(1 + \frac{\bar{\gamma} L_e}{L}\right) + \frac{1}{h}\left(\frac{1}{2}\lambda^{*}_{s} + \frac{D}{L}\right)\frac{U_g^2}{g.D}$$

$$\text{..... (2.42)}$$

This equation has two limitations which are inherent in the derivation, viz. L must be greater than L_e so that $u_{s\infty}$ can exist, and $h = U_g/u_{s\infty}$ equation (2.41). Now it was shown in section 2.2.9 that the functional relationship between the average particle velocity and the average gas velocity could be represented by an equation of the form:

$$\bar{V}_P = \alpha \bar{V}_G + \text{const.} \qquad \text{..... (2.24)}$$

where the constant term, approximates the gas velocity at which 'slug flow' may occur. Hence equation (2.41) might be expected to be of the form:

$$h = \frac{U_g}{(u_{s\infty} - \text{const.})} \qquad \ldots\ldots (2.43)$$

Consequently equations (2.41) and (2.42) would appear valid only if $u_{s\infty}$ is significantly greater than the minimum velocity required for transport. This is likely to be the case for the pneumatic transport of fine particles in a long riser where $L > L_e$ and $u_{s\infty} >> \text{const.}$ However, in view of these conditions the equations of STEMERDING (63) appear not to be appropriate for relating average particle velocity measurements to the pressure drop for moderately coarse particles in a short riser.

2.3 Derivation of a Theoretical Model for a Vertical Pneumatic Transport System

Since the literature examined did not contain a suitable function relating the average particle velocity in vertical pneumatic transport to the pressure drop, it was decided to develop a theoretical model with this requirement in mind. Because of the complexities of the real system certain simplifying assumptions must be made in the analysis. It was shown in section 2.2.9 that the ideal particle trajectory, excluding particle friction losses, is calculable from equations (2.28) and (2.29). It is proposed to derive a model which gives a functional relationship between pressure drop measurements and the average particle velocity between two points on the actual trajectory. Because of the solids-wall shear forces, the particle velocities in the actual trajectories are lower than those determined by the ideal trajectory equations. It is assumed first that the mean impulse associated with this apparent momentum change is concurrent with the solids-wall shear forces, and second that the effect of interparticle collisions is not significant at the high voidages normally encountered in vertical pneumatic transport.

2.3.1 The theoretical trajectory

The equations for calculating the theoretical trajectory are:

(i) $$S = \frac{V_T}{2g}\left[(V_G - V_T) \ln \frac{(V_G - V_T)}{(V_G - V_T - V_P)} - (V_G - V_T) \ln \frac{(V_G + V_T)}{(V_G + V_T - V_P)} \right] \quad \ldots\ldots (2.28)$$

and (ii)

$$t = \frac{V_T}{2g}\left[\ln \frac{(V_G - V_T)}{(V_G - V_T - V_P)} - \ln \frac{(V_G + V_T)}{(V_G + V_T - V_P)} \right] \quad \ldots\ldots (2.29)$$

where V_T = terminal falling velocity of the particles,

S = vertical distance travelled,

t = time,

V_G = gas velocity,

V_P = particle velocity,

and g = acceleration due to gravity.

These equations have been derived for a single particle in a uniform velocity field. In an actual pneumatic transport system, the gas velocity and possibly the particle distribution are not likely to be uniform across the riser section. The carrier gas velocity (V_G) and the particle terminal velocity (V_T) are the independent variables which completely define the particle trajectory, therefore, to apply equations (2.28) and (2.29) to a given system, estimates of their effective values must be made. It is suggested that the average gas velocity based on the fluid mass flow rate in the riser ($\overline{V_G}$) is the best estimate for a value of V_G. However, since such properties as fluid turbulence, particle shape, and particle orientation influence the fluid drag on a particle (section 2) a value of V_T for an actual system would be difficult to calculate at the present state of knowledge.

It is therefore proposed to use an experimentally determined value of $\overline{V_G}$ in equation (2.24), viz.

$$\overline{V_P} = \alpha \overline{V_G} + \text{const.} \qquad \text{..... (2.24)}$$

for which $\overline{V_P}$ is zero, i.e. the estimate of V_T is:

$$V_T = -\frac{\text{const.}}{\alpha}$$

This estimate for V_T meets requirements of a system model in that the value of the gas velocity at which the particle velocity is zero is the same for both the experimentally observed relation, equation (2.24), and the theoretical trajectory, equations (2.28) and (2.29).

2.3.2 The mean actual particle trajectory for a system of particles

Because of the retarding effect of particle-wall collisions, the collision history of a particle will influence its velocity at any point in the riser. A possible actual single particle trajectory is shown in FIGURE 2.8. In a pneumatic transport system a large number of particles continuously stream past S_1, a point in a riser, such that if all the parameters of the system are held constant, the particle velocities might be expected to be distributed according to some reproducible frequency function, $f(x_1)$, where x_1 is the velocity variable $(x = V_p)$ such that:

$$f(x_1) > 0,$$

$$\int_{-\infty}^{\infty} f(x_1)dx_1 = 1,$$

and if x_1 is bounded, $f(x_1) = 0$ outside the boundary limits.

For any point S_1 in the range of S, $S_1 < S < S_2$, the velocity can be defined by $f(x_1)$; hence, for the purpose of this analysis, it will be assumed that the actual mean particle trajectory is defined as the locus of $\overline{x_1}$, where

$$x_1 = \int_{-\infty}^{\infty} x_1 \, f(x_1)dx_1 \qquad .....(2.34)$$

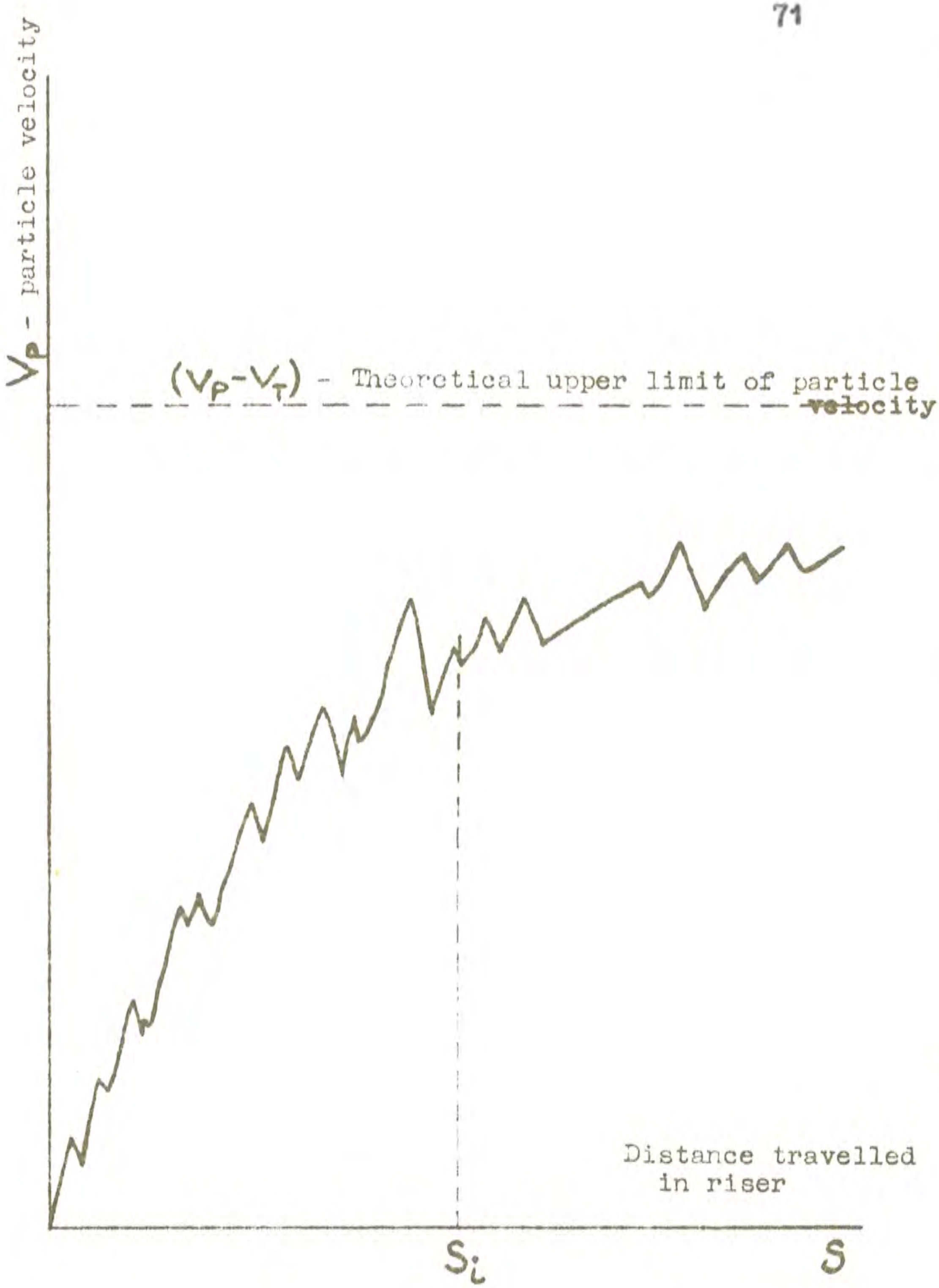

FIGURE 2.8 Example of a possible single particle trajectory in a riser

i.e. $\overline{x_1}$ is the mean velocity of particles streaming past the point S_1. The only assumption implied about $f(x_1)$ is that it is reproducible for all values of S.

FIGURE 2.9 is a schematic diagram of the hypothesis of the model which shows the relationship between the ideal and actual particle trajectories.

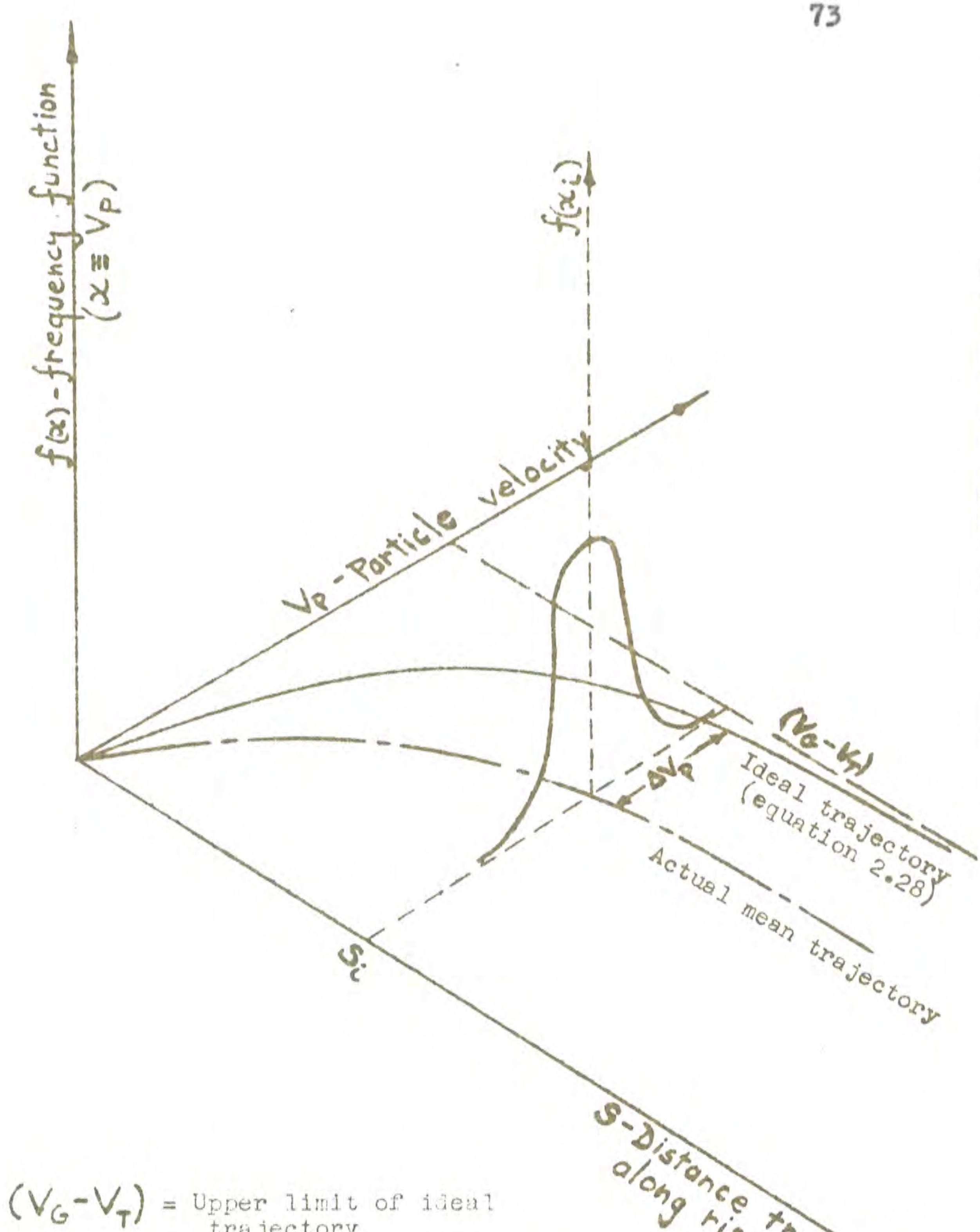

$(V_G - V_T)$ = Upper limit of ideal trajectory

ΔV_p = Associated with wall shear force

FIGURE 2.9 Graphical representation of ideal and actual particle trajectories

2.3.3 Momentum balance

The fundamental mechanism of pneumatic transport is the transfer of momentum from the gas to the dispersed solid phase. For a circular conduit the steady state momentum balance, neglecting turbulence effects, [STEMERDING (63)], can be written [BENNETT and MYERS (66)] :

$$\frac{1}{g} \triangle (w\ v_x) = R_x - F_{xp} - F_{xd} \qquad \text{..... (2.35)}$$

where x = axial coordinate,

w = mass flow rate,

v_x = axial velocity, assumed to be constant over the riser cross section,

R_x = resultant external force on the system, e.g. gravity,

F_{xp} = resultant pressure force on the system,

and F_{xd} = resultant drag force on the system.

For gas flow at a moderate pressure drop, $\triangle(w\ v_x)$ and R_x, the gravitational force, are negligible. Hence the momentum balances for two phase gas solids flow can be written:

(i) for the gas flow

$$0 = -(F_{xp})_{gas} - (F_{xd})_{gas}$$

where $(F_{xd})_{gas}$ = (gas/wall shear force) + (gas/particle dry force)

and (ii) for the solids flow

$$\frac{\Delta(W_s V_p)}{g} = -(R_x)_{solids} - (F_{xp})_{solids} - (F_{xd})_{solids}$$

where $(F_{xd})_{solids}$ = - (gas/particle drag force) + (solids/wall shear force)

The two balances solved simultaneously give:

$$\frac{\Delta(W_s V_p)}{g} = -(R_x)_{solids} - (F_{xp})_{solids} - (F_{xp})_{gas}$$

$$- (F_{xd})_{gas/wall} - (F_{xd})_{solids/wall}$$

..... (2.36)

Now since $(F_{xp})_{solids} = A_{solids} \cdot \Delta P$,

and $(F_{xp})_{gas} = A_{gas} \cdot \Delta P$, where A_{solids} and A_{gas} are the effective cross sectional areas of the conduit occupied by the solids and gas respectively, it follows that:

$$-\left[(F_{xp})_{solids} + (F_{xp})_{gas} \right] = A_c . \Delta P$$

If equation (2.36) is applied between two reference cross sections of the conduit at S_1 and S_2. the result is:

$$\overline{\Delta P} = - \frac{1}{A_c}\left[H + (\overline{F_{xd}})_{gas/wall} + (\overline{F_{xd}})_{solids/wall} + \frac{\Delta (W_s V_p)}{g} \right]$$

..... (2.37)

where $H = R_n$, the solids hold-up between S_1 and S_2.
If $\overline{\Delta P} = P_2 - P_1 = - \Delta P_T$, equation (2.37) can be written:

$$\Delta P_T = \Delta P_G + \Delta P_H + \Delta P_{SF} + \Delta P_{SA}$$

..... (2.32)

For low solids concentrations, it is assumed that $(F_{xd})_{gas/wall}$ is not modified by the presence of the solid particles, hence

$$\Delta P_{solids} = \Delta P_T - \Delta P_G \qquad ..... (2.34)$$

i.e. equation (2.37) excluding the gas/wall shear force becomes

$$\Delta P_{solids} = \frac{1}{A_c}\left[H + (\overline{F_{xd}})_{solids/wall} + \frac{\Delta (W_s\ V_p)}{g} \right]$$

..... (2.38)

2.3.4 The momentum content of a stream of particles

This analysis assumes that the particle stream is moving along a reproducible trajectory such that

$$V_P = f_{(t)} \qquad \text{..... (2.39)}$$

Under steady state conditions one particle enters and one particle leaves the system every interval of time Δt, such that for an n particle system:

$$n = \frac{T}{\Delta t} = \frac{t_2 - t_1}{\Delta t} \qquad \text{..... (2.40)}$$

where n = the number of particles in the system,

T = particle residence time in the system,

t_1 = the time a particle enters the system,

and t_2 = the time a particle leaves the system.

The momentum content, (P_M), of this stream of n particles is:

$$P_M = \sum_{i=1}^{n} m_i V_{Pi} = \sum_{i=1}^{n} n_i f(t_i) \qquad \text{..... (2.41)}$$

With particles of equal mass the hold-up (total mass) of particles between S_1 and S_2 is H where,

$$H = nm = \frac{T}{\Delta t} \; m$$

so that $m = \frac{H.\,\Delta t}{T}$ ..... (2.42)

$$\text{Hence } P_M = \sum_{i=1}^{n} \frac{H}{T}.\; \Delta t.\; f(t_i) = \frac{H}{T}\sum f(t_i).\,\Delta t$$

which is in the limit

$$P_M = \frac{H}{T} \int_{t_1}^{t_2} f(t)dt \qquad \text{..... (2.43)}$$

and since $T = t_2 - t_1$

$$P_M = H.\; \overline{V_P} \qquad \text{..... (2.44)}$$

where $\overline{V_P}$ is the average velocity of the particles between S_1 and S_2 (hence t_1 and t_2) and $\overline{V_P}$ is defined by the equation

$$\overline{V_P} = \frac{(S_2 - S_1)}{(t_2 - t_1)} \qquad \text{..... (2.45)}$$

2.3.5 The theoretical solids pressure drop in terms of the theoretical and actual particle velocities

The aim of the model is to be able to express the term

$$(\overline{F_{xd}})_{solids/wall}$$

in the equation:

$$\Delta P_{solids} = \left[\frac{H}{A_c} + \frac{(\overline{F_{xd}})_{solids/wall}}{A_c} + \frac{\Delta (W_s \; V_p)}{g \; A_c} \right] \qquad \text{..... (2.38)}$$

in terms of the apparent change of momentum between the ideal theoretical particle trajectory and the mean actual trajectory, see FIGURE 2.9. Now the mean actual trajectory has been defined as the locus of $\overline{x_1}(x = V_p)$ where:

$$\overline{x_1} = \int_{-\infty}^{\infty} x_1 \; f(x_1) \; dx_1 \qquad \text{..... (2.34)}$$

therefore the time average momentum content of the particles streaming past the point S_1 is:

$$m \; \overline{x_1} = \int_{-\infty}^{\infty} m \; x_1 \; f(x_1) \; dx_1 = m \; (V_{P_1})_{actual}$$

Hence the momentum content of the stream of particles moving along the actual trajectory is:

$$(P_M)_{actual} = H(\overline{V_P})_{actual}$$

and the momentum content of the particles moving along the theoretical trajectory is:

$$(P_M)_{theoretical} = H\ (\overline{V_P})_{theoretical}$$

since $P_M = H\ \overline{V_P}$ ..... (2.44)

By definition the impulse (J_M) due to the change in momentum is:

$$J_M = (P_M)_{theoretical} - (P_M)_{actual}$$

$$= \frac{1}{g} \int_{t_1}^{t_2} F_{xd}\ dt \text{ (where } F_{xd} = (F_{xd})_{solids/wall})$$

but since

$$\overline{F_{xd}} = \frac{1}{t_2 - t_1} \int_{t_1}^{t_2} F_{xd} \cdot dt = \frac{1}{gT} \int_{t_1}^{t_2} F_{xd} \cdot dt$$

it follows that:

$$(\overline{F_{xd}})_{solids/wall} = \frac{J_M}{Tg} = \frac{H}{gT}\left[(\overline{V_P})_{theoretical} - (\overline{V_P})_{actual} \right]$$

..... (2.46)

Therefore the solids pressure drop equation for the interval S_1 to S_2 can be written:

$$\Delta P_{solids} = \frac{1}{A_c} \left[H + \frac{H}{g\,T} (\overline{V_P}_{\ theoretical} - \overline{V_P}_{\ actual}) + \frac{H}{g\,T} (V_{P\ actual})_2 - (V_{P\ actual})_1 \right]$$

..... (2.47)

Before appropriate use can be made of equation (2.47) some assumption must be made about the relationship between $f_1(t)$ and $f_2(t)$ where,

(i) $f_1(t) = V_{P\ theoretical}$,

and (ii)

$f_2(t) = V_{P\ actual}$

i.e. the form of the relationship:

$$f_2(t) = G[f_1(t)] \qquad ..... (2.48)$$

must be known. Now if the relationship between $\overline{V_P}_{\text{ actual}}$ and $\overline{V}_{\text{theoretical}}$ can be represented by a linear or approximately linear form, the nature of the function G may be determinable from the expression:

$$\overline{V_P}_{\text{ actual}} = G\,(\overline{V}_{P\text{ theoretical}}) \qquad \text{.....(2.49)}$$

no assumption concerning the nature of the function G can be made until experimental values of $\overline{V_P}_{\text{ actual}}$ have been compared with calculated values of $\overline{V_P}_{\text{ theoretical}}$.

2.4 Experimental Technique

The object of the experiments described in this section of the thesis is to check the validity of the theoretical model developed in section 2.3 for transport in a riser similar to that shown in FIGURE 2.2. The model equation relating ΔP_{solids} and the particle velocity can be written:

$$\Delta P_{solids} = \frac{W_s}{A_c}\left[\frac{L}{\overline{V}_{P\ actual}} + \frac{[(V_{P\ actual})_2-(V_{P\ actual})_1]}{g} + \frac{(\overline{V}_{P\ theoretical}-\overline{V}_{P\ actual})}{g}\right] \quad \ldots\ldots (2.50)$$

which is an analytical expression for the equation:

$$\Delta P_{solids} = \Delta P_H + \Delta P_{SA} + \Delta P_{SF} \quad \ldots\ldots (2.38)$$

since $W_s = \frac{H}{T}$ and $H = \frac{W_s \cdot L}{\overline{V}_{P\ actual}}$. The solids pressure drop and the solids hold-up, H, are measured over the distance $L = (S_2-S_1)$.

If the system parameters A_c, L and the particle size, d, are fixed, the independent variables of the model are W_s, the solids feed rate, and $\overline{V_G}$, the average gas velocity. Therefore by measurement and control of W_s and $\overline{V_G}$, and simultaneous measurement of ΔP_{solids} and $\overline{V_P}_{actual}$, the validity of equation (2.50) can be checked, provided that a satisfactory estimate of the function G in equations (2.48) and (2.49) can be made.

2.4.1 The measurement of the average actual particle velocity ($\overline{V_P}$ actual) over a riser length L

The common method used for measuring the average actual particle velocity in a section of a riser is to trap and weigh the solids weight (H), in that particular section of the riser [CRAMP and PRIESTLEY (55), LEWIS et al (56), HARIU and MOLSTAD (57), and MEHTA et al (64)]. Then $\overline{V_P}$ is calculated from the equation:

$$\overline{V_P}_{\text{actual}} = \frac{W_s \cdot L}{H}$$

The accuracy of this method depends on the control of the solids feed rate (W_s), and on the precision of the measurement of the solids feed rate and the solids hold-up, H. Precise measurements of individual particle velocities have been made with photographic techniques [HELLINCKX (67)], and with radio-active tracer studies [GAUVIN et al (68)]. However, equation (2.50) relates the actual average particle velocity and the pressure drop between two points in a riser, S_1 and S_2. Therefore the trapping method should be a satisfactory technique for the measurement of the average particle velocity, provided that precautions are taken with the control of the solids feed rate and the synchronization of the trapping system.

2.4.2 Control of the solids feed rate

Preliminary investigations were made with horizontal screw, rotary air lock, and piston feeders. The rotary air lock feeder was rejected because of its intermittent discharge and likewise the screw feeder on account of its tendency to crush the solids (glass spheres) passing from the feed hopper into the screw mechanism. A vertical piston feeder, similar to that used by SOO (69), was chosen for the work.

2.4.3 Control of the gas velocity

The only gas used in these experiments was air. Since a source of air at 100 p.s.i.g. was readily available, the air velocity control system consisted of a pressure control valve followed by a surge tank and a throttle valve system. The flow rate was measured with a variable area flowmeter (Flowrator).

2.4.4 Measurement of the pressure drop

Because of the 'batch' nature of the piston feeder, the solids gas system is only at equilibrium for a finite time, hence the response of the pressure measuring device must be sufficiently rapid to measure the pressure drop at these equilibrium conditions. An electronic transducer would be ideal for the purpose, but, unfortunately, one was not available at the commencement of the project. An inclined tube manometer was tested and found to be satisfactory.

2.5 Description of the Apparatus

Diagrammatic sketches of the gas flow control system and the vertical transport apparatus are shown in FIGURES 2.10 and 2.11 respectively; photographs of the transport apparatus appear in FIGURES 2.12(a) and 2.12(b).

2.5.1 The gas flow control system

Air Supply

The air was supplied from a reciprocating compressor rated at 45 c.f.m. at 100 p.s.i.g.

Air filter

The air line filter combined a centrifugal separator for removing liquid droplets with a sintered ceramic filter for the removal of solid particles. Liquid (oil and/or water) could be removed either continuously or intermittently through a drain cock.

Pressure control valve and surge tank

The pressure control valve was a ¾" 'Dewrance' patent bronze reducing valve with relay control, which stabilized the delivery pressure with varying flow rates. The surge tank pressure was maintained in the vicinity of 60 p.s.i.g.

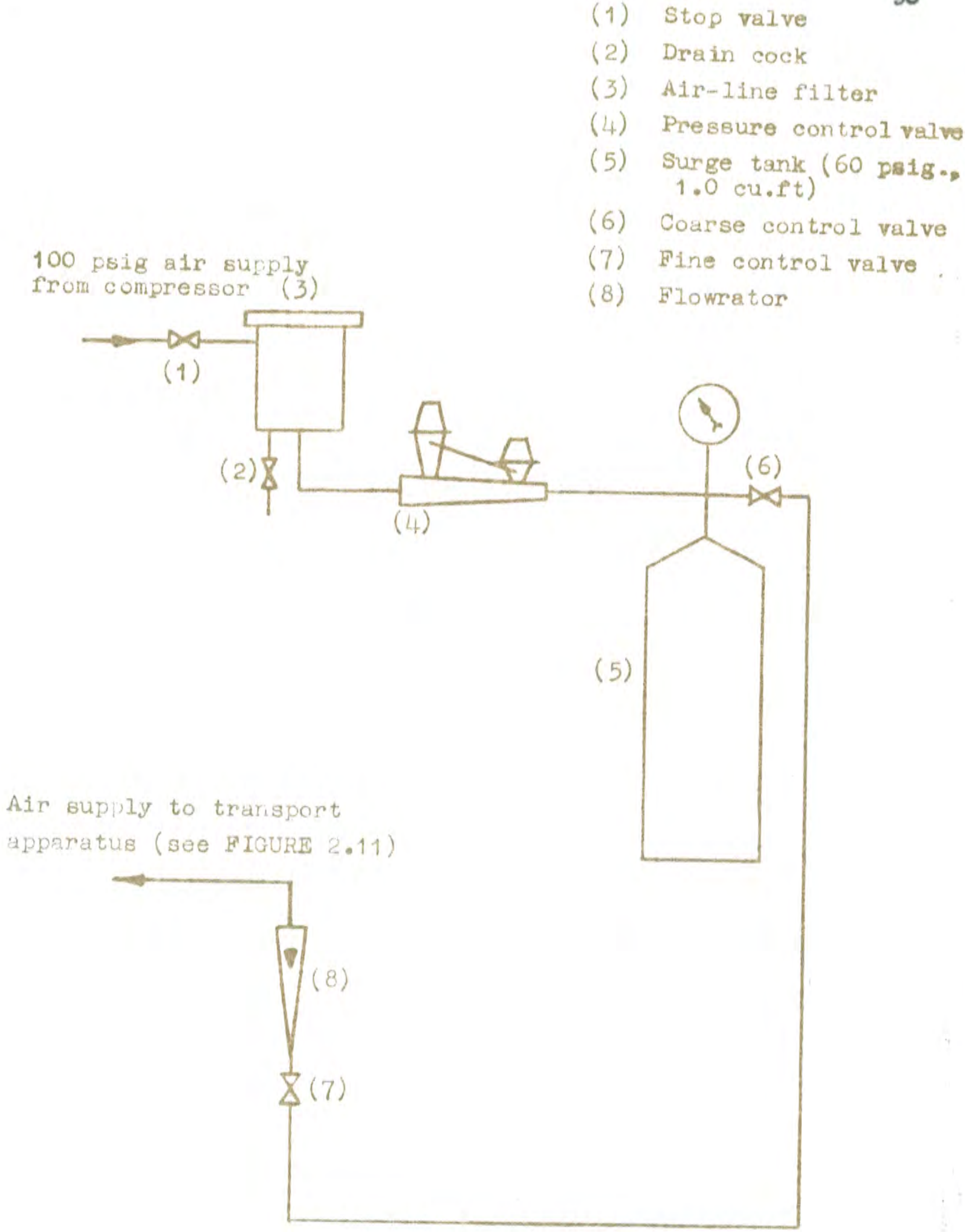

FIGURE 2.10 Gas flow control system for transport apparatus

Legend for FIGURE 2.11

(1) Riser (bore = 0.994 in)

(2) Flow straightener (inside riser)

(3) Special plug valves for trapping solids - vertical distance between valve centres 6.25 ft

(4) Plug valve operating lever

(5) Solids piston feeder

(6) 60# stainless steel gauge cylinder

(7) Solids receiver

(8) Variable speed electric motor for feeder drive

(9) Tacho-generator for motor speed measurement

(10) Motor speed controller

(11) Inclined tube manometer (vertical distance between pressure taps 6.0 ft)

(12) Auxiliary solids collection cyclone

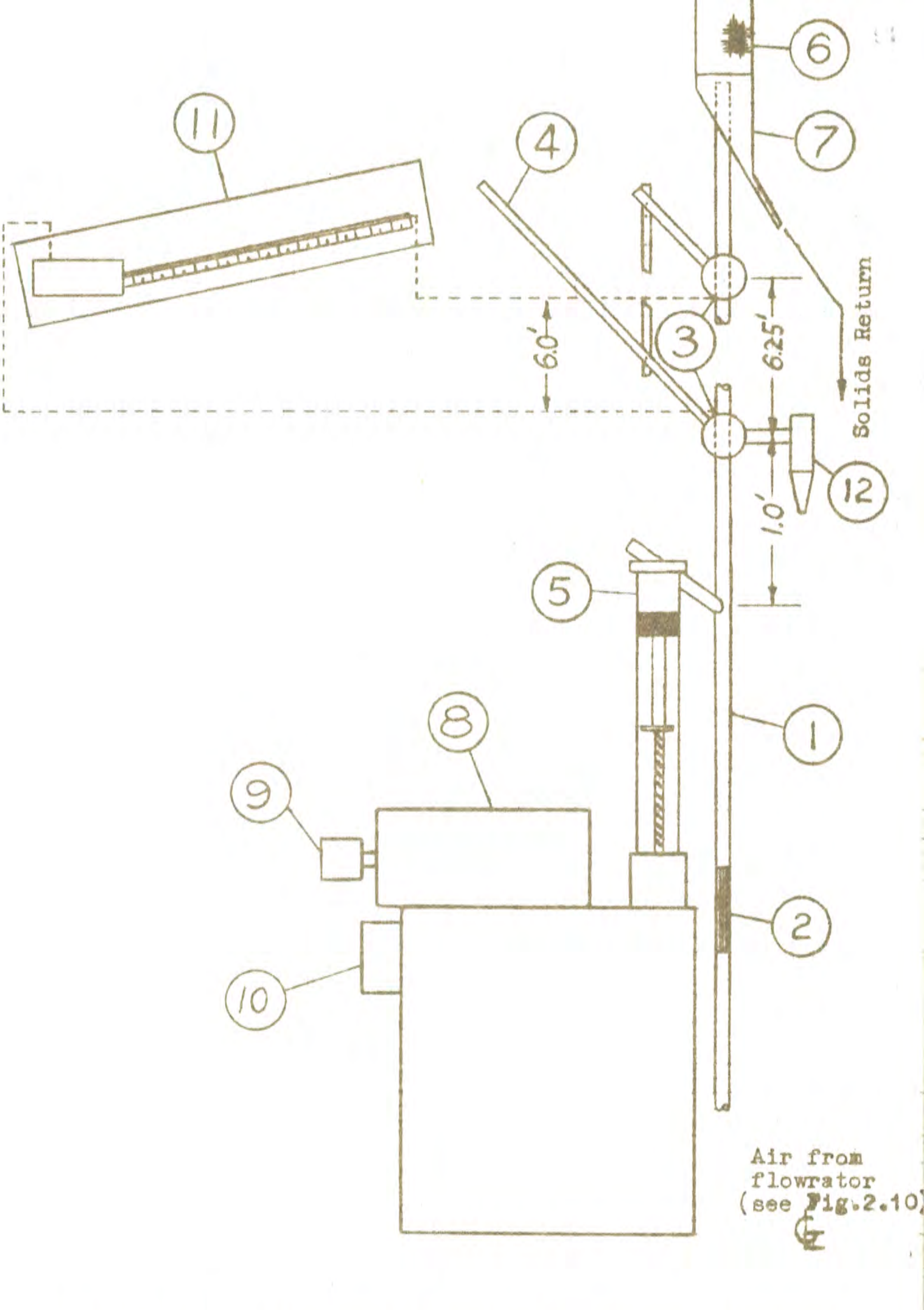

FIGURE 2.11 Diagrammatic sketch of vertical transport apparatus

Flow regulation and measurement

The surge tank acted as a constant pressure reservoir; coarse flow regulation was obtained with the first valve and fine flow control with the second valve. The flow was metered with a $\frac{3}{4}$ in Fischer and Porter series 10 A 2700 Flowrator (max. flow rate 21 c.f.m. at 14.7 p.s.i.a.). The Flowrator was calibrated with a positive displacement meter.

2.5.2 The vertical transport apparatus

The riser tube

The riser was fabricated in three sections from $1\frac{1}{8}$ in o.d. 16 gauge cold drawn copper tube (mean measured bore 0.997 in.), and the sections were joined at the trapping valves with screw threads. The riser was supported at each trapping valve and at the bottom by a 3 in. x $1\frac{1}{2}$ in. x 11 ft. aluminium channel; the lower section of the channel was stiffened with a 8 ft. length of 3 in. x $1\frac{1}{2}$ in. 'Dexion 300' angle. The solids feed point on the riser was 1.0 ft. below the bottom trapping valve, and the distance between the valve centres was 6.25 ft.

The bottom section of the riser contained a flow straightener consisting of a nest of $\frac{1}{4}$ in. o.d. x 8.0 in. copper tubes. The top of the tube nest was covered with a $60^{\#}$ stainless steel gauze, which prevented any particles from falling back and blocking the straightener, and also tended to homogenize the turbulence.

Gas solids separation

At the top of the riser the entrained solids must be separated from the gas stream and recovered. In these experiments, particular care was taken to ensure

FIGURE 2.12 (a) Photograph of the lower section of the transport apparatus

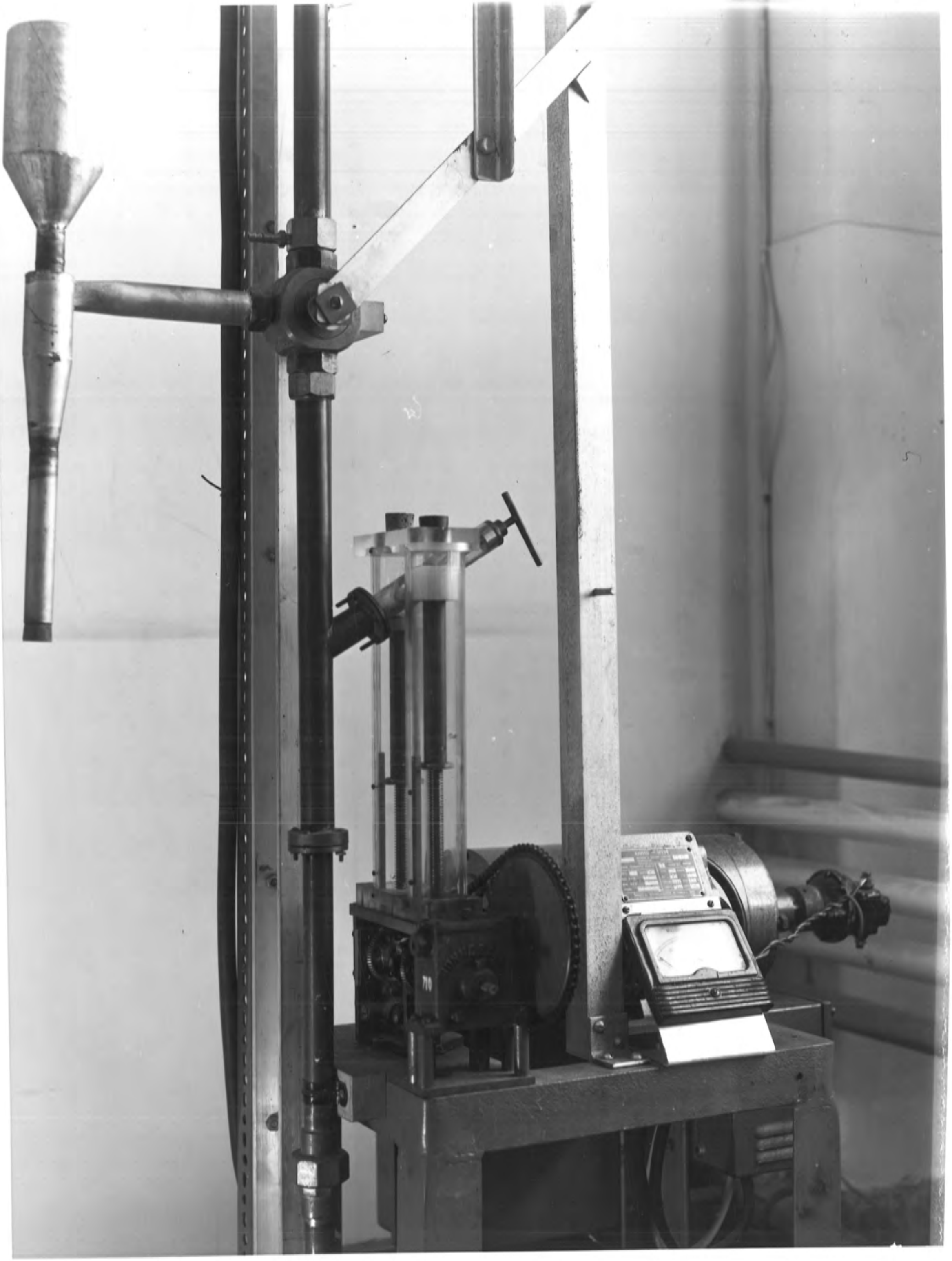

FIGURE 2.12 (b) Photograph of the upper section of the transport apparatus

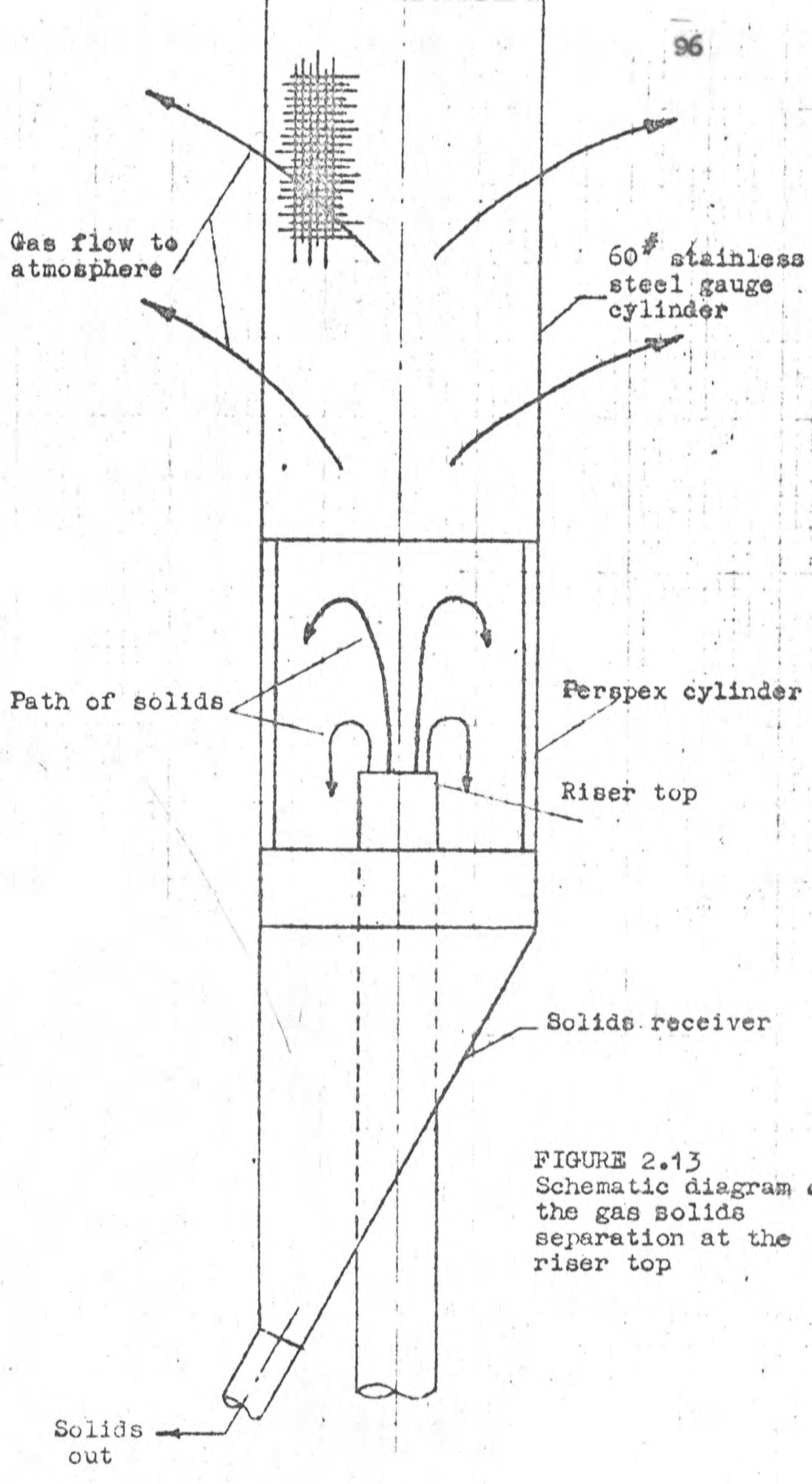

FIGURE 2.13
Schematic diagram of the gas solids separation at the riser top

that the solids separation unit produced no effects which might influence the accuracy of the measurement of the solids hold-up. Therefore, rather than use a conventional cyclone, it was decided to dis-entrain the solids by letting the air at the riser top expand in a 'free jet'. This arrangement is shown diagrammatically in FIGURE 2.13, and in the photograph, FIGURE 2.12(b). The gauze cylinder permits the air to flow out at a low average velocity and the 'dis-entrained' solids fall into the collection hopper and return to ground level by gravity flow. This technique might not be suitable if the gas velocity exceeded the solids terminal velocity by a large margin; in this case, the particles may adhere to the gauze.

The trapping valves

Both trapping valves were of the plug type especially fabricated in the departmental workshop with 1.0 in. diam. cylindrical bores so that with the valves in the open position the bore of the riser was essentially constant over its entire length. The two valves were operated simultaneously by the linked lever system shown in FIGURE 2.11. The top valve acted as a simple "on-off" valve, but the bottom valve, developed by GOMEZ (70), performed two functions. When the valve was closed the solids coming up the riser were deflected into the auxiliary solids collection cyclone (see FIGURE 2.11) while the trapped solids fell onto the bottom valve from whence they were diverted into a small envelope clipped to the valve body. The 'trapped' solids could then be removed and weighed. A photograph of the valve components is shown in FIGURE 2.14.

The solids feeder

The location of the solids feeder is shown in FIGURE 2.11 and in a photograph, FIGURE 2.12(a). FIGURE 2.15 is a more detailed sketch of the feeder. The tandem feeder was originally designed so that the apparatus could be used to study the distribution of solids residence times in the riser, by making a step change in the feed material, e.g. tagged to un-tagged particles; however, these experiments were not completed in the course of the work under review. To enable the operator to observe the feeding process the feeder cylinder walls were fabricated from clear perspex; the pistons were fabricated from nylon. The pistons were driven by coarse pitch double thread screws coupled to the drive by a bevel gear and dog clutch mechanism. The dog clutch could be engaged

FIGURE 2.14 Photograph of bottom trapping valve assembly

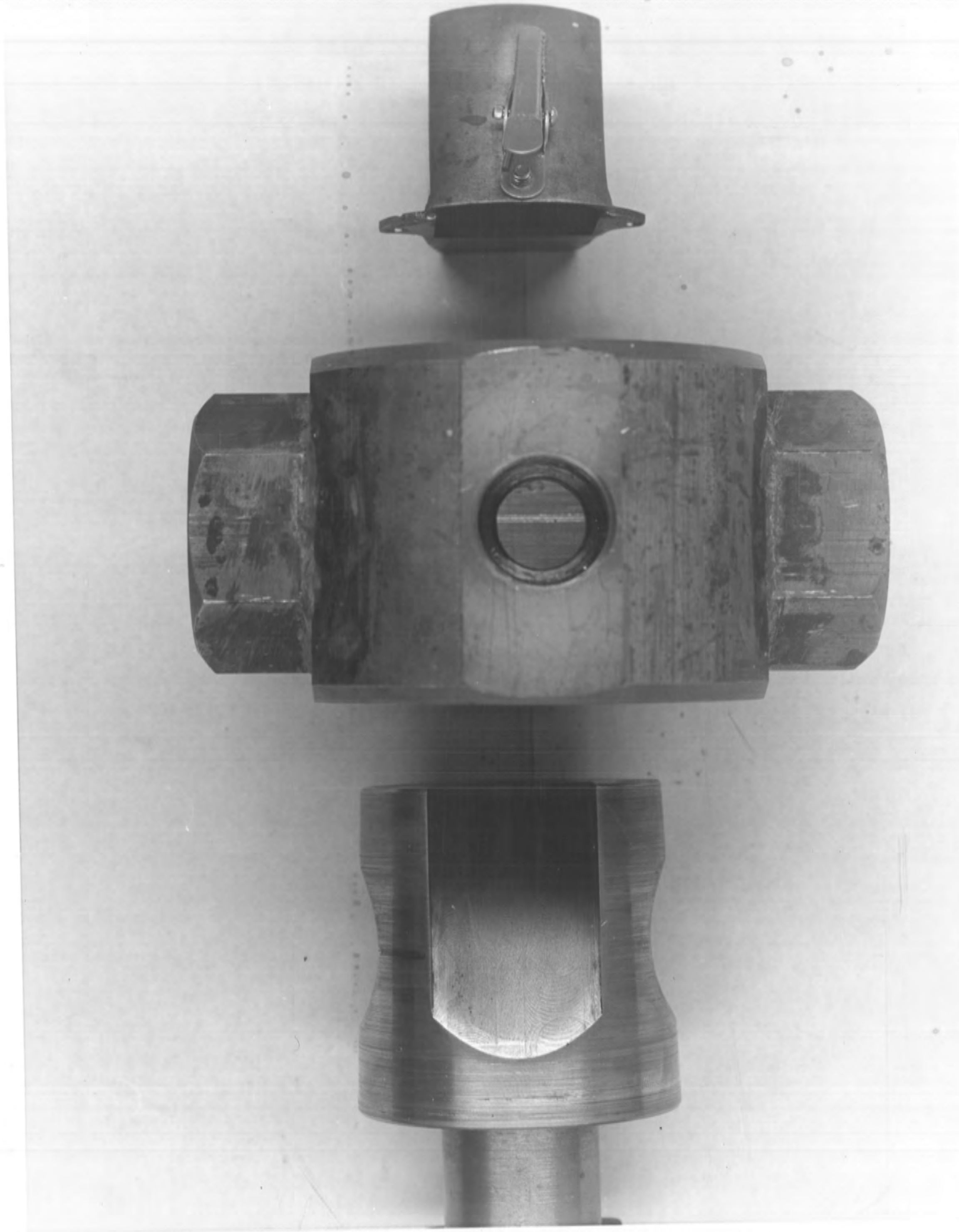

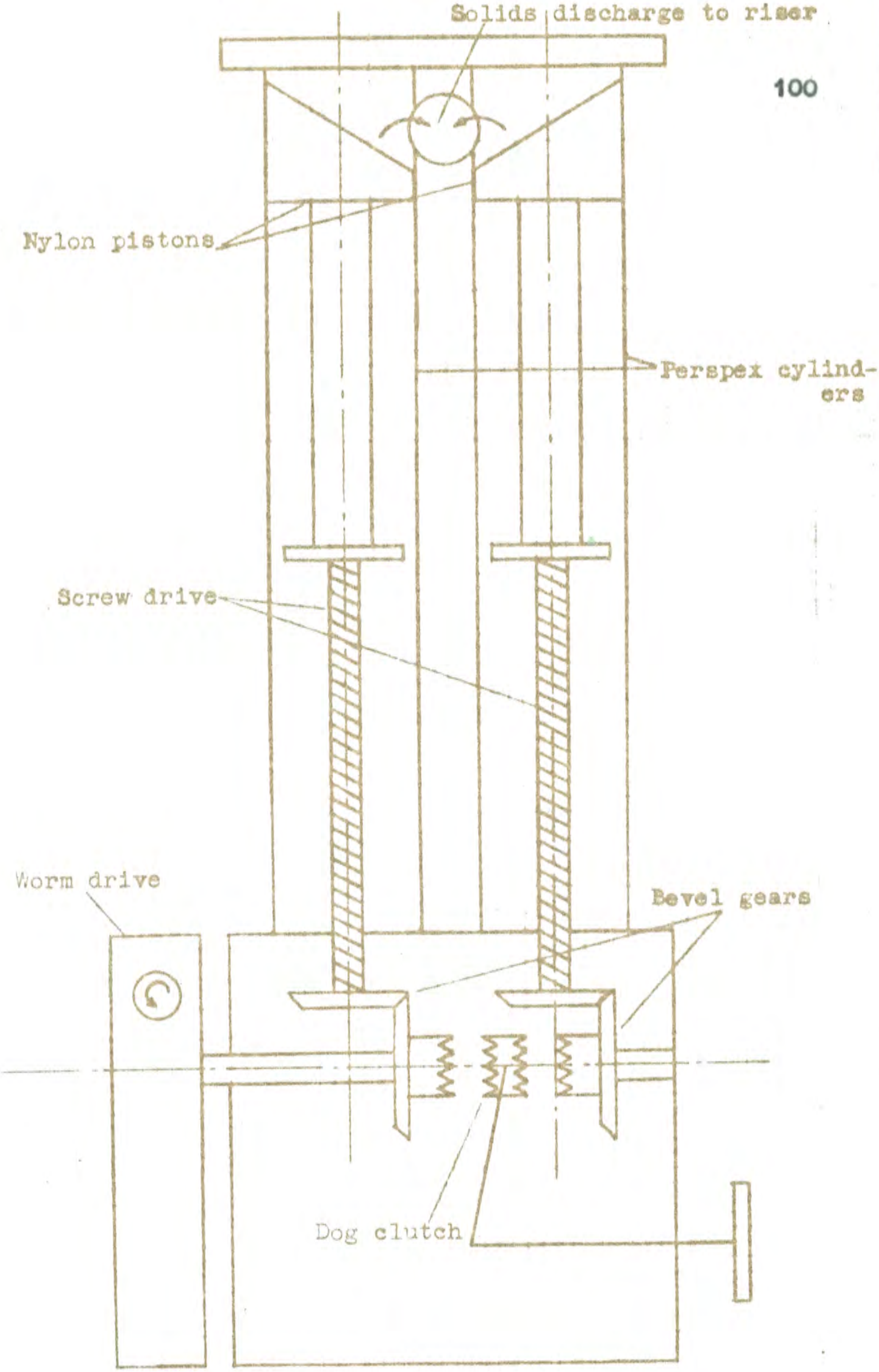

FIGURE 2.15 Schematic diagram of the piston feeder

to drive either piston (not both simultaneously) and could also be moved to a neutral position.

The unit was driven by a worm speed reduction drive and coupled to a ½ h.p. Heenan and Froude variable speed motor via a chain and sprocket drive. The motor speed was monitored with a direct coupled tacho-generator and the motor could be reversed.

Since the drive mechanism was positively engaged (no slip) and the feeder was a positive displacement device, the feeder could be calibrated in terms of weight per unit time vs. the R.P.M. indicated by the tacho-generator.

The inclined tube manometer

The inclined tube manometer shown in FIGURE 2.11 was connected to pressure taps located on the riser 6.0 ft. apart and between the trapping valves. The manometer consisted of a constant level reservoir and a 2.0 mm. bore capillary tube with a slope of 1:5. The fluid used in the manometer was di-butyl phthalate (S.G. 1.045) dyed with Sudan Red. Di-butyl phthalate was preferred to water because of the tendency of the latter to break up into slugs in the capillary tube after a rapid fall in pressure. The manometer was calibrated against an Oldham null point micromanometer. The unit had an exponential dynamic response with time constant of approximately 8.0 sec., which was satisfactory for the range of solids feed rates used.

2.6 Experimental Conditions and Procedure

2.6.1 Materials and experimental conditions

Materials

The particulate solid materials chosen for the experimental work were:*

(i) 28/32# 'Ballotini' glass spheres,
(ii) 20/24# 'Ballotini' glass spheres,
(iii) 28/32# 'Ballotini' glass spheres,
and (iv) 1.00 mm. diam. stainless steel spheres.

The physical properties of these materials are shown in TABLE 2.7; the transporting fluid used was air.

* Note: #(mesh) numbers indicated are Tyler screen mesh apertures.

Experimental conditions

For each of the three size ranges of glass spheres runs were carried out with four solids feed rates, viz. 1.14, 1.88, 2.56 and 3.25 g/sec., and for the 1.0 mm. diam stainless steel spheres three feed rates were used, viz. 3.15, 5.05 and 6.91 g/sec. For each feed rate the range of gas velocities used was from a value just above the choking point to a value about 10.0 ft/sec. greater than the choking point at intervals of about 0.7 ft/sec. Estimates of the choking velocities were made by calculating the particle terminal velocities from the standard drag relationship. Values of these velocities for the respective particles together with a summary of run numbers and solids feed rates are shown in TABLE 2.8.

TABLE 2.7 Physical properties of the particulate solids used in the pneumatic transport experiments

Material	** Mean diameter (mm)	*Specific gravity
$^{28}/_{32}$# Ballotini	0.640	2.893
$^{20}/_{24}$# Ballotini	0.857	2.898
$^{14}/_{16}$# Ballotini	1.146	2.906
1.0 mm. stainless steel spheres	1.000	7.576

* Determined with S.G. bottle technique

** These values are the means of a large number of optical micrometer measurements

TABLE 2.8 Summary of conditions and run group numbers for the pneumatic transport experiments

Material	Terminal velocity from classical data ft/sec.	Solids feed rate gm/sec / Run group number			
$^{28}/_{32}$# Ballotini	17.3	1.14 (1)	1.88 (2)	2.56 (3)	3.25 (4)
$^{20}/_{24}$# Ballotini	22.2	1.14 (5)	1.88 (6)	2.56 (7)	3.25 (8)
$^{14}/_{16}$# Ballotini	27.7	1.14 (9)	1.88 (10)	2.56 (11)	3.25 (12)
1.00 mm. stainless steel spheres	43.5	3.15 (13)	5.05 (14)	6.91 (15)	

2.6.2 Experimental procedure

To complete a run the gas velocity was first set to the selected value and the gas pressure drop recorded. A sample of the particulate solid was charged to the piston feeder, with the piston in its lower position, and the feeder drive speed was set to its selected value. Then the feeder dog clutch was engaged and the feeding process commenced. When the total gas and solids pressure drop reached its equilibrium value this value was recorded, the trapping valve mechanism was actuated, and the feeder switched off. The solids contained in the envelope attached to the bottom trapping valve (the solids hold-up) were then removed and their weight recorded.

To prepare the apparatus for the next run the trapping valves were reset, the auxiliary cyclone cleared of solids, and the piston feeder was re-wound to the lower position with the feeder drive in reverse.

2.7 Experimental Results

The data obtained from the experimental work were measurements of the pressure drop with gas only, the pressure drop with gas plus solids, and the solids hold-up for a series of gas and solid flow rates. These data are presented in detail in APPENDIX 2.1. The calculations made in the analysis of these results are described in APPENDIX 2.2.

2.7.1 The variation of the actual average solids velocity with the average gas velocity and the solids feed rate

These data are presented graphically in FIGURES 2.16 to 2.19 for the three sizes of glass spheres and the 1.0 mm. steel spheres respectively. The actual average solids velocity is plotted vs. the average gas velocity with the solids feed rate as a parameter. The actual average solids velocity is calculated from the equation:

$$\overline{V_P} = \frac{W_s \cdot L}{H} \qquad \text{..... (2.20)}$$

Run group		Solids feed rate g/sec
1	⊡	1.14
2	⊙	1.88
3	×	2.56
4	▽	3.25

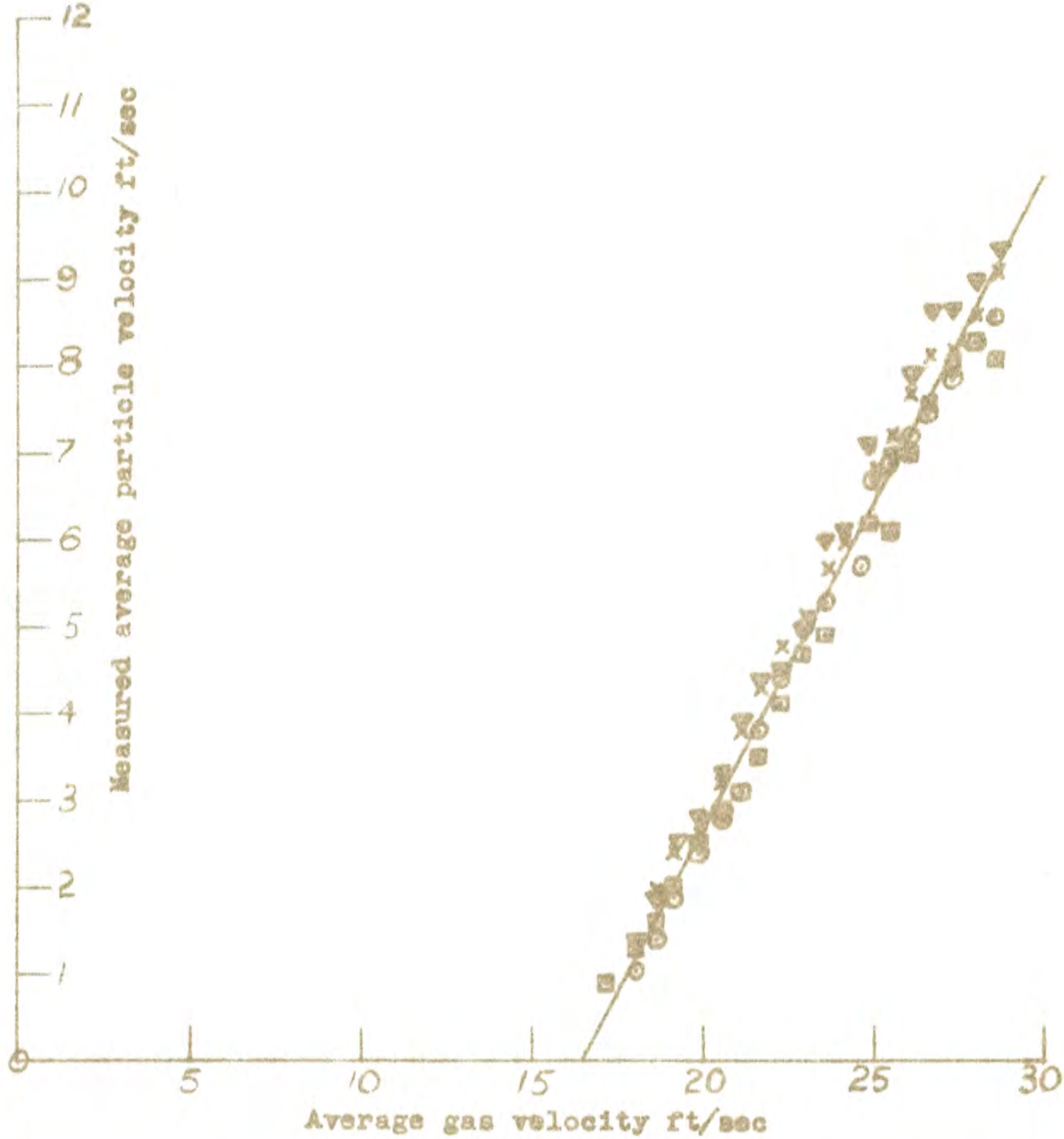

FIGURE 2.16 Graph showing the variation of actual average solids velocity with average gas velocity for $\frac{28}{32}$# glass spheres

Run group		Solids feed rate g/sec
5	⊡	1.14
6	⊙	1.88
7	×	2.56
8	▽	3.25

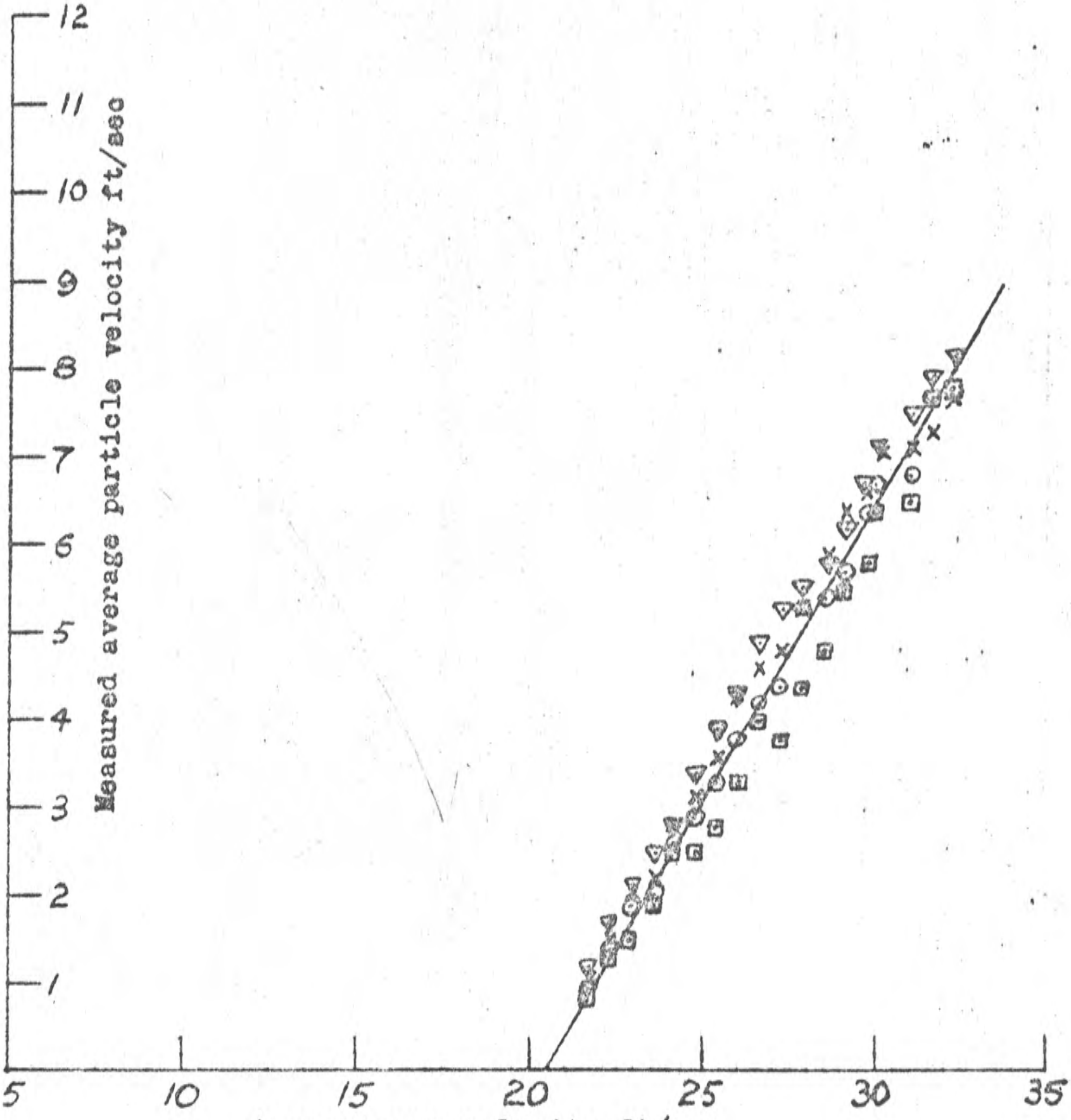

FIGURE 2.17 Graph showing the variation of the actual average solids velocity with average gas velocity for $\frac{20}{24}$ # glass spheres

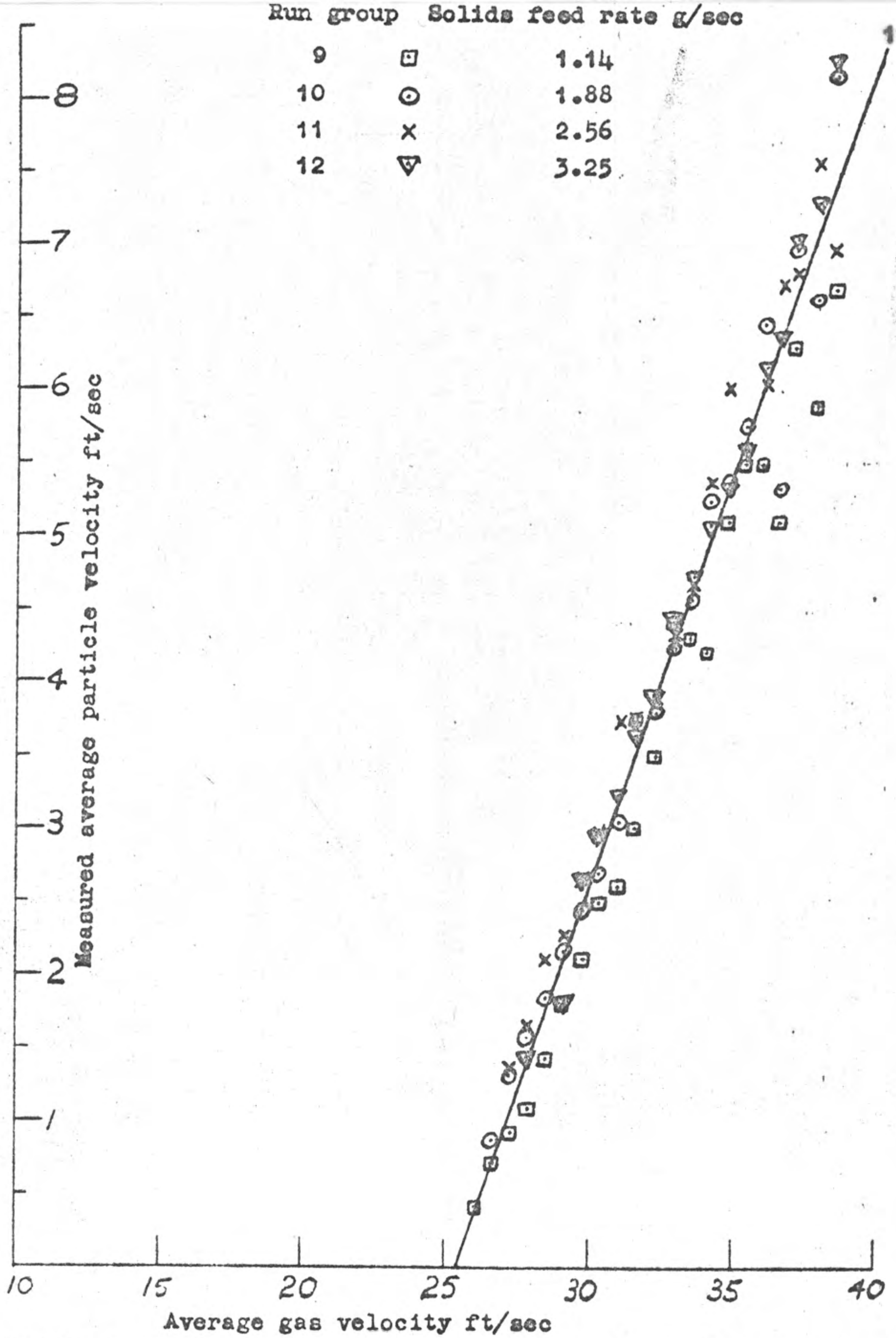

FIGURE 2.18 Graph showing the variation of actual average solids velocity with average gas velocity for $\frac{14}{16}$# glass spheres

Run group		Solids feed rate g/sec
13	⊡	3.15
14	⊙	5.05
15	×	6.91

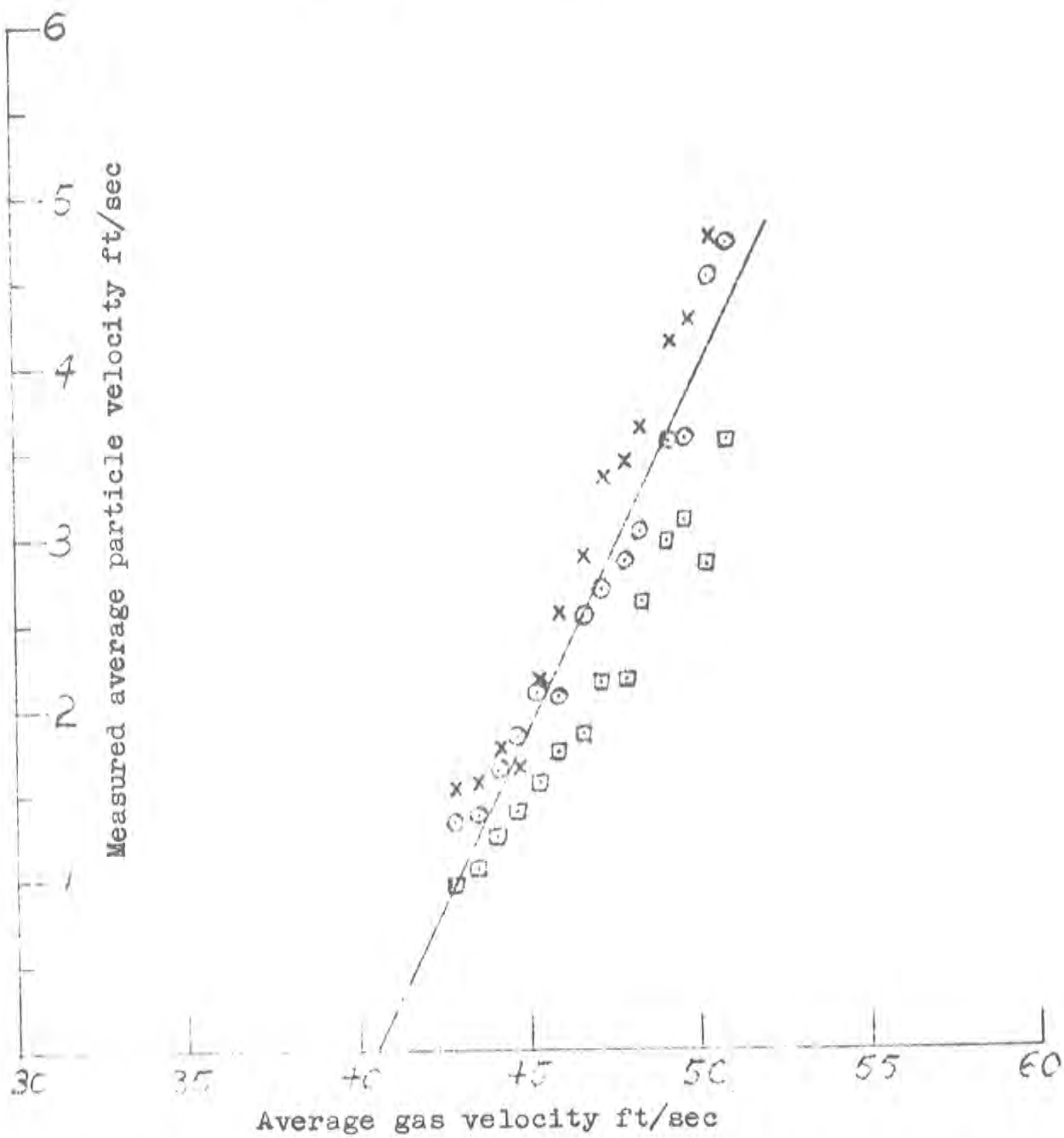

FIGURE 2.19 Graph showing the variation of actual average solids velocity with average gas velocity for 1.0 mm steel spheres

2.7.2 The variation of the pressure drop with the average gas velocity and the solids feed rate

As with the average particle velocity data described in the preceding section the pressure drop data are presented graphically. The data for the three sizes of glass spheres and the 1.0 mm. steel spheres are plotted in FIGURES 2.20 to 2.23 respectively. The total pressure drop is plotted vs. the average gas velocity, again with the solids feed rate as a parameter. In addition FIGURE 2.24 shows a typical plot of the variation of the static, acceleration, and solids/wall friction components of the theoretical solids pressure drop with the average gas velocity. These data are for Run Group 10 ($^{14}/_{16}$ # glass spheres, feed rate 1.88 g/sec) and are taken from the complete set contained in APPENDIX 2.2.

FIGURES 2.26 to 2.29 are plots of the reciprocal solids pressure drop, i.e. $^{1}/_{\Delta p_s}$, vs. the average gas velocity. These reciprocal pressure drop data are contained in APPENDIX 2.2. The aim of this analysis is to test whether the value of the gas velocity at which the actual average solids velocity is zero (ref. FIGURES 2.16 to 2.19 for the intercept on the average gas velocity axis) could be estimated from the pressure drop data. The intercept in FIGURES 2.16 to 2.19 is the estimate used for the terminal velocity to calculate the theoretical particle trajectories.

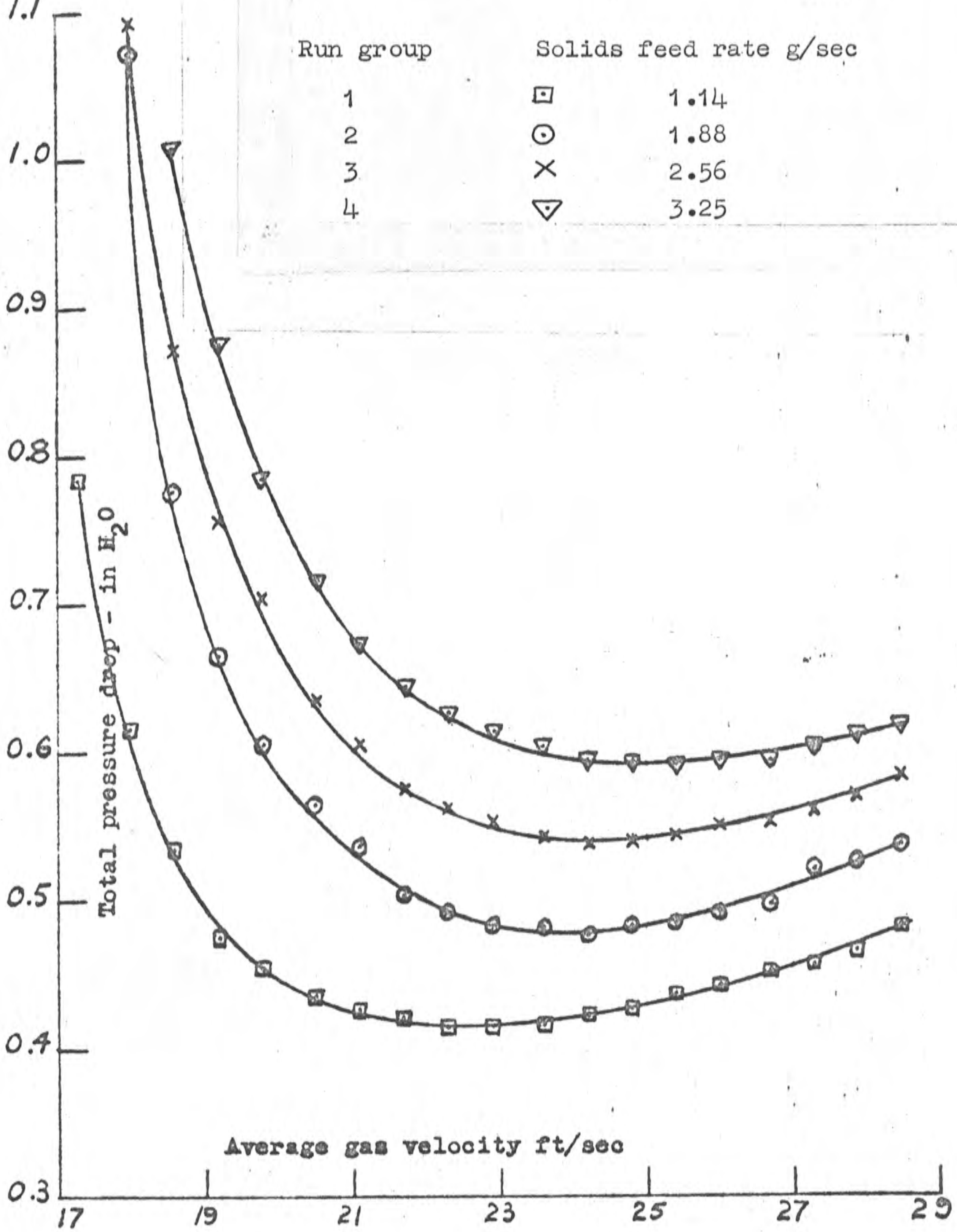

FIGURE 2.20 Graph showing the variation of total pressure drop with average gas velocity for $\frac{28}{32}$ # glass spheres

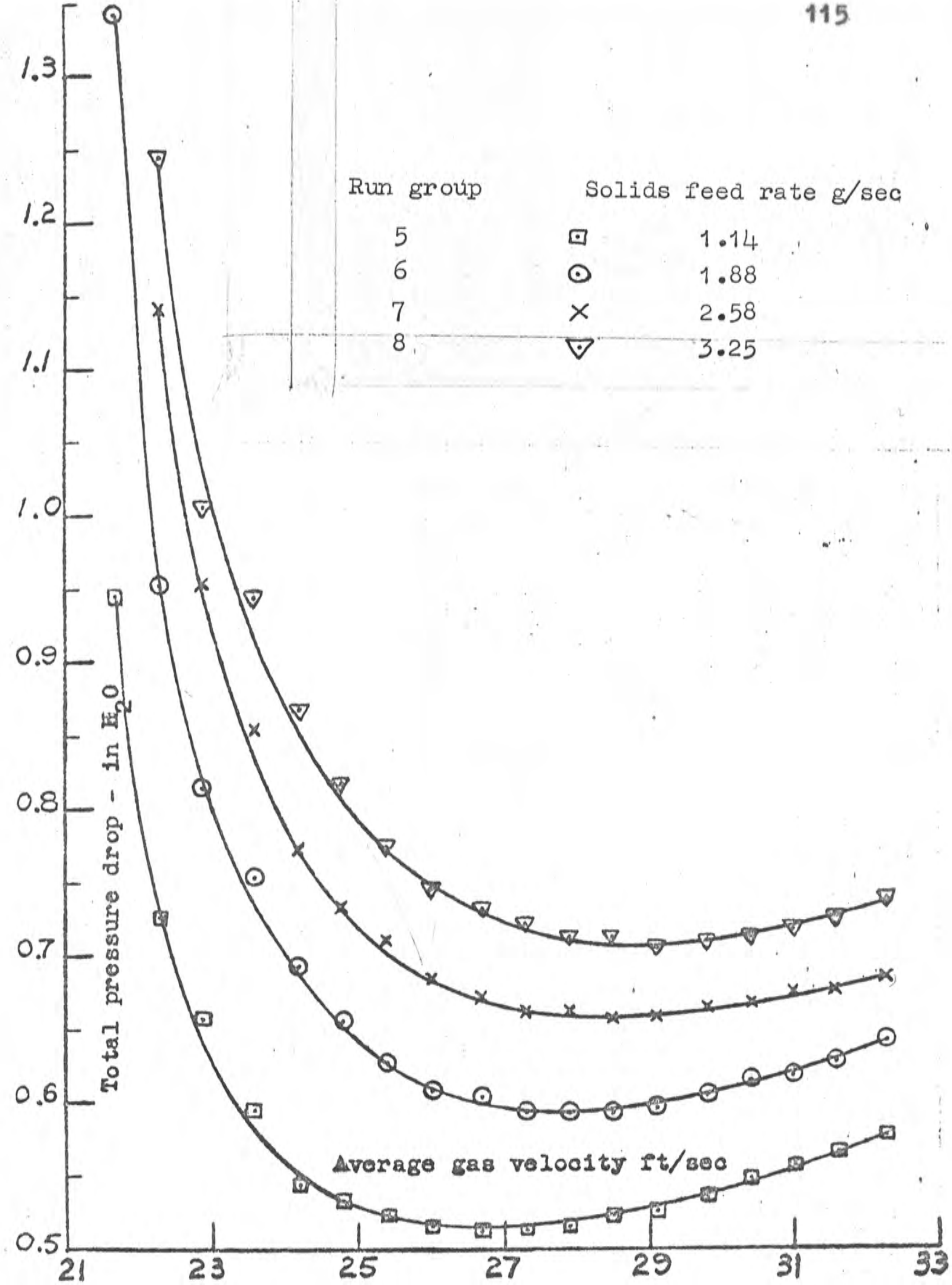

FIGURE 2.21 Graph showing the variation of total pressure drop with average gas velocity for $\frac{20}{24}$ # glass spheres

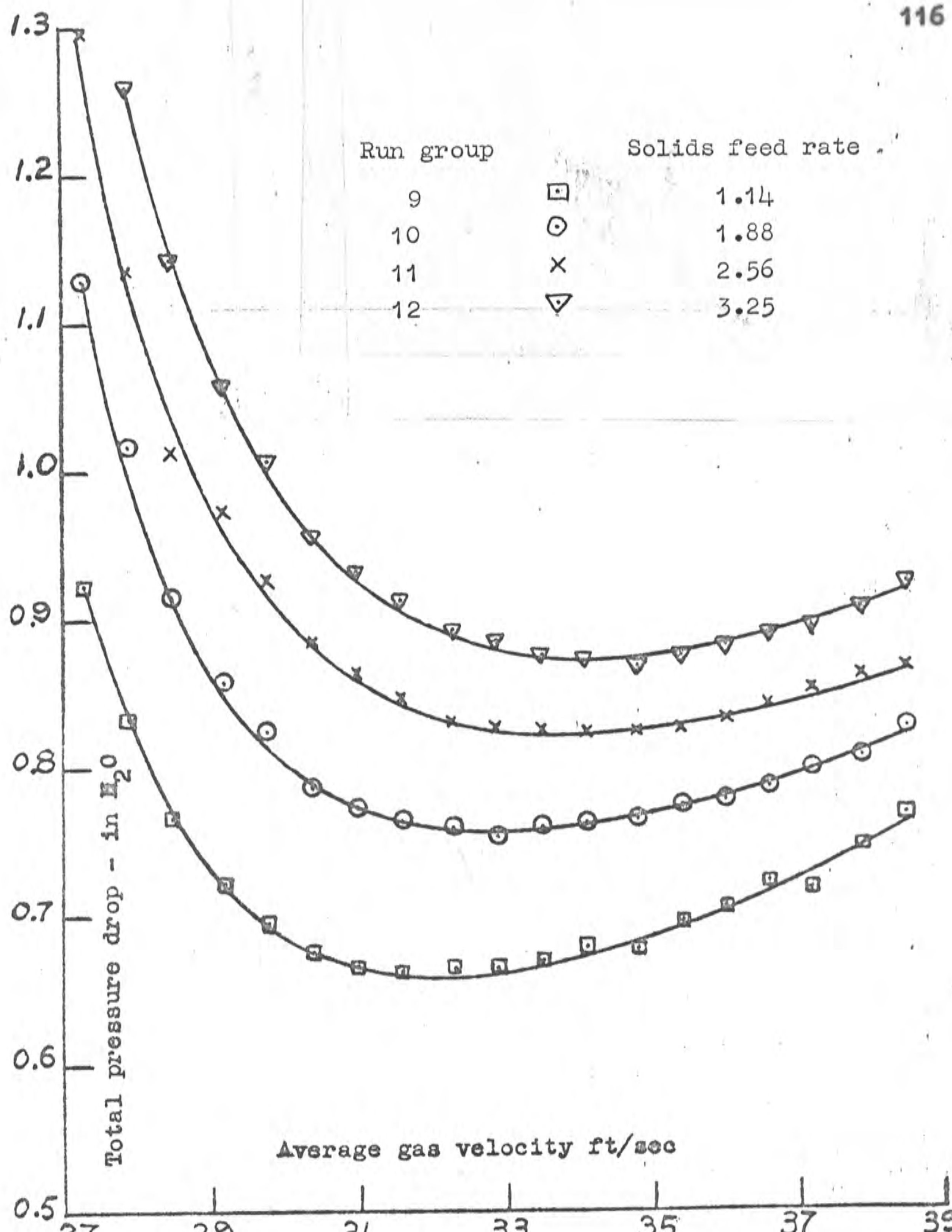

FIGURE 2.22 Graph showing the variation of total pressure drop with average gas velocity for $\frac{14}{16}$ # glass spheres

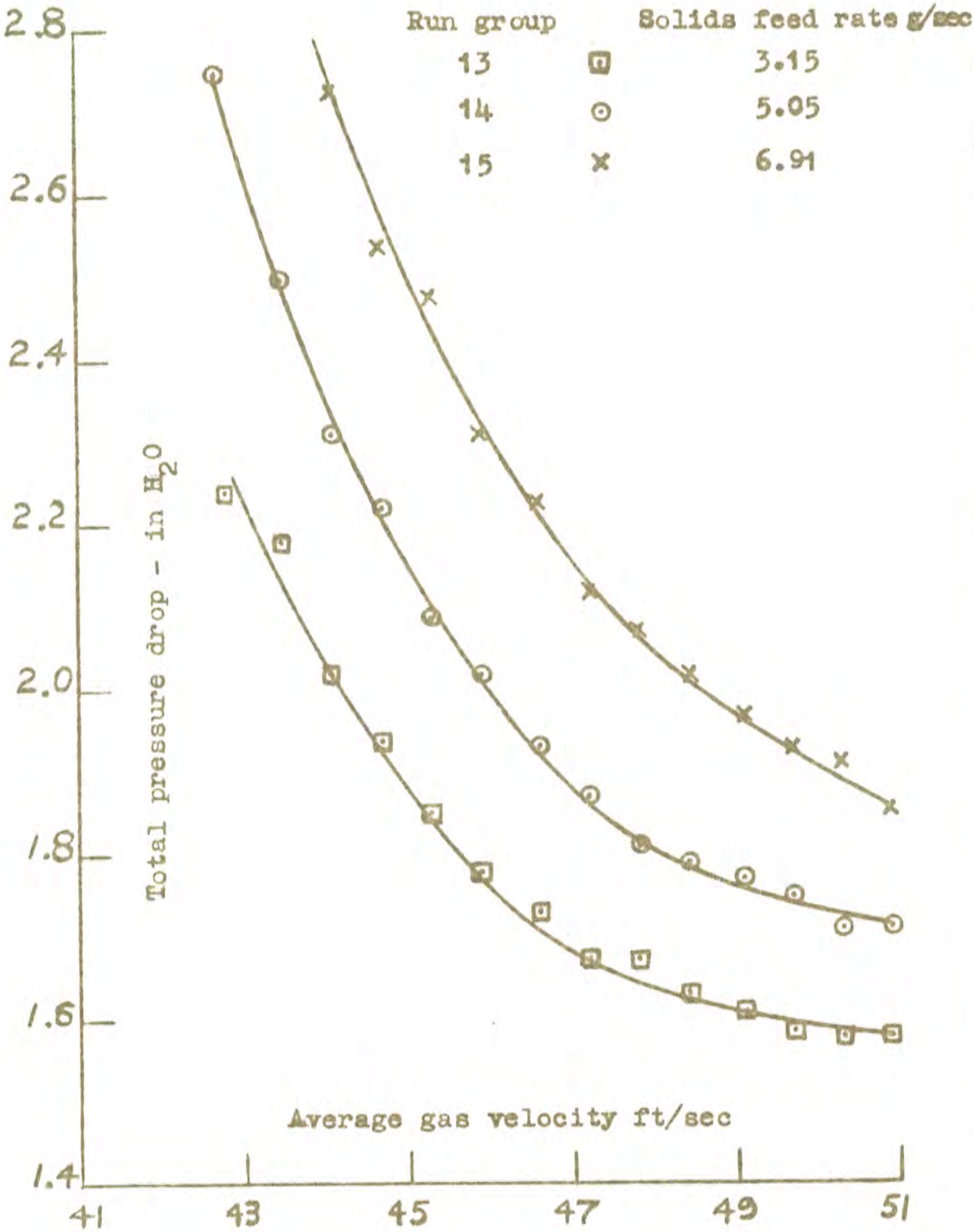

FIGURE 2.23 Graph showing the variation of total pressure drop with average gas velocity for 1.0 mm steel spheres

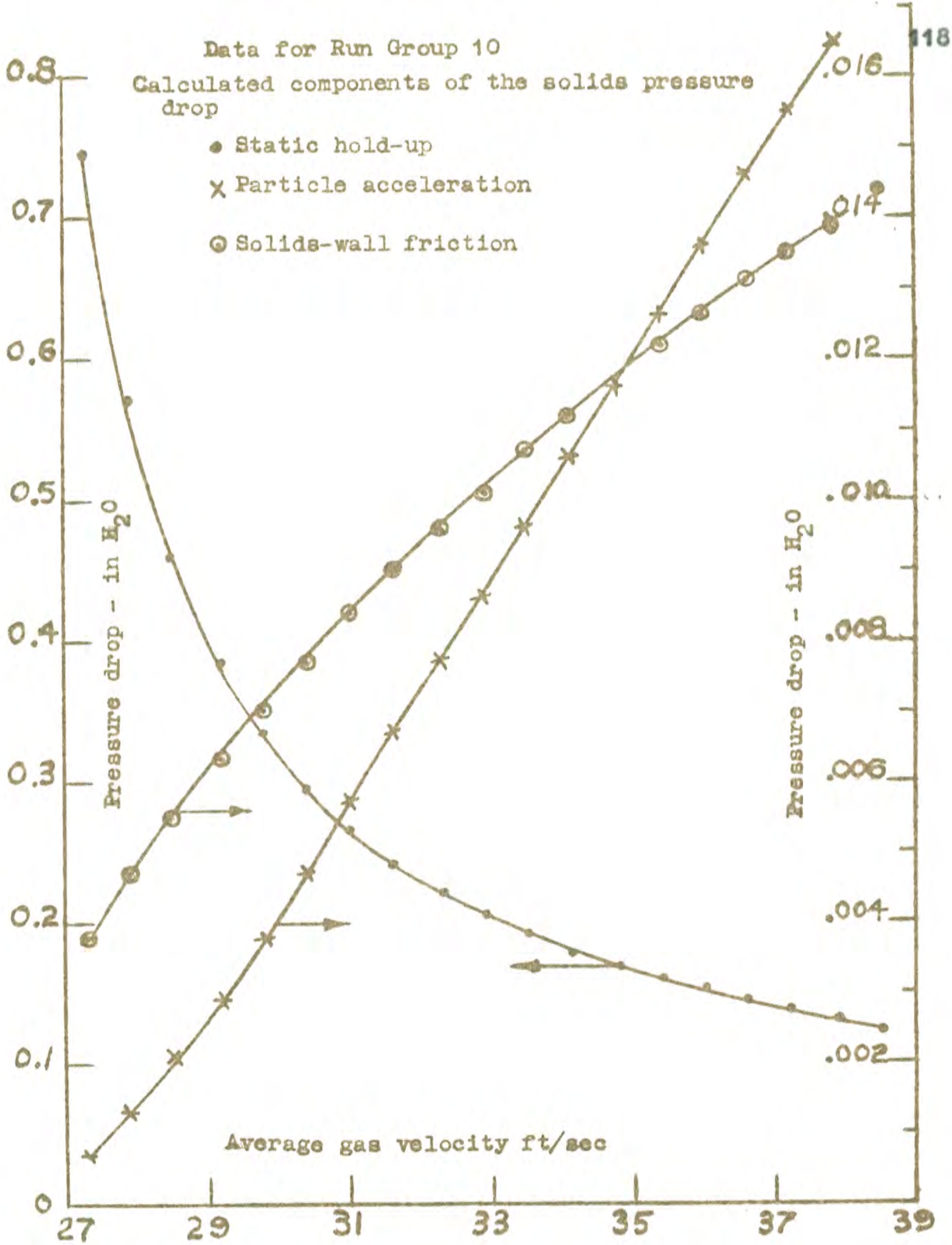

FIGURE 2.24 Graph showing a typical plot of the variation of the static, acceleration, and friction components of the solids pressure drop with the average gas velocity

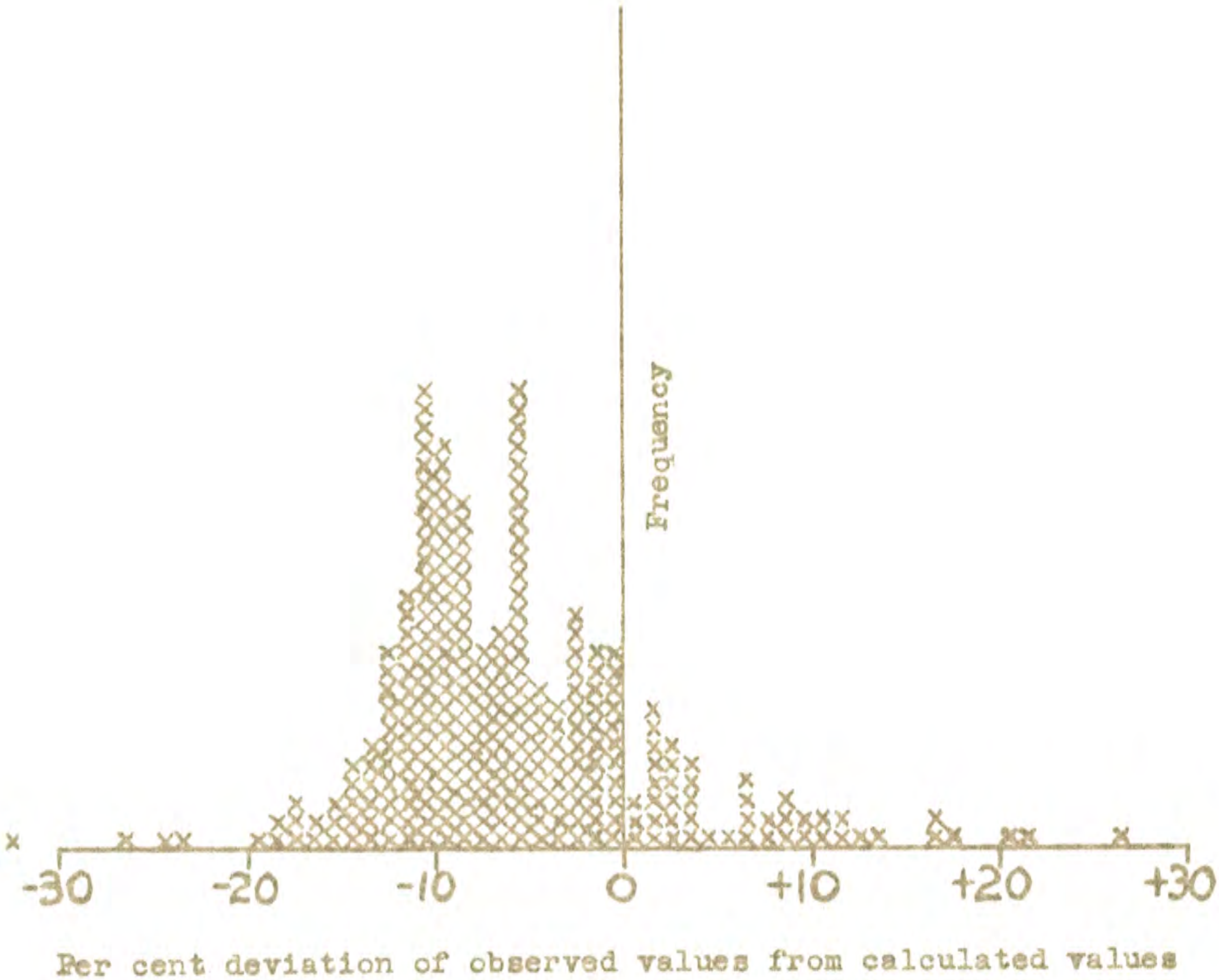

FIGURE 2.25 Histogram showing the deviation of the theoretical solids pressure drop from the observed solids pressure drop

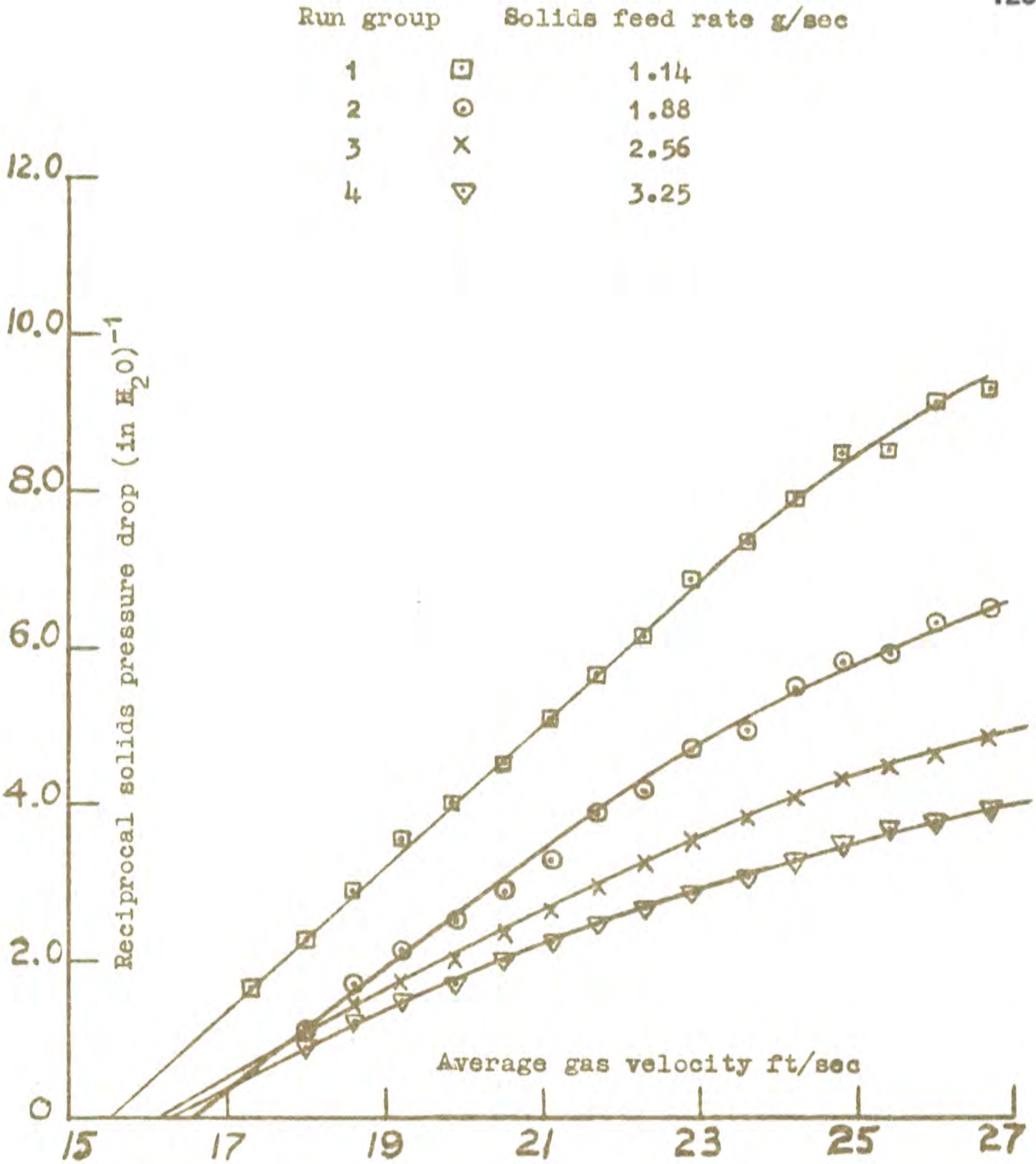

FIGURE 2.26 Plot of the reciprocal solids pressure drop vs. the average gas velocity for $\frac{28}{32}$ # glass spheres

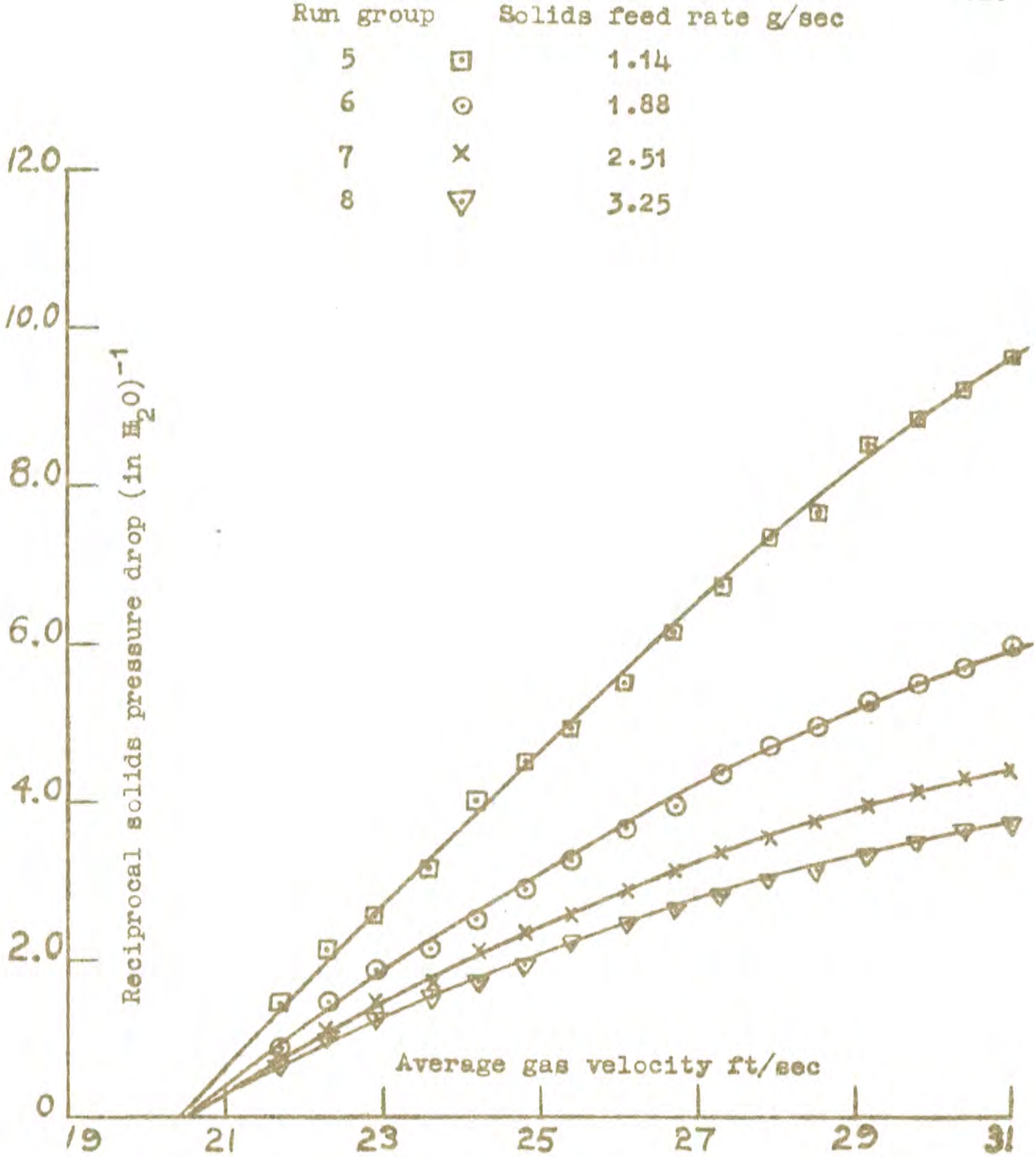

FIGURE 2.27 Plot of the reciprocal solids pressure drop vs. the average gas velocity for $\frac{20}{24}$ # glass spheres

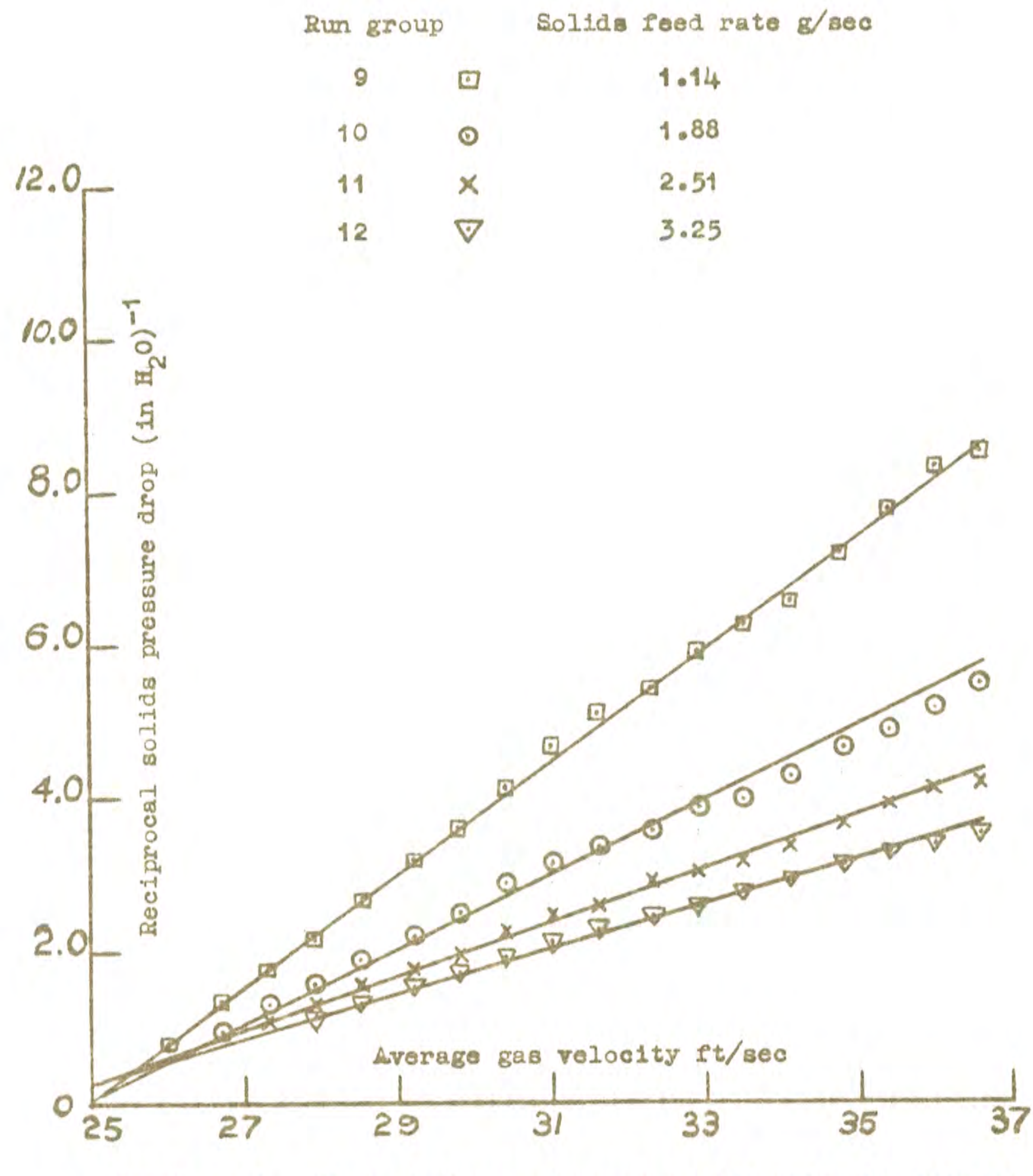

FIGURE 2.28 Plot of the reciprocal solids pressure drop vs. the average gas velocity for $\frac{14}{16}$ # glass spheres

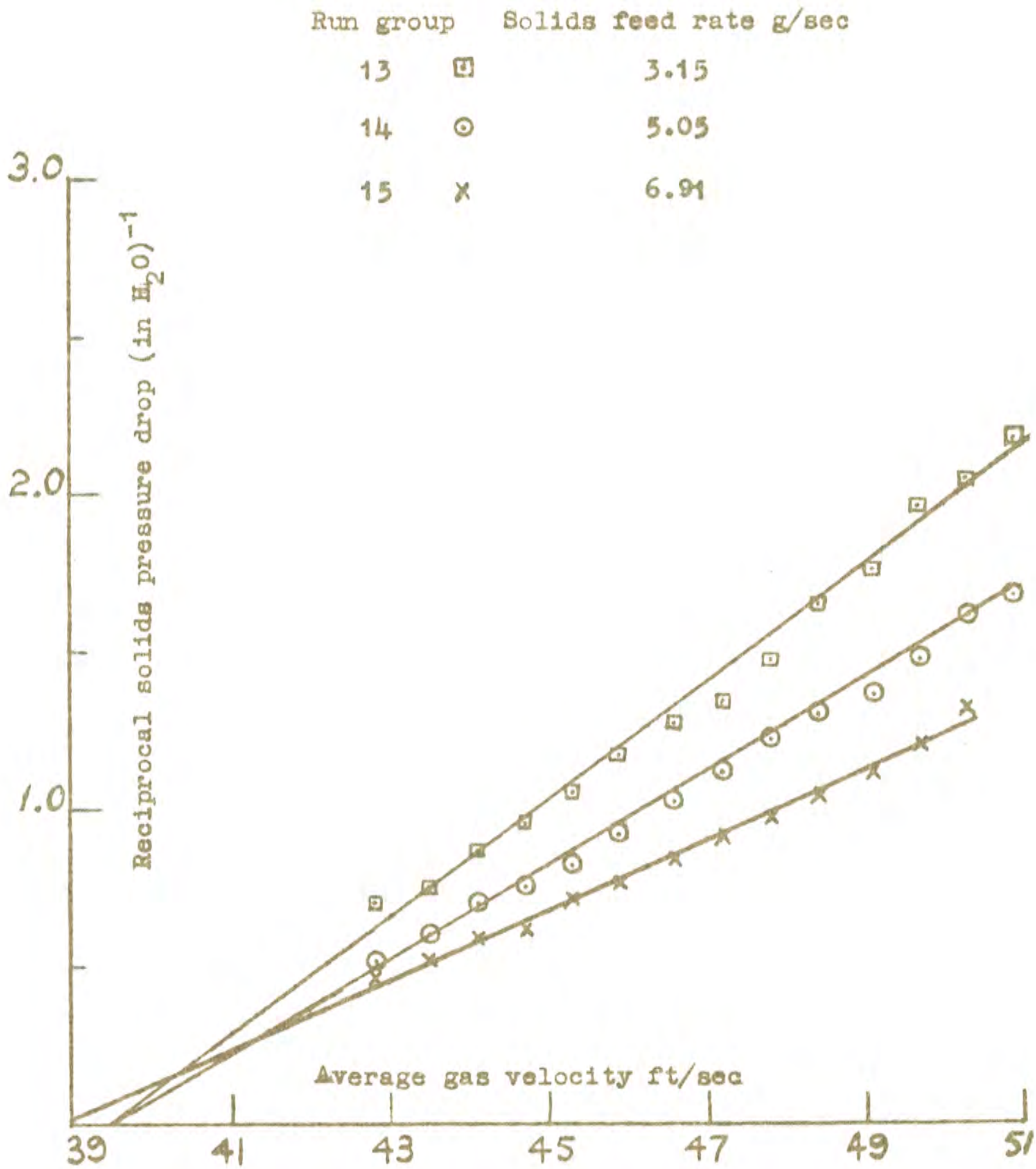

FIGURE 2.29 Plot of the reciprocal solids pressure drop vs. the average gas velocity for 1.0 mm steel spheres

2.7.3 The relationship between the actual average solids velocity and the theoretical average solids velocity

Preliminary investigations indicated that a linear correlation existed between the logarithm of the actual average solids velocity and the theoretical average solids velocity for the same section of the riser. This implies a functional relationship of the form:

$$\log_e (\overline{V_P})_{actual} = \log_e (a) + n \log_e (\overline{V_P})_{theoretical}$$

or

$$(\overline{V_P})_{actual} = (a) (\overline{V_P})^n_{theoretical}$$

The calculation of these regressions is described in APPENDIX 2.2. The values of a, n, and the correlation coefficient of the logarithmic regression are summarized in TABLE 2.9.

TABLE 2.9 Summary of the logarithmic regression results for the relationship between the actual and the theoretical average particle velocities

Run Group No.	$\log_e(a)$	(a)	n (exponent)	r (correlation coefficient)
1	-.8793	.415	1.299	.9717
2	-.6955	.499	1.250	.9861
3	-.5304	.588	1.164	.9976
4	-.5176	.596	1.177	.9949
5	-.5553	.574	1.126	.9884
6	-.6716	.511	1.195	.9926
7	-.7620	.467	1.230	.9948
8	-.6611	.517	1.194	.9974
9	-1.0313	.357	1.275	.9912
10	-.5997	.549	1.099	.9917
11	-.7796	.459	1.187	.9956
12	-.7883	.455	1.232	.9955
13	-1.2464	.287	1.187	.9823
14	-.8752	.417	1.127	.9725
15	-.7595	.468	1.144	.9600
		Mean value = .477 Standard deviation = 0.052	Mean value = 1.192 Standard deviation = 0.015	

2.7.4 Deviations of the calculated theoretical solids pressure drop from the measured solids pressure drop

The per cent deviation of the model from the measured result is calculated from the following equation:

per cent deviation = (measured solids pressure drop - theoretical solids pressure drop)/ measured solids pressure drop

Values of this per cent deviation are tabulated for each run in APPENDIX 2.2 under the heading DIFF. FIGURE 2.26 is a histogram of these deviations for all the runs in the fifteen run groups. The mean value of the per cent deviation is -5.71 per cent and the standard deviation of the distribution is 8.14. All the values of the per cent deviation have been included though some of the larger values which occur as the choking point is approached might well have been excluded as incipient 'slug flow' is the most likely cause of these large deviations. Average values of the per cent deviation for each run group are listed in TABLE 2.10.

TABLE 2.10 Summary of the per cent deviations between the observed and theoretical values of the solids pressure drop

Material	Run Group No.-Feed Rate (g/sec) / mean per cent deviation for run group			
$^{28}/_{32}$ glass spheres	1-1.14 / -9.35	2-1.88 / -7.04	3-2.56 / -10.1	4-3.25 / -8.02
$^{20}/_{24}$ glass spheres	5-1.14 / -7.29	6-1.88 / -9.57	7-2.56 / -8.60	8-3.25 / -6.4
$^{14}/_{16}$ glass spheres	9-1.14 / -3.21	10-1.88 / -9.48	11-2.56 / -6.12	12-3.25 / -3.26
1.0 mm. steel spheres	13-3.15 / +3.74	14-5.05 / +2.39	15-6.91 / +3.94	

2.8 Discussion of the Results

2.8.1 The variation of the actual average solids velocity with the average gas velocity and the solids feed rate

The results of CRAMP and PRIESTLEY (55) and LEWIS et al (56) were discussed at length in section 2.2.9. The conclusion reached was that an equation of the form

$$(\overline{V_P})_{actual} = \alpha \, \overline{V_G} + \text{const.} \qquad \ldots\ldots (2.24)$$

related the average actual particle velocity to the average gas velocity. The data plotted in FIGURES 2.16 to 2.19 sustain this conclusion.

LEWIS et al (56) concluded that the solids feed rate did not affect the slip velocity and hence the solids velocity for a given gas rate. For the range of solids feed rates covered no effect of the feed rate on the solids velocity is apparent from the data plotted in FIGURES 2.16 to 2.19. This observation is also supported by the estimates of the apparent particle terminal velocities (viz. the intercept of the line represented by equation 2.24 on the gas velocity axis) listed in APPENDIX 2.2 and summarized in TABLE 2.11.

TABLE 2.11 Summary of the terminal velocity estimates for glass and steel spheres based on zero solids velocity (ft/sec)

Solids feed rate	$^{28}/_{32}$ # glass	$^{20}/_{24}$ # glass	$^{14}/_{16}$ # glass	1.0 mm. steel
W_1	16.32	20.75	25.45	40.10
W_2	16.56	20.30	25.25	40.24
W_3	16.02	19.81	24.86	40.36
W_4	16.13	19.74	25.10	
$W_4 > W_3 > W_2 > W_1$				

2.8.2 The varistion of the observed pressure drop with the average gas velocity and the solids feed rate

The shape of the pressure drop curves plotted in FIGURES 2.20 to 2.23 conforms with the observations of ZENZ (54) which are discussed in section 2.2.8 and represented schematically in FIGURE 2.4. No attempt was made to define precisely the slugging point in the experiments so this information is not shown in FIGURES 2.20 to 2.23. Since these results are quite typical of vertical pneumatic transport systems, no further comment will be made here since they are discussed at length in section 2.2.10.

2.8.3 The agreement between the terminal velocity estimate based on zero solids velocity and the estimate based on zero reciprocal solids pressure drop

As the average solids velocity approaches zero the friction and acceleration components of the solids pressure drop approach zero and the static component approaches infinity. Hence the intercept on the gas velocity axis of a plot of the reciprocal of the observed solids pressure drop vs. the average gas velocity should provide an estimate of the gas velocity at which the solids velocity is zero and hence an estimate of the solids terminal velocity. Plots of the reciprocal solids pressure drop vs. the average gas velocity are contained in FIGURES 2.26 to 2.29 and a summary of the intercepts is listed in TABLE 2.12. The agreement between the values in TABLE 2.12 and TABLE 2.11 is quite close and indicates that the reciprocal pressure drop plots should provide a good estimate of the apparent solids terminal velocity.

TABLE 2.12 Summary of the terminal velocity estimates for glass and steel spheres based on a plot of the reciprocal solids velocity vs. the average gas velocity

	$28/_{32}$ mesh glass	$20/_{24}$ mesh glass	$14/_{16}$ mesh glass	1.0 mm steel
terminal velocity estimate ft/sec.	16.0	20.5	25.0	39.5

2.8.4 The relationship between the actual average solids velocity and the theoretical average solids velocity

The functional relationship reported in section 2.7.3 was established by purely empirical trial and error methods, it is therefore difficult to associate the form of the equation with any physical mechanism. However, the proximity of the correlation coefficient to 1.0 is a good indication that the equation is valid for the ranges of the variables covered in the experiment. The actual velocities of the particles are always less than the calculated theoretical velocities, and this result is expected because of the effect of particle/wall friction.

Because of the empirical nature of the equation it should only be used with due caution as a general relationship for vertical pneumatic transport systems. The data in TABLE 2.9 indicate that the value of the exponent 'n' is more nearly constant than the value of the term 'a', their standard deviations being 11% and 1.3% of their respective mean values. Therefore an equation of the form

$$(\overline{V_P})_{actual} = a.(\overline{V_P})^{1.192}_{theoretical}$$

may be generally applicable, where 'a' must be determined for the specific system.

2.8.5 The validity of the model for calculating the theoretical solids pressure drop

In section 2.3 the hypotheses of the model were stated and an equation derived which expressed the theoretical solids pressure drop as a function of the actual and ideal theoretical particle velocities and the solids feed rate. Since the ideal theoretical velocity is calculable from a knowledge of the gas velocity and the particle terminal velocity, the theoretical solids pressure drop can be expressed as a function of the ideal theoretical velocity and the solids feed rate provided that the nature of the relationship between the actual and ideal theoretical particle velocities is known.

i.e. if

(i) (the theoretical solids pressure drop) = f (actual particle velocity, theoretical particle velocity, solids feed rate)

(ii) (the theoretical particle velocity) = g (gas velocity, particle terminal velocity)

and

(iii) (actual particle velocity) = h (theoretical particle velocity)

it follows that :

(the theoretical solids pressure drop) = q (gas velocity, particle terminal velocity, solids feed rate).

To assess the validity of the model, the agreement between the observed and calculated values of the solids pressure drop must be examined. Data for the per cent deviation between the observed and theoretical solids pressure drop values were referred to in section 2.7.4. It is apparent from a histogram of these data FIGURE 2.25, that there is an overall bias of -5.71% between the observed and the theoretical values of the solids pressure drop. This bias may be caused by one or a combination of the following factors, viz.:

(i) an erroneous initial assumption,

(ii) an error in the development of one or more of the functions f,g, and h,

(iii) a systematic error in the measurement of one or several of the independent variables, viz. the actual particle velocity, the gas velocity, the particle terminal velocity, or the solids feed rate, or

(iv) a systematic error in the measurement of the dependent variable, the observed solids pressure drop.

Due to the complexity of the system it is considered that an attempt to allocate this bias to a specific cause is unwarranted. However, the factors contributing to the distribution of the deviations about their mean value can be examined. The theoretical model equation can be expressed as:

$$(\Delta P_s)_{theoretical} = q(\overline{V_G}, V_T, W_s)$$

or more explicitly as:

$$(\Delta P_s)_{theoretical} = W_s \cdot \phi(\overline{V_G}-V_T) = W_s \cdot \phi(y)$$

where $y = (\overline{V_G}-V_T)$.

The term $(\overline{V_G}-V_T)$ is replaced by the variable y since V_T is a special case of $\overline{V_G}$ and any per centage error in $\overline{V_G}$ will appear as a per centage error in y. Now the per centage error in $(\Delta P_s)_{theoretical}$ due to errors in W_s and $\phi(y)$ is the sum of the respective per centage errors of W_s and $\phi(y)$. Therefore if confidence limits for W_s and $\phi(y)$ are estimated as $\pm1\%$ for W_s and $\pm2\%$ for the gas velocity (the gas velocity used in the calculations is not corrected for pressure and temperature departures from calibration conditions), an inspection of the data in APPENDIX 2.2 indicates that a 2.0% change in the gas velocity produces a 3.5% change in the calculated value of $(\Delta P_s)_{theoretical}$. Hence the estimated confidence limits for $(\Delta P_s)_{theoretical}$ are $\pm(1\% + 3.5\%)$, i.e. $\pm 4.5\%$. The estimated confidence limits for the observed pressure drops, i.e. ΔP_{gas} and ΔP_{total}, are ± 0.005 in water gauge for both cases. Hence the limits for $(\Delta P_s)_{observed}$ will be ± 0.01 in water gauge since

$$(\Delta P_s)_{observed} = (\Delta P_{total} - \Delta P_{gas})$$

Therefore the factors contributing to the distribution of the per cent deviation about its mean value are the estimated $\pm 4.5\%$ limits for $\Delta P_{s_{theoretical}}$ and the ± 0.01 in water gauge limits for the observed value of ΔP_s.

2.8.6 The variation of the apparent particle drag coefficient with particle Reynolds number

While a separate study of particle drag coefficients in vertical pneumatic transport was not a specific objective for this thesis, it is considered that an examination of these data should be made to check the validity of the method suggested for estimating the particle terminal velocity which was described in section 2.3.1. The method can be checked by an examination of the relationship between the apparent drag coefficient calculated in this manner and its associated particle Reynolds number followed by a comparison of these results with the classical drag data for spheres which is listed in TABLE 2.2.

Values of the apparent drag coefficient were calculated from the mean values of the estimates of the particle terminal velocity shown in TABLE 2.11. The relationship used to calculate, C_D, the drag coefficient, was derived from equation 2.12 by equating the particle weight to the total drag force. The resulting expression is:

$$C_D = \frac{4}{3} \frac{(\rho_s - \rho_f)}{\rho_f} \frac{g.d}{V_T^2} \quad \ldots\ldots\ldots\ldots (2.54)$$

These calculated values of the apparent drag coefficient together with the associated values of the particle Reynolds number are presented in TABLE 2.13 and are plotted in FIGURE 2.30 together with the classical data for spheres.

TABLE 2.13 Values of the apparent drag coefficient and particle Reynolds numbers based on terminal velocity estimates

Material	Mean particle diameter d ft.	Estimated terminal velocity V_T ft/sec.	Particle Reynolds number $\frac{d\, V_T\, \rho_f}{\mu}$	Apparent drag coefficient C_D
28/32 glass spheres	.00209	16.25	216	.815
20/24 glass spheres	.00281	20.2	361	.710
14/16 glass spheres	.00376	25.2	602	.613
1.0 mm. steel spheres	.00328	40.23	838	.565

Note: The values of ρ_f and μ used were for air at 70°F.

Inspection of FIGURE 2.30 shows that the values of the apparent drag coefficient for vertical pneumatic transport

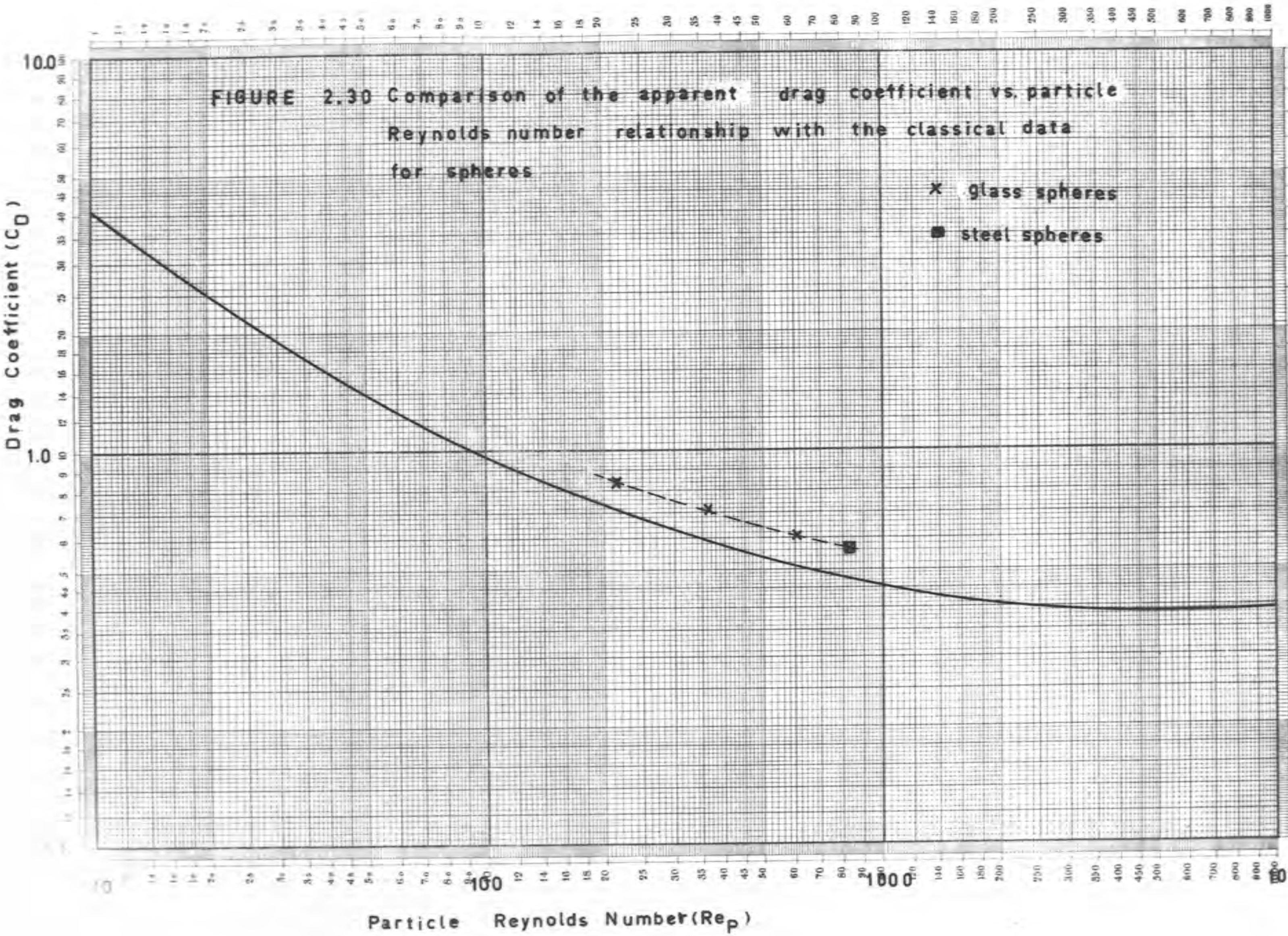

FIGURE 2.30 Comparison of the apparent drag coefficient vs. particle Reynolds number relationship with the classical data for spheres

are slightly higher than those corresponding to the classical relationship. Now drag coefficients in vertical gas-solids flow systems were discussed in section 2.2.7 where it was pointed out that the results of ZIJNEN (41), WILHELM and VALENTINE (44) and TOROBIN and GAUVIN (48) all indicated that at sub-critical Reynolds numbers free stream turbulence caused a moderate increase in the drag coefficient. Therefore, as it is likely that free stream turbulence existed under the experimental conditions that were used when the terminal velocity data were obtained, it is considered that the results are in agreement with those described in references (41), (44) and (48) and that the methods proposed in section 2.3.1 for estimating the particle terminal velocity are valid.

2.9 Conclusions

The conclusions reached during the course of the investigation of a theoretical model relating the solids pressure drop (ΔP_s) to the theoretical average solids velocity were:

(i) The relationship between the actual average solids velocity and the average gas velocity may be expressed as a linear equation of the form:

$$(\overline{V_P})_{actual} = \alpha (\overline{V_G}) + const. \quad .... (2.24)$$

The values of α and const. will depend on the nature of the material being transported and the dimensions and construction of the transport system. For the range of solids feed rates considered the values of α and const. were apparently independent of the solids feed rate.

(ii) For the glass and steel spheres tested the empirical relationship between the average actual solids velocity and the average theoretical solids velocity was found to be

$$(\overline{V_P})_{actual} = a.(\overline{V_P})^{1.192}_{theoretical}$$

where $(\overline{V_P})_{theoretical}$ was calculated from equations 2.28 and 2.29.

(iii) A theoretical model relating the solids pressure drop to the theoretical average solids velocity in a vertical pneumatic transport system has been developed. The model is derived from a momentum balance for two phase gas/solids flow and utilizes the relationships stated in conclusions (i) and (ii). The derived equation relating the pressure drop to the theoretical average solids velocity is:

$$(\Delta P_s)_{theoretical} = \frac{W_s}{A_c}\text{ (static component + acceleration component + solids/wall friction component)}$$

where (a) the static component = $\dfrac{L}{a.(\overline{V_P})^{1.192}_{theoretical}}$,

(b) the acceleration component

$$= a\left[(V_P)^{1.192}_{theoretical,2} - (V_P)^{1.192}_{theoretical,1}\right] \div g,$$

and (c) the solids/wall friction component

$$= \left[(\overline{V_P})_{theoretical} - a(\overline{V_P})^{1.192}_{theoretical}\right] \div g.$$

The calculation of the acceleration component is based on the relation

$$(V_P)_{actual} = a(V_P)^{1.192}_{theoretical}$$

and the solids/wall friction component on the relation

$$(\overline{V_P})_{actual} = a(\overline{V_P})^{1.192}_{theoretical}$$

The parameter 'a' must be experimentally determined for a given system. It follows from this that the actual average particle velocity between two points may be estimated from pressure drop measurements by solving the theoretical solids pressure drop equation for the parameter 'a', since the theoretical velocities are calculable.

(iv) Values of the average gas velocity and the apparent particle terminal velocity are required for the calculation of the theoretical particle velocities referred to in the previous section. It is considered that the intercept on the average gas velocity axis of a plot of the reciprocal solids pressure drop vs. the average gas velocity (i.e. $1/\Delta P_s$ vs. $\overline{V_G}$) should provide a satisfactory estimate of V_T, the apparent particle terminal velocity.

The conclusions stated are only confirmed for the particular materials investigated, i.e. glass and steel spheres transported with air; however, it is considered that the derived pressure drop equation has sufficient fundamental basis to justify its application to other materials in vertical pneumatic transport systems. Exceptions to the generality of the equation might arise in any situation in which the drag coefficient was not reasonably constant over the range of particle Reynolds numbers encountered during acceleration, viz. when dealing with very fine particles in the Stokes law region or very large particles in highly turbulent fluids when the upper critical Reynolds number may be reached.

3 THE FIXED BED REDUCTION OF NICKEL MONOXIDE WITH HYDROGEN

3.1 Introduction

In order to provide a basis for the analysis of the kinetics of the reduction of N_1O with H_2 in a transport reactor it was decided to examine first the kinetics of the fixed bed reduction of N_1O together with the necessary thermodynamic data for determining the chemical equilibrium of the reaction at the relevant temperatures. In the first instance an examination of the literature was undertaken. The material reported in the literature indicated that certain differences of opinion existed as to the actual mechanism of the reduction. Only one reference contained a quantitative expression for the reaction rate, however, this reference did not present an integrated form of the rate equation. It was also reported that the method of preparation of the oxide sample was likely to affect the kinetic characteristics of the reduction. In view of these observations it was decided to proceed with an experimental investigation of the kinetics of the fixed bed reduction of N_1O with H_2 with samples of the N_1O to be used in the transport reactor experiments. It was decided to use three size ranges of material in the experiments, viz. $^{35}/_{42}$#, $^{42}/_{48}$# and $^{48}/_{60}$# Tyler screen series; the method of preparation of these samples is described in APPENDIX 3.1.

The objectives of the experiments referred to above are:

(i) to establish a satisfactory kinetic model for the fixed bed reduction of N_1O with hydrogen, preferably with a single temperature dependent parameter, and

(ii) to determine the effect of particle size on the rate of reduction within the size range $35^{\#}$ to $60^{\#}$.

3.2 Literature Review

3.2.1 Chemical equilibrium and kinetics for the reduction of N_1O with H_2

Equilibrium

The reduction of N_1O with H_2 is a heterogeneous gas-solid reaction which may be written:

$$N_1O_{(s)} + H_{2(g)} = N_{1(s)} + H_2O_{(g)}$$

Calculations to determine the chemical equilibrium of the reaction are contained in APPENDIX 3.2, the data of ELLIOTT and GLEISER (2) were used. The equilibrium favours almost complete conversion of the oxide to metallic nickel in the temperature range 300°C to 700°C.

Kinetics of reduction

The most relevant papers published concerning the fixed bed reduction of N_1O are by BENTON and EMMETT (2), PARRAVANO (3), HAUFFE and RAHMEL (4), KUZNETSOV (5) and BANDROWSKI et al (6). A paper by KIVNICK and HIXSON (7) is of related interest but describes the fluidized bed reduction of N_1O with H_2 diluted with nitrogen. BENTON and EMMETT (2) and BANDROWSKI et al (6) used a dynamic system in which a stream of hydrogen was passed through a bed of heated N_1O. The water vapour content of the reactor exit gas was monitored by adsorption of the H_2O on a solid desiccant in reference (2) and by measuring the dew point of the reactor exit gas in reference (6). PARRAVANO (3) used a closed constant volume apparatus together with a mercury displacement pump to circulate the reducing gas. The water vapour was removed with a liquid nitrogen trap and the course of the reaction was observed by measuring the changes in the absolute pressure of the system. HAUFFE and RAHMEL (4) used a similar apparatus but maintained it at constant pressure by means of a mercury filled gas burette. Water vapour was removed by absorption in concentrated H_2SO_4 and the degree of reduction was measured by measuring volume changes with the gas burette. The thermosyphon principle was used to circulate the gas. KUZNETSOV (5) also used a sealed apparatus but did not describe it.

A similar reduction rate curve is reported in all the references (2), (3), (4), (5) and (6). Plots of the rate of reduction vs. time start from zero, rise to a maximum, then decline as complete reduction is approached. This is the characteristic shape of the rate curve of an 'autocatalytic' reaction. FIGURE 3.1 is a reproduction from reference (6) which illustrates

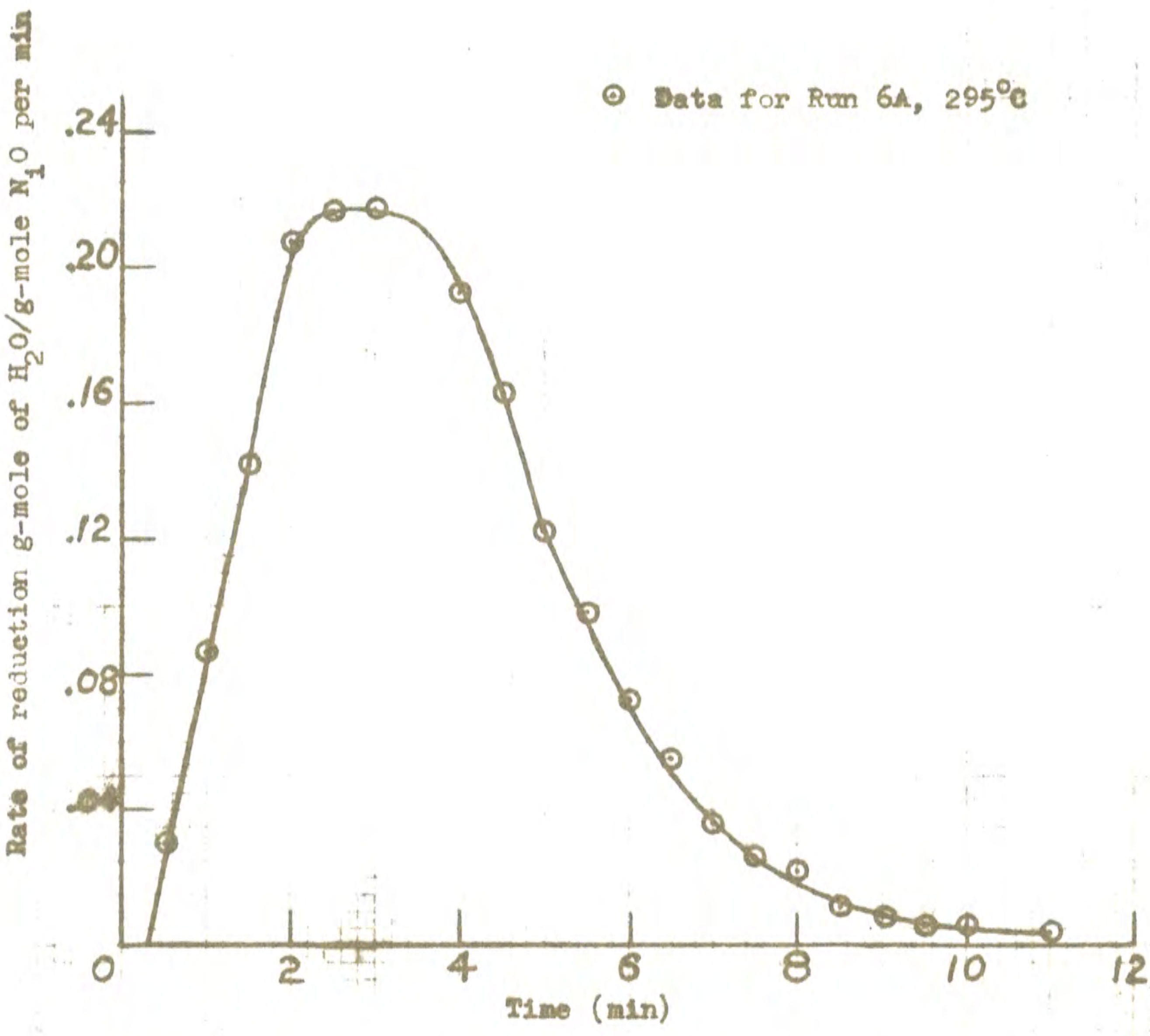

FIGURE 3.1 Reproduction of Figure 4 from the data of BANDROWSKI et al (6)

this point. Now the characteristics of this rate curve will be determined by the reaction mechanism. Generally gas-solid reactions involve four basic processes, LEVENSPIEL (9), these are:

(i) the transport of the reacting gas molecules to the reaction zone in the solid,

(ii) a chemical reaction between the molecules of the gas and the unreacted solid,

(iii) the transport of gaseous reaction products, if present, away from the reaction zone and their replacement by fresh reactant gas, and

(iv) since temperature is an important variable in chemical kinetics, the transfer of heat to and from the reaction zone.

Steps (i), (iii) and (iv) usually depend on convection, diffusion, and conduction, while step (ii) involves the formation of chemical bonds. The overall kinetics of the reaction are determined by the relative rates at which these processes occur. A predominantly slow step, or steps, may control the reaction rate to such an extent that the faster steps may be ignored, YANG and HOUGEN (16).

3.2.2 Rate controlling steps in the reduction of N_1O with H_2

Possible rate controlling steps have been considered in references (2), (3), (4) and (6). However, none of these writers claim to have confirmed an actual reaction mechanism. Simplified qualitative explanations of the mechanism are given in references (2) and (3). BENTON and EMMETT (2) cited LANGMUIR (8) to support the hypothesis that a solid state reaction involving two immiscible solid phases must occur at the solid A-solid B interface. They deduced that the apparent 'autocatalytic' nature of the reaction was caused by the interfacial area increasing from preferred adsorption sites, and then decreasing as the advancing reaction zones competed for the unreacted N_1O. A more comprehensive explanation was given in reference (3); it was suggested here that the following steps can be envisaged as occurring during the reduction process:

(i) chemisorption of the H_2 on the solid surface,

(ii) a chemical reaction between the adsorbed H_2 and the N_1O, and

(iii) evaporation of the H_2O.

It was suggested that the chemisorption of the H_2 was the rate controlling step, this chemisorption being a nonequilibrium process at all stages of the reaction. It was also suggested that diffusional and convective rate transfer of the H_2 and the H_2O did not influence the reaction rate. Contrary to the opinion expressed in reference (3), it was suggested by HAUFFE and RAHMEL (4) that solid state processes and not chemisorption determined the reaction rate.

BANDROWSKI et al (6) proposed a quantitative mathematical model for the reaction; (quote) "The form of the curve relating reaction rate to conversion of N_1O, as shown in Fig. 6, suggests that the reaction consists of two rates, one involving the reaction between N_1O and H_2 adsorbed on N_1O, and a second involving an interfacial surface reaction between N_1O and H_2 adsorbed on the nickel." These reactions are considered to proceed in parallel, the first rate predominating in the initial stages and rapidly diminishing as the second rate takes over; the second rate would increase progressively from an initial value of zero to a maximum rate and then reduce to zero at complete conversion. The expression derived for the rate equation was:

$$r = r_1 + r_2 = k_1(1 - \theta)p^{0.43} + k_2(1 - \theta)(\theta)p^{0.05}$$

where r = overall reaction rate, g mole H_2O/g mole N_1O per min.,

θ = total g mole of N_1O reduced per g mole N_1O charged,

k_1, k_2 = rate constants, and

p = partial pressure of H_2, atm.

Constants k_1 and k_2 were determined by regression analyses, giving the equations:

$$\log k_1 = \log(3.43 \times 10^4) - \frac{\Delta H_1}{4.576\ T},$$

and $$\log k_2 = \log(2.51 \times 10^4) - \frac{\Delta H_2}{4.576\ T},$$

where ΔH_1 = 14,388 cal/g mole and ΔH_2 = 12,420 cal/g mole are the respective activation energies for the two reactions.

The other workers in references (2), (3), (4) and (5) also noticed a marked dependence of the rate on the reaction temperature, Arrhenius activation energies are presented in references (3), (4) and (5). These published activation energies are shown in TABLE 3.1 together with the value obtained by KIVNICK and HIXSON (7).

TABLE 3.1 Published activation energies for the reduction of N_1O with H_2

Source of data	Reported Arrhenius activation energy at 1.0 atm. pressure cal/g mole	Temperature range ^oC
PARRAVANO (3) (Fixed bed)	26,400	155-200
HAUFFE and RAHMEL (4) (Fixed bed)	23,000	270-360
KUZNETSOV (5) (Fixed bed)	10,400	82-346
BANDROWSKI et al (6) (Fixed bed)	14,380) parallel 12,420) reactions	261-300
KIVNICK and HIXSON (7) (Fluidized bed with H_2-N_2 mixture)	10,200	177-399

3.2.3 Summary

The study of the literature indicates that the different workers agree on the processes involved in the reduction of NiO with H_2, i.e. the adsorption of hydrogen followed by an interfacial reaction in the solid and subsequently desorption of H_2O, but they do not agree as to which step controls the reaction rate. Their views are summarized in TABLE 3.2. The work of BANDROWSKI et al (6) is probably the most complete as they were the only workers to formulate a mathematical model. However, from a practical standpoint this model has several limitations, viz.

(i) the method of obtaining the rate curve involves numerical differentiation which can introduce errors in addition to the experimental errors already present,

(ii) the equation resulting from the mathematical model has two constants which must be determined by experiment,

(iii) the range of validity of the equation is only between 5 and 95 per cent reduction, and

(iv) extrapolation from the range 261-300°C to 325°C gave results consistently high compared with measured values.

TABLE 3.2 Summary of proposed rate controlling processes for the reduction of N_1O with H_2

MECHANISM	SOURCE OF DATA				
Possible controlling processes in the reduction of N_1O with H_2	BENTON and EMMETT (2)	PARRAVANO (3)	HAUFFE and RAHMEL (4)	KUZNETSOV (5)	BANDROWSKI et al (6)
Chemisorption of H_2	Not controlling	Probably controlling	Not controlling	No comment	Not controlling
Interfacial reaction between adsorbed H_2 and N_1O	Probably controlling	Not controlling	Probably controlling	No comment	Two parallel reactions: probably controlling
Evaporation of H_2O	No comment	Not controlling	No comment	No comment	No comment
Heat transfer effects	There was no reference to this effect as the heat of reaction is quite small, see APPENDIX 3.2				

In addition to these points the only boundary conditions available for integration of the rate equation are $(t=0, \theta=0)$, which are outside the range, $0.05 < \theta < 0.95$, specified for the validity of the model.

In view of these limitations and the fact that the reported values for the reaction rate by different workers show considerable variation, it is proposed to formulate a reaction model based on the chemisorption theory of PARRAVANO (3) and to experimentally investigate its applicability to several samples of N_1O prepared by the method described in APPENDIX 3.1.

3.3 Development of a Reaction Model

In this section a mathematical expression is proposed which describes the kinetics of the fixed bed reduction of N_2O. The approach adopted is semi-empirical, but is based on the hydrogen chemisorption theory proposed by PARRAVANO (3). While a successful application of the model to the experimental data would not be sufficient proof to establish a definite reaction mechanism, successful results could be taken as evidence to support PARRAVANO (3).

In selecting a model to describe the gas-solid reaction the following factors must be considered:

(i) the model should be based on some qualitative assessment of the four basic processes previously discussed, section 3.2.1.,

(ii) the mathematics of the model must be manageable, and

(iii) the parameters and constants resulting from the mathematical analysis must be determinable from fundamental knowledge or experiment.

The first point is most important when extrapolation beyond the range of the experimentally confirmed validity of the model is considered.

3.3.1 Derivation of the rate equation

It is proposed that the rate controlling step in the reaction initial stages of the reaction is the chemisorption of H_2 on N_1O. Further it is proposed that this chemisorbed H_2 then reacts with the available N_1O to produce metallic nickel. It is assumed that N_1O prepared according to the method described in APPENDIX 3.1 will be sufficiently porous to absorb H_2 throughout its bulk. The proposed semi-empirical rate equation then becomes:

$$(\text{rate of reduction}) = (\text{constant})(\text{moles of oxygen as } N_1O)(\text{moles of chemisorbed } H_2) \qquad \ldots\ldots(3.1)$$

Chemisorption of hydrogen

The chemisorption of H_2 on N_1O has been shown to obey the Roginsky-Zeldovich equation, GARNER (10). This equation may be written:

$$\frac{dq}{dt} = a\ e^{-bq} \qquad \ldots\ldots(3.2)$$

which yields on integration

$$q = \frac{1}{b}\left[\ln\left(t + \frac{1}{a.b}\right) - \ln\left(\frac{1}{ab}\right)\right] \quad .....(3.3)$$

where q is the moles of gas adsorbed at time t and a,b are constants. Now since the reaction model is to fit the autocatalytic shape of the reaction curve, it is assumed that there is no rapid initial adsorption at time zero, as has been observed in some instances, TAYLOR and THON (11). Further, since no published values of a,b for the chemisorption of hydrogen on N_1O could be found in the literature, some empirically determined values must be assigned to the product ab to test the model. A preliminary investigation of the data of BANDROWSKI et al (6) indicated that if the product ab was assigned the value 1.0 good agreement was obtained between the observed results and those predicted by the reaction model. This fit is discussed in detail in section 3.4. In this case equation 3.3 can be written:

$$q = \frac{1}{b}\left[\ln(t + 1.0)\right] \quad .....(3.4)$$

and the boundary condition t=0, q=0 is satisfied.

The rate equation

This equation is chosen to represent the rate of reduction of a mass of N_1O containing X_T moles of oxygen at time zero. Let the moles of oxygen removed at time t (min.) be X, and let y be the degree of reduction of the N_1O (c.f.θ used in reference (6)), defined as the fraction of total oxygen which has been removed at time t. Since $X = y.X_T$; $\frac{dX}{dt}$, the rate of reaction may be written as:

$$\frac{dX}{dt} = \frac{dy}{dt} \cdot X_T \qquad \text{.....(3.5)}$$

so that equation 3.1 becomes

$$\frac{dX}{dt} = \frac{dy}{dt} \cdot X_T = (\text{const.})(X_T - X)(q) \qquad \text{.....(3.6)}$$

Equations 3.6 and 3.4 can then be combined to give:

$$\frac{dX}{dt} = \frac{dy}{dt} \cdot X_T = (\text{const.})(X_T - X)\left[\frac{1}{b}\ln(t + 1.0)\right]$$

$$= A_1 (X_T - X)\left[A_2 \ln(t + 1.0)\right] \qquad \text{.....(3.7)}$$

where A_1 = const. and $A_2 = \frac{1}{b}$

and since $y = \frac{X}{X_T}$, equation 3.7 reduces to

$$\frac{dy}{dt} = A(1-y)\ln(t + 1.0) \qquad \text{.....(3.8)}$$

where A is a constant for constant temperature and pressure and $A = A_1 \cdot A_2$

Now for chemisorption, the Arrhenius activation energy, E, can be defined by the following relationship, PORTER and TOMPKINS (78):

$$\frac{d(\ln a - bq)}{d(\frac{1}{T})} = \frac{E}{R}$$

since rate of chemisorption $= \frac{dq}{dt} = a\, e^{-bq}$ .....(3.2)

Hence if q, the amount of H_2 in the chemisorbed state on N_1O, is assumed to be relatively small at all stages during the reaction due to the formation of H_2O, A_2 (which is equal to a and $\frac{1}{b}$) can be considered as the rate constant for the chemisorption process of the model. Hence, if A_1 is the rate constant for the surface reaction, $A = A_1 \cdot A_2$, can be considered as the rate constant for the overall reaction and the Arrhenius equation:

$$\frac{d \ln A}{d(\frac{1}{T})} = \frac{E}{R}$$

will give the activation energy for the reaction if the model is valid.

3.3.2 Integration of the rate equation

Equation 3.8 may be written:

$$\frac{1}{(1-y)} \cdot \frac{dy}{dt} = A \ln(t+1.0)$$

which on integration and application of the boundary conditions yields

$$y = 1 - \exp - A\ \{(t+1.0)\ [\ln(t+1.0) - 1.0] + 1.0\}$$

..... (3.9)

[Note: $\int \ln x\, dx = x \ln x - x + c$]

Equation 3.9 may be written:

$$y = 1 - \exp - A\,[f(t)] \qquad \text{..... (3.10)}$$

$$\text{or} \quad -\ln(1-y) = A.f(t) \qquad \text{..... (3.11)}$$

where $f(t) = \{(t+1.0)\ [\ln(t+1.0) - 1.0] + 1.0\}$

..... (3.12)

3.4 The evaluation of parameter A and the validity of the model

The validity of the proposed model may be tested by plotting $-\ln(1-y_e)$ vs. $f(t)$ where y_e is the observed experimental degree of reduction at time t. The plot should yield a straight line of slope A passing through the origin. The parameter A could also be determined from rate data using equation 3.8 and a plot of $(\frac{dy_e}{dt})(\frac{1}{1-y_e})$ vs. $\ln(t + 1.0)$; however, this is undesirable for the following reasons:

(i) the use of integral data (i.e. y_e only) avoids numerical differentiation, and

(ii) it is proposed to measure the actual degree of conversion and not reaction rates in the experimental equipment; hence the model parameters should be determined as directly as possible from the observed values of y_e.

The published data of BANDROWSKI et al (6) are used to test the model. These data are reproduced in TABLE 3.3 together with values of $-\ln(1-y_e)$ and $f(t)$, the estimated value of A, the values predicted from the model for the rate $\frac{dy}{dt}$, (equation 3.8), and the model fractional conversion y, (equation 3.9). The value of A was determined by a linear regression of $-\ln(1-y_e)$ vs. $f(t)$ neglecting the last datum, the repeated value of

TABLE 3.3 Application of the adsorption model to the data of BANDRWOSKI et al (6)

Data of BANDROWSKI et al (6) Run 6A 295 °C 1.0 atm.			$-\ln(1-y_e)$ equation 3.11	f(t) equation 3.12	Values predicted from model, A = 0.2804	
Time (min.)	Reduction rate g mole H_2O / g mole N_1O per min.	Per cent reduction $100.y_e$			Rate $\frac{dy}{dt}$ equation 3.8	Fractional conversion y Equation 3.9
0.5	0.02958	0.214	0.00214	0.1082	.1103	.0298
1.0	.09227	4.112	.04199	.3863	.1744	.1026
1.5	.1423	10.68	.1129	.7907	.2058	.1988
2.0	.2069	19.63	.2185	1.296	.2142	.3046
2.5	.2161	30.24	.3601	1.885	.2071	.4104
3.0	.2196	41.45	.5353	2.545	.1904	.6000
4.0	.1933	62.32	.9760	4.047	.1451	.6785
4.5	.1630	71.62	1.259	4.876	.1218	.7451
5.0	.1216	79.16	1.568	5.751	.1002	.8006
5.5	.09768	84.57	1.869	6.667	.0809	.8457
6.0	.07260	88.86	2.195	7.621	.0644	.8819
6.5	.05479	91.92	2.516	8.612	.0505	.9106
7.0	.03619	94.14	2.837	9.636	.0391	.9329
7.5	.02739	95.75	3.158	10.690	.0300	.9500
8.0	.02169	96.91	3.477	11.775	.0227	.9631
8.5	.01130	97.91	3.868	12.887	.0170	.9730
9.0	.00885	98.35	4.104	14.025	.0127	.9804
9.5	.00648	98.76	4.390	15.189	.00932	.9858
10	.00602	99.22	4.854	16.376	.00682	.9898
11	.00362	99.56	5.426	18.818	.00356	.9948
12	.00076	99.72	5.878	21.344	.00181	.9974
13	.0000	99.73	5.915	23.946	.000898	.9987
14		99.73				

99.73 per cent conversion. From the regression calculation, the value of the intercept on the $-\ln(1-y)$ axis was found to be -0.1506, the value of A was 0.2804 and the correlation coefficient was 0.9935. These data are plotted in FIGURE 3.2. A comparison is made in FIGURE 3.3 between the reaction rate predicted by the model with the parameter A=0.2804 and the experimental results of BANDROWSKI et al (6). It is apparent from the graph that the experimental results lag behind the predicted results. BANDROWSKI et al (6) suggest that at low conversions, i.e. $y_e < 0.05$, the rate was retarded by the initial displacement of nitrogen from the reactor charge. Because the rate equation in reference (6) was not a function of time, viz.:

$$r = r_1 + r_2 = k_1(1-\theta).p^{0.43} + k_2(1-\theta)(\theta).p^{0.05}$$

(Note: $\theta = y$)

the initial displacement of nitrogen will only affect the results if $\theta < .05$, a region which is ignored by BANDROWSKI et al (6). However, in equation 3.8 the reaction rate is expressed as a function of both the degree of reduction and time. This means that the initial time lag δt will effect the prediction of results throughout the reaction and cause the model to yield high results for the predicted

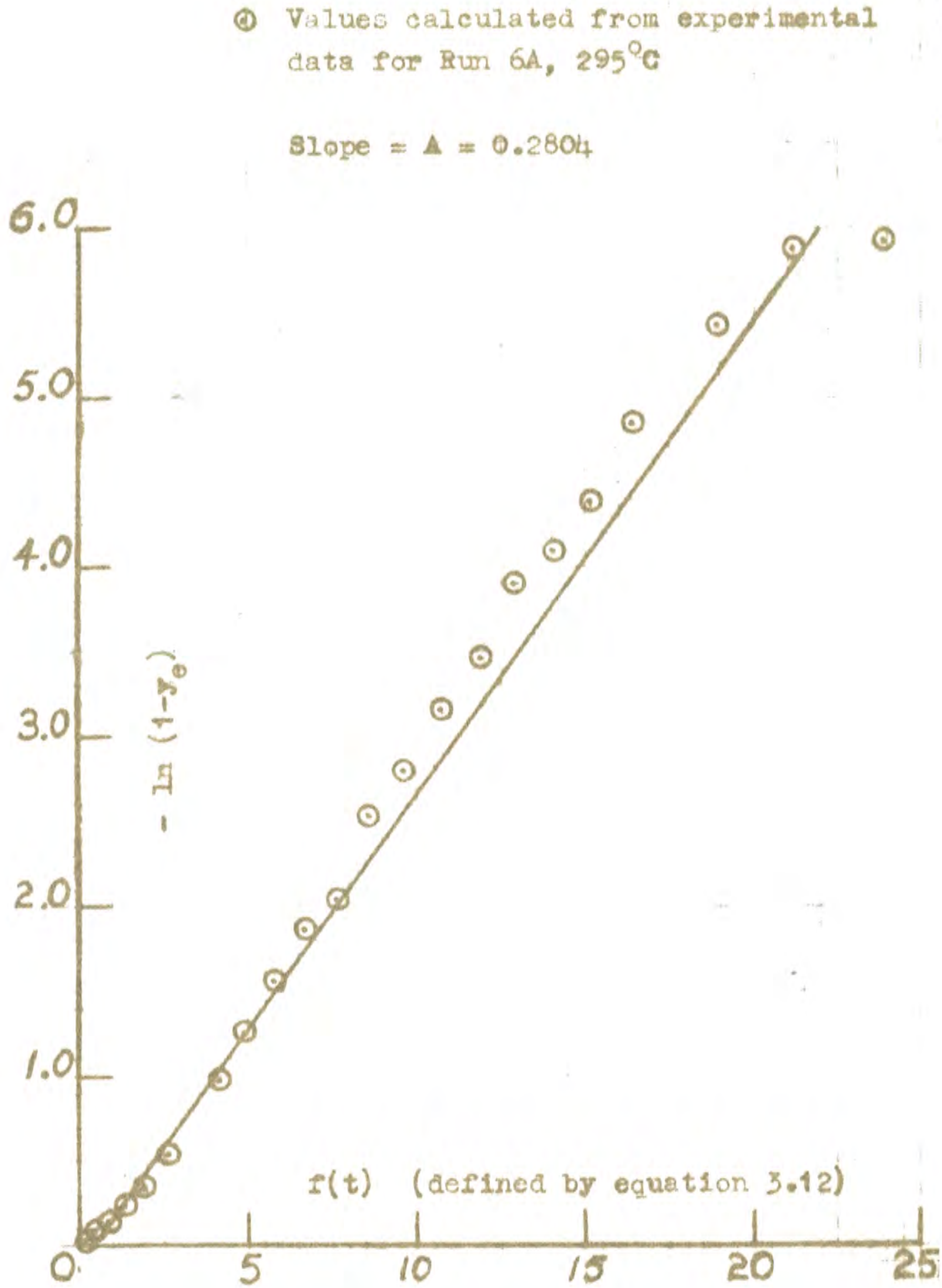

FIGURE 3.2 Plot of $-\ln(1-y_e)$ vs. $f(t)$ for the data of BANDROWSKI et al (6)

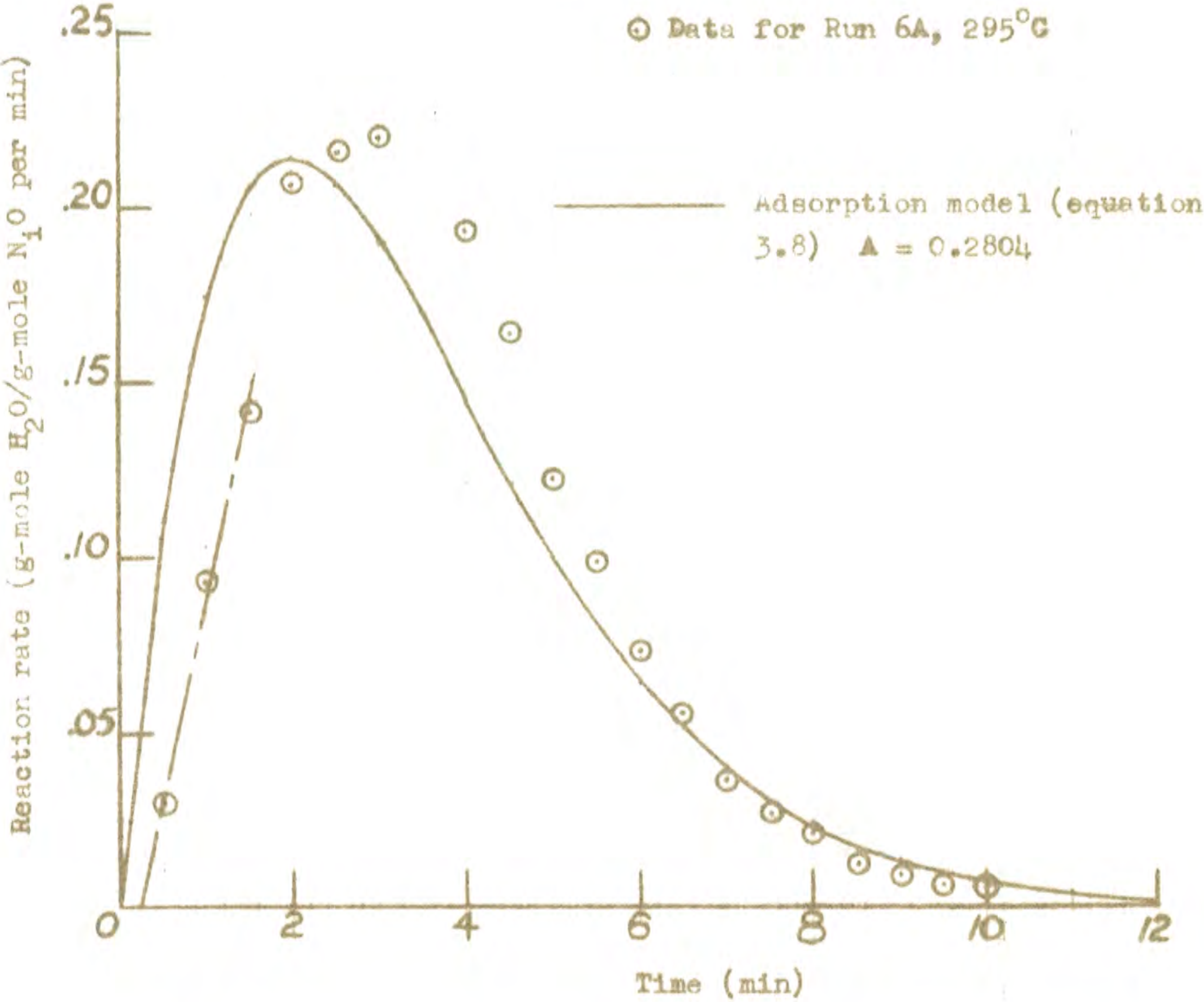

FIGURE 3.3 Plot of reaction rate vs. time for the comparison of the data of BALDROWSKI et al (6) with the values calculated from the proposed model

degree of conversion vs. time. From FIGURE 3.3 it is apparent that the initial increase in reaction rate approximates a linear function of time. Extrapolation back to zero rate gives a positive intercept on the time axis of 0.25 min. It is proposed that this is a valid estimate of the time, δt, taken for the initial displacement of the nitrogen from the pellets, and that the true reaction time, t_c, can be expressed by the equation:

$$t_c = t - \delta t \qquad \ldots\ldots (3.13)$$

where $\delta t = 0.25$ min. TABLE 3.4 shows the results from reference (6) with both the reaction rate and the degree of reduction tabulated with corresponding values of the corrected time, t_c. In addition corresponding values of $-\ln(1-y_e)$ and $f(t_c)$ are listed. The values of $f(t_c)$ are calculated from equation 3.12 using the corrected time, t_c.

From the results of a linear regression between $-\ln(1-y_e)$ and $f(t_c)$ the intercept on the $-\ln(1-y_e)$ axis was found to be 0.06113, the slope of the line A was 0.2862, and the correlation coefficient was 0.9931. The plotted data are almost identical with those in FIGURE 3.2. The results predicted by the model for the reaction rate, $\frac{dy}{dt}$, and the degree of reduction, y, for A = 0.2862 are

TABLE 3.4 Results of BANDROWSKI et al (6) at 295°C and 1.0 atm., corrected for time lag

Time t (min)	Corrected time t_c=t-0.25 (min)	*Rate r_e	Per cent reduction y_e	$-\ln(1-y_e)$	$f(t_c)$
0.5	0.25	0.02958	0.214	0.002142	0.02893
1.0	0.75	0.09227	4.112	0.04199	0.2293
1.5	1.25	0.1423	10.68	.1129	.5746
2.0	1.75	0.2069	19.63	.2185	1.032
2.5	2.25	0.2161	30.24	.3601	1.581
3.0	2.75	0.2196	41.45	.5353	2.207
4.0	3.75	0.1933	62.32	.9760	3.651
4.5	4.25	0.1630	71.62	1.259	4.456
5.0	4.75	0.1216	79.16	1.578	5.308
5.5	5.25	0.09768	84.57	1.869	6.204
6.0	5.75	0.07260	88.86	2.195	7.394
6.5	6.25	0.05479	91.92	2.516	8.112
7.0	6.75	0.03619	94.14	2.837	9.120
7.5	7.25	0.02739	95.75	3.158	10.16
8.0	7.75	0.02169	96.91	3.477	11.23
8.5	8.25	0.01130	97.91	3.868	12.33
9.0	8.75	0.00885	98.35	4.104	13.45
9.5	9.25	0.00648	98.76	4.390	14.60
10.0	9.75	0.00602	99.22	4.854	15.78
11.0	10.75	0.00362	99.56	5.261	18.20
12.0	11.75	0.00076	99.72	5.878	20.71
13.0	12.75	0.0000	99.73	5.915	23.29
14.0	13.75	0.0000	99.73	-	-

* g mole H_2O/g mole initial N_1O per min

listed in TABLE 3.5. These calculations were made at arbitrary 0.5 min. intervals to generate the curve predicted by the model and are independent of the time correction, δt. A comparison between the time corrected data from reference (6) and the model predictions for A = 0.2862 is shown in FIGURE 3.4. A similar plot for the degree of reduction data is seen in FIGURE 3.5. It is suggested that these graphs may be regarded as qualitative evidence to support the validity of the proposed model.

In addition the degree of fit of BANDROWSKI'S model and the model now proposed are compared in APPENDIX 3.3. To eliminate any bias the original data from reference (6) are used without any time correction for the initial displacement of nitrogen. The range of fractional conversion taken for the comparison was from 0.05 to 0.95 and the basis chosen for the comparison was the R.M.S. value of the difference between the observed experimental values of the reaction rate and the degree of reduction and the values predicted by each model. For the model proposed by BANDROWSKI et al (6) the R.M.S. deviation for the reaction rate was 0.0349 and the R.M.S. deviation for the degree of conversion was 0.1015. By comparison for the model now proposed the R.M.S. deviation

TABLE 3.5 Rate and degree of reduction predicted by model, A = 0.2862

Time (min)	Rate $\frac{dy}{dt}$ equation 3.8	Degree of reduction y, equation 3.9
0.5	0.1125	0.0304
1.0	.1776	.1046
1.5	.2091	.2025
2.0	.2170	.3098
2.5	.2091	.4168
3.0	.1915	.5173
3.5	.1689	.6075
4.0	.1446	.6859
4.5	.1209	.7523
5.0	.09890	.8071
5.5	.07949	.8516
6.0	.06288	.8870
6.5	.04904	.9149
7.0	.03775	.9365
7.5	.02873	.9530
8.0	.02163	.9656
8.5	.01612	.9749
9.0	.01190	.9819
9.5	.008710	.9879
10.0	.006323	.9907
11.0	.003258	.9954
12.0	.001632	.9977
13.0	.0007973	.9984

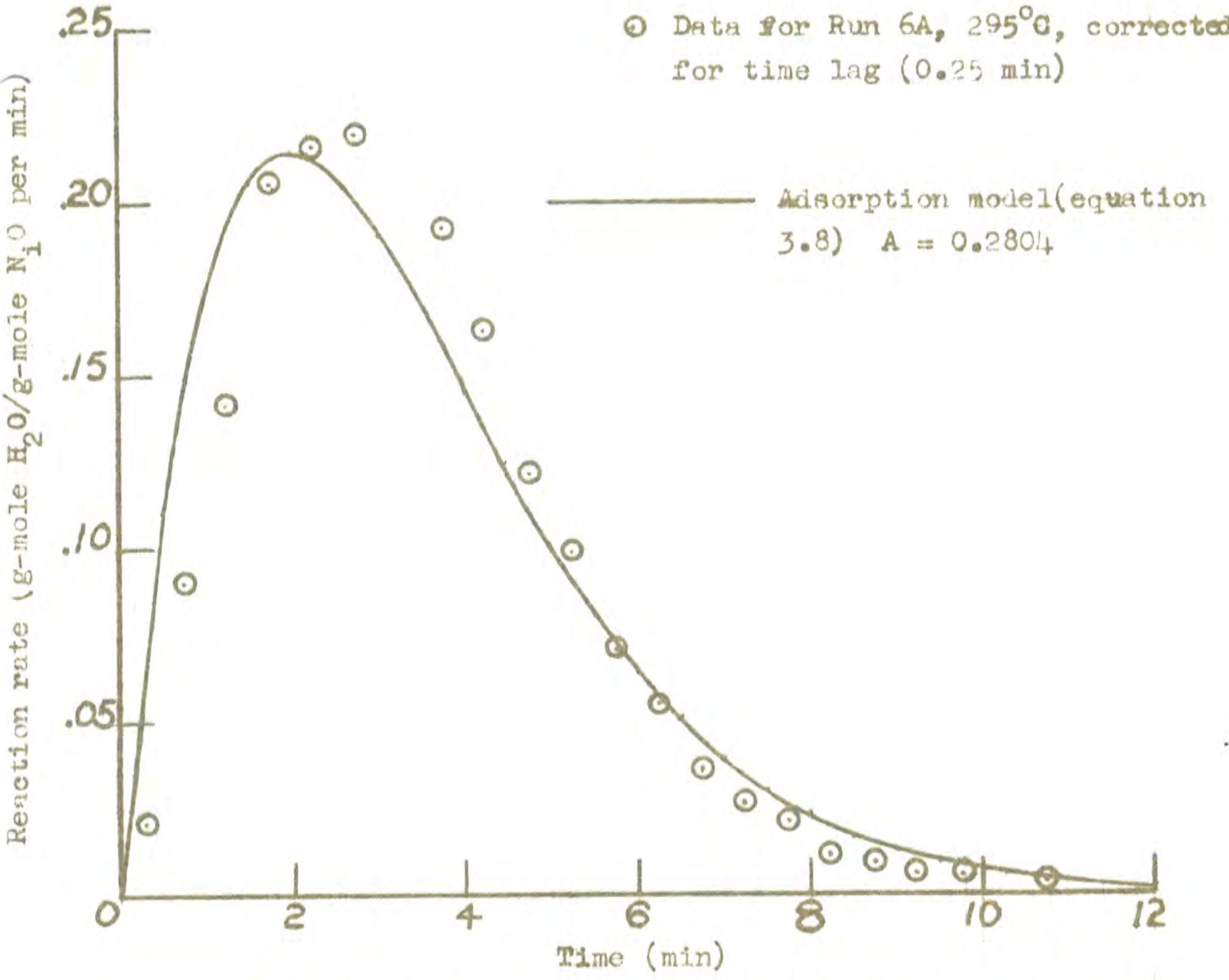

FIGURE 3.4 Plot of reaction rate vs. time for the data of BANDROWSKI et al (6) using the time lag (0.25 min) correction

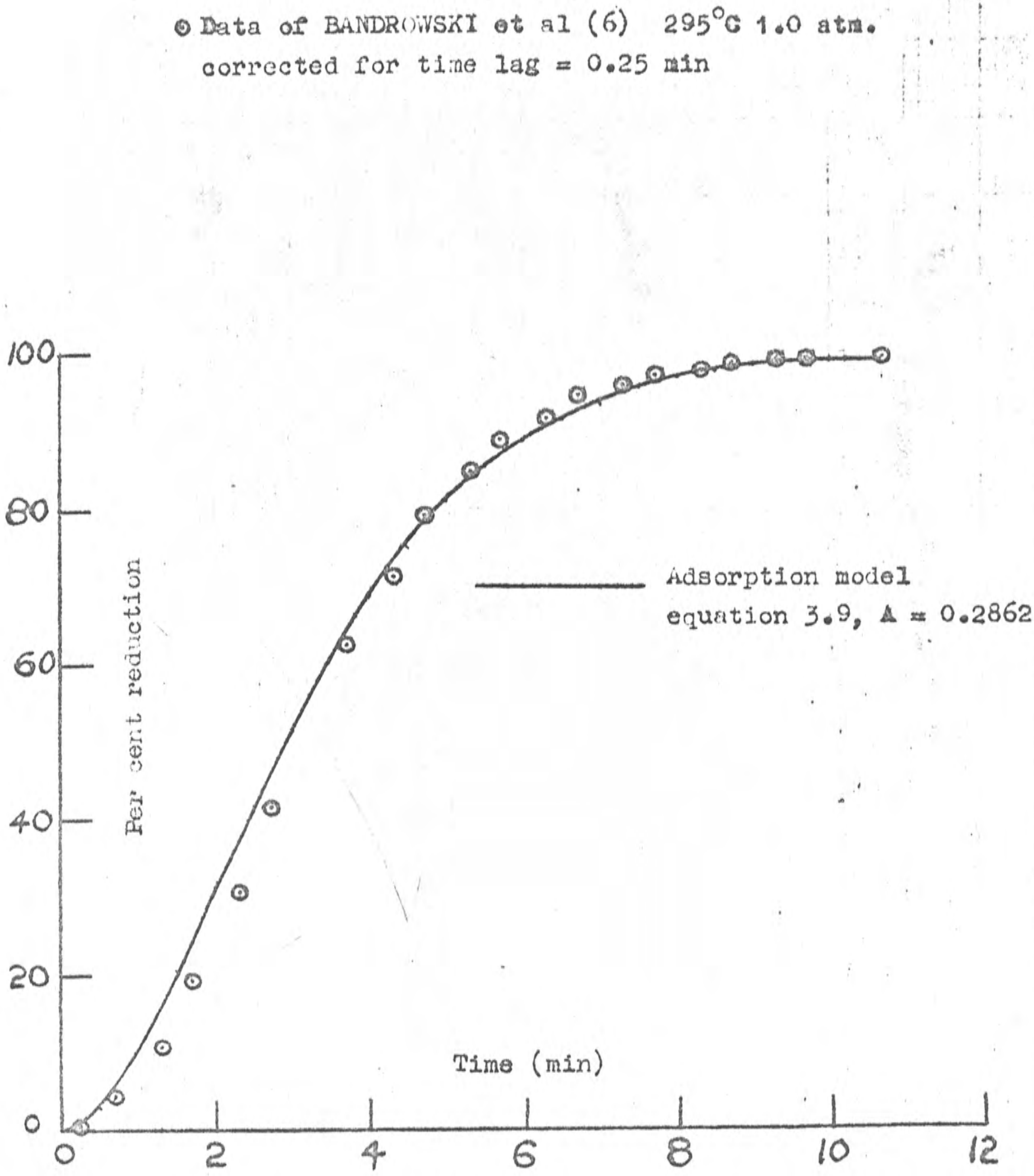

FIGURE 3.5 Plot of per cent reduction vs. time, for the data of BANDROWSKI et al (6) corrected for time lag

for the reaction rate was 0.02984 and the R.M.S. deviation for the degree of conversion was 0.0799.

An inspection of the R.M.S. deviations indicates that the proposed model fits the observed data better than the model derived by BANDROWSKI et al (6).

3.5 Experimental technique

As stated in the introduction, the object of the proposed series of experiments was to obtain kinetic data for the fixed bed reduction of N_1O with a view to using these data to make a comparison between the observed reaction rates in the fixed bed and transport reactors. Ideally the fixed bed experiments should have been carried out with the same conditions of temperature, pressure, gas composition, and mass transfer as occur in a transport reactor. However, the attainment of exactly similar reaction zone conditions in the two reactors is not practicable. Various techniques have been considered with a view to minimizing these differences.

A dynamic reaction system, SMITH (14), was chosen in preference to a static system in order to minimize the effect of mass transfer rates on the overall kinetics of the reaction. Three possible dynamic techniques were considered:

(1) the method of PARRAVANO (3) which involved circulation of the H_2 through the N_1O bed and a desiccant in series in a constant volume apparatus, the progress of the reaction being observed by measurement of the pressure changes; there are two disadvantages with this technique,

first the partial pressure of the H_2 changes as the reaction proceeds and second for accurate work the apparatus must be kept at constant temperature;

(ii) Circulation of the H_2 through the N_1O bed and a desiccant in series, make up gas being supplied to keep the system at constant pressure; this method was used by HAMDORF (13) to study the fluidized bed reduction of $BaSO_4$; the reaction could be followed either by weighing the desiccant or by measuring the make up volume of H_2; and

(iii) Passing the H_2 through the N_1O bed and measuring the exit gas composition and then venting the gas to atmosphere, the reaction rate can be determined by measuring the dew point of the gas and metering the gas flow rate (BANDROWSKI et al (6); alternatively the degree of reduction can be determined by absorbing the H_2O contained in the exit gas with a desiccant and recording weight changes, the method used by BENTON and EMMETT (2) and MATTHEW (12).

Because of the disadvantages of method (i) attention was directed towards methods (ii) and (iii).

Method (iii) was chosen for the experiments described in this section because of its simplicity and suitability for bench scale work, i.e. no circulating pump is required as the hydrogen can be regulated from a high pressure gas cylinder. The desiccant method of observing the degree of reduction vs. time was used.

3.6 Description of the apparatus

The design of the apparatus was based on the apparatus used by MATTHEW (12). A flow sheet of the apparatus used in this work is shown in FIGURE 3.6 and a photograph appears in FIGURE 3.7. In both the photograph and the flow sheet the H_2 flow is from right to left. With the valve arrangement shown nitrogen could be used to purge the apparatus before H_2 is admitted. Both the H_2 and the N_2 were supplied from high pressure gas cylinders, their flow rates being controlled with standard two-stage pressure regulators followed by needle valves. As the experimental technique is based on the absorption of water vapour from the reactor exit gas, care was taken to remove any oxygen or water from the gas streams before they entered the reduction unit proper. After purification the H_2 stream flowed through the following stages in turn - the flowmeters, the gas preheater, the reactor, and the absorption section. The drying bottles in the absorption unit could be removed for weighing. After leaving the absorption unit the dry effluent H_2 was discharged to atmosphere through a vent.

LEGEND FOR FIGURE 3.6

F1	Hydrogen flowrators
F2	Nitrogen flowrators
NV1	Hydrogen needle valve
NV2	Nitrogen needle valve

V1, V2, V3, V4 — Three-way cocks

V5, V6 — Stop-cocks

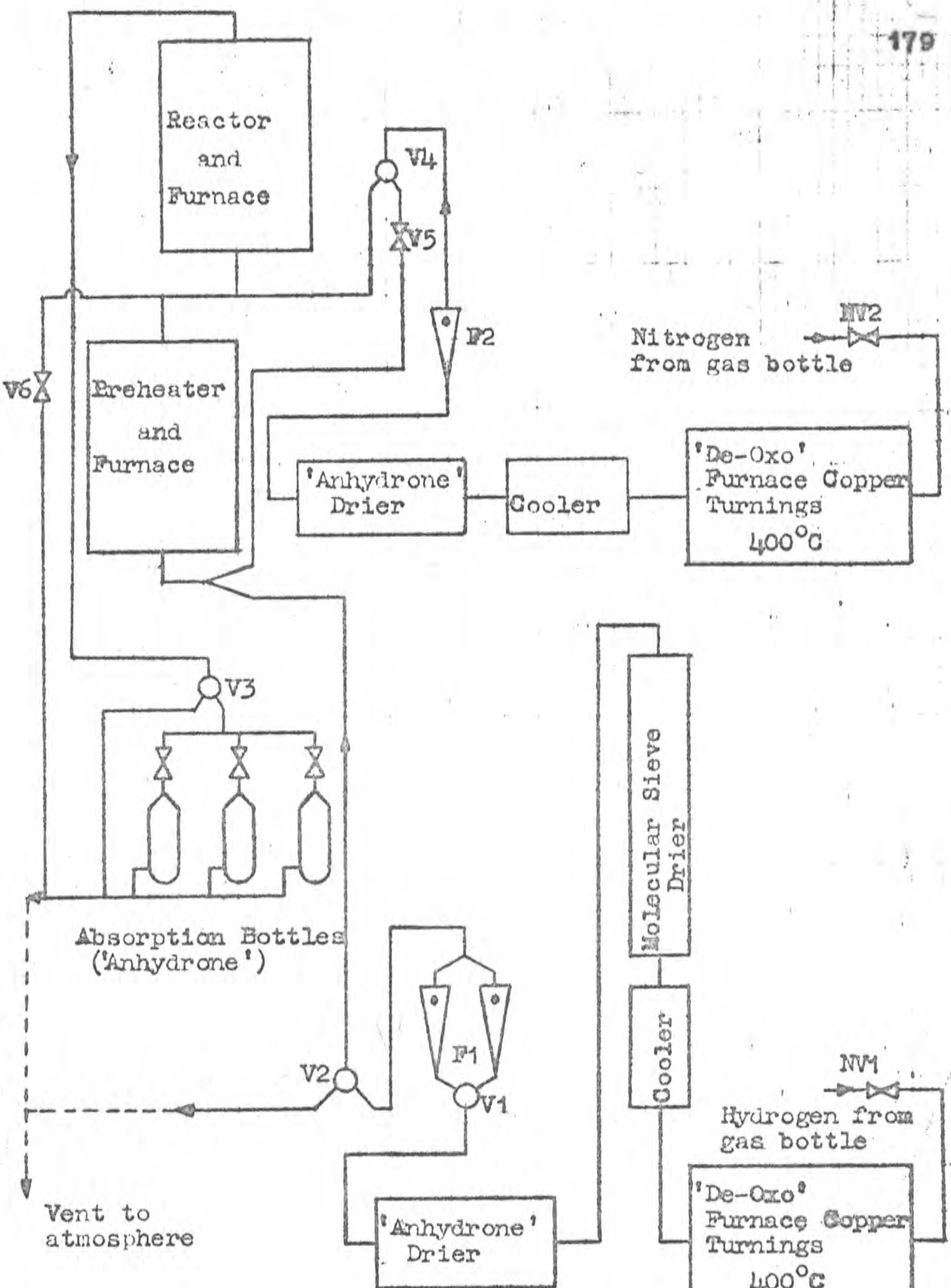

FIGURE 3.6 Flowsheet of the apparatus used for the fixed bed reduction of N_1O.

FIGURE 3.7 Photograph of the apparatus used for the fixed bed reduction of NiO

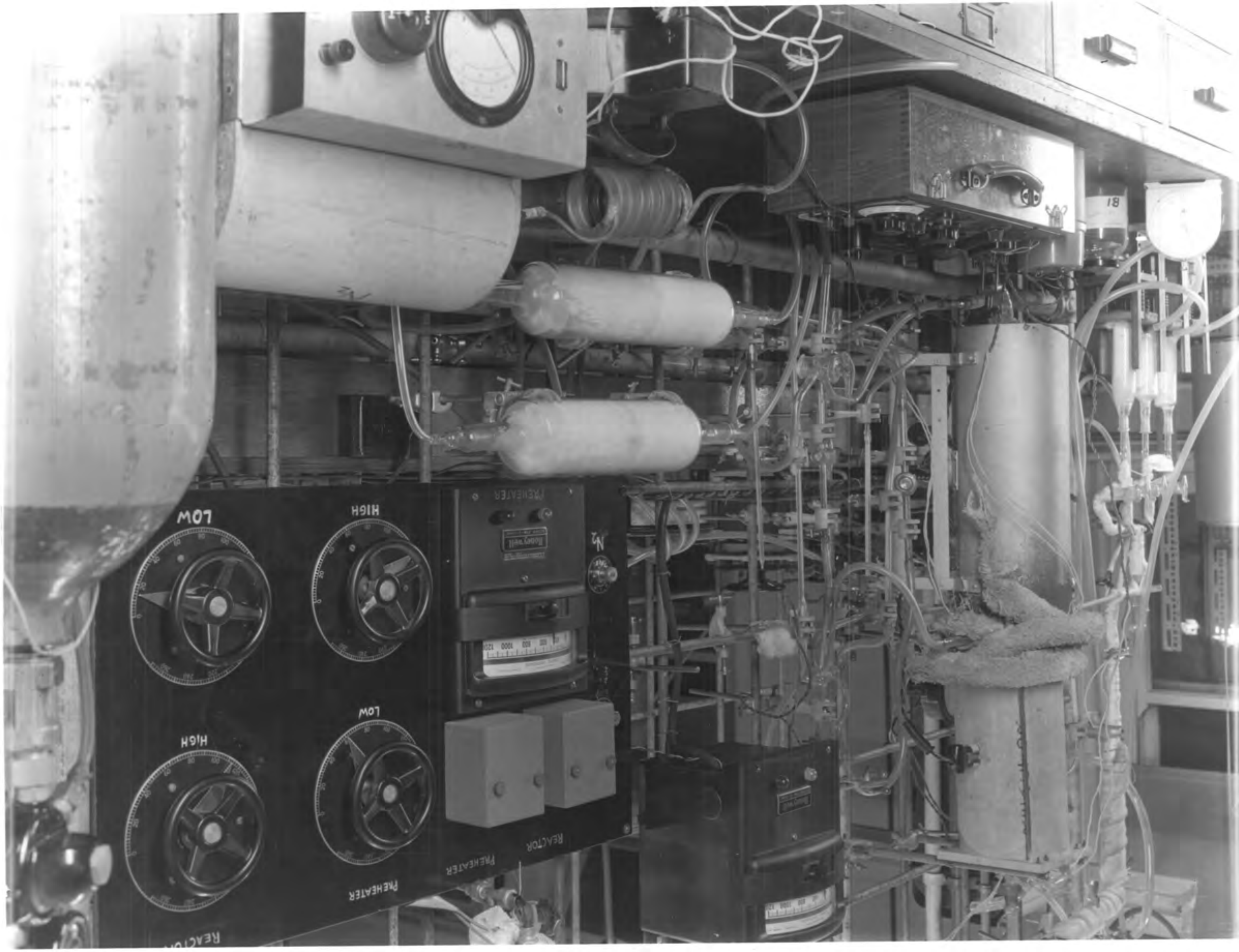
LOW
HIGH
PREHEATER
HIGH
LOW
PREHEATER
REACTOR
REACTOR
18

3.6.1 Gas purification

The function of the purification unit was to remove the oxygen and water vapour impurities from the H_2 and N_2 streams; they are seen in the lower left portion of FIGURE 3.7. The gas specifications are listed in APPENDIX 3.1. The 'De-Oxo' furnaces were identical and consisted of copper tubes 1.0 in. in diameter and 15 in. in length packed with copper turnings. These tubes were supported inside horizontal tubular silica muffles maintained at 400°C with 1.0 Kw electric heaters. The hydrogen stream at this stage contained water vapour originally present in the gas cylinder together with water vapour formed by the reaction:

$$H_2 + \tfrac{1}{2} O_2 = H_2O$$

which occurs on the copper surface. From the 'De-Oxo' furnace the H_2 passed through a cooler to a molecular sieve drier, then to an 'Anhydrone' (magnesium per chlorate) drier. The N_2 stream received similar treatment except that the only water removed was that originally present in the gas cylinder, the oxygen remained with the copper as CuO. N_2 passed from the 'De-Oxo' furnace through a cooler to an 'Anhydrone' drier from whence it was distributed for flushing the reduction apparatus.

3.6.2 Flow control

Both the N_2 and H_2 streams were metered with 'Flowrators' previously calibrated against a positive displacement flowmeter. Two flow ranges were available for the H_2 stream and one range for the N_2 stream, viz. 0-20 litres/min. for the N_2 and 0-15 litres/min. for the H_2 stream.

3.6.3 Gas preheater unit

The position of this unit is shown in FIGURE 3.6 and may be seen in the photograph, FIGURE 3.7, immediately above the left-hand end of the Cambridge potentiometer; a schematic diagram is shown in FIGURE 3.8. The gas passed through a vertical silica tube 12.0 in. long x 1 3/16 in. diameter packed with silica chips. This tube was contained in a tubular 2.0 Kw silica muffle furnace the temperature of which was controlled by a Honeywell-Brown Pyrovane temperature controller. FIGURE 3.8 shows the two power level control systems used, one auto-transformer setting slowly raised the temperature above the set point, while the other setting allowed the temperature to fall slowly. The thermocouple which actuated the controller was located between the furnace wall and the preheater tube. The thermocouple in the well indicated in FIGURE 3.8 was monitored by a Cambridge

LEGEND FOR FIGURE 3.8

V1	}	'Variac' Autotransformers
V3	}	
V4	}	
V5	}	

R1	}	Relays
R2	}	

A Silica chips

B N_1O bed

C Silica wool

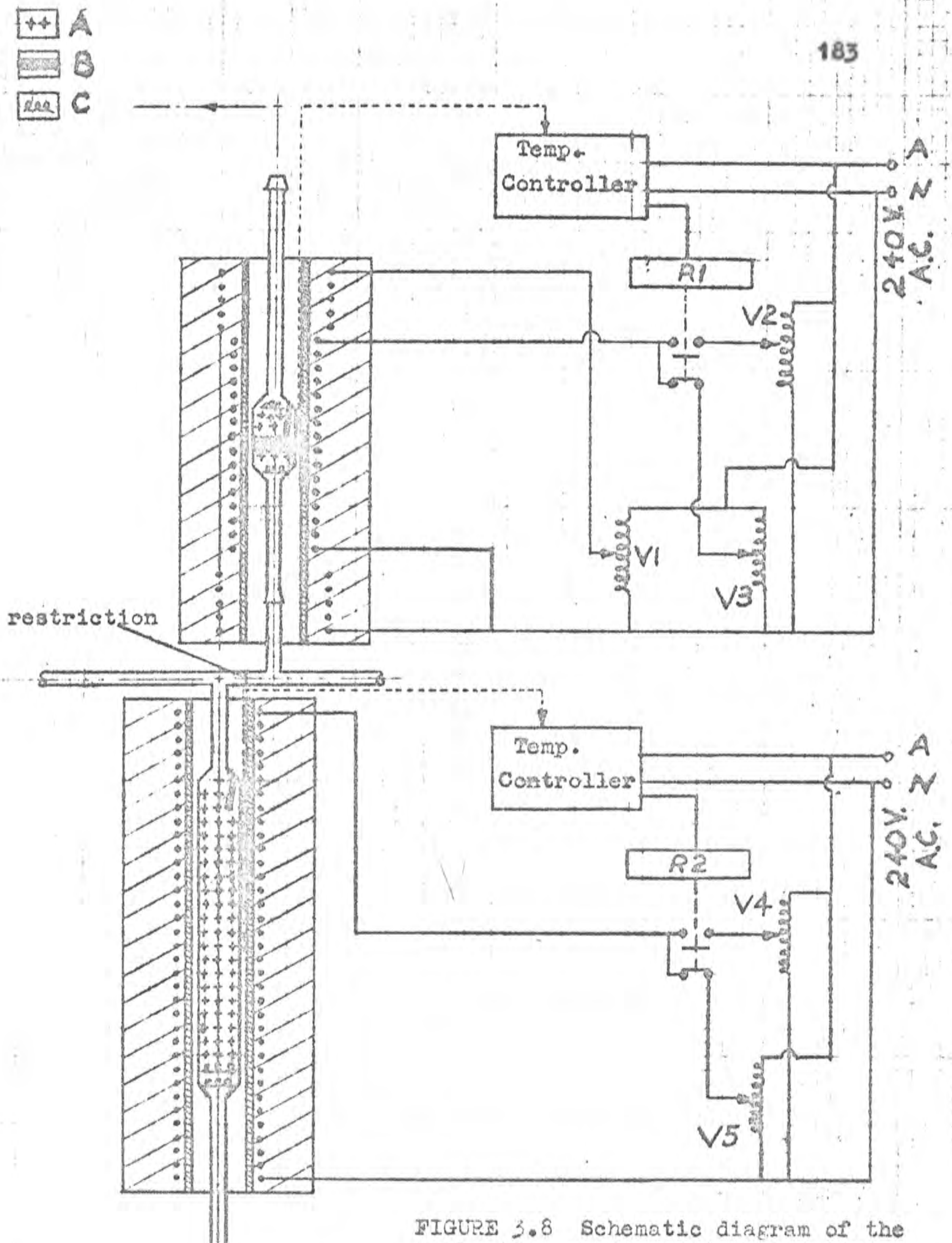

FIGURE 3.8 Schematic diagram of the preheater, reactor and temperature control units used in the fixed bed reduction apparatus

potentiometer, the controller set point was adjusted to keep this temperature at the value required for the reaction.

3.6.4 Reactor unit

The reactor unit was located above the preheater section, see FIGURE 3.6. The reactor itself was fabricated from 1.0 in. bore silica tubing and was detachable from the apparatus by means of cone and socket joints, see FIGURE 3.9. The system of heating and temperature control was similar to the preheater except that the furnace had two windings. The main 2.0 Kw winding was located in the central section of the furnace, and a secondary winding was distributed over 2.0 in of each end of the furnace. As with the preheater the 2.0 Kw winding was controlled by a Pyrovane temperature controller with a two power level input, see FIGURE 3.8. Again the controller thermocouple was located between the reactor and the tubular furnace. The input to the subsidiary winding was regulated by an auto-transformer. The controller and auto-transformers were set to give the desired reaction temperature which was monitored with a thermocouple located in the well of the reactor. The silica tube which joined the preheater to the reactor had a 1.0 cm. bore. To assist in starting a reduction

FIGURE 3.9 Photograph of the reactor used in the fixed bed reduction apparatus

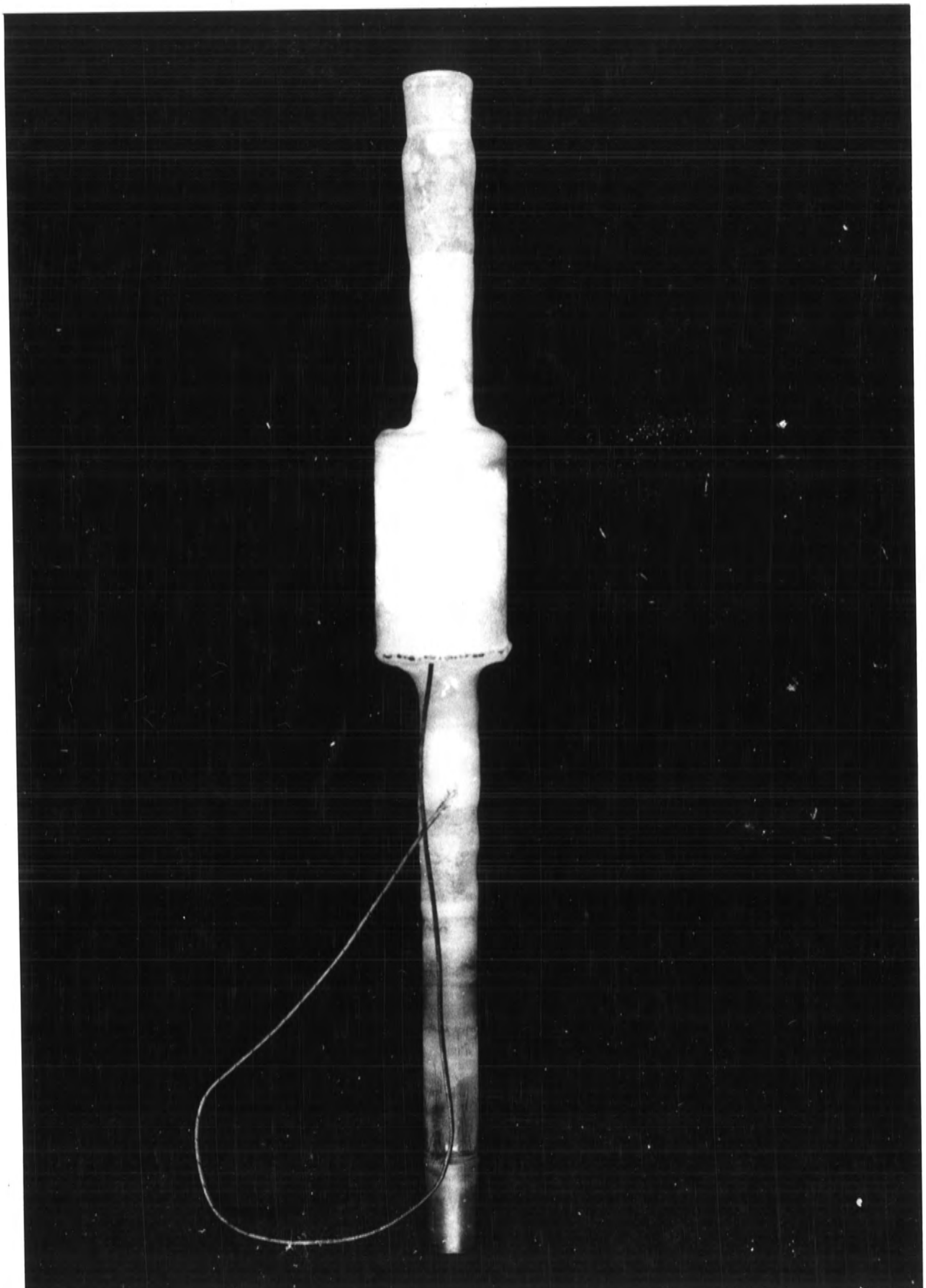

run, a 5.0 mm. diam. constriction was located between the preheater outlet and the reactor inlet. The function of the constriction was to enable a stream of hydrogen to be passed through the preheater while nitrogen flowed through the reactor.

3.6.5 H_2O absorption system

The excess hydrogen and the water generated by the reaction

$$N_1O + H_2 = N_1 + H_2O$$

passed from the top of the reactor to the absorption unit, as indicated in FIGURE 3.6. This unit comprised a three outlet manifold to which drying bottles were attached for absorption and removed for weighing during a run. The gas line from the reactor to the manifold was made from glass and traced with Isomantle heating tapes to prevent condensation. The drying bottles were packed with magnesium per-chlorate. After drying the hydrogen stream was vented to atmosphere.

3.7 Experimental conditions

These conditions were chosen to minimize the differences in reaction zone variables such as pressure, temperature and mass transfer conditions, between the fixed bed and the transport reactors. The factors which determine the conditions in the transport reactor and the approach to these conditions attainable in the fixed bed reactor are summarized below.

Pressure

The proposed transport reactor was a pilot scale apparatus, hence a certain amount of difficulty was expected in containing H_2 at elevated temperatures. Therefore it was decided to operate with the proposed transport reactor pressure in the vicinity of several inches of water above atmospheric pressure. With the experimental technique described these conditions could be matched very closely in the bixed bed experiments.

Temperature

The operation of the transport reactor is characterized by low solids residence times. It is applicable therefore to fast reactions attainable only at comparitively high temperatures. From the data of BENTON and EMMETT (2) and BANDROWSKI et al (6) it was estimated that temperatures of the order of 650°C would be required in the transport reactor to give an adequate amount of reaction with a residence time of several seconds. Because of the time required to change the absorption bottles, it was estimated that the upper working limit of temperature for the fixed bed experiments was in the vicinity of 400°C. It was therefore proposed to use the following temperatures for the fixed bed reduction of N_1O, viz. 300, 325, 350, 375, 400 and 425°C, the aim being to find the functional relationship between temperature and the parameter A of equation 3.9, viz.

$$y = 1 - \exp - A\left\{(t+1.0)\left[\ln(t+1.0) - 1.0\right] + 1.0\right\} \qquad \ldots\ldots(3.9)$$

and then for comparison to extrapolate the data for the fixed bed to the higher temperatures occurring in the transport reactor. This extrapolation, together with its inherent limitations is discussed in section 4.

Mass transfer effects

In the transport reactor the diffusional resistance to the mass transfer of the reactants (H_2) and the reaction product (H_2O) should be low as each N_1O

particle would be completely surrounded by H_2 and in addition the relative velocity between the N_1O particles and the hydrogen stream would approximate the terminal velocity of the particle. There is no evidence in the literature (refs. (2), (3), (4) or (6)) to suggest that mass transfer is a rate controlling step in the reaction, however, to allow for marginal errors, the experiments were carried out with a H_2 flow of 12 litres/min. at N.T.P., the highest gas flow commensurate with temperature and bed stability in the reactor.

Particle size

The N_1O particle sizes chosen for the transport reactor experiments were 35/42#, 42/48# and 48/60#, Tyler screen series. Samples riffled from these batches were used in the transport reactor.

Summary of experimental conditions

The proposed conditions for the fixed bed reduction runs were to use samples from three sizes of sintered N_1O (viz. 35/42#, 42/48# and 48/60#) and to reduce them with a H_2 flow rate of 12.0 litres/min. at N.T.P. at the following temperatures, 300, 325, 350, 375 and 400°C. It was further proposed to carry out three additional runs at 425°C with $^{42}/_{48}$# material, the H_2 flow rate remaining at 12 litres/min. at N.T.P.

3.8 Experimental Procedure

Charging the reactor

The reactor was removed from the furnace and charged with layers of the following materials:

(i) silica wool,
(ii) alumina chips,
(iii) N_1O sample,
(iv) alumina chips, and
(v) silica wool.

The quantities of silica wool and alumina chips were adjusted to locate the bed of N_1O in the middle of the reactor. The cone and socket joints were then smeared with silicone grease and the reactor replaced in the apparatus.

Purging the apparatus with nitrogen

The apparatus was purged with N_2 while the preheater and the reactor were brought up to the operating temperature. For the initial purge the following sequence was observed, reference should be made to FIGURE 3.6 for flow sheet and legend.

(a) Hydrogen was admitted through NVI and discharged to atmosphere through V2; then V2 was shut and the H_2 turned off.

(b) Nitrogen was admitted through NV2, directed with V4 through V5 to the preheater and reactor and then passed through V3 to atmosphere.

(c) When the air was purged from the preheater and reactor, V5 and V3 were closed and the N_2 flow was directed through V4 to V6 and then vented to atmosphere.

This completed the initial purging. The heaters were then switched on and a stream of N_2 was passed through the apparatus using the valve settings for operation (b). The controllers were set to keep the reactor $3^{o}C$ below the desired reaction temperature and the preheater $8^{o}C$ below the desired reaction temperature.

Procedure for a reduction run

After the temperatures had stabilized, the N_2 stream was directed with V4 to flow into the junction between the preheater and the reactor, the main stream was passed through the reactor and V3 to atmosphere and a subsidiary stream passed through the junction constriction (see FIGURE 3.6 for detail) and V6 to atmosphere. Almost simultaneously the H_2 was turned on and admitted through V2 to the bottom of the preheater. The H_2 stream passed up through the preheater and was flushed out to atmosphere by the N_2 flowing through the constriction in the preheater-reactor junction. The preheater temperature then rose approximately 8°C on the admission of the H_2 due to the better heat transfer properties of H_2.

The reduction run was started by two operators who carried out the following procedures concurrently:

(i) the nitrogen stream was switched off and V6 closed. This admitted the H_2 stream to the reactor.

(ii) V3 was switched to the absorption manifold and a manifold cock was opened to the selected absorption bottle, and

(iii) the stop-clock was started.

The reactor temperature rose approximately 3°C on the admission of the H_2.

The progress of the reaction was observed by changing and weighing the absorption bottles at predetermined time intervals; the reaction temperature was monitored throughout the run with the Cambridge potentiometer. The experimental data obtained from a run are for the cumulative per cent H_2O generated at a particular time after the commencement of the reaction.

3.9 Experimental Results

Eighteen reduction runs were completed and a summary of the experimental conditions is shown in TABLE 3.6.

TABLE 3.6 Summary of the experimental conditions for the fixed bed reduction of N_1O

Hydrogen flow rate: 12 litres/min., N.T.P. N_1O sample wgt.: 5,000 g.			
Nominal temp. °C	Run numbers		
300	1	6	11
325	2	7	12
350	3	8	13
375	4	9	14
400	6	10	15
425		16, 17, 18	
	35/42#	42/48#	48/60#
	Particle size		

3.9.1 Evaluation of the per cent reduction

The results of runs 1 to 18 are tabulated in TABLES 3.7.1 to 3.7.6; the data presented for each temperature are corresponding values of time (min.) and the observed per cent reduction ($y_e \times 10^2$). Time is a direct measurement, but y_e is derived from the H_2O absorption measurements and is calculated by the equation:

$$y_e = \left(\sum_{i=1}^{n} w_{H_2O_i} \right) \Big/ W_{H_2O} \qquad \ldots\ldots (3.14)$$

where

$$\sum_{i=1}^{n} w_{H_2O_i}$$

is the cumulative weight of water absorbed up to time t, n is the number of weight determinations made up to time t, and W_{H_2O} is the total weight of water equivalent to 5.000 g. of N_1O, i.e. W_{H_2O} = 1.205 g.

The runs at 350, 375, 400 and 425°C, in which the N_1O was completely reduced, were repeated if the total weight of water absorbed was not within ± 1.5 per cent of the stoichiometric quantity. This check was not available for the runs at 300° and 325°C as they were not taken to completion.

FIGURES 3.10.1 to 3.10.3 show the results for the three size ranges plotted from the data in TABLES 3.7.1 to 3.7.6. A logarithmic time scale was chosen to avoid congestion of the data in the initial reaction stages.

3.9.2 Estimation of the parameter A

Assuming that the reaction model is correct and that A is only a function of temperature, and possibly particle size for a given N_1O sample, the value of $(A)_{Temp., size}$ may be estimated from the equation:

$$-\ln(1-y_e) = A.f(t) \qquad ..... (3.11)$$

since each run was carried out at constant temperature and particle size. The observed values of y, i.e. y_e, were calculated from equation 3.14, and f(t) is defined by equation (3.12).

If the model is valid, a plot of $-\ln(1-y_e)$ vs. f(t), for corresponding values of y_e and t, should yield a straight line. Hence, if the variance of $-\ln(1-y_e)$ is constant over the range of y_e, A can be efficiently determined by linear regression. Now over most of the experimental range, the weight increments, $w_{H_2O_1}$, were approximately equal, hence:

$$\sum_{i=1}^{n} w_{H_2O_i} \approx N . w_{H_2O}$$

Therefore, since the value of time may be considered to be without error relative to the values of $-\ln(1-y_e)$, the variance of y_e ($\sigma^2_{y_e}$) is approximately equal to $N.\sigma^2_w$. This means that $\sigma^2_{y_e} \propto y_e$ (approx.) and that the variance of $-\ln(1-y_e)$ should be constant within sufficient limits over the range of y_e for the regression to be efficient. TABLES 3.8.1 to 3.8.3 list corresponding values of t, f(t), and $-\ln(1-y_e)$ for runs 1 to 18. These data are plotted in FIGURES 3.11.1 to 3.11.6; the slopes of these lines, which are the estimated values of A, were obtained by linear regression passing through the origin since y_e=0, t=0 is a boundary condition for the reaction. The values of A are summarized in TABLE 3.9.

3.10 Discussion of the Results

3.10.1 Cumulative degree of reduction vs. time

Time correction

Data for the cumulative degree of reduction vs. time are shown in TABLES 3.7.1 to 3.7.6. No time correction for the initial displacement of N_2 was introduced as the mean residence time of the gases in the reactor was of the order of 0.3 sec.

Error estimate for the observed degree of reduction

It is estimated that the accuracy of any one weighing to determine a weight increment $w_{H_2O_1}$, is within ±0.001 g. The mean value of the increments is of the order of 0.1 g, therefore the expected experimental error in the observed cumulative per cent reduction data is of the order of ± 1.0 per cent for any individual run.

The shape of the cumulative degree of reduction curve

These curves display the characteristic 'autocatalytic' shape reported in references (2), (3), (4), (5) and (6). In the present instance this shape is assumed to be caused by the slow initial rate of chemisorption of H_2 on the N_1O surface.

3.10.2 Evaluation of the parameter A

The linearity of $-\ln(1-y_e)$ vs. $f(t)$

As described in section 3.9.2, the value of the parameter A for each run is determined from a plot of $-\ln(1-y_e)$ vs. $f(t)$. For this estimation to be valid the data must exhibit a linear relationship. FIGURES 3.11.1 to 3.11.6 show plots of $-\ln(1-y_e)$ vs. $f(t)$. It is noticeable that for some runs the line has a slight 'wave' departure from linearity; this is particularly noticeable in FIGURE 3.11.1, run 11, and in FIGURE 3.11.2, run 7. The probable cause of this departure from linearity is the temperature transient, which due to the slightly exothermic nature of the reaction (see APPENDIX 3.2), was observed to follow a geometrically similar pattern. These temperature transient data are listed in TABLES 3.7.1 to 3.7.6. The values of temperature shown were attenuated and lag in time because of the 20 sec. time constant of the temperature measurement system.

It was thought that calculating A from a regression passing through the origin might unfavourably bias the estimate of A. However, a similar computation to that in APPENDIX 3.4 using estimates of A obtained with ordinary linear regression, gave statistically less significant results for the co-variation between $\log_{10}A$ and $\frac{1}{T}$, where T is the absolute reaction temperature K.

The variation of A for a particular nominal temperature

From FIGURES 3.11.1 to 3.11.6 and TABLE 3.9 it is evident that some variation exists in the values of A determined for any particular nominal temperature. This variation is not readily attributable to the differences in the mean run temperatures. Possible causes of this variation are:

(i) that the particle size affects the rate of reaction, or

(ii) some error in the temperature control and measurement for the duration of a reduction run.

Now the analysis in section 3.10.4 indicates that differences in particle size do not significantly affect the reaction rate. Therefore, it is probable that the observed differences in the values of A for a given nominal temperature are associated with errors in the temperature control and measurement.

3.10.3 The effect of temperature on the parameter A

An inspection of TABLE 3.9 shows that the temperature of reduction has a marked influence on the value of A, which ranges from 0.004 to 0.140 for a change in temperature from 300°C to 425°C. One of the assumptions of the model was that activated adsorption of H_2 was the rate controlling step for the reaction. Therefore, if the model is valid, it would be reasonable to expect that the relationship between the model parameter A and the absolute temperature of reaction could be represented by the Arrhenius equation:

$$\ln A = \text{const.} - \frac{E}{RT}$$

where A= model parameter, i.e. rate constant,

E= energy of activation, cal. per g mole,

R= gas constant, 1.987 cal.per g mole per .K,

and T= absolute temp. °K.

The data from TABLE 3.7 are plotted in FIGURE 3.12 with a logarithmic ordinate and a linear abscissa. The graph clearly indicates that the form of the Arrhenius equation accounts for the temperature dependence of A very satisfactorily. The numerical v alues of the const. and E are determined in section 3.10.5 from an equation developed in section 3.10.4.

3.10.4 The relative effects of particle size and temperature on the value of parameter A

From the data in TABLE 3.9 and from FIGURE 3.12 it is not immediately apparent whether variations in particle size significantly affect the value of A. To test for this significance an analysis of variance using the technique of multiple linear regression was made. For this regression the dependent variate was A, and the independent variates are the absolute temperature, T, and the mean particle size, $\bar{d}$. Because of the apparent functional relationship between A and T, indicated by FIGURE 2.12, and because the effect of variations in particle size on A, if any, would probably depend on the particle surface area, the multiple regression was calculated with the assumption that:

$$\log_{10}A = \phi\left(\frac{1}{T}, \log_{10}(\bar{d})\right) \qquad \ldots\ldots (3.15)$$

where A = model parameter,

T = absolute temp., $^{\circ}K$,

and $\bar{d}$ = mean particle size, in.

The analysis for which it was assumed that there was no interaction between the variates $\frac{1}{T}$ and $\log_{10}(\bar{d})$, is contained in APPENDIX 3.4. The results indicated that the regression coefficient for the size effect was very probably zero, hence, for the size range examined, the value of A may be considered to be independent of size. The final regression equation determined in APPENDIX 3.4 was:

$$\log_{10} A = \left(8.2717 - \frac{6.0634 \times 10^3}{T}\right) \qquad \ldots\ldots (3.16)$$

with $S.E._{\log_{10} A}$ = 0.1002 (standard error of estimate).

3.10.5 Estimation of the activation energy

Since equation 3.16 is similar in form to the Arrhenius equation, the activation energy can be estimated by changing the base of the logarithm and including R=1.987 in the equation, i.e.

$$\log_{10}A = (8.2717 - \frac{6.0634 \times 1.987 \times 10^3}{1.987 \times T})$$

$$\therefore \quad \ln A = (19.05 - \frac{27.75 \times 10^3}{RT}) \qquad \ldots\ldots (3.17)$$

Equation 3.17 indicates that the activation energy is 27,750 cal. per g mole. Fixed bed activation energies observed by other workers are listed in TABLE 3.1.

The values observed by PARRAVANO (3), 26,400 cal. per g mole, and HAUFFE and RAHMEL, 23,000 cal. per g mole, are in good agreement with the present value of 27,750 cal. per g mole. KUZNETSOV (5) quotes a value of 10,400 cal. per g mole, but does not indicate how it was determined. BANDROWSKI et al (6) obtained values for two parallel reactions of 14,380 and 12,420 cal. per g mole, respectively, which cannot be compared directly with a single estimate. From these data it is evident that the value of 27,750 cal. per g. mole is in reasonable agreement with the data obtained by other workers.

Because of the good fit of the Arrhenius relationship to the experimental data, it is likely that the overall reaction rate for the reduction of N_1O by H_2 under the experimental conditions existing in the fixed bed reactor, is determined by the chemical reaction rather than by mass transfer rates.

3.10.6 The validity of the model

For the purposes of this thesis an acceptable reaction model must be capable of describing the experimental data, and provided that the experimental conditions are known, must be able to predict results in good agreement with these data.

The linearity observed in FIGURES 3.11.1 to 3.11.6 is qualitative evidence to support the hypothesis of the model. In addition the values of y_e, the observed degree of reduction, and y, the degree of reduction predicted by the model equation, are compared in APPENDIX 3.5, using equations 3.9 and 3.16. The R.M.S. deviations between y and y_e were calculated for the eighteen experimental runs. The average of the R.M.S. values was 6.5 per cent. The maximum R.M.S. deviation observed was 12.8 per cent and the minimum 1.39 per cent. Since most of the variation can be assigned to the standard error of equation 3.16 for estimating A (presumably caused by lack of precision in the temperature measurement and control) it can reasonably be concluded that the model fulfils the requirements referred to in the introduction, section 3.1.

The fact that the observed functional relationship between ln A and $\frac{1}{T}$ conforms with the Arrhenius equation may be regarded as additional evidence supporting the model. However, the model is based only on broad theoretical considerations: the assumption that one step in a series of reaction processes can control the overall rate is not theoretically sound, but it is often a justifiable simplification for chemical engineering calculations, YANG and HOUGEN (16). In formulating this model scant consideration has been given to the intricacies of the actual heterogeneous mechanism which may involve mass transfer, heat transfer, adsorption, chemical reaction, solid state diffusion processes, and desorption. Hence, no claim is made by the writer that the simplified reaction mechanism shown to fit the observed values of reaction rate and degree of reduction actually establishes a definite reaction mechanism as this type of proof was beyond the scope of the present work.

3.11 Conclusions

The aim of the work described in this section was to attempt to establish the kinetic characteristics for the reduction of a sample of N_1O with H_2 with a view to using the information as a basis for studying the reduction of N_1O in a transport reactor. A study of the literature was made, and it was considered that although the literature provided a valuable qualitative guide the current state of published knowledge was inadequate for the purpose outlined above. Therefore a suitable reaction model was derived based on the adsorption theory of PARRAVANO (3) and a series of experiments carried out to check the validity of the model.

It is considered that the following conclusions are valid for the N_1O used in the work and that it could be reasonably assumed that other samples of N_1O would reduce in a similar way. The derived model fits the experimental data of BANDROWSKI et al (6) with the same degree of precision that it fits the experimental data obtained by the writer. Therefore, from the theoretical and experimental data discussed in this section of the thesis it may be concluded that:

(1) The degree of reduction, y, at time t of the sample of N_1O reduced at T^oK may be calculated from the following equations for $300^oC < Temp. < 425^oC$.

$$y = 1 - \exp - A\ \{(t + 1.0)[\ln(t + 1.0) - 1.0] + 1.0\} \quad \ldots\ldots (3.9)$$

$$\log_{10}A = (8.2717 - \frac{6.0634 \times 10^3}{T}) \quad \ldots\ldots (3.16)$$

with a mean expected precision of $\pm$ 6.5 per cent.

(2) The particle size over the range $^{35}/_{42}$, $^{42}/_{48}$ and $^{48}/_{60}$ (Tyler screen series), has no significant effect on the kinetics of the reduction of N_1O with hydrogen in a fixed bed.

(3) The activation energy for the reduction of the N_1O sample was 27,750 cal. per g mole which is in good agreement with the value of 26,400 observed by PARRAVANO (3).

TABLE 3.7.1 Results for the fixed bed reduction of N_1O at 300 °C

Results of runs: 1, 6, 11 Nominal Temperature: 300 °C Hydrogen flow rate: 12 litres/min N_1O sample weight: 5,000 g						
Mesh	35/42 #		42/48 #		48/60 #	
Run No.	1		6		11	
Time min.	$y_e \times 10^2$	Temp. °C	$y_e \times 10^2$	Temp. °C	$y_e \times 10^2$	Temp. °C
0	0.00	299	0.00	297	0.00	299
4	2.6	300	2.4	300	3.2	302
8	5.9	302	5.2	303	7.6	302
12	9.7	302	8.9	302	12.1	304
16	13.5	300	12.7	302	16.6	302
20	17.1	301	15.9	300	20.6	302
24	20.6	300	19.1	300	24.6	301
28	24.4	301	22.3	301	28.5	301
32	27.8	300	26.1	301	32.5	301
40	35.1	301	32.3	301	40.4	302
48	42.9	302	39.2	301	49.1	305
56	50.3	301	46.0	302	56.8	305
64	56.9	302	52.7	-	64.5	305

TABLE 3.7.2 Results for the fixed bed reduction of N_1O at 325°C

Results of runs: 2, 7 , 12
Nominal Temperature: 325°C
Hydrogen flow rate: 12 litres/min.
N_1O sample weight: 5,000 g

Mesh	35/42 #		42/48 #		48/60 #	
Run No.	2		7		12	
Time min.	$y_e \times 10^2$	Temp. °C	$y_e \times 10^2$	Temp. °C	$y_e \times 10^2$	Temp. °C
0	0.00	322	0.00	321	0.00	323
2	6.11	323	5.67	325	3.2	323
4	11.1	324	11.8	325	7.4	323
6	16.4	325	17.6	326	11.9	323
8	22.2	325	23.1	326	15.7	323
12	34.0	321	34.4	326	23.3	325
16	44.2	321	41.1	326	30.4	324
20	53.8	326	52.1	325	37.2	324
24	62.7	324	58.8	325	43.8	325
28	69.6	327	64.8	323	49.7	323
32	76.3	328	70.1	325	55.8	327
36	81.1	323	75.4	327	61.9	327
40	85.5	320	80.1	326	67.4	325
44	88.6	325	84.1	327	72.1	324
48	91.5	325	87.7	325	76.4	325
52	93.8	325	90.6	325	80.0	324
56	-	-	93.0	325	83.4	325
60	-	-	-	-	86.2	325

TABLE 3.7.3 Results for the fixed bed reduction of N_1O at 350°C

Results of runs: 3, 8, 13 Nominal Temperature: 350°C Hydrogen flow rate: 12 litres/min. N_1O sample weight: 5,000 g						
Mesh	35/42 #		42/48 #		48/60 #	
Run. No.	3		8		13	
Time min.	$y_e \times 10^2$	Temp. °C	$y_e \times 10^2$	Temp. °C	$y_e \times 10^2$	Temp. °C
0	0.00	344	0.00	345	0.00	347
2	9.58	345	11.8	348	5.20	347
4	21.4	348	29.4	353	12.7	343
6	32.9	350	40.0	355	20.3	345
8	43.2	350	51.3	354	29.1	351
10	52.4	350	61.2	347	38.8	353
12	61.3	351	69.5	348	48.1	353
16	75.7	349	82.8	349	64.7	354
20	85.7	349	91.4	347	78.0	351
24	92.3	349	96.0	345	87.4	350
28	96.1	347	98.0	349	93.4	353
32	98.1	348	98.7	348	97.1	349
36	98.9	-	98.9	350	98.8	350
40	99.4	-	99.1	347	-	-

TABLE 3.7.4 Results for the fixed bed reduction of N_1O at 375°C

Results of runs: 4, 9, 14 Nominal Temperature: 375°C Hydrogen flow rate: 12 litres/min. N_1O sample weight: 5,000 g						
Mesh	35/42 #		42/48 #		48/60 #	
Run No.	4		9		14	
Time min.	$y_e \times 10^2$	Temp. °C	$y_e \times 10^2$	Temp. °C	$y_e \times 10^2$	Temp. °C
0	0.00	369	0.00	369	0.00	367
1	10.2	372	9.9	375	4.3	370
2	22.7	373	22.1	378	11.0	371
3	33.2	374	32.4	379	19.1	373
4	42.0	374	41.3	379	27.4	374
6	56.6	375	56.6	378	43.9	377
8	68.0	374	70.3	379	60.3	379
10	77.5	374	80.2	379	74.7	378
12	85.4	374	87.1	379	86.9	375
16	95.3	374	94.3	378	97.3	373
20	98.6	373	97.7	378	-	-
24	99.3	373	98.7	377	-	-
28	99.6	375	-	-	-	-
32	99.9	-	-	-	-	-

TABLE 3.7.5 Results for the fixed bed reduction of N_1O at 400°C

Results of runs: 5, 10, 21
Nominal Temperature: 400°C
Hydrogen flow rate: 12 litres/min.
N_1O sample weight, 5,000 g

Mesh	35/42 #		42/48 #		48/60 #	
Run No.	5		10		15	
Time min.	$y_e \times 10^2$	Temp. °C	$y_e \times 10^2$	Temp. °C	$y_e \times 10^2$	Temp. °C
0	0.00	392	0.00	393	0.00	392
1	11.6	397	8.38	396	12.1	398
2	30.0	400	26.9	399	31.0	401
3	43.6	401	40.7	399	43.2	402
4	56.3	401	52.6	399	58.0	403
6	73.8	401	68.5	401	73.8	404
8	83.9	400	76.9	401	84.0	404
10	90.3	400	88.8	402	90.8	402
12	94.7	399	93.5	402	96.1	399
16	99.1	401	98.4	402	98.7	401
20	-	-	99.3	402	99.7	402

TABLE 3.7.6 Results for the fixed bed reduction of N_1O at 425°C

Results of runs: 16, 17, 18 Nominal Temperature: 425°C Hydrogen flow rate: 12 litres/min. N_1O sample weight: 5,000 g						
Mesh	35/42#		42/48#		48/60#	
Run No.	16		17		18	
Time min.	$y_e \times 10^2$	Temp. °C	$y_e \times 10^2$	Temp. °C	$y_e \times 10^2$	Temp. °C
0	0.00	419	0.00	417	0.00	414
1	18.4	426	33.9	421	30.6	421
2	46.7	427	56.1	424	51.8	424
3	72.7	427	72.6	424	66.9	426
4	89.4	425	83.2	424	77.8	426
6	94.7	424	95.7	425	90.0	424
8	97.4	425	99.1	425	96.4	423
10	-	-	-	-	98.8	423

TABLE 3.8.1 Tabulated data for corresponding values of t, f(t) and $-\ln(1-y_e)$ for runs 1, 6, 11, 2, 7 and 12.

Temperature		300°C			325°C		
Mesh		35/42 #	42/48 #	48/60 #	35/42 #	42/48 #	48/60 #
Run No.		1	6	11	2	7	12
Time min.	f(t)	$-\ln(1-y_e)$	$-\ln(1-y_e)$	$-\ln(1-y_e)$	$-\ln(1-y_e)$	$-\ln(1-y_e)$	$-\ln(1-y_e)$
0	0.00	0.00	0.00	0.00	0.00	0.00	0.00
2	1.30	-	-	-	.0629	.0584	.0325
4	4.05	.0263	.0242	.0325	.117	.125	.0767
6	7.65	-	-	-	.180	.194	.127
8	11.80	.0608	.0534	.0790	.250	.263	.171
12	21.4	.102	.0932	.129	.415	.420	.265
16	32.3	.145	.136	.182	.581	.530	.362
20	44.0	.188	.173	.231	.774	.735	.465
24	56.6	.231	.212	.282	.986	.887	.526
28	70.6	.280	.252	.336	1.19	1.04	.686
32	83.5	.326	.303	.393	1.44	1.21	.816
36	97.9	-	-	-	1.67	1.40	.964
40	113	.432	.390	.517	1.93	1.61	1.12
44	127	-	-	-	2.18	1.84	1.28
48	143	.560	.496	.675	2.46	2.10	1.44
52	159	-	-	-	2.76	2.36	1.61
56	175	.700	.616	.838	-	2.66	1.80
60	192	-	-	-	-	-	1.98
64	208	.840	.706	1.035	-	-	-

TABLE 3.8.2 Tabulated data for corresponding values of t, f(t) and $-\ln(1-y_e)$ for runs 3, 8, 13, 4, 9 and 14.

Temperature		350°C			375°C		
Mesh		35/42	42/48	48/60	35/42	42/48	48/60
Run No.		3	8	13	4	9	14
Time min.	f(t)	$-\ln(1-y_e)$	$-\ln(1-y_e)$	$-\ln(1-y_e)$	$-\ln(1-y_e)$	$-\ln(1-y_e)$	$-\ln(1-y_e)$
0	0.00	0.00	0.00	0.00	0.00	0.00	0.00
1	0.38	-	-	-	.109	.104	.0440
2	1.30	.101	.126	.0534	.254	.250	.116
3	2.56	-	-	-	.403	.392	.212
4	4.05	.242	.334	.138	.545	.533	.320
6	7.65	.398	.510	.227	.835	.835	.577
8	11.8	.566	.720	.344	1.14	1.21	.924
10	16.3	.745	.946	.490	1.49	1.62	1.37
12	21.4	.948	1.19	.655	1.92	2.04	2.03
16	32.3	1.41	1.76	1.04	3.04	2.86	3.61
20	44.0	1.94	2.44	1.51	-	3.76	-
24	56.6	2.44	3.22	2.07	-	4.35	-
28	70.6	3.26	3.90	2.72	-	-	-
32	83.5	3.94	4.30	3.54	-	-	-
36	97.9	4.55	4.55	4.42	-	-	-
40	113	-	4.71	-	-	-	-

TABLE 3.8.3 Tabulated data for corresponding values of t, f(t) and $-\ln(1-y_e)$ for runs 5, 10, 15, 16, 17 and 18.

Temperature		400°C			425°C		
Mesh		35/42	42/48	48/60	35/42	42/48	48/60
Run No.		5	10	15	16	17	18
Time min.	f(t)	$-\ln(1-y_e)$	$-\ln(1-y_e)$	$-\ln(1-y_e)$	$-\ln(1-y_e)$	$-\ln(1-y_e)$	$-\ln(1-y_e)$
0	0.00	0.00	0.00	0.00	0.00	0.00	0.00
1	0.38	.123	.0875	.129	.203	.416	.368
2	1.30	.361	.314	.371	.629	.823	.733
3	2.56	.573	.522	.565	1.30	1.30	1.11
4	4.05	.832	.746	.867	2.24	1.78	1.51
6	7.65	1.34	1.15	1.34	2.94	3.15	2.31
8	11.8	1.83	1.59	1.83	3.65	4.71	3.32
10	16.3	2.33	2.12	2.38	-	-	4.42
12	21.4	2.94	2.74	3.24	-	-	-
16	32.3	4.70	4.14	4.34	-	-	-
20	44.0	-	4.96	5.80	-	-	-

TABLE 3.9 Summary of predicted values of A for runs 1-18 inclusive

			Predicted values of A, runs 1-18		
Temperature			Mesh		
°C	°K=T	$10^3/T$	35/42#	42/48#	48/60#
300	573	1.745	.00404	.00359	.00491
325	598	1.672	.0175	.0152	.0102
350	623	1.605	.0459	.0512	.0385
375	648	1.543	.0996	.0905	.0942
400	673	1.486	.154	.130	.147
425	698	1.433		.395 .439 .313	

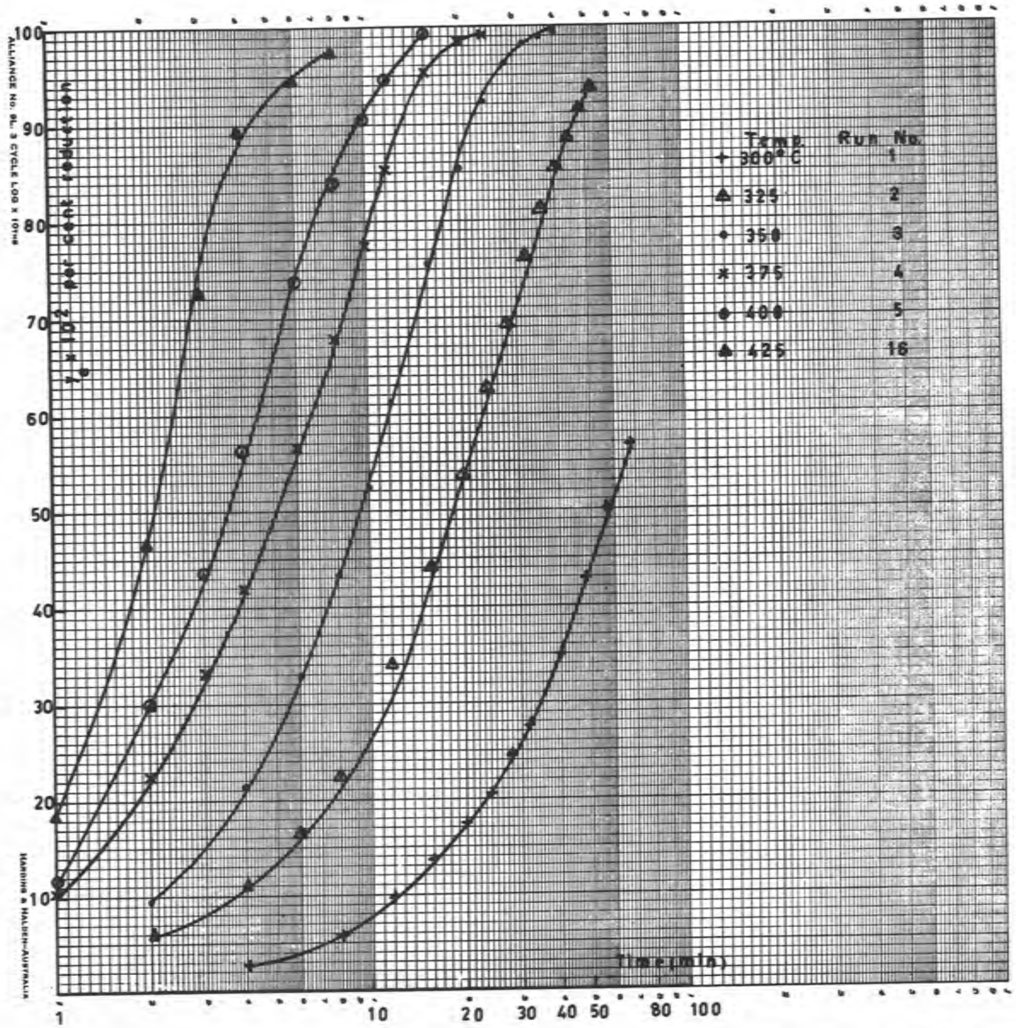

FIGURE 3.10.1 Per cent reduction vs. log time(min) for the reduction of NiO ($^{35}/_{42}$ mesh) with H_2 in a fixed bed

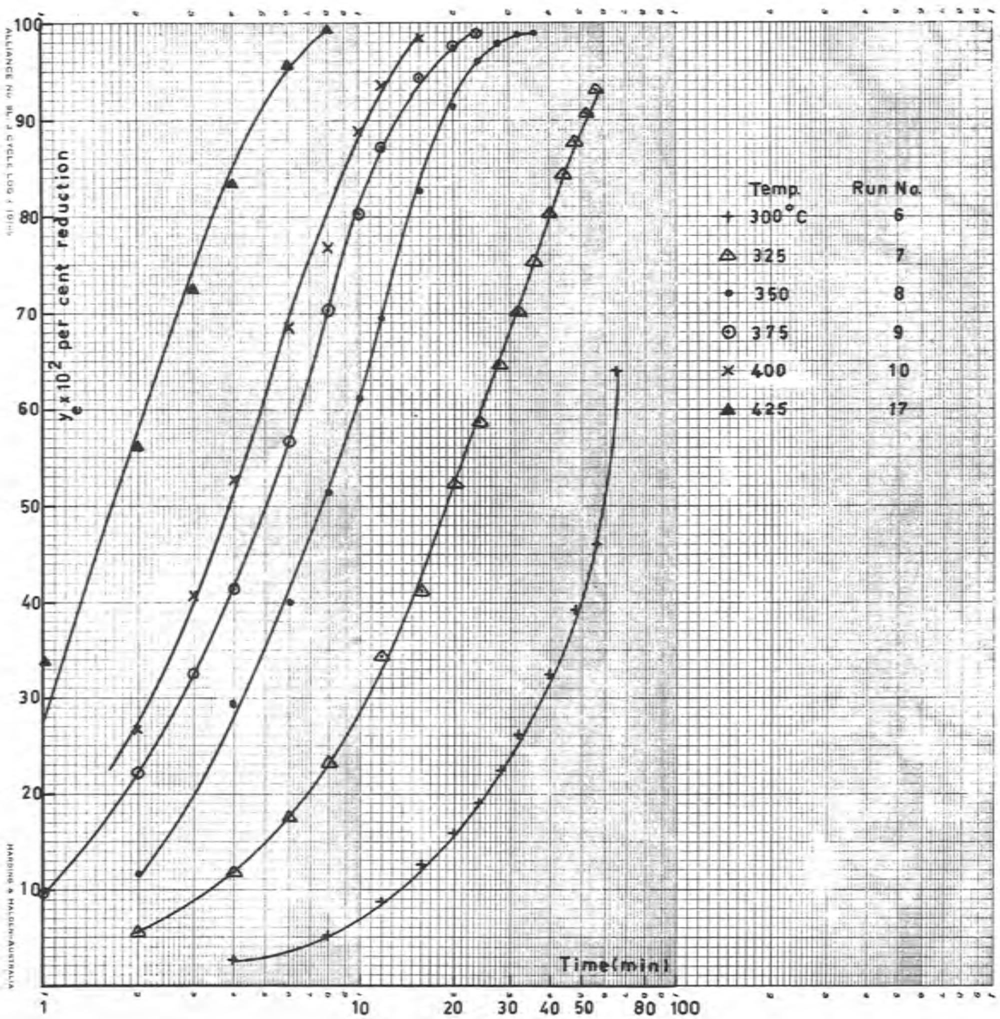

FIGURE 3.10.2 Per cent reduction vs. log time(min) for the reduction of NiO($^{42}/_{48}$mesh) with H_2 in a fixed bed

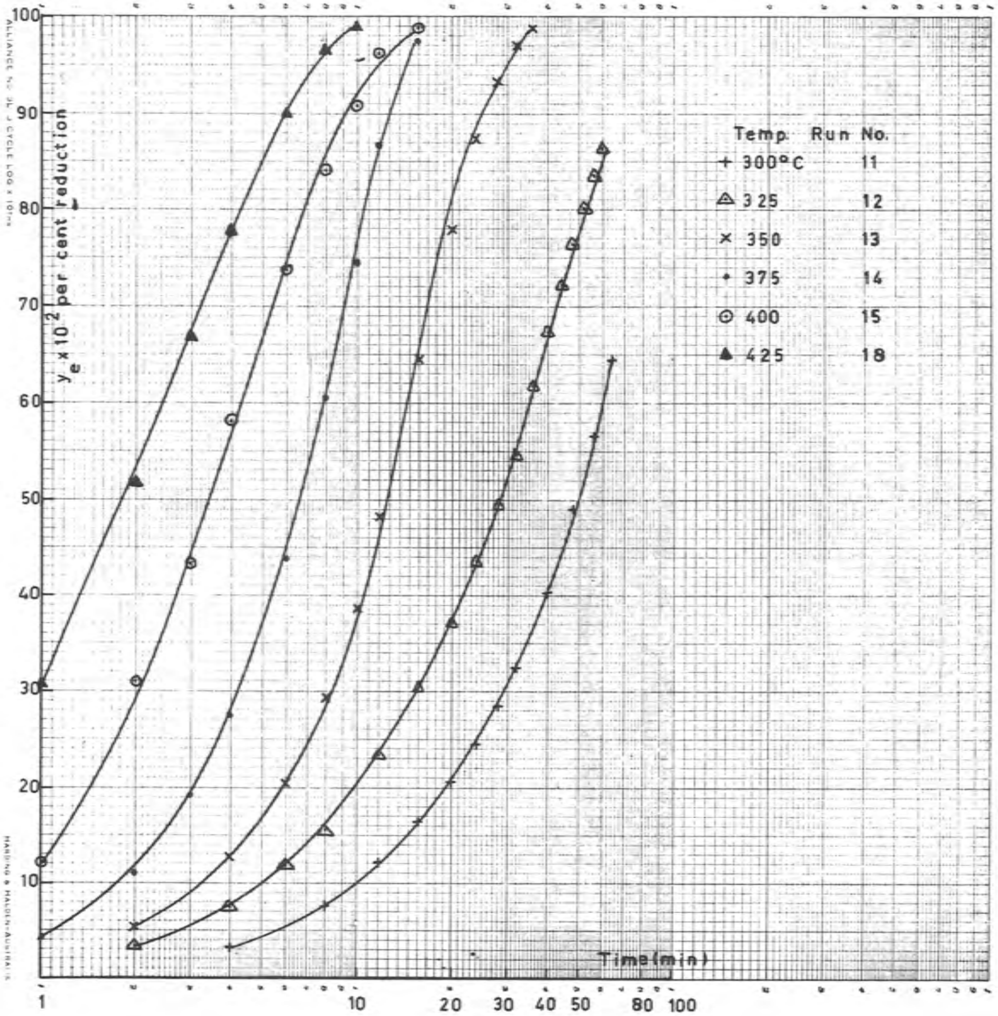

FIGURE 3.10.3 Per cent reduction vs. log time(min) for the reduction of NiO($^{48}/_{60}$ mesh) with H_2 in a fixed bed

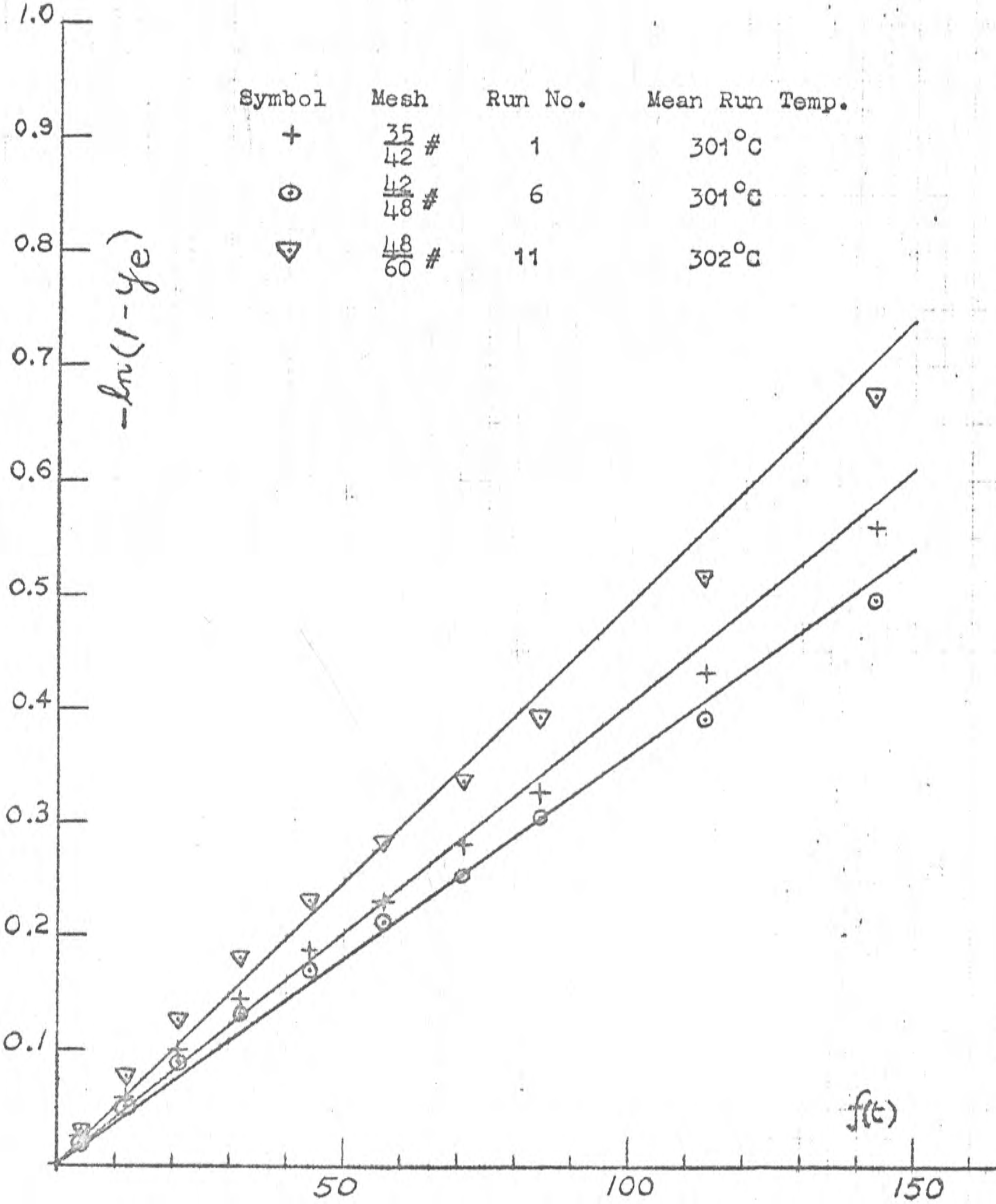

FIGURE 3.11.1 Linear plot of $-\ln(1-y_e)$ vs. $f(t)$ for the determination of parameter A for nominal run temperature 300°C

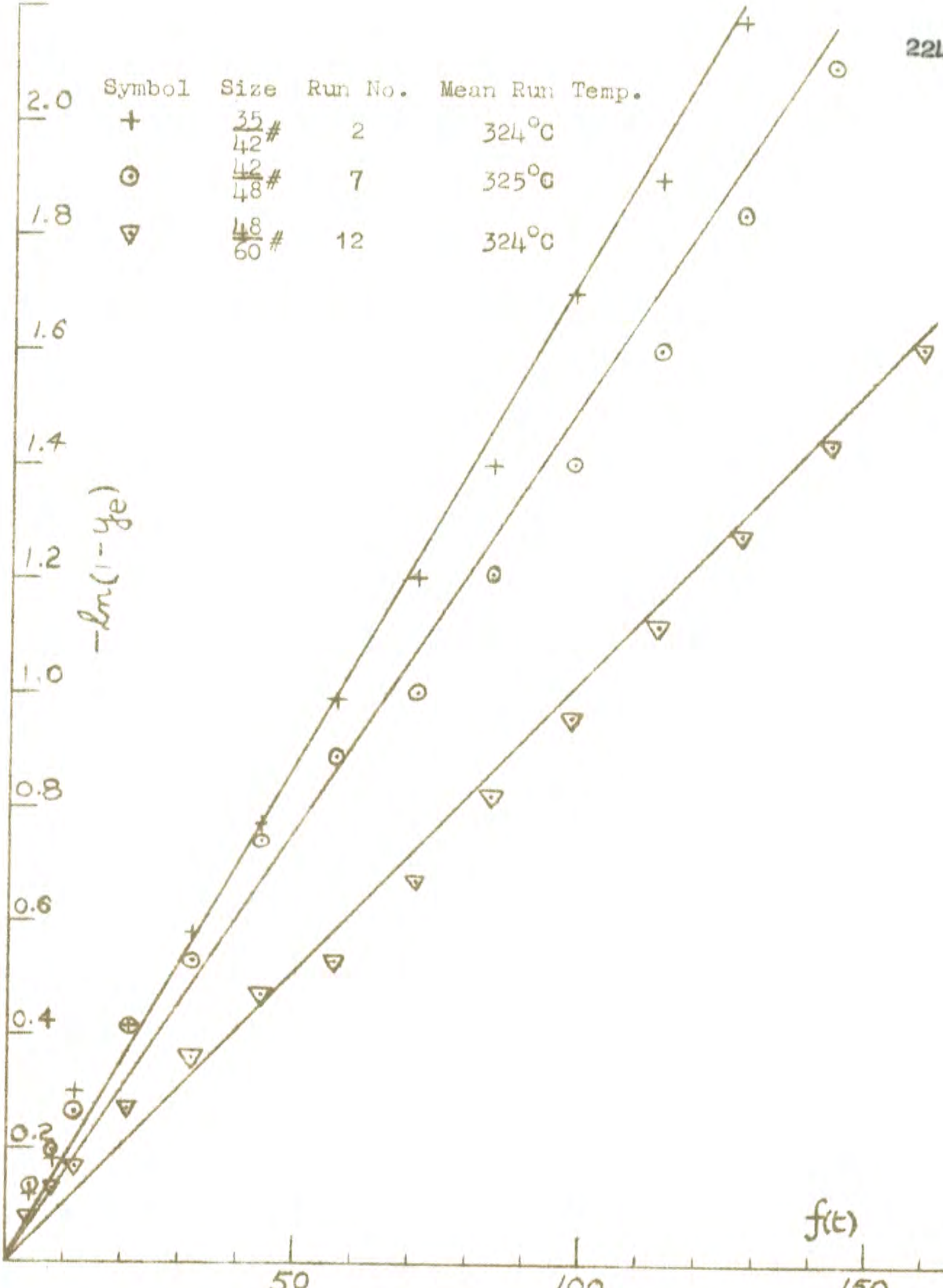

FIGURE 3.11.2 Linear plot of $-\ln(1-y_e)$ vs. $f(t)$ for the determination of parameter A for a nominal run temperature of 325°C

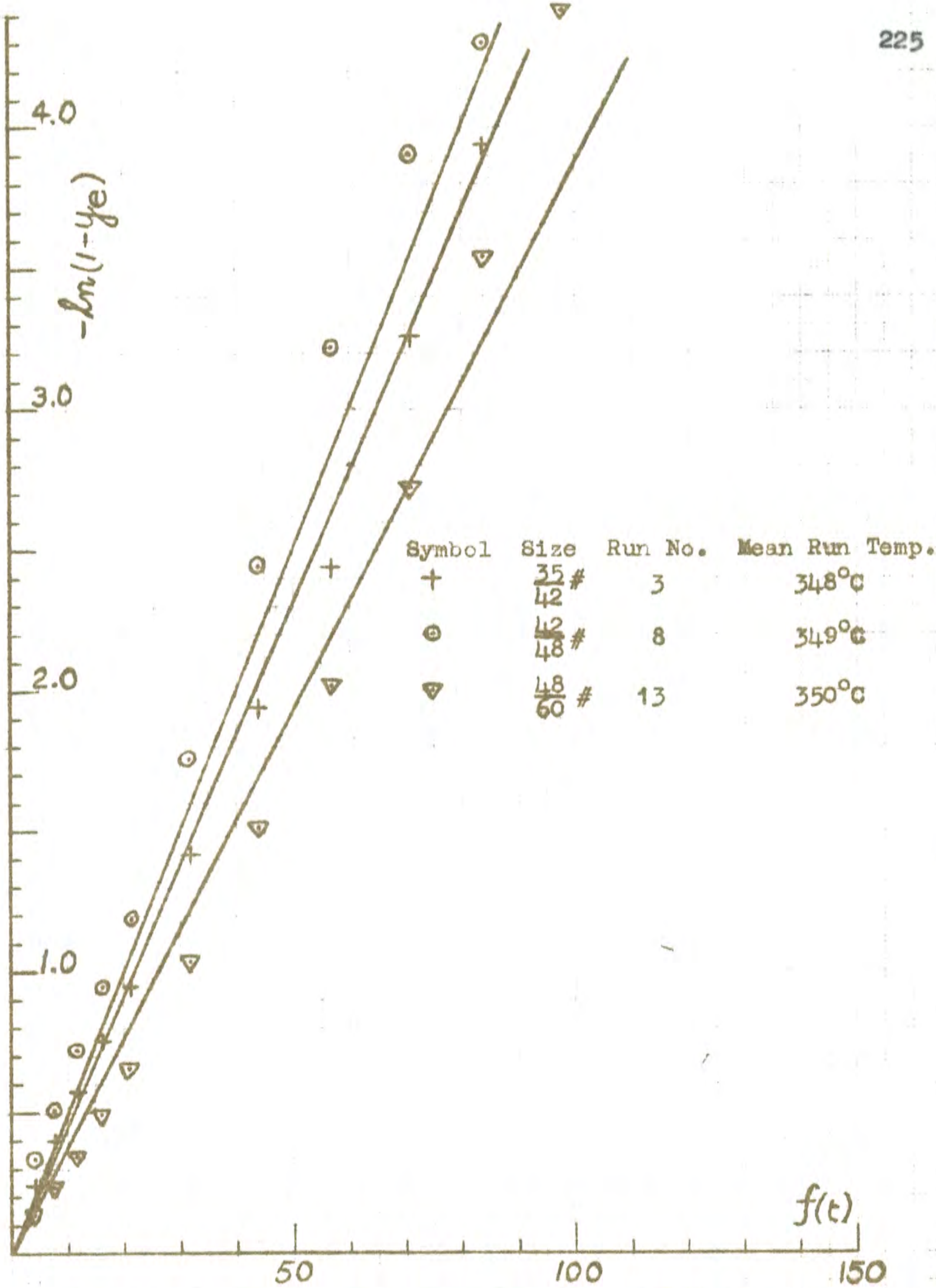

FIGURE 3.11.3 Linear plot of $-\ln(1-y_e)$ vs. f(t) for the determination of parameter A for nominal run temperature 350°C

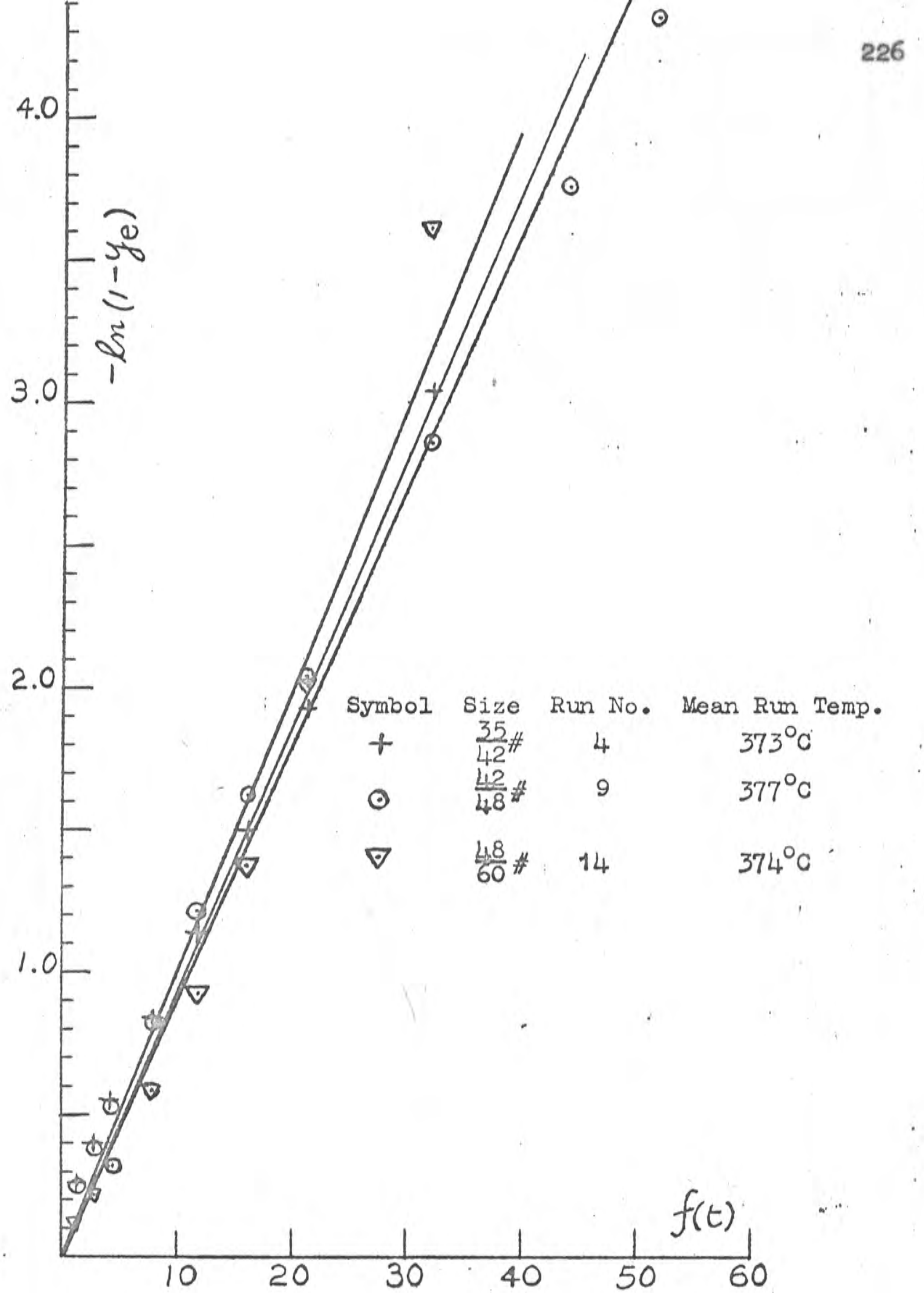

FIGURE 3.11.4 Linear plot of $-\ln(1-y_e)$ vs. f(t) for the determination of parameter A for nominal run temperature 375°C

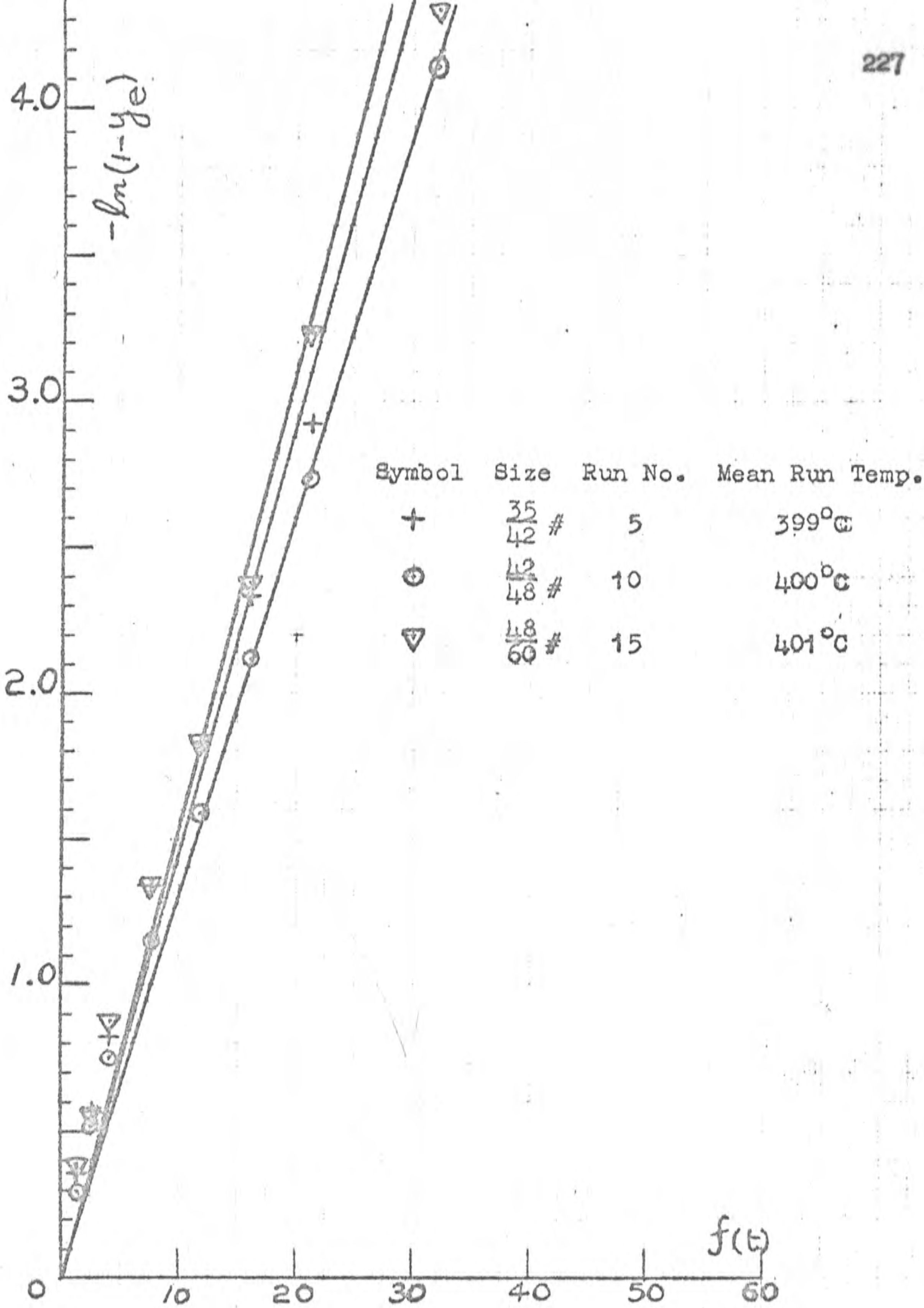

FIGURE 3.11.5 Linear plot of $-\ln(1-y_e)$ vs. $f(t)$ for the determination of the parameter A for nominal run temperature 400°C

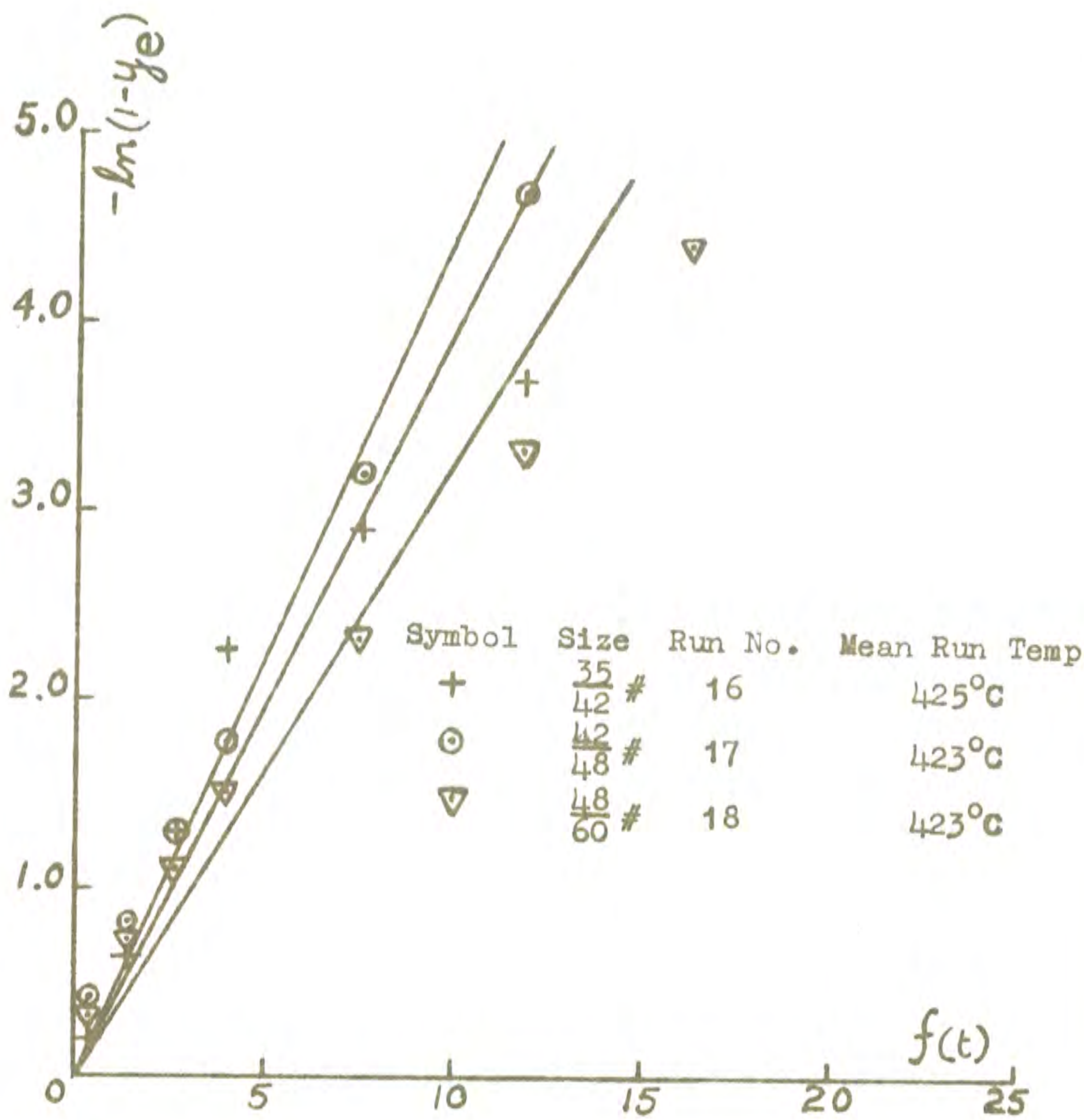

FIGURE 3.11.6 Linear plot of $-\ln(1-y_e)$ vs. f(t) for the determination of the parameter A for nominal run temperature 425°C

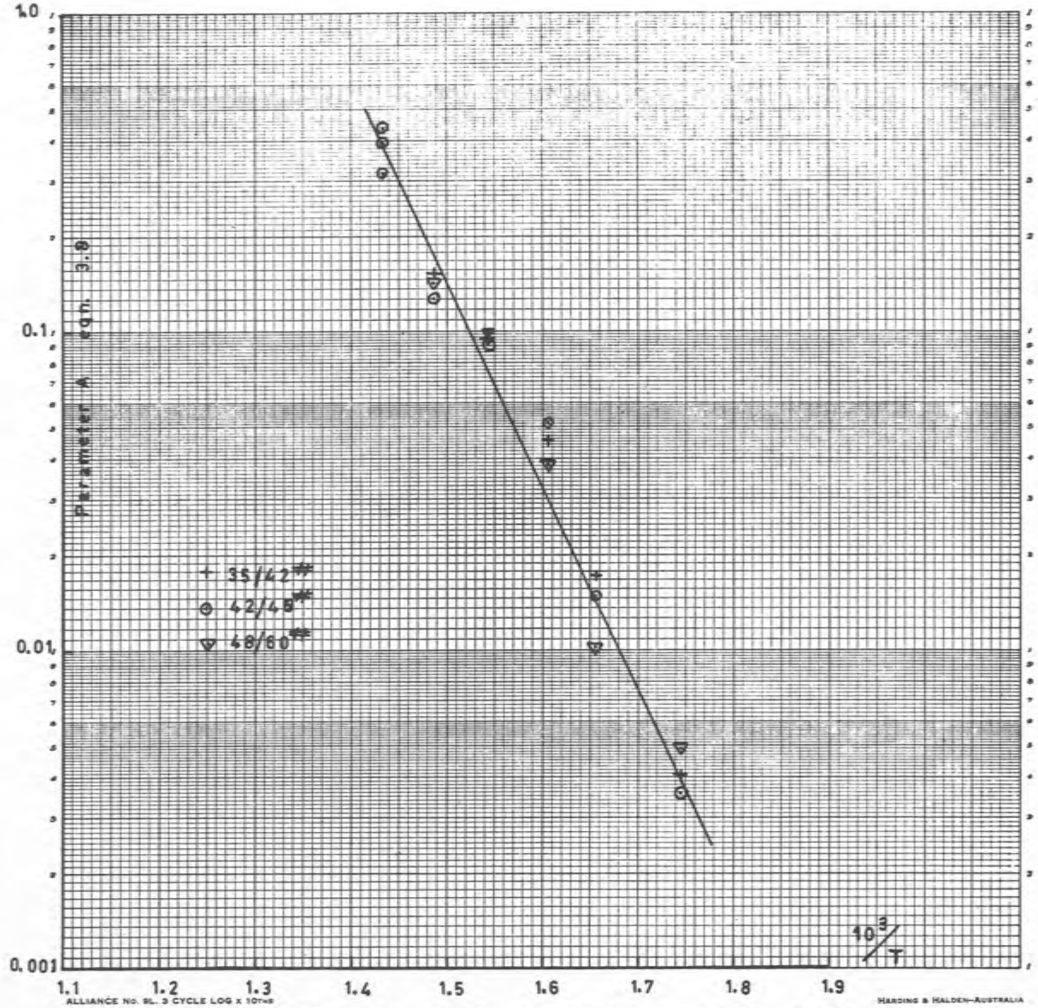

FIGURE 3.12 Arrhenius plot for the fixed bed reduction of NiO with hydrogen

4 THE TRANSPORT REDUCTION OF NICKEL MONOXIDE WITH HYDROGEN

4.1 Introduction

The aim of the work described in this section is to study the kinetics of the reduction of N_1O with H_2 in a transport reactor and to compare the results with those obtained for the reduction of N_1O in a fixed bed. As with the fixed bed work, actual reaction rates are not measured but rather the degree of conversion for various residence times and temperatures. Because the method of preparation of the N_1O has been shown to effect the kinetics of the reaction (BENTON and EMMETT (2)), the N_1O used in these experiments was taken from the same sample as the material used in section 3.

In order to obtain some quantitative measure of the reaction rates occurring in the transport reactor and the degree of control of the particle residence time, some estimate of the particle residence time must be made. It is proposed to use the model developed in section 2 relating the average solids velocity to the solids pressure drop for this purpose.

In addition to the above objectives, which are specific to the reduction of N_1O with H_2, the experiments should give some indication of the general suitability of this type of reactor for gas-solids reactions at high rates which require low residence times.

Following a discussion of the literature the experimental technique is explained and the apparatus described. The remaining sections deal with the experimental procedure and the analysis of the results.

4.2 Literature Review

Chemical reactions in the dilute fluidized phase have been described in the literature by LLOYD and AMUNDSON (71), DALLA LANA and AMUNDSON (72), THEMELIS and GAUVIN (73), GAUVIN and GRAVEL (74), and CULVER and GOMEZ (75). The work reported by THEMELIS and GAUVIN (73), and GAUVIN and GRAVEL (74), was for downward co-current gas-solids flow. THEMELIS and GAUVIN (73) studied the reduction of fine (5 to 102 microns) iron oxide with hydrogen. GAUVIN and GRAVEL (74) reported studies of the following reactions: reduction of iron oxide with hydrogen, denitration of uranyl nitrate, roasting of pyrites, decomposition of ferrous and nickel sulphates and conversion of sodium sulphate to sodium carbonate. The uranyl nitrate, the ferrous and nickel sulphates, and the sodium sulphate were fed into the top of the reactor as solutions. The iron oxide was fed into the reactor from a spouted bed and the pyrites from a screw feeder. While these studies are only of secondary interest to the present work, many of the problems associated with furnaces, temperature measurement, gas flow control and metering, solids separation and solids feeding, are similar to those encountered in upward gas flow co-current gas-solid reactions.

The equipment used for the experimental work described in this section of the thesis is a unit in which gas-solid reactions are carried out during the upward flow of both phases; this unit is defined as a transport reactor. LLOYD and AMUNDSON (71) investigated the reduction of fine iron oxides with hydrogen in a transport reactor while CULVER and GOMEZ (75) studied the oxidation of galena (PbS) with oxygen-nitrogen mixtures. In the transport reactor the solid and gas phases are contacted by means of techniques similar to those described in section 2.4. However, when a chemical reaction occurs between the gas and the solid particles, an analysis of the system must include the factors which influence the rates and the equilibrium states of the chemical reactions. The main factors concerned are the temperature of the reacting particles in the reaction zone and the length of time the particles remain in this zone; and in some instances the reaction zone pressure may be important.

4.2.1 Reactor design and materials handling

Reactor design

Risers with high length:diameter ratios have been used for transport reactors, viz. 2.7 m:27 mm (71), 16 ft:2.0 in (72), and 36 in.:1.0 in (75). The reaction zone is usually confined to the lower part of the riser, the upper section being used to cool the gas-solid mixture; the gas entering the reaction zone being normally preheated. The apparatus as described in references (72) and (75) both used concentric tube water cooled heat exchangers in the upper section of the riser, and in addition CULVER and GOMEZ (75) chilled the stream leaving the reaction zone by admitting cold nitrogen at the top of the reactor.

Gas flow control

Single pass gas flow systems were employed in the three apparatuses described in references (71), (72) and (75). The gases were supplied in high pressure cylinders, passed through the apparatus and vented to atmosphere. LLOYD and AMUNDSON (71) and CULVER and GOMEZ (75) metered both inlet and outlet gas flows, but DALLA LANA and AMUNDSON (72) metered only the inlet gas flow. Control of the gas flow in all cases (refs. (71),

(72) and (75)) was achieved with suitable pressure regulators and needle valves.

Solids handling

DALLA LANA and AMUNDSON (72) and CULVER and GOMEZ (75) used similar solids feeding techniques, viz. screw feeders discharging into an auxiliary gas stream which in turn passed into the bottom of the reactor. LLOYD and AMUNDSON (71) simply elutriated particles from a fluidized bed situated below the reactor and hence had no direct control over the particle feed rate. The reacted solids have usually been separated from the gas in small cyclones (refs. (72), (75)), but LLOYD and AMUNDSON (71) made use of an electro-magnet as the reacted solid (Fe_3O_4) was magnetic.

4.2.2 Particle residence times

The concept of average particle velocity was discussed in section 2.3 and a model was proposed which related the average particle velocity to the solids pressure drop. If the particle residence time is uniform, i.e. the particles move through the reactor in plug flow, (or approximate plug flow to such an extent that deviations of individual particle residence times from the mean particle residence time are small compared with the mean value), then the mean residence time calculated from the average velocity should be valid for a kinetic analysis of reactions carried out in a transport reactor. However, conditions in the reactor could give rise to a wide distribution of particle residence times, especially at low average velocities when some particles could have negative (i.e. downward) velocities for some of the time spent in the reaction zone. Downward particle flow near the riser walls was noticed by STEMERDING (63) in his study of the vertical transport of fine catalyst particles. Particle size distribution gas velocity distribution over the riser cross section, and solids friction could contribute to the distribution of particle residence times.

DALLA LANA and AMUNDSON (72) developed an expression for the mean particle residence time when the transporting fluid was in laminar flow. The analysis included the distribution of residence times due to the particle size and gas velocity distributions; however, the derivation is not valid if the particle diameter exceeds 30 microns. Serious limitations of their model include the assumptions that particles settling near the wall are not re-entrained and particles are not transported radially. This latter assumption means that the effect of particle-wall friction has been neglected.

4.2.3 Particle temperature

The temperature reached by particles in the reaction zone of a transport reactor will depend on the relative contributions of the following factors:

(i) the rate of heat transfer to or from the particle by convection,

(ii) the rate of heat transfer to or from the particle by radiation, and

(iii) the heat of reaction, whether endothermic or exothermic.

LLOYD and AMUNDSON (71) and DALLA LANA and AMUNDSON (72) both assumed that fine particles reached the reaction zone temperature very rapidly. Recently THEMELIS and GAUVIN (76) have calculated particle temperatures in the reaction zone assuming that the gas did not absorb or emit significant thermal radiation. This analysis refers to fine particles where $R_{e_p} < 1.0$ and takes convection, radiation and heat of reaction into account; allowance is also made for a longitudinal temperature gradient in the reaction zone. For the hydrogen reduction of fine iron oxide it was concluded that heat transfer by convection was the most significant factor determining the particle temperature and that the particle temperature very rapidly approached the gas temperature (to within 2°F in approximately 0.1 sec. for a 76 micron particle.)

4.3 Experimental Technique

The object of the experimental work described in section 4 was to study the reduction of nickel oxide with hydrogen in a transport reactor and to compare the rates of reduction observed with those obtained for the fixed bed reduction of nickel oxide.

In order that some assessment of the performance of the reactor can be made the following information is required:

(i) kinetic and thermodynamic data, including reaction equilibria and heats of reaction for the conditions prevailing in the reactor, as discussed in section 3,

(ii) the temperature of the transporting fluid in the reaction zone,

(iii) the residence time of the particles in the reaction zone, and

(iv) the degree of conversion obtained in the transport reactor.

The experiments should enable estimates of the values of the variables mentioned in (ii), (iii) and (iv) to be made. Ideally the particle temperature should have been measured, but THEMELIS and GAUVIN (76) have shown that this approaches the gas temperature very rapidly, therefore the gas temperature will be used as a measure of the particle temperature.

4.3.1 Basic flowsheet of the apparatus

The apparatus had to incorporate all the facilities normally associated with a pneumatic transport system plus those required for a chemical reactor, i.e. provision had to be made for gas heating and cooling, and special gas metering, as well as solids feeding, gas circulation, and gas-solids separation. The apparatuses of several previous workers [refs. (71), (72) and (73)] were designed with single pass gas flow systems, i.e. the gas flowed from high pressure storage cylinders through the apparatus and was then vented to atmosphere. However, for the reaction:

$$N_1O_{(s)} + H_{2(g)} = N_{1(s)} + H_2O_{(g)}$$

the only gaseous reaction product formed is easily removable from the reactor exit stream, therefore it was proposed to maintain the apparatus at constant pressure with make-up hydrogen and to recirculate the gas. This procedure had two distinct advantages when compared with a single pass system, viz.:

(i) in transport reactors there is always a high gas:solid ratio, and in a single pass system the excess of gaseous reactant is wasted, and

(ii) the degree of conversion of NiO could be monitored by measuring the amount of water vapour removed from the system and also by measuring the make up hydrogen required to keep the system at constant pressure.

A schematic flowsheet of the apparatus is shown in FIGURE 4.1. The reaction zone can be considered as the section of the riser between the solids feed point and the bottom of the reactor cooler.

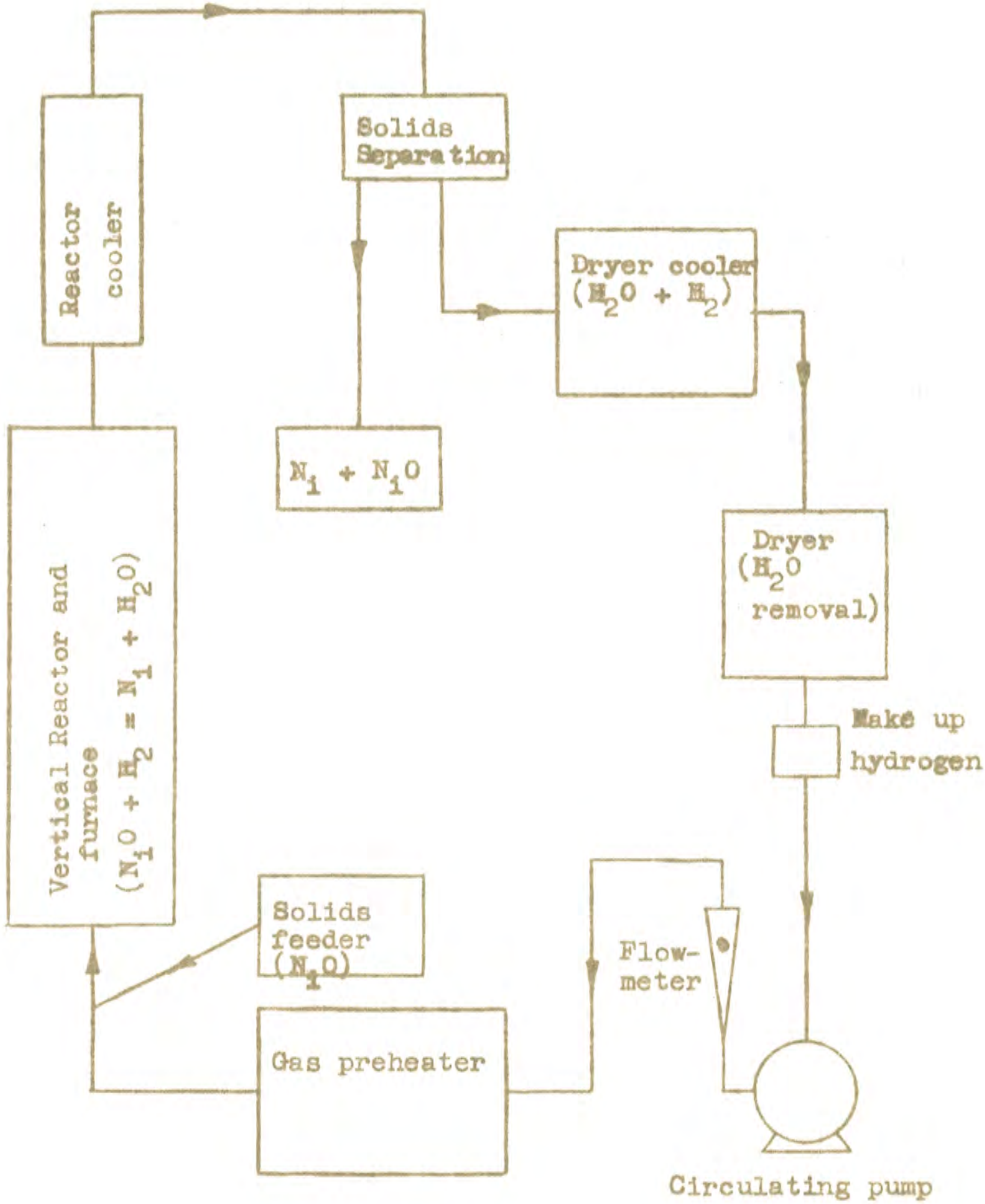

FIGURE 4.1 Schematic diagram of a transport reduction system

4.3.2 Temperature control and measurement

Since the heat capacity of the gas stream in dilute phase transport is much greater than that of the entrained solids, an isothermal reaction zone was maintained by controlling the gas temperature at both the reactor inlet and outlet. These temperatures were controlled by varying the power input to the preheater and the reactor furnaces respectively. Because of the effect of thermal radiation on the temperature sensing devices (thermocouples) it was difficult to obtain an accurate measure of the gas temperature. However, to obtain an estimate of the required radiation correction, which was calculated with the aid of a computer, provision was made for monitoring the pipe wall temperature near the temperature measuring elements.

4.3.3 Estimation of the particle residence time

It is proposed to estimate the average particle residence time in the system from measurements of the pressure drop over the reactor and the model developed in section 2 which relates the average particle velocity to the solids pressure drop.

4.3.4 Measurement of the degree of conversion

It was mentioned in section 4.3.1 that with the reaction:

$$N_1O + H_2 = N_1 + H_2O$$

occurring in a closed system, two simultaneous methods were available for measuring the degree of conversion. First the water formed during the reaction could be removed with a suitable desiccating agent and weighed, or second the volume of make up hydrogen to keep the system at constant pressure could be measured. The stoichiometry of the reaction shows that for every mole of hydrogen consumed a mole of water is formed. Therefore, if both methods are used a check is obtained on the estimate of the degree of reaction. In the experiments described in this part of the work this latter technique is adopted.

The degree of conversion could also have been measured by direct analysis of the partially reduced product; however, re-oxidation may occur when the product is exposed to the air.

4.4 Description of the Apparatus

A flowsheet of the transport reduction apparatus is shown in FIGURE 4.2 and the arrangement of the pressure regulated gas supply is shown in FIGURE 4.3. FIGURE 4.4 is a more detailed diagram of the reactor, reactor furnace, and solids feeder. FIGURE 4.5 shows the main wiring layout for the reactor and preheater furnaces and includes the thermocouple connections for the preheater and reactor exit thermocouples (T1 and T2). FIGURES 4.6 to 4.8 illustrate sections of the apparatus, viz.:

- FIGURE 4.6 Photograph of control panel and reactor section
- FIGURE 4.7 Photograph of vane pump, valve system, dryer cooler and dryer
- FIGURE 4.8 Photograph of reactor cooler and solids collection system

4.4.1 Pipework, jointing and valves

Pipework

The pipework in the apparatus was fabricated from "COMSTEEL 25/20" heat resistant stainless steel in the high temperature zones and from cold drawn copper

Legend for FIGURE 4.2

(1) Preheater

(2) Solids feeder

(3) Reactor and reactor furnace

(4) Reactor cooler

(5) Expansion loop

(6) Solids separation system

(7) Cooler fro drying unit

(8) Drying unit

(9) Vane pump

(10) Flowrator

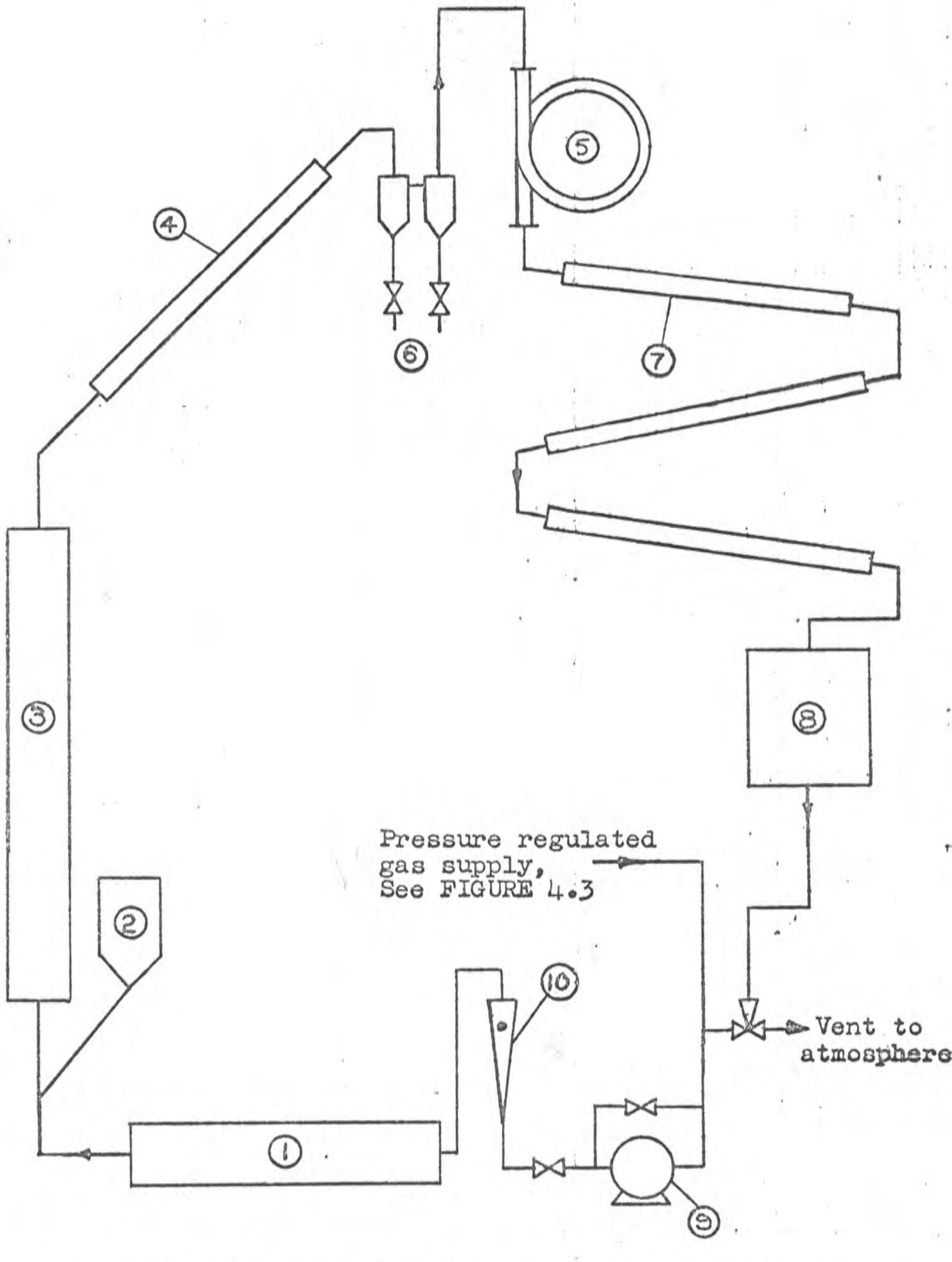

FIGURE 4.2 Flowsheet of apparatus used for the transport reduction of N_iO with H_2

tubing in the low temperature zones. In the low temperature zones some connections were made with plastic hose where flexibility was required.

Jointing

In view of the hazard presented by hydrogen-air mixtures, especially at high temperatures, care was taken to minimize hydrogen leakage from the apparatus. This was done by reducing the number of breakable joints to a minimum (in fact, as far as possible the high temperature circuit was welded 'in situ') and by the use of effective jointing techniques. Joints in the high temperature zone were made by bolting 3.0 in. diam. flanges together with six ½ in. high tensile steel bolts located on a 2½ in. diam. pitch circle. The gaskets were cut from asbestos millboard and were soaked in water for 12 hr. before fitting. Screw threads (e.g. thermocouple glands) in the high temperature zone were sealed with a litharge and glycerine cement. Joints in the cold drawn copper tubing were made with "Flowline" capillary soldered fittings; screw threads in the low temperature zone were sealed with "PERMACEL" Teflon tape. Plastic hoses were sealed with "CHEYNEY" threaded band hose clips.

Valves

The vane pump and the low pressure gas make up flows were controlled by ¼ in. needle valves, as seen in FIGURE 4.3; elsewhere plug valves were used.

4.4.2 Solids feeder

The function of this unit was to admit fine granular N_1O particles to the bottom of the reactor. The N_1O was charged to the feeder from the twin valve gas lock, which was always maintained at a positive hydrogen pressure, so that no air could leak into the apparatus. As shown in FIGURE 4.4, the feeder was driven via a speed reduction unit by a variable speed D.C. motor. The motor speed was controlled by varying the armature voltage with an autotransformer coupled to a silicon diode full wave rectifier. Also shown in FIGURE 4.4 is a mercury seal which prevents hydrogen leakage along the screw spindle where it passes through the top of the feeder. To ensure free flow of the solids in the connecting tube between the feeder and the reactor base, a magnetic vibrator was connected to the tube.

4.4.3 Reactor

A schematic diagram of the reactor assembly is shown in FIGURE 4.4. The reactor tube was fabricated from 1.0 in. bore 16 gauge heat resistant stainless steel tube (COMSTEEL 25/20) and was heated by a 2.0 Kw silica tube furnace wound with nichrome wire and then coated with alundum cement, and the furnace contained in a 6.0 in.

bore asbestolite pipe packed with Kieselguhr insulation. The actual reactor length was 6 ft. 3 in.

4.4.4 Reactor cooler

The reactor cooler was a concentric tube water cooled heat exchanger fabricated from molybdenum stabilized stainless steel with an effective heat transfer surface of 0.5 sq.ft.

4.4.5 Reacted solids collection system

The collection system comprised two units in series, a reverse flow particle trap for coarse particles and a 1.0 in. diam. cyclone for fine particles. The particles dropped into two small canisters, as shown in FIGURE 4.2.

4.4.6 Expansion loop

The reactor expanded approximately $\frac{1}{2}$ in. in length when heated to temperatures in the vicinity of 700°C. A loop of $\frac{3}{4}$ in. diam. annealed copper tubing, located after the solids collection system, allowed for this expansion.

4.4.7 Dryer cooler

Before the reactor effluent gases entered the dryer they were further cooled to ensure efficient drying. The dryer cooler was a concentric tube water cooled heat exchanger with a total heat transfer area of 6.0 sq. ft.

4.4.8 Drying unit

The water formed in the reaction, viz.:

$$N_1O + H_2 = N_1 + H_2O$$

was removed in this unit, which is shown in the foreground of the photograph FIGURE 4.7. The two main problems in the design of a suitable dryer were:

(i) the drying unit must be removable and of sufficiently small bulk to be weighed on an accurate balance,

and (ii) the pressure drop had to be kept to a reasonably low figure commensurate with the design of the rest of the apparatus, i.e. several inches water gauge.

The requirement of the first point is self explanatory while that of the second indicates that a unit with a low length:diameter ratio and a coarse granular desiccant should be used. The dryer was constructed from a B55 Pyrex cone and socket joint and filled with ⅛ in. cylindrical pellets of Union Carbide 5A Linde molecular sieves. The weight changes of the dryer (and the amount of water adsorbed) were measured with a Mettler B4 C1000 (up to 1.0 Kg ± 0.001 g) balance.

With the small drying unit described above all the water vapour might not have been removed in a single pass. However, since the N_1O was supplied to the apparatus in batches, any water vapour not adsorbed in the first pass through the dryer would be removed in the successive passes before the next N_1O sample was introduced.

4.4.9 Vane pump

The hydrogen was circulated through the apparatus with a water cooled, oil (S.A.E. 30) sealed, vane pump. Coarse control of the hydrogen displacement was achieved with a variable speed drive, and fine control with the throttle and feed back valves shown in FIGURE 4.2. It was necessary to return a large amount of hydrogen directly from the pump outlet to the pump inlet (feedback) to obtain a stable gas flow reading. The maximum pump displacement was 20 c.f.m. at N.T.P.

4.4.10 Flowrator

This unit, used to meter the hydrogen flow rate through the apparatus, was a Fischer and Porter 'Flowrator'. The Flowrator, range 0.0-8.0 c.f.m. at N.T.P., was calibrated against a positive displacement meter.

4.4.11 Gas preheaters

There were two preheating furnaces constructed in a similar manner to the reactor unit. The pipe carrying the gas stream was fabricated from 1.0 in. bore 16 gauge heat resistant stainless steel tube, COMSTEEL 25/20. The first preheater had two tube passes with a single 2.0 Kw nichrome winding; the second unit had three tube passes with two 2.0 Kw windings.

4.4.12 Pressure regulated gas supply

FIGURE 4.3 is a schematic diagram of the pressure regulated gas supply which could supply either hydrogen or nitrogen to the apparatus.

Medium pressure regulators

The gases were supplied in 200 cub.ft. high pressure cylinders (2,000 p.s.i.g.). The cylinders used were fitted with standard medium pressure gas regulators with which gas could be supplied up to 60 p.s.i.g.

Low pressure demand valves

These units, made by modifying airforce disposals oxygen regulators, were sensitive pressure regulators which were used to supply gas from the medium pressure regulators to the apparatus at +7.0 in. water gauge. For high flow rates, as used for purging the transport apparatus, the demand valves were by-passed, but for normal operation the vane pump inlet pressure was maintained at + 7.0 in. water gauge by the hydrogen demand valve. As the water formed by the reaction was removed in the dryer the pump inlet pressure fell and hydrogen flowed through the demand valve until the pump inlet pressure was again + 7.0 in. water gauge.

Positive displacement flow meter

A Parkinson-Cowan wet type laboratory gas meter was used to measure the quantity of make up hydrogen admitted to the apparatus through the demand valve. One revolution of the drum was equivalent to $^{1}/_{50}$ of 1.0 cub.ft. displacement. To avoid contamination of the hydrogen stream the fluid used in the meter was Energol LPT 50.

Catalytic 'De-Oxo' unit and dryer

The hydrogen, supplied in cylinders, may have contained water vapour and/or oxygen, therefore a palladized asbestos 'De-Oxo' unit was attached to the hydrogen medium pressure regulator. This converts any oxygen present in the hydrogen to water vapour. The gas was then passed through a solid desiccant dryer before entering the apparatus.

4.4.13 Temperature measurement and control

Two gas temperatures were measured and controlled, viz. the reactor inlet (i.e. preheater exit) and the reactor exit temperatures. Chromel-Alumel thermocouples in $^3/_{16}$ in. diam. heat resistant stainless steel sheaths were axially located in the 1.0 in. bore preheater and reactor exit tubes which carried the hydrogen. These thermocouples were normally connected to "on-off" temperature controllers; however, special thermocouple switches enabled the two temperatures to be accurately measured at any time with a potentiometer. Thermocouples were attached to the pipe wall near these gas temperature thermocouples and were connected to temperature indicators. A third indicator was connected to a thermocouple used to measure the gas temperature at the top of the reactor cooler.

4.4.14 Measurement of the differential pressure across the reactor

The unit used to measure the differential pressure across the reactor (the distance between pressure taps was 5 ft. 10 in.) was a pressure transducer manufactured by the Infrared Development Company, United Kingdom. The range of the instrument was from -1.0 to + 1.0 in. water gauge with a central zero; the output from the transducer was ± 10 mV over the indicated range. During the experimental work the output signal was recorded on a fast response Leeds and Northrup chart recorder.

R1 } Medium pressure gas regulators
R2 }

D1 } Low pressure (7 in H_2O) gas demand valves
D2 }

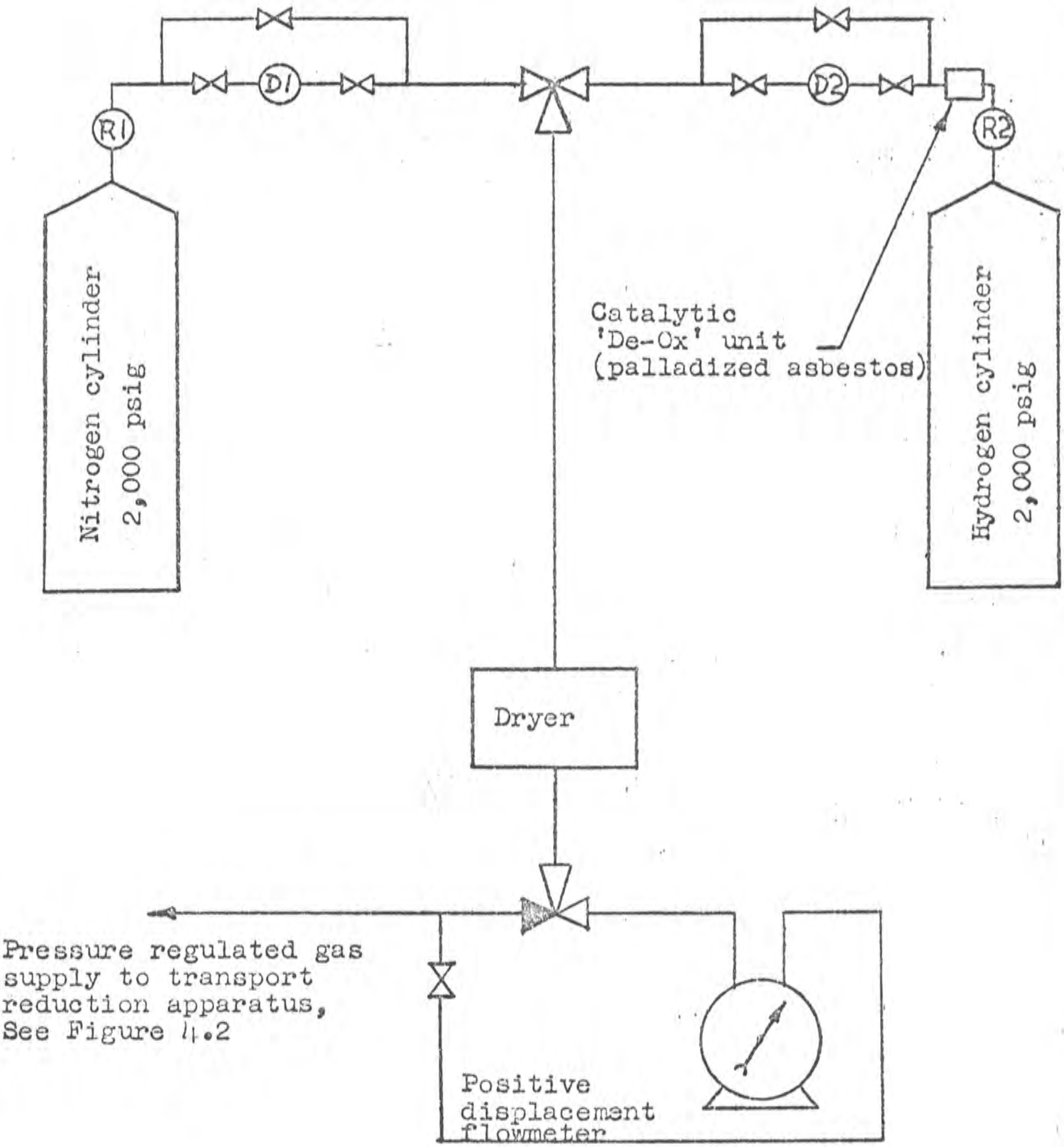

FIGURE 4.3 Diagram of pressure regulated gas supply used for the transport reduction of N_iO

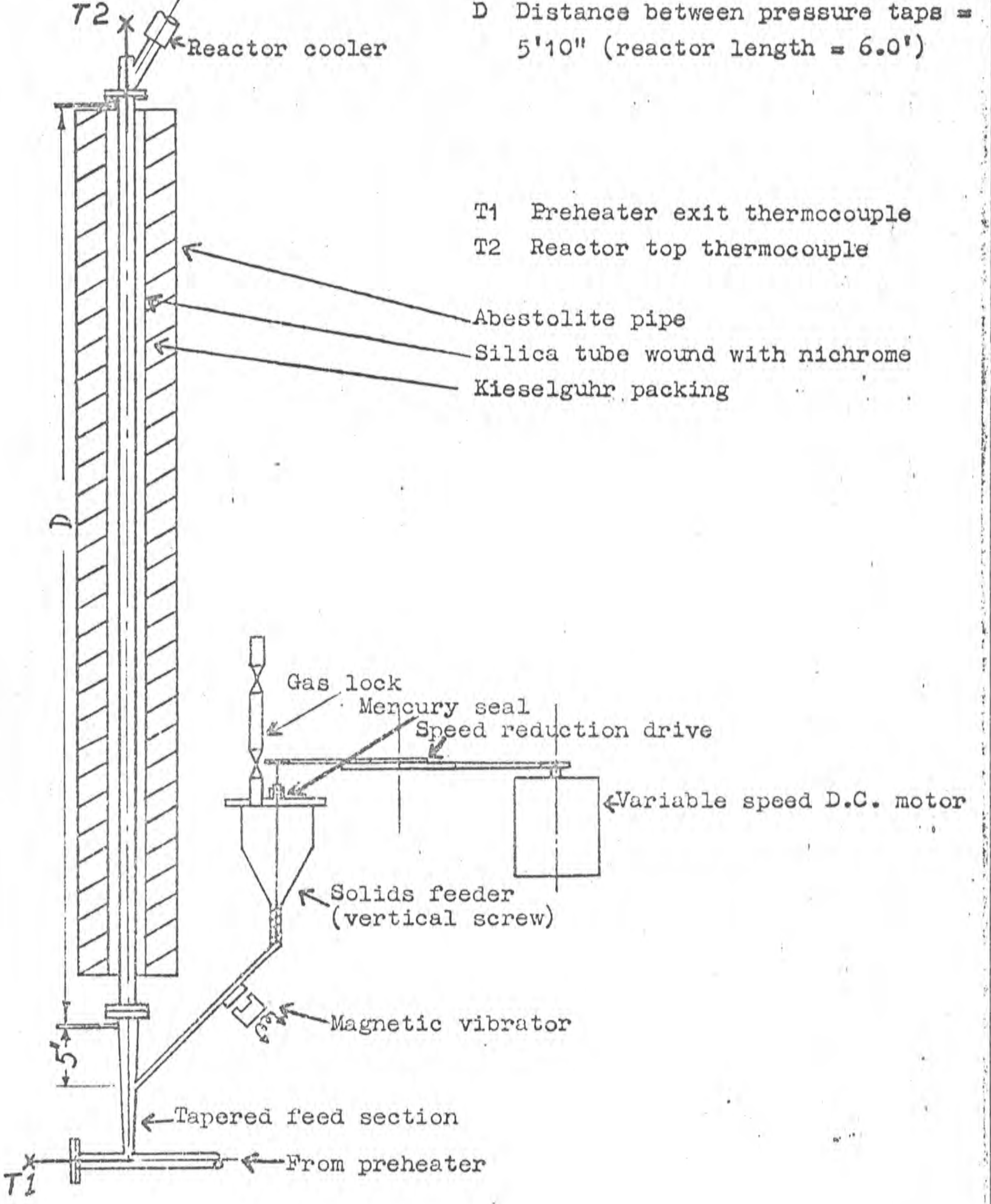

FIGURE 4.4 Schematic diagram of reactor, reactor furnace and solids feeder used for the transport reduction of N_iO

Legend for FIGURE 4.5

A, N — Active and neutral of 240 v A.C. supply

V_1, V_2, V_3, V_4 — 2.0 KW auto-transformers ('Variac')

S_1, S_2, S_3, S_4 — Controller by-pass switches

R_1 — Nichrome winding reactor furnace

R_2, R_3 — Nichrome windings second preheater furnace(3 pass)

R_4 — Nichrome winding first preheater furnace(2 pass)

DP1, DP2, — Double-pole double-throw thermocouple switches to enable potentiometer monitoring of preheater and reactor exit temperatures

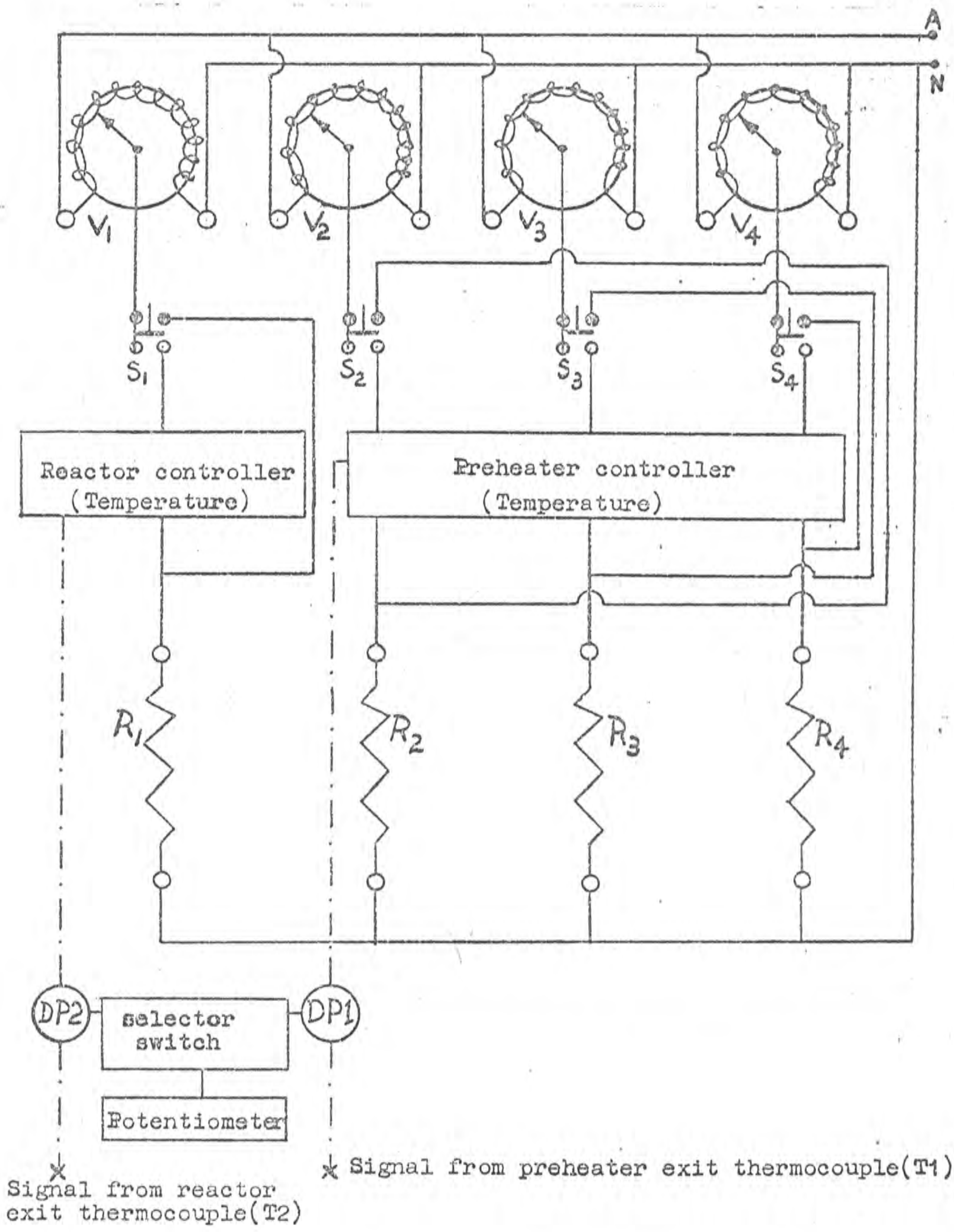

FIGURE 4.5 Wiring diagram for the transport reactor

FIGURE 4.6 Photograph of control panel and reactor section


K159
KENT
CAMBRIDGE
INDICATING CONTROLLER

FIGURE 4.7 Photograph of vane pump, valve system, dryer cooler and dryer

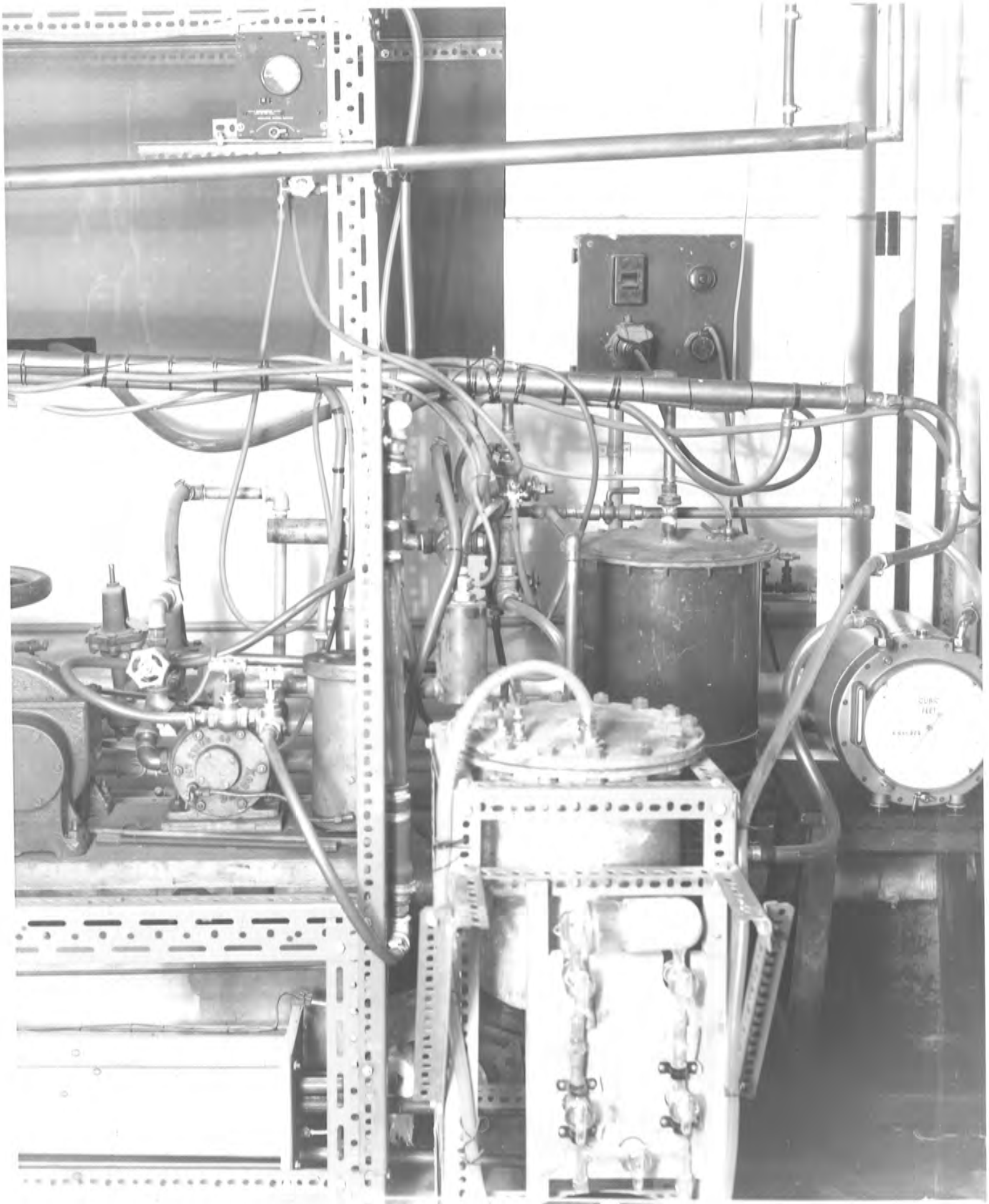

FIGURE 4.8 Photograph of the reactor cooler and the solids collection system

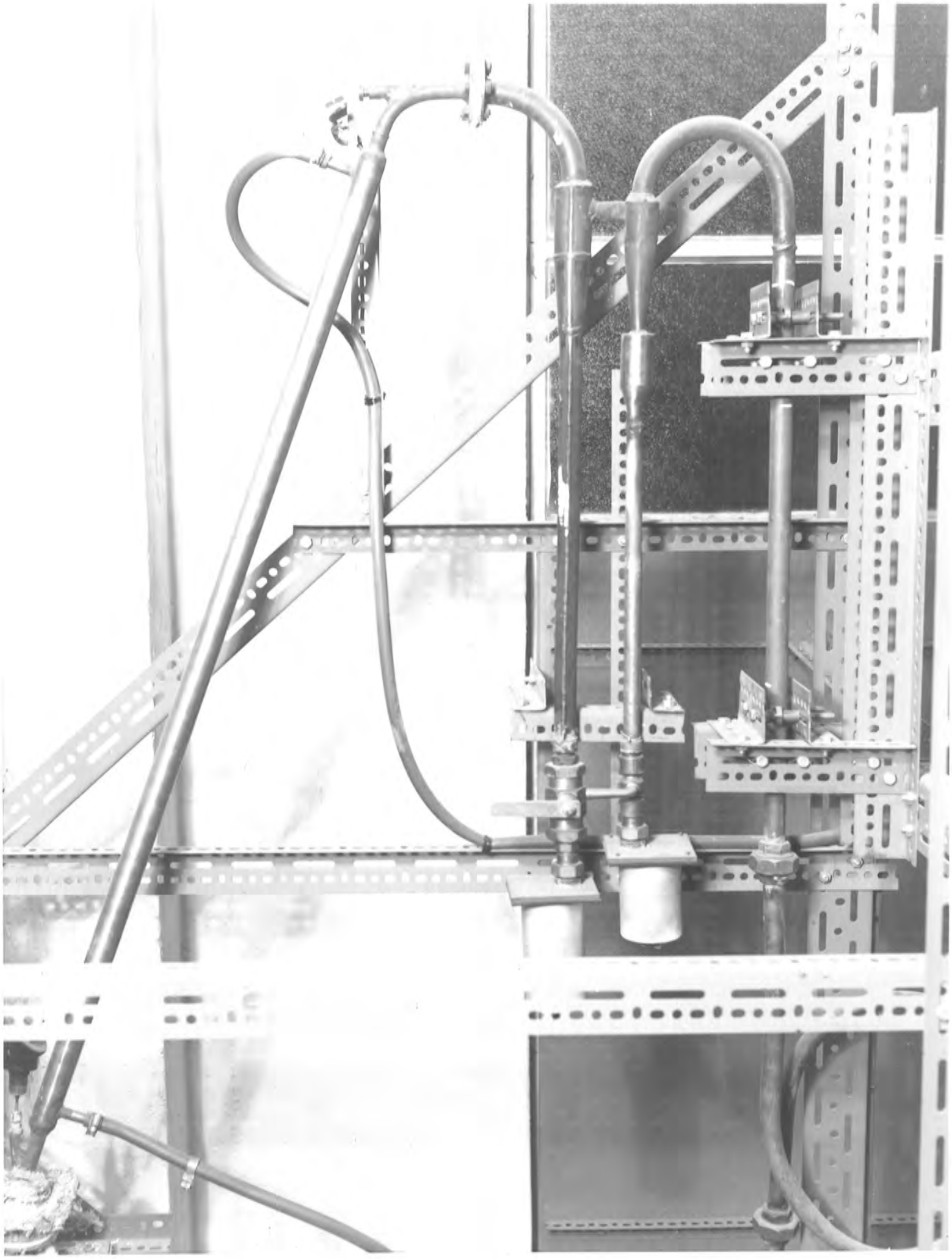

4.5 The Experimental Procedure

4.5.1 The start up procedure

Because of the hazardous nature of hydrogen at high temperatures a rigorous start up procedure was observed. The runs were usually conducted during the forenoon, therefore, as the furnaces required several hours to reach operating temperature, a time switch was used to switch the heaters on at 0400 hours. As the operating temperatures were approached (approx. 5 hours after the initial 'switch on') all the functional parts of the apparatus were carefully checked and the gas charging procedure started. The following operations were then completed in sequence, viz.:

(i) A stream of nitrogen was passed through the apparatus and vented to atmosphere until the apparatus was completely purged of air. During this purge the temperature controllers were set to a value 80°C less than the required operating temperature because of the difference in the thermal properties of hydrogen and nitrogen.

(ii) When the air purge was complete the nitrogen was purged from the apparatus with a stream of hydrogen, the hydrogen demand valve and the positive displacement flowmeter being by-passed for this operation.

(iii) On the completion of this second purge the hydrogen demand valve was placed on line and the vent valves set to re-cycle the hydrogen stream.

(iv) The circulating pump was switched on, the hydrogen circulating rate set, and the temperature controller settings corrected to the desired value. At this stage the positive displacement hydrogen flowmeter was placed on line and the hydrogen leak rate checked. The maximum acceptable leak rate was 0.015 cub.ft. per min.

On the completion of this sequence the apparatus was ready for operation.

4.5.2 The procedure for a reduction run

Two operators were needed to run the apparatus, the assistant being required to record readings from the positive displacement gas meter. The dryer absorption bottle was weighed before and after each group of runs, the absorption bottle being full of hydrogen for both weighings.

The following schedule shows the exact procedure used by the operator for a reduction run, viz.:

(i) The feed sample (N_1O powder) was charged to the feeder gas-lock.

(ii) The zeros of the differential pressure transducer and the Leeds and Northrup chart recorder were checked.

(iii) The feeder speed setting was checked and the feed sample was introduced into the screw feeder section from the gas-lock.

(iv) The Flowrator setting was checked and recorded together with the temperature and pressure of the gas passing through the Flowrator and the reactor pressure.

(v) The following temperatures were checked and recorded, the reactor exit gas, the reactor exit wall, the reactor inlet gas, and the reactor inlet wall.

(vi) The solids feeder was switched on and the actual reduction run started. The feeding process was timed with a stopwatch by observation of the N_1O powder flow through a P.V.C. window in the bottom of the feeder. From the knowledge of this feeding time and the weight of solid charged, the average solids feed rate for each run was calculated.

(vii) When the N_1O sample had completely discharged from the screw feeder the temperature measurements made in step (v) were repeated. The reduced sample of $N_1O + N_1$ was then recovered from the collection canisters.

Before, during, and after these operations the assistant recorded the readings of the positive displacement gas meter. The readings before and after the run were taken at 30 second intervals to establish the hydrogen leak rate: the readings taken during the run measured the amount of hydrogen consumed by the reaction and were recorded at 15 second intervals.

4.6 Summary of the Experimental Conditions

The nickel oxide used for the transport reduction experiments came from the same samples that were used in the work described in section 3, i.e. three size ranges of N_iO were used, viz. $^{35}/_{42}$#, $^{42}/_{48}$# and $^{48}/_{60}$#. Samples from each of the three size ranges were reduced at four levels of temperature, viz. 550, 600, 650 and 700°C, which enabled classification of the experiments into twelve run groups. Within each run group the gas velocity was varied to give a range of particle residence times for a given hydrogen temperature and particle size. A summary of the experimental conditions and the number of runs in each run group is presented in TABLE 4.1.

TABLE 4.1 Summary of the experimental conditions for the transport reduction of N_iO

Particle size	Nominal run temperature			
	500°C	550°C	600°C	700°C
48/60#	Run group 1 6 runs	Run group 2 6 runs	Run group 3 6 runs	Run group 4 7 runs
42/48#	Run group 5 7 runs	Run group 6 6 runs	Run group 7 7 runs	Run group 8 7 runs
35/42#	Run group 9 7 runs	Run group 10 7 runs	Run group 11 8 runs	Run group 12 6 runs

4.7 Experimental Results

The experimental results obtained for the twelve run groups are contained in APPENDIX 4.1. For each run group there are three categories of data, i.e. mass balance data, residence time data, and temperature data.

4.7.1 Mass balance data

The mass balance data presented for each run are the solids feed weight, the reduced product weight, and the volume and temperature of the make up hydrogen required to keep the system at constant pressure, i.e. the pump inlet pressure at + 7.0 in water gauge. In addition the total weight of water adsorbed for each run group is presented.

As the total water adsorbed was only measured for each run group, the mass balance calculations are made with the data from a complete run group. Therefore, the input to the system was the total weight of nickel oxide charged plus the weight of make up hydrogen, and the output was the total weight of reduced product collected plus the total weight of water adsorbed.

4.7.2 Residence time data

The residence time data consist of the Flowrator setting (from which gas velocity is calculated), the solids feed rate, and the differential pressure transducer output taken from the chart recorder. The pressure transducer output is converted to actual pressure drop readings (in H_2O) by use of the computer program referred to in section 4.8. A subsequent program was used to estimate the average particle residence time by application of the model developed in section 2. No pressure drop data are presented for run group 12 because the manometer lines became blocked.

4.7.3 Temperature data

The temperature data presented are:

(i) the reactor exit gas temperature and the reactor exit wall temperature,

(ii) the reactor inlet gas temperature and the reactor inlet wall temperature,

and (iii) the temperature of the gas leaving the reactor cooler.

The first four temperatures were used to estimate the true mean gas temperature while the gas cooler temperature was monitored as an operating guide.

4.8 Analysis of the results

The bulk of the results was analysed with the aid of an I.B.M. 1620 digital computer. Two programs were employed. The first program was used to make the following calculations:

(i) the degree of reduction of the N_iO,

(ii) the mass balance for each run group,

(iii) an iterative analysis to estimate the corrected mean temperature and the mean gas velocity in the reactor, and

(iv) values of the solids pressure drop and the reciprocal solids pressure drop.

These data are tabulated in APPENDIX 4.2.

The second program was used to estimate the average particle residence time for each run from the relationship developed in section 2 relating the average particle velocity to the solids pressure drop. These data are contained in APPENDIX 4.3.

4.8.1 Calculation of the degree of reduction

The degree of reduction is defined in the same manner as it was in section 3; however, the calculation is based on measurements of hydrogen consumption rather than water formation:

i.e.

$$\text{observed degree of reduction} = y_e = \frac{\text{g oxygen removed}}{\text{g initial oxygen}}$$

$$= \frac{(\text{g } H_2 \text{ consumed})(\text{equivalent g } O_2 \text{ per g } H_2)}{(\text{equivalent g } O_2 \text{ per g } N_1O \text{ feed})(\text{g } N_1O \text{ feed})}$$

which can be expressed in the form

$$y_e = \left[\frac{453.6(\text{mol.wgt.}H_2)(H_2 \text{ pressure atm.})(\text{cub.ft.}H_2 \text{ consumed})}{0.7302 \quad (H_2 \text{ temp. } ^{\circ}R)}\right]$$

$$\left[\frac{(7.936)}{(0.2142)(\text{g } N_1O)}\right] \qquad \text{......} \quad (4.1)$$

4.8.2 Calculation of the mass balance

The mass balance was determined for each run group with the exception of run group 12. The relationship used to compute the mass balance was:

(Input - Output) = (Residual)

which can be expressed in the form

$$\left[\Sigma(N_1O)_{feed} + \Sigma(H_2)_{make-up}\right]_g - \left[\Sigma(N_1O + N_1)_{product} + \Sigma(H_2O)_{adsorbed}\right]_g = \left[\text{Residual}\right]_g \quad \ldots\ldots (4.2)$$

The summations were made over all runs in a given group and the proximity of the residual term to zero gave a measure of the efficiency of the operation of the apparatus. For run groups 1-11 inclusive the grand total mass balance figures are:

Total input ($N_1O + H_2$) = 1303.165 g

Total output ($N_1O + N_1 + H_2O$) = 1286.742 g

Total residual = 16.423 g

The residual quantity, approximately 1.3% of the total input can be almost completely accounted for by the 14 g of material removed from the manometer lines from time to time during the experiments.

4.8.3 Temperature correction and gas velocity estimation

For a given mass flow rate of gas in the reactor, determined by the Flowrator setting, the average gas velocity is a function of the mean gas temperature and pressure. The mean gas temperature was estimated with two pairs of temperature measurements, viz. the temperature indicated by a thermocouple probe in the gas stream and the wall temperature near the thermocouple probe at both the reactor inlet and outlet points. The estimation was based on a thermal energy balance, i.e. the gas temperature required for the consistency of the equation:

(heat transferred to the probe from the gas by convection)

= (heat transferred from the probe to the wall by radiation)

..... (4.3)

The location and dimensions of the thermocouple probe were chosen to minimize heat losses by conduction along the axis of the probe. Because the value of the gas velocity affects the rate of heat transfer by convection an iterative technique was used to obtain the solution of equation 4.3. The calculation was repeated until two successive estimates of the gas temperature were within half a centigrade degree.

4.8.4 Estimation of the average solids residence time

A relationship was developed in section 2 which expressed the solids pressure drop as a function of the theoretical solids velocity and the solids feed rate, viz.:

$$\Delta P_{solids} = \frac{W_s}{A_c}\left[\frac{L}{a\,\bar{V}_{P_{theoretical}}^{1.192}} + \frac{a\{(V_{P_{theoretical}})_2^{1.192} - (V_{P_{theoretical}})_1^{1.192}\}}{g} + \frac{(\bar{V}_{P_{theoretical}} - a.\,\bar{V}_{P_{theoretical}}^{1.192})}{g}\right]$$

This equation can be rearranged and written as a quadratic equation in the constant 'a'; for convenience the variable x is used to replace $V_{P_{theoretical}}$, viz.

$$a^2\{\bar{x}^{1.192} - (x_2^{1.192} - x_1^{1.192})\} + a\left(\frac{g.A_c}{W_s}.\,\Delta P_s - \bar{x}\right) - \frac{L.g}{\bar{x}^{1.192}} = 0 \qquad \ldots\ldots (4.4)$$

NOTE: $\bar{x}^{1.192}$ = (mean value of x)$^{1.192}$

In the program used to estimate the average particle residence times, values of the theoretical velocities (x, $\bar{\bar{x}}$) were calculated using the following data:

(i) the average gas velocity,

*(ii) an estimate of the particle terminal velocity obtained from the intercept on the gas velocity axis of a plot of the reciprocal solids pressure drop vs. the average gas velocity for all the observed pairs of points for a given run group,

(iii) the solids feed rate, and

(iv) the dimensions of the reactor, see FIGURE 4.4.

The values of x and $\bar{\bar{x}}$, calculated from equations 2.28 and 2.29, were substituted in equation 4.4 and the quadratic equation solved for 'a'. The value of the actual average particle velocity, and hence the average particle residence time, was then estimated from the equation:

$$(\overline{V_P})_{actual} = a.(\overline{V_P})^{1.192}_{theoretical} \qquad ..... (2.53)$$

The residence time estimation are listed in APPENDIX 4.3 and exclude the data for run groups 5 and 12. The data are also presented in TABLES 4.2 to 4.4 together with the corresponding values of the degree of reduction.

*See FIGURES 4.13 to 4.16 for estimates of the terminal velocity.

TABLE 4.2 Summary of degree of reduction and residence time data for $^{48}/_{60}{}^{\#}$ N_iO

Run group 1 500°C			Run group 2 550°C			Run group 3 600°C			Run group 4 700°C		
y_e	$-\ln(1-y_e)$	t (sec)	y_e	$-\ln(1-y_e)$	t (sec)	y_e	$-\ln(1-y_e)$	t (sec)	y_e	$-\ln(1-y_e)$	t (sec)
.106	.112	2.91	.442	.583	2.74	.722	1.48	3.32	.938	2.78	3.04
.207	.232	3.10	.500	.693	2.83	.773	1.48	3.31	.928	2.50	3.02
.263	.305	3.45	.581	.870	3.08	.806	1.64	3.22	.948	2.96	3.03
.293	.347	5.59	.620	.968	3.10	.870	2.04	5.24	.964	3.32	4.40
.329	.399	9.02	.624	.978	3.86	.874	2.07	6.45	.975	3.69	5.71
.424	.552	13.1	.726	1.29	8.97	.916	2.48	9.37	.948	2.96	2.62

TABLE 4.3 Summary of degree of reduction and residence time data for 42/48# N_1O

Run group 5 500°C			Run group 6 550°C			Run group 7 600°C			Run group 8 700°C		
y_e	$-\ln(1-y_e)$	t (sec)	y_e	$-\ln(1-y_e)$	t (sec)	y_e	$-\ln(1-y_e)$	t (sec)	y_e	$-\ln(1-y_e)$	t (sec)
No analysis because of nitrogen leak into system			.281	.330	2.93	.693	1.18	2.88	.912	2.43	2.91
			.340	.416	3.33	.738	1.34	3.15	.930	2.66	3.06
			.408	.524	4.00	.772	1.48	3.31	.919	2.51	3.38
			.473	.641	7.59	.786	1.54	3.53	.949	2.98	3.53
			.543	.783	11.3	.810	1.66	3.52	.957	3.15	6.10
			.581	-	-	.866	2.01	6.80	.957	3.15	9.79
						.868	1.95	3.94	.915	2.47	5.40

TABLE 4.4 Summary of degree of reduction and residence time data for $^{35}/_{42}$# NiO

Run group 9 500°C			Run group 10 550°C			Run group 11 600°C			Run group 12 700°C		
y_e	$-\ln(1-y_e)$	t (sec)	y_e	$-\ln(1-y_e)$	t (sec)	y_e	$-\ln(1-y_e)$	t (sec)	y_e	$-\ln(1-y_e)$	t (sec)
.071	.0737	3.65	.298	.354	4.29	.661	1.08	3.53	No analysis because of blocked manometer lines		
.152	.165	4.22	.431	.564	6.48	.738	1.34	3.64			
.168	.184	5.41	.505	.703	9.53	.798	1.60	5.01			
.247	.284	8.38	.653	1.06	18.6	.822	1.73	6.59			
.306	.365	7.66	(.684)	-	-	.831	1.78	8.19			
.373	.467	17.5	(.568)	-	-	.931	2.67	11.6			
.300	.357	13.9	.271	.316	10.0	.855	1.93	10.3			
						.851	1.90	8.03			

4.8.5 The kinetic characteristics of the reduction of N_1O in a transport reactor

To make a quantitative assessment of the performance of a reactor it is desirable to try and establish some explicit relationship between the degree of conversion and the independent variables which affect the degree of conversion. In the case of the fixed bed reactor discussed in section 3, the degree of reduction was found to be a function of temperature and time; no significant effect was observed for the different values of particle size used,

i.e. observed degree of reduction = y_e = $\phi(T, t)$

where T = absolute temperature ^oK,

and t = time elapsed after the start of the reaction, min.

An equation was established that gave quite good agreement between the predicted and observed results, viz.

$$y = 1-\exp-A\,\{(t+1.0)\,[\ln(t+1.0)-1.0] + 1.0\} \quad \ldots\ldots (3.9)$$

or $$-\ln(1-y) = A.f(t) \quad \ldots\ldots (3.11)$$

where

$$f(t) = \{(t+1.0)\,[\ln(t+1.0)-1.0] + 1.0\} \quad \ldots. (3.12)$$

Equation 3.9 was obtained by integration of an assumed rate equation:

$$\frac{dy}{dt} = A(1-y).\ln(t+1.0) \qquad .... (3.8)$$

The value of A was determined by plotting $-\ln(1-y_e)$ vs. f(t) and calculating the slope of the line with a linear regression analysis assuming that the line passed through the origin. The relationship between the value of A and the absolute temperature was found to be

$$\ln A = (19.05 - \frac{27.75.10^3}{R\,T}) \qquad .... (3.17)$$

It was decided to test the adequacy of these equations as a means of representing the relationship between the observed values of the degree of reduction, the temperature of reaction, and the estimated residence time for the transport reactor. Values of $-\ln(1-y_e)$ and f(t) for the relevant run groups are tabulated in APPENDIX 4.4, and the results of the regressions for the determination of A are listed in TABLE 4.5, together with the mean run temperature data. The standard error estimate is also listed and is based on the distribution of the values of $-\ln(1-y_e)$ about the mean line and so is a measure of the fit of the data to the assumed relationship. In this case the fit was not good, the standard

TABLE 4.5 Summary of the Arrhenius[a] constant (A) estimates for the transport reduction of N_1O

Run group 1 (i) A=47.1 (ii) Std. error estimate = .2702 (iii) mean run temp. = 509°C (iv) $\frac{10^3}{T}$ = 1.28	Run group 2 (i) A= 309 (ii) Std. error estimate = .9862 (iii) mean run temp. = 561°C (iv) $\frac{10^3}{T}$ = 1.20	Run group 3 (i) A=442 (ii) Std. error estimate = 1.395 (iii) mean run temp. = 611°C (iv) $\frac{10^3}{T}$ = 1.13	Run group 4 (i) A=806 (ii) Std. error estimate = 3.978 (iii) mean run temp. = 716°C (iv) $\frac{10^3}{T}$ = 1.01
Run group 5 No data	Run group 6 (i) A=92.1 (ii) Std. error estimate = .4489 (iii) mean run temp. =560°C (iv) $\frac{10^3}{T}$ = 1.20	Run group 7 (i) A=717 (ii) Std. error estimate = 1.073 (iii) mean run temp. =610°C (iv) $\frac{10^3}{T}$ = 1.13	Run group 8 (i) A=709 (ii) Std. error estimate = 2.736 (iii) mean run temp. = 715°C (iv) $\frac{10^3}{T}$ = 1.01
Run group 9 (i) A=21.2 (ii) Std. error estimate = .1961 (iii) mean run temp. =506°C (iv) $\frac{10^3}{T}$ = 1.28	Run group 10 (i) A=39.7 (ii) Std. error estimate = .4221 (iii) mean run temp. =561°C (iv) $\frac{10^3}{T}$ = 1.20	Run group 11 (i) A=227 (ii) Std. error estimate = .8903 (iii) mean run temp. =613°C (iv) $\frac{10^3}{T}$ = 1.13	Run group 12 No data

(a) In the case of the fixed bed work the relationship between A, the rate constant, and the absolute temperature was found to be of the form: ln A = (const. - E/RT) error of $-\ln(1-y_e)$ being of the same order as the mean value, $-\ln(1-\bar{y}_e)$.

In view of the above results it was decided to modify the rate equation developed for the fixed bed data. The following rate equation was found to be satisfactory, viz.:

$$\frac{dy}{dt} = K(1-y) \qquad \text{.....(4.5)}$$

This equation, with the boundary condition y=0, t=0 yields on integration the following equation:

$$-\ln(1-y) = K.t \qquad \text{.....(4.6)}$$

or

$$y = 1 - e^{-Kt} \qquad \text{.....(4.7)}$$

As with the determination of A, values of K were estimated by calculating the linear regression passing through the origin between $-\ln(1-y_e)$ and t. They are summarized in TABLE 4.6. Values of y_e, $-\ln(1-y_e)$ and t(sec) are listed in TABLES 4.2 to 4.4 for the relevant run groups. These data are plotted in FIGURES 4.9 to 4.11 with the mean reduction temperature as a parameter for the three sizes of N_1O used in the experiments, viz. 48/60#, 42/48# and 35/42#.

FIGURE 4.12 is an Arrhenius plot of log K vs.

TABLE 4.6 Summary of the Arrhenius[(a)] constant (K) estimates for the transport reduction of N_1O

Run group 1 (i) K = 3.14 (ii) Std. error estimate = .0983 (iii) mean run temp. = 509°C (iv) $\frac{10^3}{T}$ = 1.28	Run group 2 (i) K = 13.14 (ii) Std. error estimate = .3463 (iii) mean run temp. = 561°C (iv) $\frac{10^3}{T}$ = 1.20	Run group 3 (i) K = 21.72 (ii) Std. error estimate = .5108 (iii) mean run temp. = 611°C (iv) $\frac{10^3}{T}$ = 1.13	Run group 4 (i) K = 50.08 (ii) Std. error estimate = .6518 (iii) mean run temp. = 716°C (iv) $\frac{10^3}{T}$ = 1.01
Run group 5 No data	Run group 6 (i) K = 5.54 (ii) Std. error estimate = .1666 (iii) mean run temp. = 560°C (iv) $\frac{10^3}{T}$ = 1.20	Run group 7 (i) K = 24.68 (ii) Std. error estimate = .3644 (iii) mean run temp. = 610°C (iv) $\frac{10^3}{T}$ = 1.13	Run group 8 (i) K = 33.98 (ii) Std. error estimate = 1.2219 (iii) mean run temp. = 715°C (iv) $\frac{10^3}{T}$ = 1.01
Run group 9 (i) K = 1.87 (ii) Std. error estimate = .0725 (iii) mean run temp. = 506°C (iv) $\frac{10^3}{T}$ = 1.28	Run group 10 (i) K = 3.68 (ii) Std. error estimate = .1903 (iii) mean run temp. = 561°C (iv) $\frac{10^3}{T}$ = 1.20	Run group 11 (i) K = 14.80 (ii) Std. error estimate = .3497 (iii) mean run temp. = 613°C (iv) $\frac{10^3}{T}$ = 1.13	Run group 12 No data

(a) The rate constant K, based on time (min.), is referred to as an Arrhenius constant as the relationship between K and the absolute temperature was found to be of the form: $\ln K = (\text{const.} - E/RT)$

$\frac{10^3}{T}$, and the regression equation for these data is:

$$\ln K = (14.86 - \frac{10.78 . 10^3}{T}) \qquad .....(4.8)$$

To obtain an estimate of the activation energy this equation may be written:

$$\ln K = (14.86 - \frac{21,400}{RT}) \qquad .....(4.9)$$

where 21,400 cal per g mole is an estimate of the Arrhenius activation energy for the reduction of the N_1O sample in a transport reactor.

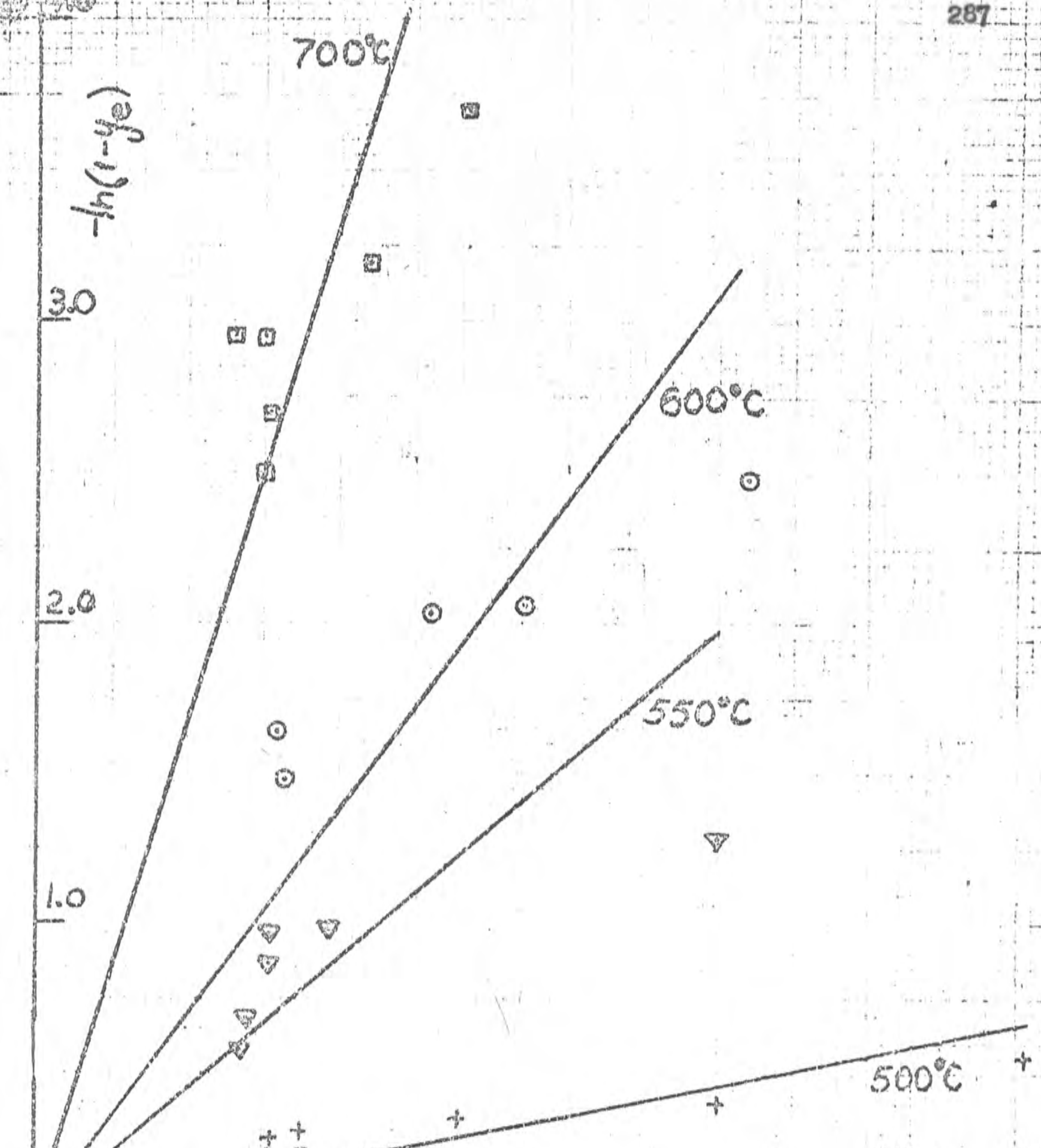

FIGURE 4.9 Relationship between $-\ln(1-y_e)$ and the residence time estimate (t) for the transport reduction of $\frac{48}{60}$ # NiO

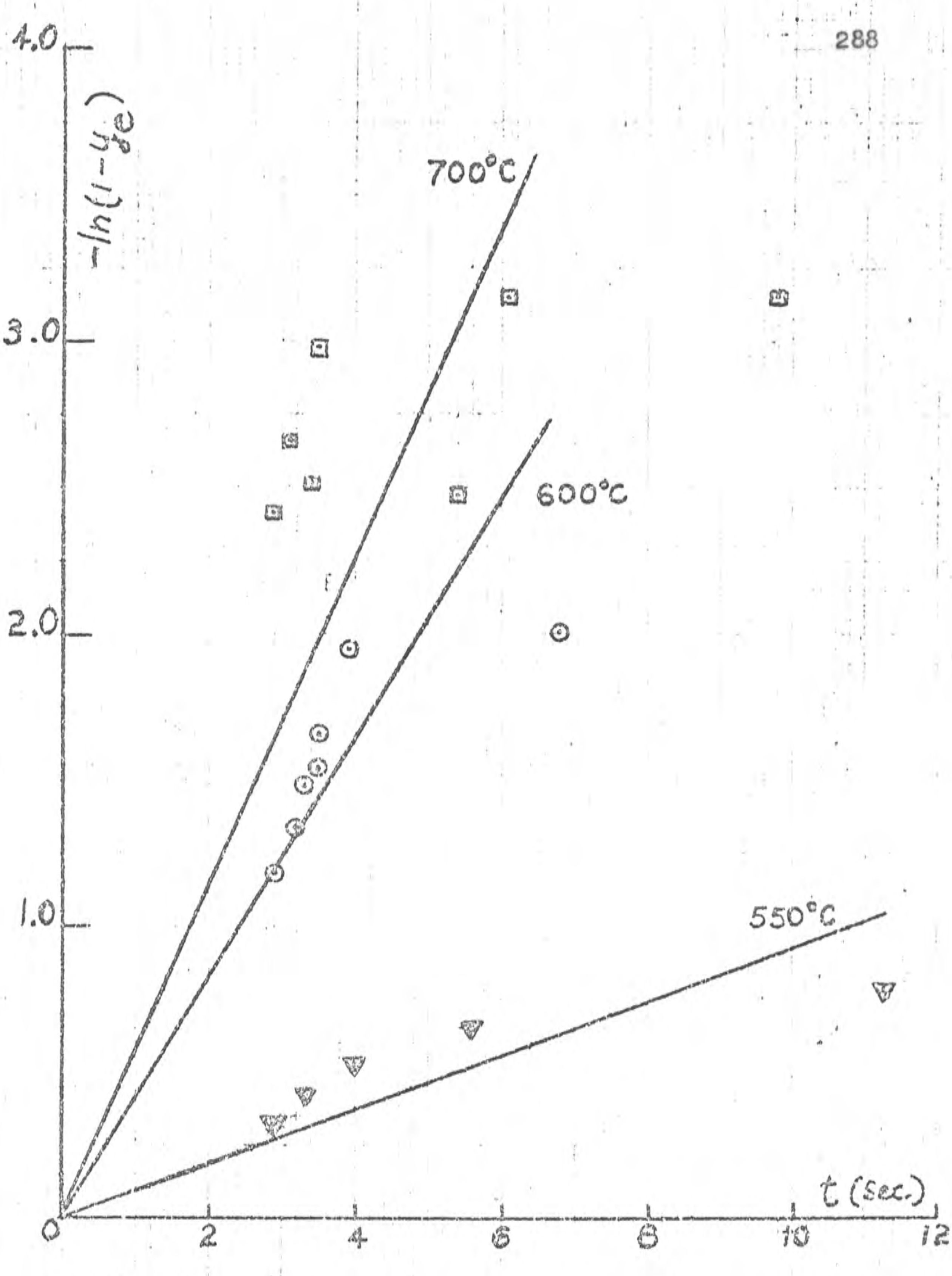

FIGURE 4.10 Relationship between $-\ln(1-y_e)$ and the residence time estimate (t) for the transport reduction of $\frac{42}{48}$# N_2O

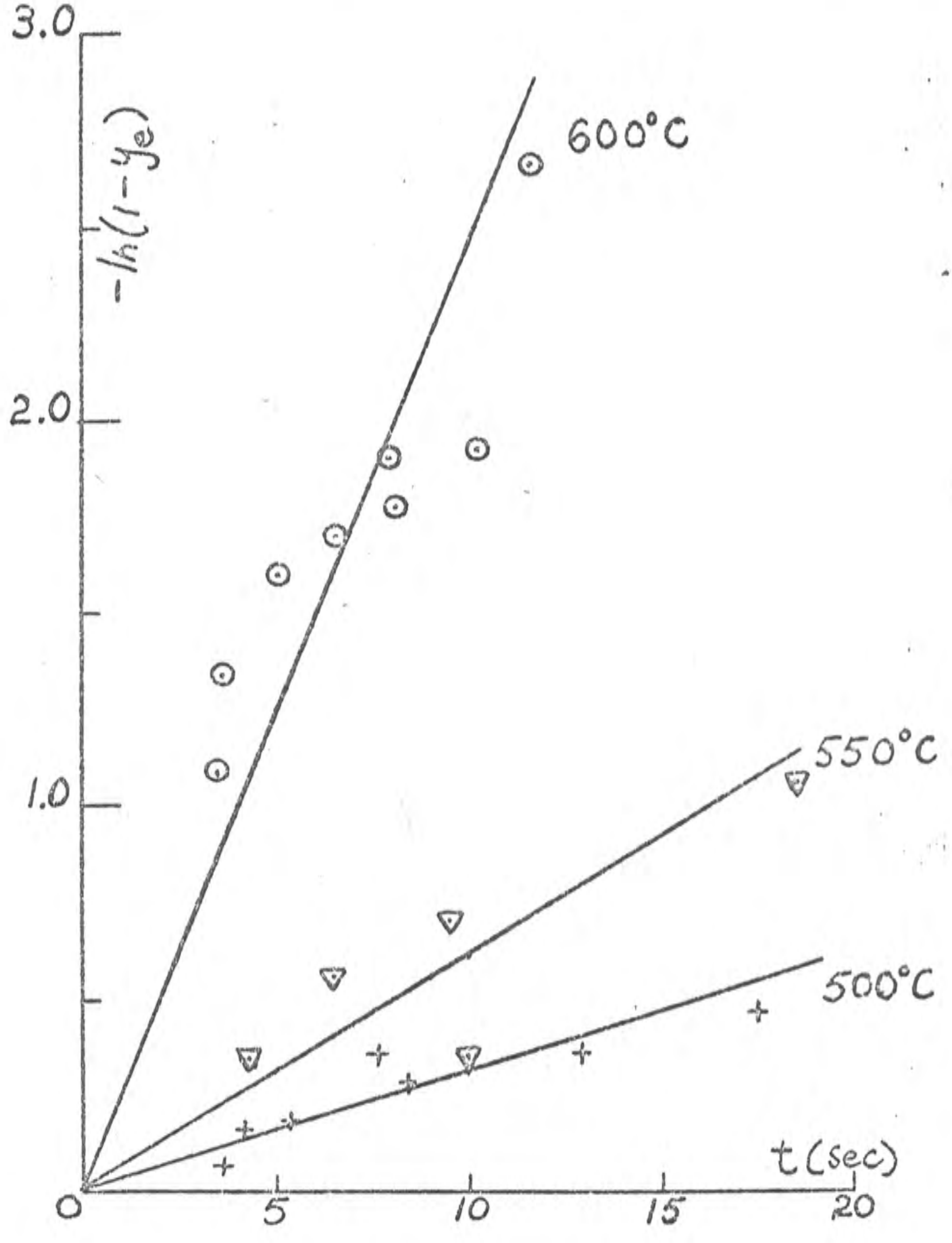

FIGURE 4.11 Relationship between $-\ln(1-y_e)$ and the residence time estimate for the transport reduction of $\frac{35}{42}$ # N_iO

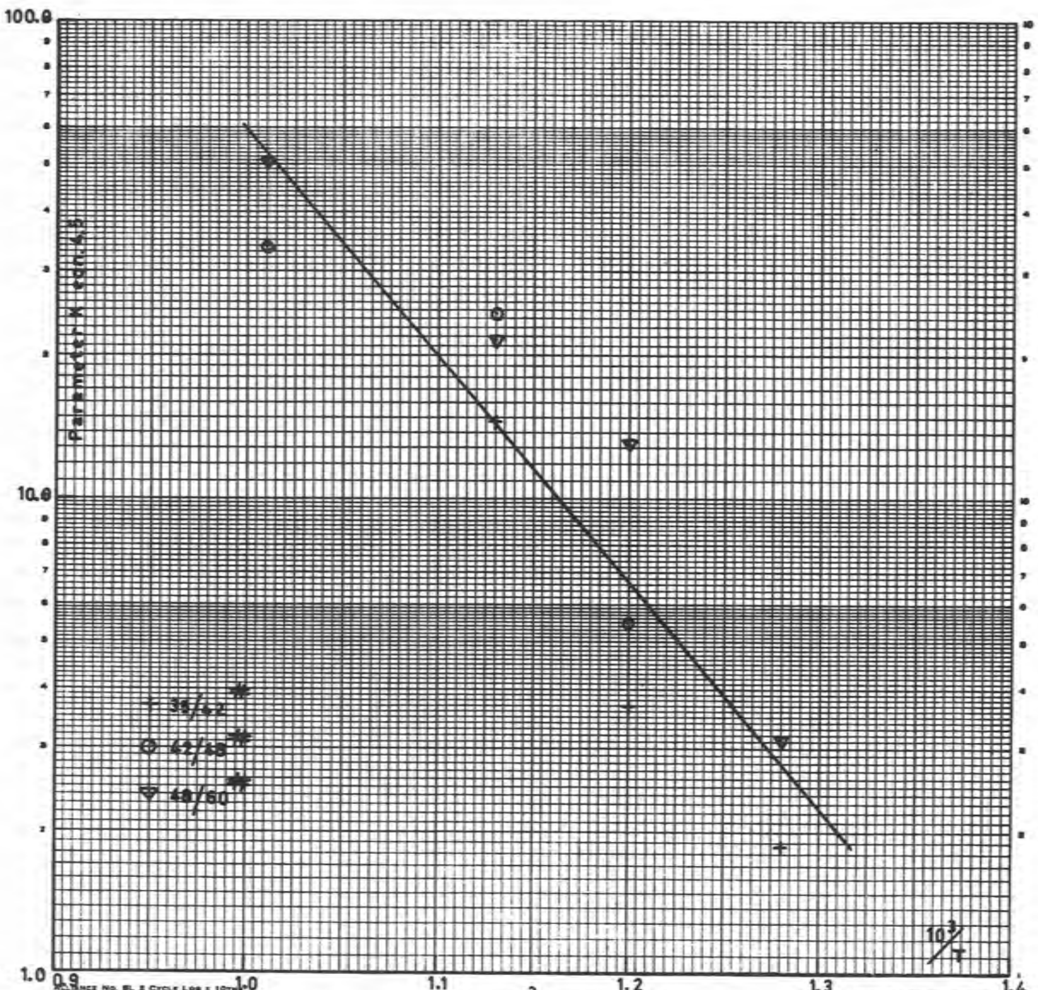

FIGURE 4.12 Arrhenius plot of log K vs. $10^3/T$ for the transport reduction of NiO

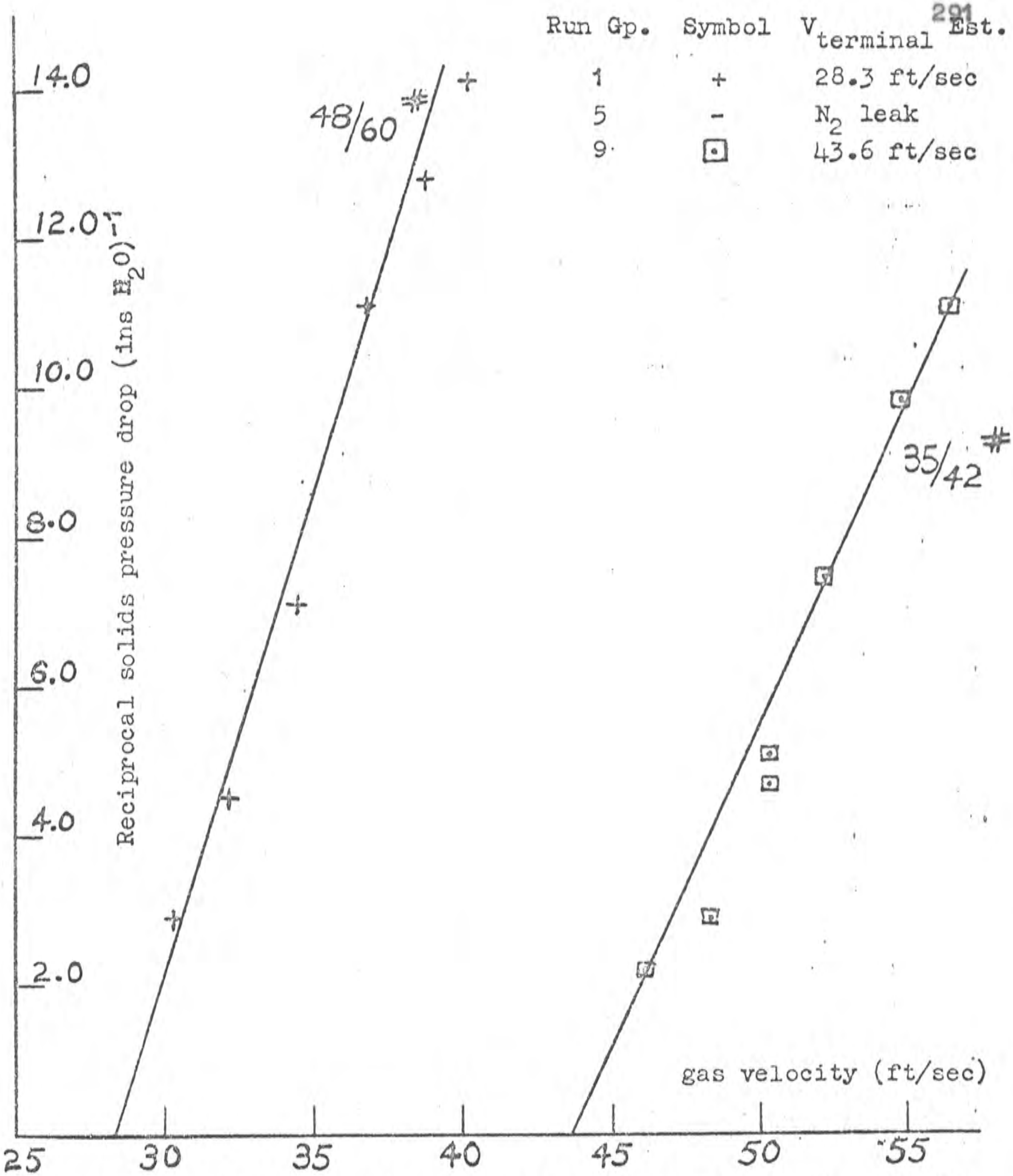

FIGURE 4.13 Plot of reciprocal solids pressure drop vs. average gas velocity for the 500°C runs

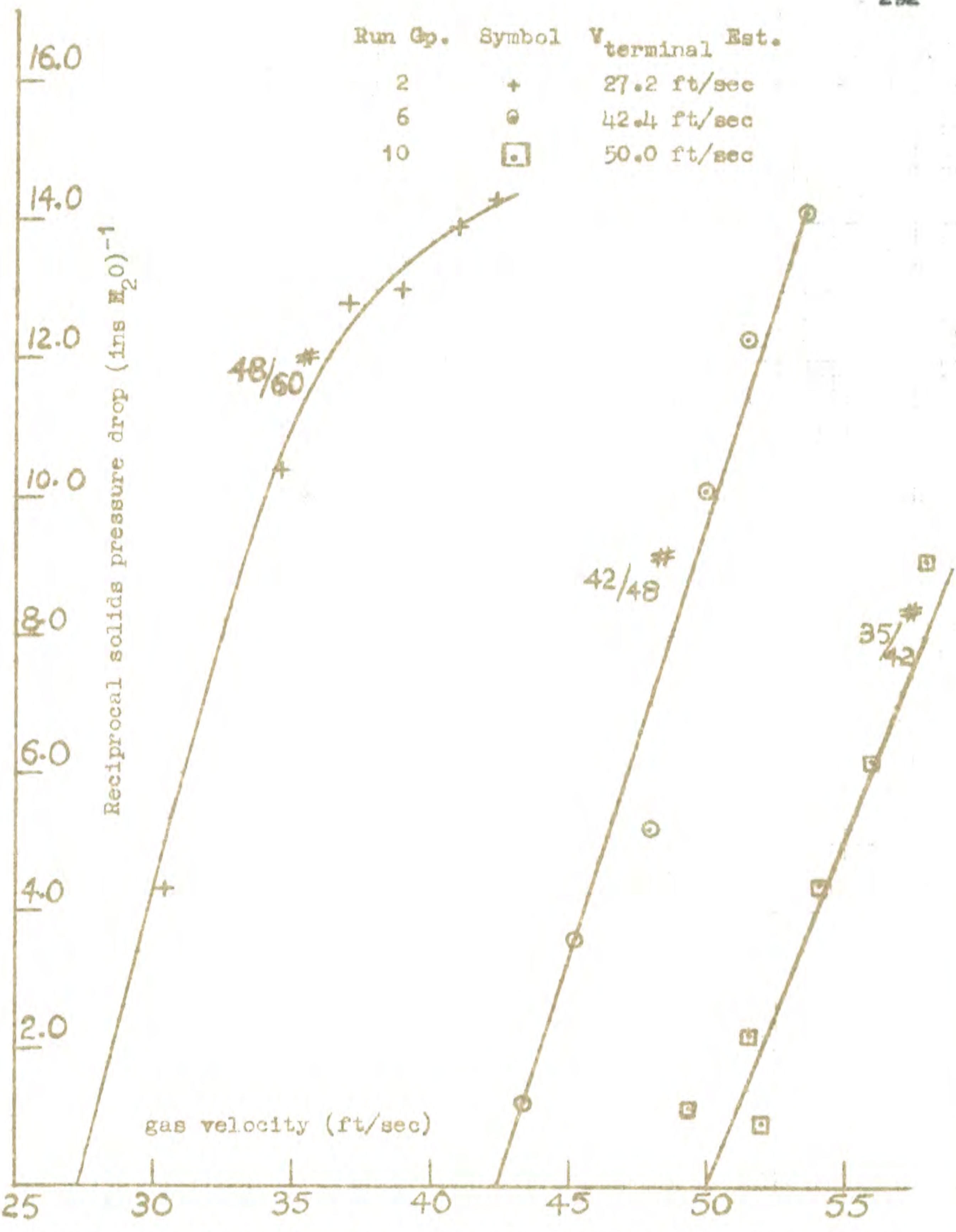

FIGURE 4.14 Plot of reciprocal solids pressure drop vs. average gas velocity for the 550°C runs

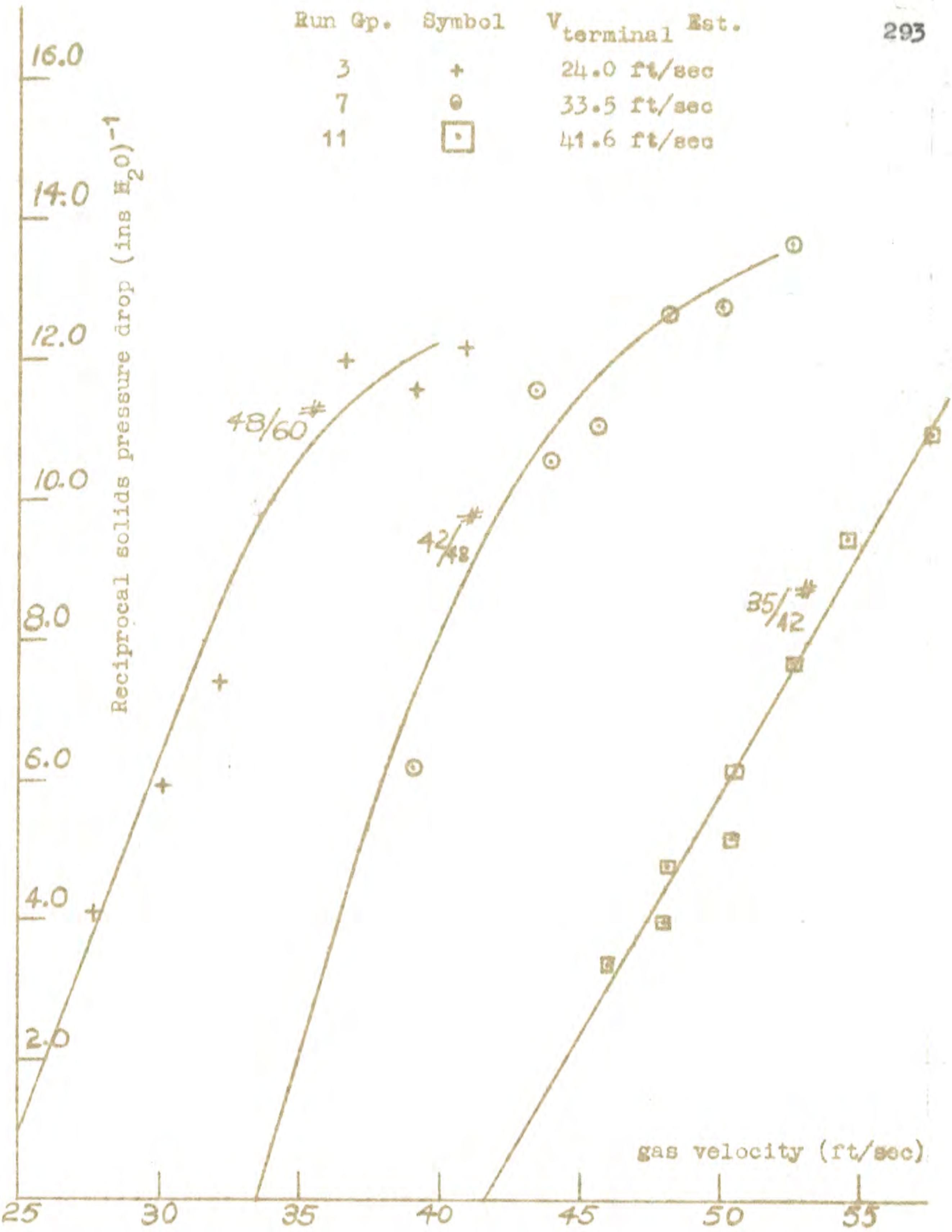

FIGURE 4.15 Plot of reciprocal solids pressure drop vs average gas velocity for the 600°C runs

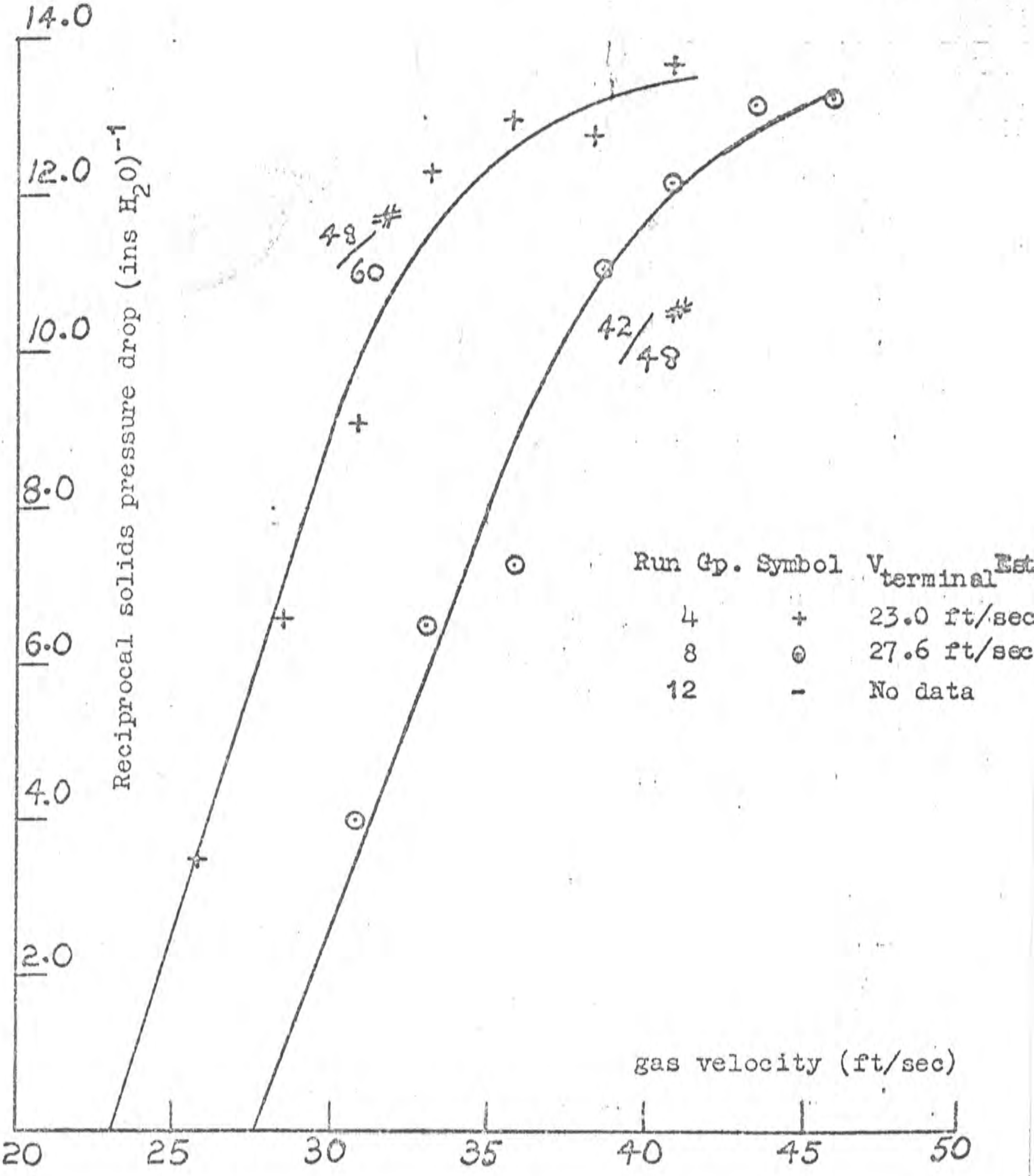

FIGURE 4.16 Plot of reciprocal solids pressure drop vs. average gas velocity for the 700°C runs

4.9 Discussion of Results

The analysis of the results indicates that much higher rates of reduction were attained in the transport reactor than were obtained with the fixed bed reactor. For comparison the observed degree of conversion for run 7-4 (chosen because it approximates average conditions) is compared with a value of the degree of conversion calculated by extrapolation of the rate equations which describe the fixed bed data, viz.

(i) the degree of reduction observed for run 7-4 was 78.6% at 608°C with an estimated residence time of 3.53 sec., and

(ii)* the degree of reduction predicted by the fixed bed equations 3.9 and 3.17 for identical temperature and time conditions is 2.1%.

This marked difference is typical of the other data and it is apparent that the kinetic relationships established for the fixed bed results are not satisfactory when applied to the transport reactor data.

The differences in the experimental conditions between the two reactors were reaction temperature,

---

* Note: Time is in minutes for these equations.

reaction time, and the method of gas solid contact. In the transport reactor the temperatures were higher, the residence times much shorter, and the gas-solid contact was achieved in the dilute fluidized phase. The higher reaction rates observed in the transport reactor could be due to one or a combination of the following factors:

(i) a large systematic error in the particle temperature estimation,

(ii) a large systematic error in the estimate of the particle residence time,

(iii) a change in a rate controlling step due to the effect of temperature,

or (iv) a change in a rate controlling step due to altered mass transfer characteristics, i.e. diffusion of reactants and products to and from the reaction interface.

Particle temperature estimation

The estimate of the particle temperature was made with the assumption that the particle temperature was equal to the gas temperature. This assumption was based on the observations of THEMELIS and GAUVIN (73) and the fact that the reaction is slightly exothermic. Therefore, since the instruments involved in the gas temperature measurement could be read to better than ± 1°C and the corrections for radiation errors were found to be small, (approximately 2% of the gas thermocouple reading due to the excellent convective heat transfer properties of hydrogen), it is considered unlikely that any error in the method of the estimation of the particle temperature would be sufficiently large to account for the observed difference in the reaction rates.

Particle residence time estimation

The particle residence time estimates, based on the momentum balance developed in section 2, are subject to the same systematic errors that were discussed in the analysis of the particle dynamics results, i.e. the confidence limits for the estimate would be of the order of ± 8%. In addition there are two other possible sources of error which may be significant in the application of the model to the transport reactor, viz.

(a) the fact that the particle weight and probably the particle drag coefficient would change during the period of residence in the reaction zone, and

(b) the possibility that the residence times of particles passing through the reactor might not have been uniformly distributed about the mean value.

Since the terminal velocity estimates used for the analysis were based on pressure drop measurements made during actual reduction runs (FIGURES 4.13 to 4.16) errors due to the factors mentioned in point (a) should be minimized. It is therefore considered that the resultant systematic error in the estimation of the mean particle residence time should be within the limits ± 20%. With regard to point (b) no measurements were made to determine the distribution function for the individual particle residence times, this measurement being beyond the scope of the present work. However, if back mixing occurred it would tend to skew the distribution in the direction of low particle residence times, which means that conversion estimates based on the fixed bed rate equation would be too high if the mean residence was used in the calculation. Therefore, since the possible ± 20% systematic error in the residence time estimate would not be sufficient to account for the observed difference in the reaction rates, it is considered that the difference is due to a true change in reaction rate, i.e. either point (iii) or point (iv).

Discussion of possible rate controlling factors

If the rate of diffusion of reactants and products to and from the reaction interface were rate controlling steps, the observed difference in the reaction rates might be attributed to the more efficient gas-solid contact obtained with the transport reactor. In the transport reactor each reacting particle is surrounded by a continuously changing atmosphere in which the partial pressure of H_2 is relatively higher and the partial pressure of H_2O is relatively lower than for a fixed bed. However, in the fixed bed reactor described in section 3, the maximum gas flow commensurate with bed stability was chosen to minimize diffusional effects and it is unlikely that the reaction rates were processes.

Additional evidence to support the hypothesis that the rate of reaction is chemically controlled can be found in the literature and in the observed relationship between the rate constants and the absolute temperature of reaction. This view is upheld in references (2), (3), (4), (5) and (6). The findings of KIVNICK and HIXSON (7) that the rate constant for the reduction of fine N_1O in a fluidized bed depended on the gas velocity, are not considered relevant for the comparison as the hydrogen was diluted with nitrogen and the maximum mole fraction of hydrogen used was only 0.25.

Now the relationships between the fixed bed and the transport reactor rate constants, A and K, respectively, and the absolute temperature, can both be represented by the Arrhenius equation. These observations together with the views advanced in the literature support the argument that the reduction of NiO with hydrogen was chemically controlled in both the fixed bed and transport reactors.

Comparison of the two rate equations

Although the experiments in this and the previous section were designed to compare actual average rates of reaction rather than reaction mechanisms, some interesting observations can be made regarding the form of the rate equations found to fit the experimental data. Two reaction rate equations have been proposed, viz.

(i) $$\frac{dy}{dt} = A(1-y)\ln(t + 1.0) \qquad .....(3.8)$$

for the fixed bed reduction of nickel oxide in the temperature range 300 to 425°C, and

(ii) $$\frac{dy}{dt} = K(1-y) \qquad .....(4.5)$$

for the transport reduction of nickel oxide in the temperature range 550 to 700°C.

It is apparent from the form of the equations that the first rate equation represents an 'autocatalytic' reaction and the second represents a reaction commencing at the maximum rate. The difference is possibly caused by the difference in the temperatures of reaction.

Now equation 3.8 may be written

$$\frac{dy}{dt} = A_1(1-y)\,A_2 \ln(t+1.0) \quad \ldots\ldots (3.8a)$$

where $A_2 \ln(t+1.0) = q =$ the amount of hydrogen adsorbed at time t, see equation 3.7 section 3.3.1.

There are two rate constants in this form of the equation, A_1 represents the rate constant for the surface reaction between adsorbed hydrogen and the available N_1O and A_2 represents the rate constant for the chemisorption of hydrogen. GARNER (10) reports that frequently in chemisorption there is an initial rapid uptake followed by a slow process which can be expressed by an equation of the form:

$$q = \text{constant} \,.\, \ln t + \text{constant}$$

If the difference in the level of temperature between the fixed bed experiments and the transport reactor experiments was sufficient to cause a change of this type in the mechanism of the hydrogen adsorption, i.e. from a steadily increasing rate process to a process with an initial rapid uptake, the fixed bed rate equation could be written:

$$\frac{dy}{dt} = A_1.(1-y).q_o \qquad \text{..... (4.9)}$$

If this equation were valid, the transport reactor could be a special case of the fixed bed rate equation, i.e.

$$\frac{dy}{dt} = K(1-y) \qquad \text{..... (4.5)}$$

and equation 4.9 could be identical with equation 4.5 if

$$K = A_1.q_o \qquad \text{..... (4.10)}$$

A change in mechanism of this kind could also explain the observed difference in Arrhenius activation energies. The relationship between the rate constant A and the absolute temperature has been shown to be of the form:

$$\ln A = \text{const.} - \frac{E}{RT}$$

where E = activation energy of the reaction,

R = gas constant,

and T = absolute temperature.

Now if $A = A_1 \cdot A_2$, it follows that

$$\ln A = \ln A_1 + \ln A_2$$

and hence that the Arrhenius equation for the reaction could be written:

$$\ln A = \ln A_1 + \ln A_2 = \text{const.} - \frac{(E_1 + E_2)}{RT}$$

where $E = E_1 + E_2$,

i.e. E_1 = activation energy for the reaction between adsorbed hydrogen and the available N_1O,

and E_2 = activation energy for the chemisorption of hydrogen on the nickel oxide surface.

The observed value of E for the fixed bed results was 27,750 cal.per g.mole and the observed value of E_1 for the transport reactor results was 21,400 cal. per g. mole. By subtraction the value of E_2 is 6,350 cal. per g. mole. If the hypothesis discussed were true, this value of E_2 should represent the activation energy for the chemisorption of hydrogen on N_1O. Unfortunately no value for the activation energy for the chemisorption of H_2 on N_1O could be found in the literature. However, ROGINSKY and TSELINSKAYA (79) observed values of E ranging between 3,500 and 7,500 cal. per g. mole for the chemisorption of CO on N_1O. This reaction could be expected to have similar kinetic characteristics to the hydrogen chemisorption and hence the value of E_2 = 6,350 cal. per g. mole is of the right order.

The observations of BENTON and EMMETT (2) that the manner of preparation of the N_1O has a significant effect on the kinetics of the reduction, especially the temperature at which the oxide was prepared, might also be explained in terms of the adsorption mechanism. Higher temperatures of preparation of the oxide may lower the number of potential chemisorption sites on the oxide surface.

Confirmation or rejection of the reaction mechanism hypothesis proposed in this section would have required further experimentation in an apparatus specifically designed for the purpose. This additional work was beyond the scope of the current project but will be included in the recommendations for future work.

4.10 Conclusions

4.10.1 Particle residence times

Particle residence times in the transport reactor were estimated from the relationships developed in section 2 which related the average particle velocity to the solids pressure drop. The theoretical velocity at each pressure tap, and the average theoretical velocity between these taps, were estimated with the equations.

(i) $$S = \frac{V_T}{2g}\left[(V_G - V_T)\ \ln\frac{(V_G - V_T)}{(V_G - V_T - V_P)} - (V_G - V_T)\ \ln\frac{(V_G + V_T)}{(V_G + V_T - V_P)}\right]$$

..... (2.28)

and (ii)

$$t = \frac{V_T}{2g}\left[\ln\frac{(V_G - V_T)}{(V_G - V_T - V_P)} - \ln\frac{V_G + V_T}{(V_G + V_T - V_P)}\right]$$

..... (2.29)

Then equation 4.4 was solved for 'a', i.e.

$$a^2(\bar{\bar{x}}^{1.192}-(x_2^{1.192}-x_1^{1.192}))+a(\frac{g.A_c}{W_s}.\Delta P_s-\bar{\bar{x}})-\frac{Lg}{\bar{\bar{x}}^{1.192}}=0$$

..... (4.4)

where $x = V_{P\ \text{theoretical}}$ and $\bar{\bar{x}} = \bar{\bar{V}}_{P\ \text{theoretical}}$.
($V_{P\ \text{theoretical}}$ is written as V_P in equations 2.28 and 2.29).
The estimate of the actual average particle velocity, and hence the mean residence time, was calculated from equation 2.53, viz.:

$$(\overline{V_P})_{\text{actual}} = a\,(\overline{V_P})^{1.192}_{\text{theoretical}} \qquad ..... (2.53)$$

It is considered that residence times calculated with this technique should be within the range ± 20% of the true value.

4.10.2 Reaction rates and degree of conversion in the transport reactor

The observed values for the degree of reduction obtained in the transport reactor ranged from 10 to 90 per cent in a reaction temperature range from 500°C to 700°C. With the residence time estimates summarized in section 4.10.1 the rate equations found to describe the data were:

$$\frac{dy}{dt} = K(1-y) \qquad \text{..... (4.5)}$$

and

$$\ln K = 14.86 - \frac{21,400}{RT} \qquad \text{..... (4.9)}$$

Equation 4.5 integrates to

$$y = 1 - \exp(-Kt) \qquad \text{..... (4.7)}$$

In these equations y = degree of reduction,

t = estimate of the mean particle residence time, min.

K = reaction rate constant,

R = gas constant,

and T = absolute temperature, °K.

These reaction rates were approximately forty times as fast as those predicted by extrapolation of the rate equations which were found to describe the fixed bed data.

Equation 4.9 indicates that the observed activation energy for the reduction of N_1O with hydrogen in a transport reactor was 21,400 cal. per g mole.

It is considered that a likely cause of the higher reduction rates is that in the range of temperatures investigated in the transport reactor the reaction is no longer 'autocatalytic'. This is possibly due to the very rapid initial chemisorption of hydrogen at these temperatures.

4.10.3 The performance of the transport reactor

The experimental results indicate that for the reduction of N_1O with H_2 the transport reactor provides an effective means of contacting the gaseous and solid reactants in the reaction zone with controlled low residence times. This means that efficient utilization can be made of the high reaction rates obtainable with high reaction temperatures, as the particles are contained in the reaction zone no longer than is necessary to achieve the desired degree of conversion, whether partial or complete.

It is considered that this advantage could be utilized with other gas-solid reactions provided that no operational difficulties such as particle sticking or scaling were encountered. One disadvantage of the system is the high gas/solid ratio required for the transport of the solid particles; however, this disadvantage can be minimized by re-circulation provided that the gaseous reaction products are readily removable from the gas stream.

5. RECOMMENDATIONS FOR FUTURE WORK

5.1 Particle Dynamics

In the field of particle dynamics in vertical pneumatic transport it is considered that two aspects of the work warrant further investigation. These aspects are directly related, viz. the nature of the distribution function for the velocities of entrained particles streaming past a point in the riser, see FIGURE 2.9, and secondly the relation of this distribution function to the distribution of particle residence times in a riser of finite length. These recommendations are made because of the possible application of the results to the study of transport reactors.

5.2 Kinetics of the Reduction of N_1O with H_2

In view of the findings discussed in sections 3.10 and 4.9, particularly with regard to the very high reaction rates observed in the transport reactor, it is suggested that a fundamental investigation of the reduction of N_1O with H_2 would be worth-while over a wide temperature range, e.g. 300-700^oC. It would be of particular interest to check the hypothesis that a very rapid initial adsorption occurs at high temperatures thus making the reaction no longer 'autocatalytic'. It was suggested in this thesis that this effect was responsible for the higher than anticipated reaction rates in the transport system and also for the change in the observed Arrhenius activation energy.

BIBLIOGRAPHY

(1) ELLIOTT, J.F. and GLEISER, M., 'Thermochemistry for Steel Making', Addison-Wesley, 1960.

(2) BENTON, A.F. and EMMETT, P.H., Jnl.Amer.Chem.Soc., 38, 2263, (1916)

(3) PARRAVANO, G., Jnl.Amer.Chem.Soc., 74, 1194, (1952)

(4) HAUFFE, K. and RAHMEL, A., Z.phys.Chem., 1, 104 (1954).

(5) KUZNETSOV, A.N., Russian Jnl.Phys.Chem.(English Trans., 34, 15, (1960)

(6) BANDROWSKI, J., BICKLING, C.R., YANG, K.H. and HOUGEN, O.A., Chem.Eng.Sci., 17, 379, (1962).

(7) KIVNICK, A. and HIXSON, A.N., Chem.Eng.Prog., 48, 394,(1952).

(8) LANGMUIR, I., Jnl.Amer.Chem.Soc., 38, 2263, (1916).

(9) LEVENSPIEL, O., 'Chemical Reaction Engineering', John Wiley and Sons, New York, 1960, Ch. 11.

(10) GARNER, W.E., 'Chemistry of the Solid State', Butterworths, London, 1955, p. 385.

(11) TAYLOR, H and THON, N , Jnl.Amer.Chem.Soc., 74, 4169, (1952).

(12) MATTHEW, I.G., 'The Kinetics of the Reduction of Lead Monoxide by Hydrogen', Ph.D. Thesis, Chem.Eng.Department, University of Adelaide (1959).

(13) HAMDORF, C.J. 'Reaction Rates in the Fluidized State - Barium Sulphate Reduction', Ph.D. Thesis, Chem.Eng.Dept., University of Adelaide, (1956).

(14) SMITH, J.M., 'Chemical Engineering Kinetics', McGraw-Hill, 1956, Ch. 3.

(15) DAVIES, O.L., 'Statistical Methods in Research and Production', 2nd Ed., Oliver and Boyd, 1954.

(16) YANG, K.H. and HOUGEN, O.A., Chem.Eng.Prog., 46, 176, (1958).

(17) LAUFER, J., 'The Structure of Turbulence in Fully Developed Pipe Flow', N.A.C.A. Report 1174, (1954).

(18) SANDBORN, V.A., 'Experimental Evaluation of Momentum Terms in Turbulent Pipe Flow', N.A.C.A. Technical Note 3266, (1955).

(19) HINZE, J.O., 'Turbulence', McGraw-Hill, N.Y., 1959, p.4.

(20) PRANDTL, L. and TIETJENS, O.G., 'Applied Hydro and Aeromechanics', Dover N.Y., 1957, p. 46.

(21) SCHLICHTING, H., 'Boundary Layer Theory', Pergamon Press, London, 1955, p. 312 (First Ed.)

(22) HINZE, J.O., op.cit., p. 519.

(23) SCHLICHTING, H., op.cit., p. 402.

(24) SCHLICHTING, H., op.cit., p. 401.

(25) SCHLICHTING, H., op.cit., p. 413.

(26) PRANDTL, L. and TIETJENS, O.G., op.cit., p.88.

(27) SCHLICHTING, H., op.cit., p. 507.

(28) PRANDTL, L. and TIETJENS, O.G., op.cit., p. 92.

(29) SCHLICHTING, H., op.cit., p. 15.

(30) BROWN, G.G., 'Unit Operations', Wiley, 1950, p. 76.

(31) LAPPLE, C.E., 'Fluid and Particle Mechanics', University of Delawere, Newark, Delawere, 1954, p. 283.

(32) TOROBIN, L.B. and GAUVIN, W.H., Canadian Jnl. of Chem.Eng., 37, 134, (1959).

(33) NEMENYI, P., Trans.Amer.Geophys.Union, 31, 633, (1940).

(34) COULSON, J.M. and RICHARDSON, J.F. Chemical Engineering, Vol. II, Pergamon, London, 1955, p. 488.

(35) COULSON, J.M. and RICHARDSON, J.F., ibid, p. 482.

(36) PRANDTL, L. and TIETJENS, O.G., op.cit., p. 99.

(37) TOROBIN, L.B. and GAUVIN, W.H., Canadian Jnl.Chem. Eng., 38, 189, (1960).

(38) HOERNER, S. Luftfahrtforschung, 12, 42, (1935).

(39) TAYLOR, G.I., Proc.Roy.Soc.London, A156, 307, (1936).

(40) DRYDEN, H.L., N.A.C.A. 392.

(41) van der HEGGE ZIJNEN, App.Sci.Res., A7, 205, (1958).

(42) ROUSE, H., 'Elementary Mechanics of Fluids', Wiley N.Y., 1956, p. 245.

(43) BROWN, G.G., 'Unit Operations', Wiley N.Y., 1950, p.77.

(44) WILHELM, R.H. and VALENTINE, S., Ind.Eng.Chem., 43, 1199, (1951).

(45) MILLER, W.and McINNALLY, T.W., Jnl.Roy.Tech.College Glasgow, 3, Part 4, p. 682 (1936).

(46) WHETTON, J.T. and BROADHURST, P.H., Trans.Instn. Mining Engineers, 111, 920, (1951-1952).

(47) GARNER, F.H. and KENDRICK, P., Trans.Inst.Chemical Engineers, 37, 155, (1959).

(48) TOROBIN, L.B. and GAUVIN, W.H., A.I.Ch.E.Jnl., 7, 615, (1961).

(49) TOROBIN, L.B. and GAUVIN, W.H., ibid, 7, 406, (1961).

(50) ROWE, P.N., Trans.Inst.Chem.Engineers, 39, 175, (1961).

(51) DALLEVALLE, J.M., 'Micromeritics', 2nd Edition, Pitman, 1948, p. 129.

(52) TOROBIN, L.B. and GAUVIN, W.H., Canadian Jnl.Chem. Eng., 39, 113, (1961).

(53) LEVA, M., 'Fluidization', McGraw-Hill, N.Y., 1959, p. 134.

(54) ZENZ, F.A., Ind.Eng.Chem., 41, 2801, (1949).

(55) CRAMP, W. and PRIESTLEY, A., The Engineer, 137, 34, (1924).

(56) LEWIS, W., GILLIAND, E. and BAUER, W., Ind.Eng.Chem., 41, 1104, (1949).

(57) HARIU, O. and MOLSTAD, M., Ind.Eng.Chem., 41, 1148, (1949).

(58) CRAMP, W., Jnl.Roy.Soc.Arts, 69, 283, (1921).

(59) TRIPURANENI GOPICHAND, SARMA, K.J.R., NARASINGA, RAO, Ind.Eng.Chem., 51, 1449, (1959).

(60) JENNINGS, M., Engineering, 150, 361, (1940).

(61) VOGT, E. and WHITE, R., Ind.Eng.Chem., 40, 1731, (1948).

(62) BARTH, W., Chemie Ing.Technik, 30, 171-180, (1958).

(63) STEMERDING, S., Chem.Eng.Sci., 17, 599, (1962).

(64) MEHTA, N.C., SMITH, J.M. and COMINGS, E., Ind.Eng. Chem., 49, 986, (1957).

(65) HINZE, J.O., App.Sci.Res., 11, 33, (1962).

(66) BENNETT, C.O. and MEYERS, J.E., 'Momentum, Heat and Mass Transfer', McGraw-Hill, 1962, p. 36.

(67) HELLINCKX, L.J., 'Interaction Between Fluids and Particles', Symposium, London Inst.Chem.Engineers, 1962, p. 72.

(68) GAUVIN, W.H., PASTERNAK, I.S., TOROBIN, L.B. and YAFFE, L., Canadian Jnl.Chem.Eng., 37, 95, (1959).

(69) SOO, S.L. and REGALBUTO, J.A., Canadian Jnl.Chem. Eng., 38, 160 (1960).

(70) GOMEZ, R.M., M.Sc. Thesis, University of Adelaide, 'The Transport Reactor: The Reduction of Lead Sinter and the Oxidation of Lead Sulphide in a Transport Reactor', (1960).

(71) LLOYD, W.A., and AMUNDSON, N.R., Ind.Eng.Chem., 53, 19, (1961).

(72) DALLA LANA, I.G. and AMUNDSON, N.R., Ind.Eng.Chem., 53, 22, (1961).

(73) THEMELIS, N.J. and GAUVIN, W.H., A.I.Ch.E. Jnl., 8, 437, (1962).

(74) GAUVIN, W.H. and GRAVEL, J.J.O., 'Interaction Between Fluids and Particles', Symposium, London Inst.Chem.Engineers, 1962, p. 250.

(75) CULVER, R.V. and GOMEZ, R.M., Aust.Jnl.of App.Sci., 14, 22, (1963).

(76) THEMELIS, N.J. and GAUVIN, W.H., Canadian Jnl.Chem. Eng., 41, 1, (1963).

(77) HOUGEN, O.A., WATSON, K.M. and RAGATZ, R.A., Chemical Process Principles, Vol. II, Wiley, 1947, p. 982.

(78) PORTER, A.S., and TOMPKINS, F.C., Proc. Roy. Soc. A, 217, 529, (1953).

(79) ROGINSKY and TSELINSKAYA, Zhur. fig. Khim. S.S.S.R. 21, 919, (1947).

NOMENCLATURE

A	reaction rate constant for the fixed bed reduction of N_1O
A_c	cross sectional area of a pipe
A_p	projected area of a particle
a	constant, equation 2.53
C_D	drag coefficient
D	pipe diameter
d	particle diameter
E	Arrhenius activation energy
F_D	drag force on a particle
$F_{D\infty}$	drag force on a particle in an array at infinite separation from neighbouring particles
f_s	solids friction factor
$f(t)$	function of time defined by equation 3.12
H	solids hold-up in a vertical pipe
K	reaction rate constant for the transport reduction of N_1O
L	length of pipe
L_s	scale of turbulence
M	mass flow rate
m	particle mass
P	total pressure
p	partial pressure H_2

q moles of H_2 adsorbed at time t

q_o moles of H_2 adsorbed instantaneously

Re pipe Reynolds number

Re_p particle Reynolds number

R gas constant

r reaction rate for model of BANDROWSKI et al (6) or radial cylindrical coordinate

T absolute temperature, ^oK

t time, minutes unless otherwise stated

U instantaneous point velocity in turbulent flow

$\bar{U}$ time average point velocity in turbulent flow

u fluctuating point velocity component in turbulent flow, $\bar{u} = 0$

$V_{av.}$ average velocity based on mass flow rate

V_R relative velocity between particle and fluid

V_P particle velocity in vertical direction

V_G gas velocity in vertical direction

V_T particle terminal velocity

W_s solids feed rate

W_{H_2O} total weight of water formed during the reduction of a sample of N_1O

w_{H_2O} weight of water formed during an element of time during the reduction of a sample of N_1O

X_T moles of oxygen initially present in a sample of N_1O

X moles of oxygen removed from N_1O by reduction with H_2

x axial cylindrical coordinate, or distance between neighbouring particles in an array, or dummy variable.

y degree of reduction for adsorption model

$$\frac{\text{g mole } H_2O}{\text{g mole initial } N_1O} \equiv \frac{\text{g mole } O_2 \text{ removed}}{\text{g mole initial } O_2}$$

$$\equiv \frac{\text{g } O_2 \text{ removed}}{\text{g initial } O_2}$$

y_e observed degree of reduction

α $d\bar{V}_P/d\bar{V}_G$

δ x/d, separation ratio for particles in an array

ΔP_T total pressure drop in vertical pneumatic transport

ΔP_G gas pressure drop in vertical pneumatic transport

ΔP_{sF} pressure drop due to solids-wall friction in vertical pneumatic transport

ΔP_{sA} pressure drop due to solids acceleration in vertical pneumatic transport

ϵ fraction of void space

θ degree of reduction for model of BANDROWSKI et al (6)

λ dimensionless friction factor

μ fluid viscosity

ρ_s solids density

ρ_f gas density

ϕ azimuthal cylindrical coordinate or function name

APPENDIX 2.1 Experimental results for the pneumatic transport experiments

The results which follow are tabulated for each run group designated in TABLE 2.8. Each block of data corresponds to one run group. The headings used for the data that follows are summarized below:

Heading	Description	Units
FEED RATE	solids feed rate, W_s.	g/sec
FLOWRATOR	flowrator setting	-
GASP	gas pressure drop	in H_2O
TOTP	total gas + solids pressure drop	in H_2O
HOLD UP	solids hold-up between trapping valves	g

RUN GROUP NO. 1 FEED RATE 1.14

RUN	NO.	FLOWRATOR	GASP	TOTP	HOLD UP
1	1	44.	.392	.483	.879
1	2	43.	.380	.469	.862
1	3	42.	.364	.457	.890
1	4	41.	.345	.452	.935
1	5	40.	.334	.443	1.023
1	6	39.	.320	.437	1.166
1	7	38.	.310	.428	1.154
1	8	37.	.296	.422	1.449
1	9	36.	.280	.416	1.457
1	10	35.	.270	.416	1.507
1	11	34.	.254	.416	1.727
1	12	33.	.243	.421	2.022
1	13	32.	.231	.428	2.265
1	14	31.	.218	.436	2.498
1	15	30.	.206	.455	2.897
1	16	29.	.198	.476	3.587
1	17	28.	.186	.535	4.349
1	18	27.	.175	.618	5.482
1	19	26.	.165	.785	8.097

RUN GROUP NO. 2 FEED RATE 1.88

RUN	NO.	FLOWRATOR	GASP	TOTP	HOLD UP
2	1	44.	.392	.539	1.366
2	2	43.	.380	.527	1.411
2	3	42.	.364	.521	1.487
2	4	41.	.345	.499	1.568
2	5	40.	.334	.491	1.627
2	6	39.	.320	.487	1.712
2	7	38.	.310	.482	1.760
2	8	37.	.296	.478	2.078
2	9	36.	.280	.481	2.206
2	10	35.	.270	.483	2.371
2	11	34.	.254	.493	2.689
2	12	33.	.243	.504	3.107
2	13	32.	.231	.539	3.769
2	14	31.	.218	.566	4.145
2	15	30.	.206	.607	4.838
2	16	29.	.198	.665	6.164
2	17	28.	.186	.778	8.150
2	18	27.	.175	1.071	11.423

RUN GROUP NO. 3 FEED RATE 2.56

RUN	NO.	FLOWRATOR	GASP	TOTP	HOLD UP
3	1	44.	.392	.583	1.753
3	2	43.	.380	.570	1.852
3	3	42.	.364	.560	1.947
3	4	41.	.345	.552	1.954
3	5	40.	.334	.550	2.088
3	6	39.	.320	.544	2.210
3	7	38.	.310	.540	2.361
3	8	37.	.296	.540	2.668
3	9	36.	.280	.543	2.798
3	10	35.	.270	.552	3.134
3	11	34.	.254	.562	3.302
3	12	33.	.243	.577	3.732
3	13	32.	.231	.607	4.203
3	14	31.	.218	.636	5.072
3	15	30.	.206	.704	6.046
3	16	29.	.198	.758	6.777
3	17	28.	.186	.871	8.003
3	18	27.	.175	1.093	11.860

RUN GROUP NO. 4 FEED RATE 3.25

RUN	NO.	FLOWRATOR	GASP	TOTP	HOLD UP
4	1	44.	.392	.618	2.168
4	2	43.	.380	.612	2.255
4	3	42.	.364	.603	2.346
4	4	41.	.345	.597	2.330
4	5	40.	.334	.597	2.583
4	6	39.	.320	.593	2.895
4	7	38.	.310	.597	2.873
4	8	37.	.296	.595	3.338
4	9	36.	.280	.603	3.382
4	10	35.	.270	.614	4.053
4	11	34.	.254	.628	4.541
4	12	33.	.243	.645	4.642
4	13	32.	.231	.673	5.207
4	14	31.	.218	.717	6.081
4	15	30.	.206	.787	7.161
4	16	29.	.198	.875	8.210
4	17	28.	.186	1.009	10.670
4	18	27.	.175	1.318	14.162

RUN GROUP NO. 5 FEED RATE 1.14

RUN	NO.	FLOWRATOR	GASP	TOTP	HOLD UP
5	1	50.	.474	.577	.917
5	2	49.	.461	.564	.922
5	3	48.	.450	.554	1.095
5	4	47.	.438	.546	1.108
5	5	46.	.422	.535	1.229
5	6	45.	.408	.525	1.306
5	7	44.	.392	.523	1.477
5	8	43.	.379	.515	1.609
5	9	42.	.365	.513	1.891
5	10	41.	.349	.511	1.773
5	11	40.	.334	.515	2.143
5	12	39.	.321	.523	2.577
5	13	38.	.309	.531	2.885
5	14	37.	.294	.544	2.844
5	15	36.	.280	.597	3.782
5	16	35.	.268	.659	4.848
5	17	34.	.256	.729	5.496
5	18	33.	.244	.947	8.654

RUN GROUP NO. 6 FEED RATE 1.88

RUN	NO.	FLOWRATOR	GASP	TOTP	HOLD UP
6	1	50.	.474	.642	1.510
6	2	49.	.461	.628	1.518
6	3	48.	.450	.618	1.739
6	4	47.	.438	.614	1.747
6	5	46.	.422	.603	1.834
6	6	45.	.408	.597	2.051
6	7	44.	.392	.593	2.166
6	8	43.	.379	.593	2.201
6	9	42.	.365	.593	2.680
6	10	41.	.349	.601	2.776
6	11	40.	.334	.607	3.092
6	12	39.	.321	.628	3.578
6	13	38.	.309	.655	4.072
6	14	37.	.294	.692	4.598
6	15	36.	.280	.752	5.894
6	16	35.	.268	.813	6.103
6	17	34.	.256	.951	8.535
6	18	33.	.244	1.342	13.077

RUN GROUP NO. 7 FEED RATE 2.56

RUN	NO.	FLOWRATOR	GASP	TOTP	HOLD UP
7	1	50.	.474	.686	2.085
7	2	49.	.461	.677	2.198
7	3	48.	.450	.677	2.262
7	4	47.	.438	.669	2.265
7	5	46.	.422	.663	2.429
7	6	45.	.408	.659	2.503
7	7	44.	.392	.657	2.719
7	8	43.	.379	.661	2.993
7	9	42.	.365	.661	3.312
7	10	41.	.349	.671	3.461
7	11	40.	.334	.684	3.689
7	12	39.	.321	.710	4.449
7	13	38.	.309	.733	5.093
7	14	37.	.294	.772	5.637
7	15	36.	.280	.852	7.184
7	16	35.	.268	.953	8.132
7	17	34.	.256	1.141	10.582
7	18	33.	.244	1.452	15.075

RUN GROUP NO. 8 FEED RATE 3.25

RUN	NO.	FLOWRATOR	GASP	TOTP	HOLD UP
8	1	50.	.474	.739	2.486
8	2	49.	.461	.725	2.557
8	3	48.	.450	.719	2.702
8	4	47.	.438	.712	2.852
8	5	46.	.422	.710	3.023
8	6	45.	.408	.704	3.296
8	7	44.	.392	.712	3.521
8	8	43.	.379	.712	3.660
8	9	42.	.365	.721	3.853
8	10	41.	.349	.731	4.187
8	11	40.	.334	.747	4.716
8	12	39.	.321	.774	5.237
8	13	38.	.309	.819	6.043
8	14	37.	.294	.869	7.199
8	15	36.	.280	.943	8.082
8	16	35.	.268	1.050	9.658
8	17	34.	.256	1.246	12.209
8	18	33.	.244	1.555	17.052

RUN GROUP NO. 9 FEED RATE 1.14

RUN	NO.	FLOWRATOR	GASP	TOTP	HOLD UP
9	1	60.	.660	.768	1.056
9	2	59.	.647	.745	1.215
9	3	58.	.623	.731	1.140
9	4	57.	.603	.721	1.408
9	5	56.	.584	.704	1.285
9	6	55.	.567	.696	1.294
9	7	54.	.547	.686	1.409
9	8	53.	.526	.679	1.709
9	9	52.	.508	.669	1.671
9	10	51.	.493	.663	1.630
9	11	50.	.478	.663	2.031
9	12	49.	.463	.661	2.340
9	13	48.	.449	.665	2.729
9	14	47.	.433	.677	2.868
9	15	46.	.418	.696	3.433
9	16	45.	.403	.721	3.985
9	17	44.	.389	.768	4.959
9	18	43.	.374	.832	6.212
9	19	42.	.359	.922	7.564
9	20	41.	.347	1.081	9.865
9	21	40.	.329	1.575	17.153

RUN GROUP NO. 10 FEED RATE 1.88

RUN	NO.	FLOWRATOR	GASP	TOTP	HOLD UP
10	1	60.	.660	.826	1.437
10	2	59.	.647	.807	1.769
10	3	58.	.623	.799	1.684
10	4	57.	.603	.787	2.207
10	5	56.	.584	.778	1.822
10	6	55.	.567	.774	2.037
10	7	54.	.547	.764	2.177
10	8	53.	.526	.762	2.242
10	9	52.	.508	.760	2.566
10	10	51.	.493	.752	2.783
10	11	50.	.478	.760	3.089
10	12	49.	.463	.764	3.149
10	13	48.	.449	.772	3.856
10	14	47.	.433	.787	4.345
10	15	46.	.418	.824	4.801
10	16	45.	.403	.859	5.373
10	17	44.	.389	.916	6.358
10	18	43.	.374	1.019	7.466
10	19	42.	.359	1.130	8.959
10	20	41.	.347	1.363	13.183

RUN GROUP NO. 11 FEED RATE 2.56

RUN	NO.	FLOWRATOR	GASP	TOTP	HOLD UP
11	1	60.	.660	.869	2.290
11	2	59.	.647	.863	2.108
11	3	58.	.623	.852	2.344
11	4	57.	.603	.842	2.375
11	5	56.	.584	.832	2.641
11	6	55.	.567	.826	2.852
11	7	54.	.547	.824	2.661
11	8	53.	.526	.824	2.982
11	9	52.	.508	.824	3.424
11	10	51.	.493	.826	3.700
11	11	50.	.478	.830	4.113
11	12	49.	.463	.848	4.283
11	13	48.	.449	.861	4.290
11	14	47.	.433	.885	5.335
11	15	46.	.418	.927	6.022
11	16	45.	.403	.972	7.048
11	17	44.	.389	1.036	7.586
11	18	43.	.374	1.137	9.717
11	19	42.	.359	1.297	12.023

RUN GROUP NO. 12 FEED RATE 3.25

RUN	NO.	FLOWRATOR	GASP	TOTP	HOLD UP
12	1	60.	.660	.924	2.456
12	2	59.	.647	.906	2.791
12	3	58.	.623	.894	2.787
12	4	57.	.603	.890	2.885
12	5	56.	.584	.881	3.174
12	6	55.	.567	.875	3.290
12	7	54.	.547	.869	3.627
12	8	53.	.526	.871	3.807
12	9	52.	.508	.875	3.996
12	10	51.	.493	.885	4.307
12	11	50.	.478	.892	4.600
12	12	49.	.463	.912	5.200
12	13	48.	.449	.931	5.574
12	14	47.	.433	.957	6.270
12	15	46.	.418	1.009	6.806
12	16	45.	.403	1.058	7.736
12	17	44.	.389	1.143	11.142
12	18	43.	.374	1.260	14.012

RUN GROUP NO. 13 FEED RATE 3.15

RUN	NO.	FLOWRATOR	GASP	TOTP	HOLD UP
13	1	80.	1.113	1.575	5.487
13	2	79.	1.085	1.575	6.980
13	3	78.	1.073	1.585	6.340
13	4	77.	1.035	1.606	6.599
13	5	76.	1.018	1.627	7.535
13	6	75.	.989	1.668	9.024
13	7	74.	.967	1.688	9.130
13	8	73.	.942	1.734	10.608
13	9	72.	.921	1.781	11.294
13	10	71.	.898	1.853	12.433
13	11	70.	.878	1.938	14.020
13	12	69.	.857	2.018	15.891
13	13	68.	.834	2.183	18.495
13	14	67.	.812	2.240	19.723

RUN GROUP NO. 14 FEED RATE 5.05

RUN	NO.	FLOWRATOR	GASP	TOTP	HOLD UP
14	1	80.	1.113	1.709	6.689
14	2	79.	1.085	1.709	6.989
14	3	78.	1.073	1.750	8.815
14	4	77.	1.035	1.771	8.847
14	5	76.	1.018	1.790	10.455
14	6	75.	.989	1.812	11.147
14	7	74.	.967	1.874	11.684
14	8	73.	.942	1.925	12.514
14	9	72.	.921	2.018	15.302
14	10	71.	.898	2.090	14.980
14	11	70.	.878	2.224	17.317
14	12	69.	.857	2.306	19.462
14	13	68.	.834	2.512	22.706
14	14	67.	.812	2.749	23.449

RUN GROUP NO. 15 FEED RATE 6.91

RUN	NO.	FLOWRATOR	GASP	TOTP	HOLD UP
15	1	79.	1.085	1.848	9.105
15	2	78.	1.073	1.911	10.066
15	3	77.	1.035	1.932	9.288
15	4	76.	1.018	1.974	11.895
15	5	75.	.989	2.016	12.560
15	6	74.	.967	2.069	12.877
15	7	73.	.942	2.121	14.861
15	8	72.	.921	2.226	17.056
15	9	71.	.898	2.310	19.993
15	10	70.	.878	2.478	26.018
15	11	69.	.857	2.541	24.541
15	12	68.	.834	2.730	27.365
15	13	67.	.812	2.940	28.131

APPENDIX 2.2 Analysis of the experimental results

The analysis of the experimental results was made with the aid of an I.B.M. 1620 computer. Two programs were used, the first calculated the actual and theoretical average particle velocities between the pressure taps, and the second program used these results to calculate a theoretical solids pressure drop based on the model developed in section 2.3 and then compared these results with the measured values. Schematic outlines of the two programs are shown in FIGURES A.2.2.1 and A.2.2.2 respectively. The input data for the first program are the experimental results listed in APPENDIX 2.1. The input data for the second program are the output data from the first program. The output data from both programs are listed on the succeeding fifteen pages of this APPENDIX after FIGURES A.2.2.1 and A.2.2.2. Each of the fifteen run groups occupies a complete page, the first block of data being the results of PROGRAM A.2.2.1 and the second block the results of PROGRAM A.2.2.2. The headings used for these lists are described in TABLE A.2.2.1.

TABLE A.2.2.1 Summary of headings used for computer output lists

Heading	Description	Units
FEED RATE	solids feed rate, W_s.	g/sec
XBAR	mean value of X's in regression calculation	-
YBAR	mean value of Y's in regression calculation	
A, B	linear regression equation coeffs. $Y = A + B.X$	
CORR	correlation coeff. of the regression	
SXX, SYY, SXY	respectively the sum of the squares of the X's, Y's and the sum of the X,Y products	
INTERCEPT = - A/B	particle terminal velocity estimate, where X=gas velocity, Y=solids velocity.	ft/sec
SOLP	measured solids pressure drop	in H_2O
GASV	gas velocity	ft/sec
Y(I)	average solids velocity between the pressure taps calculated from the hold-up measurement	ft/sec

(continued)

TABLE A.2.2.1 (continued)

Heading	Description	Units
VPBAR	average theoretical solids velocity between the pressure taps calculated from equations 2.28 and 2.29	ft/sec
LN(Y)	$\log_e$ (Y(I)), i.e. the logarithm of the actual average solids velocity	
LNV	$\log_e$ VPBAR, i.e. the logarithm of the theoretical average solids velocity	
DELPS	ΔP_s, the theoretical solids pressure drop calculated from equation 2.50	in H_2O
REC (equal to 1./SOLP)	reciprocal of the measured solids pressure drop	in^{-1} H_2O
DIFF	the per cent difference between the measured solids pressure drop (SOLP) and the calculated solids pressure drop (DELPS)	
STAT ACC FRI	respectively the static, acceleration, and friction components of the total theoretical solids pressure drop	in H_2O and per cent of the total theoretical solids pressure drop

FIGURE A.2.2.1 Schematic outline of computer PROGRAM A.2.2.1.

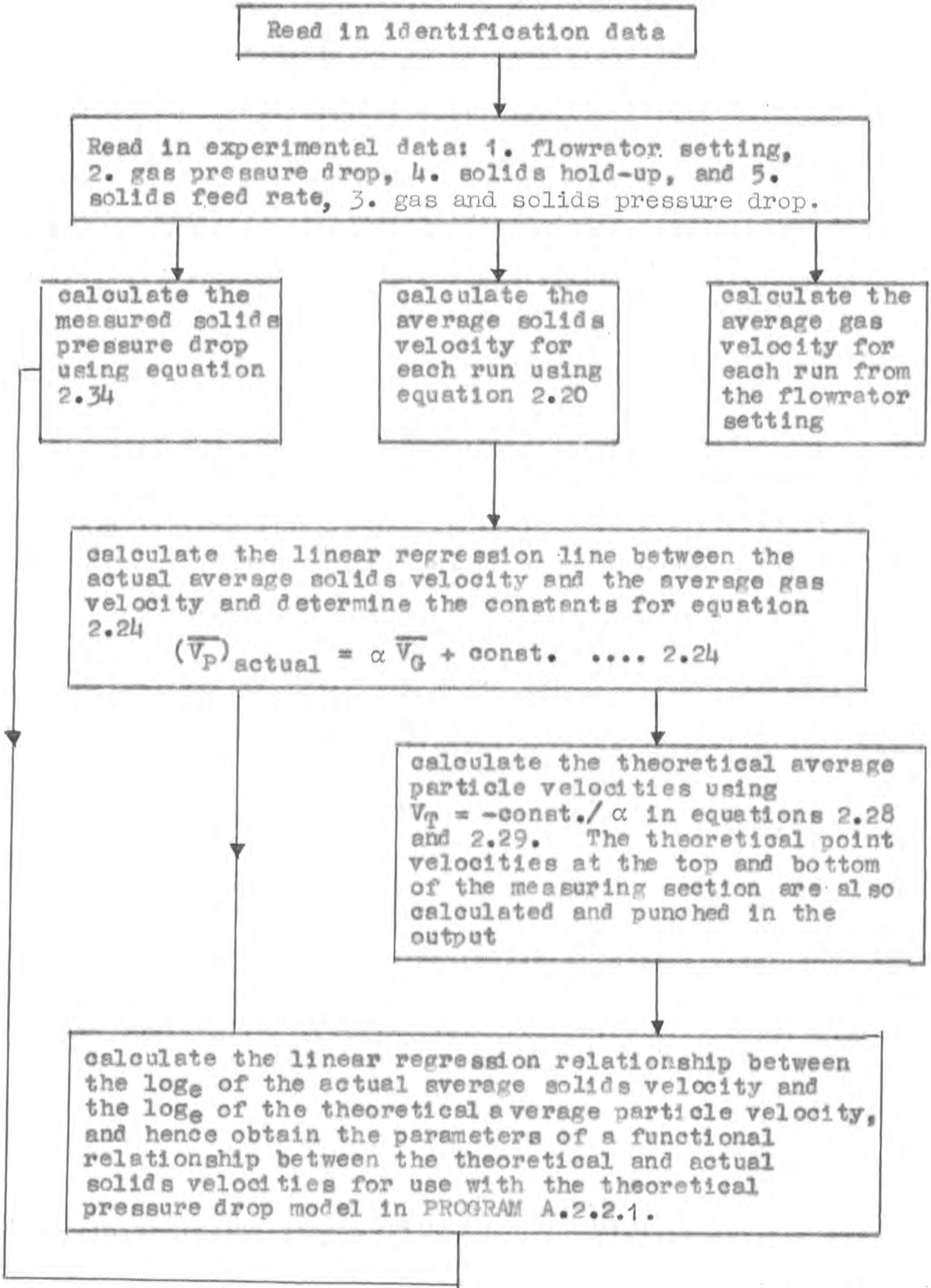

(cont.)

Output results of calculations on punched cards as a suitable input for PROGRAM A.2.2 and for listing, i.e. 1. identification, 2. results of first regression, 3. results of particle trajectory calculations, and 4. results of second regression.

FIGURE A .2.2.2 Schematic outline of computer PROGRAM A.2.2.2.

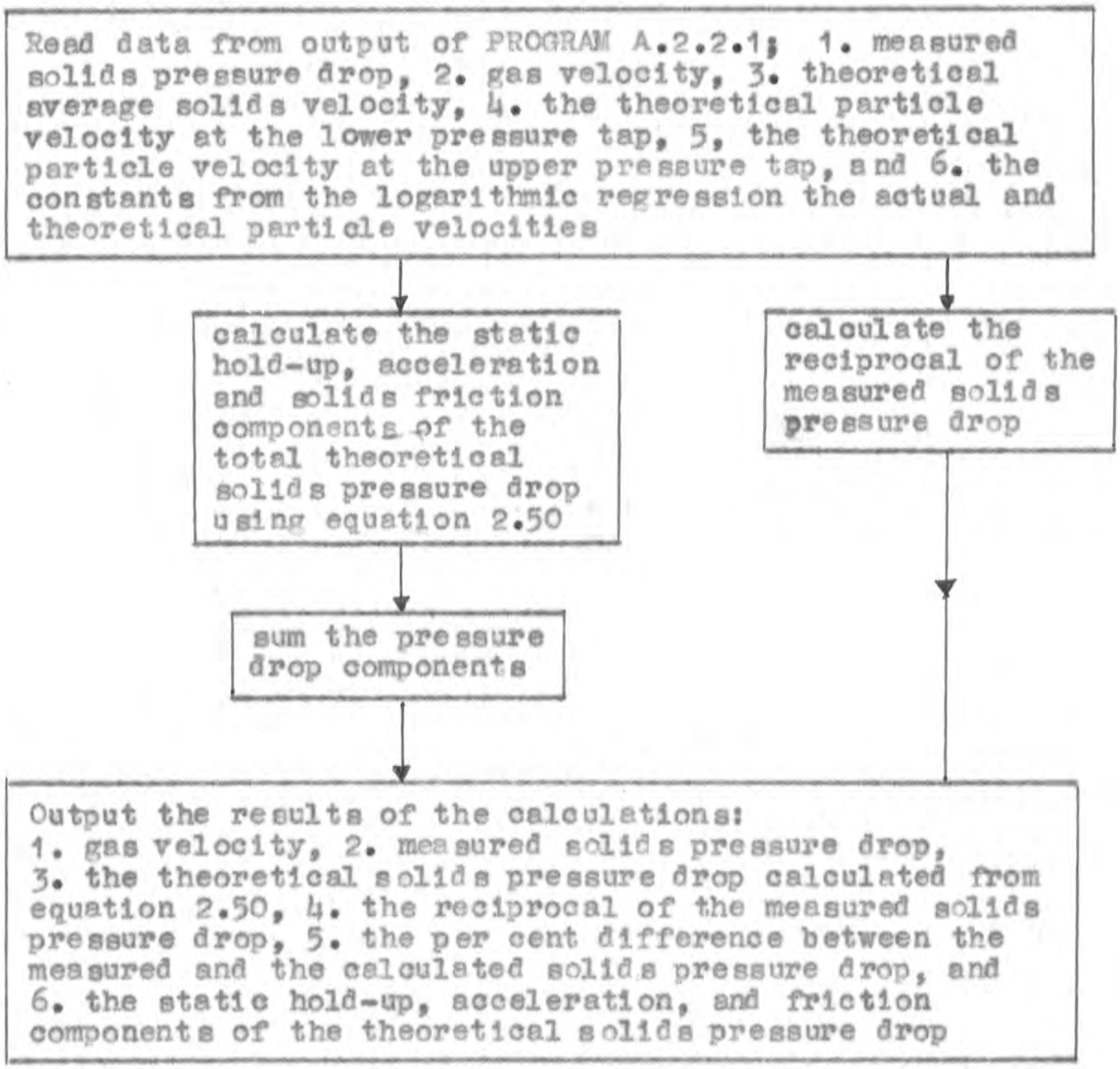

RUN GROUP NO.= 1 FEED RATE=.1140E+01 N=19

XBAR= .2294E+02 YBAR= .4615E+01

A=-.113962E+02 B= .6979E+00 CORR= .9947E+00

SXX= .2203E+03 SXY= .1537E+03 SYY= .1084E+03

INTERCEPT=-A/B= .1632E+02

SOLP	GASV	Y(I)	VPBAR	V1	V2	LN(Y)	LNV
.091	28.53	8.10	10.55	7.770	11.796	2.09258	2.35628
.089	27.91	8.26	10.09	7.478	11.240	2.11210	2.31218
.093	27.29	8.00	9.63	7.181	10.677	2.08014	2.26549
.107	26.67	7.62	9.16	6.880	10.109	2.03081	2.21592
.109	26.04	6.96	8.69	6.574	9.536	1.94087	2.16282
.117	25.42	6.11	8.21	6.263	8.956	1.81003	2.10595
.118	24.80	6.17	7.72	5.945	8.370	1.82037	2.04442
.126	24.18	4.91	7.22	5.620	7.779	1.59273	1.97785
.136	23.56	4.89	6.71	5.286	7.181	1.58723	1.90478
.146	22.94	4.72	6.19	4.944	6.579	1.55348	1.82450
.162	22.31	4.12	5.67	4.590	5.971	1.41722	1.73587
.178	21.69	3.52	5.13	4.225	5.358	1.25952	1.63541
.197	21.07	3.14	4.58	3.844	4.742	1.14603	1.52255
.218	20.45	2.85	4.01	3.446	4.124	1.04811	1.38988
.249	19.83	2.45	3.44	3.026	3.503	.89993	1.23617
.278	19.21	1.98	2.93	2.580	2.882	.68629	1.07682
.349	18.58	1.63	2.71	2.100	2.260	.49366	.99711
.443	17.96	1.29	2.31	1.579	1.639	.26213	.84141
.620	17.34	.87	2.77	1.008	1.017	-.12788	1.02140

XBAR= .1717E+01 YBAR= .1352E+01

A=-.879292E+00 B= .1299E+01 CORR= .9717E+00

SXX= .4446E+01 SXY= .5779E+01 SYY= .7956E+01

GASV	SOLP	DELPS	REC	DIFF	STAT		ACC		FRI	
28.53	.091	.077	10.98	-14.9	.0607	78.4	.0119	15.4	.0047	6.0
27.91	.089	.080	11.23	-9.8	.0643	80.2	.0110	13.7	.0048	6.0
27.29	.093	.083	10.75	-10.3	.0684	82.0	.0100	12.0	.0049	5.8
26.67	.107	.087	9.34	-18.5	.0730	83.7	.0091	10.5	.0049	5.7
26.04	.109	.091	9.17	-16.0	.0781	85.4	.0082	9.0	.0050	5.4
25.42	.117	.096	8.54	-17.4	.0841	87.0	.0074	7.6	.0050	5.2
24.80	.118	.102	8.47	-12.8	.0911	88.7	.0065	6.3	.0050	4.9
24.18	.126	.110	7.93	-12.5	.0994	90.2	.0057	5.1	.0050	4.5
23.56	.136	.119	7.35	-12.2	.1093	91.7	.0049	4.1	.0049	4.1
22.94	.146	.130	6.84	-10.6	.1214	93.0	.0041	3.1	.0048	3.7
22.31	.162	.144	6.17	-10.9	.1361	94.3	.0034	2.3	.0047	3.3
21.69	.178	.162	5.61	-8.7	.1550	95.4	.0027	1.6	.0046	2.8
21.07	.197	.186	5.07	-5.5	.1796	96.5	.0020	1.1	.0044	2.3
20.45	.218	.219	4.58	.5	.2134	97.4	.0015	.6	.0041	1.8
19.83	.249	.265	4.01	6.5	.2605	98.1	.0010	.3	.0038	1.4
19.21	.278	.325	3.59	16.9	.3209	98.7	.0006	.1	.0034	1.0
18.58	.349	.358	2.86	2.8	.3551	98.9	.0003	.0	.0033	.9
17.96	.443	.440	2.25	-.6	.4370	99.2	.0001	.0	.0030	.6
17.34	.620	.348	1.61	-43.7	.3451	99.0	.0000	.0	.0033	.9

```
        RUN GROUP NO.=  2  FEED RATE= .1880E+01 N=18
    XBAR= .2325E+02      YBAR= .4996E+01
    A=-.123758E+02  B= .7471E+00  CORR= .9969E+00
    SXX= .1872E+03       SXY= .1399E+03     SYY= .1051E+03
            INTERCEPT=-A/B= .1656E+02
```

SOLP	GASV	Y(I)	VPBAR	V1	V2	LN(Y)	LNV
.147	28.53	8.60	10.35	7.619	11.571	2.15196	2.33701
.147	27.91	8.32	9.89	7.327	11.014	2.11955	2.29203
.157	27.29	7.90	9.43	7.031	10.451	2.06709	2.24439
.154	26.67	7.49	8.96	6.731	9.883	2.01405	2.19357
.157	26.04	7.22	8.49	6.425	9.308	1.97711	2.13923
.167	25.42	6.86	8.01	6.113	8.728	1.92619	2.08083
.172	24.80	6.67	7.52	5.795	8.141	1.89853	2.01759
.182	24.18	5.65	7.01	5.469	7.548	1.73244	1.94874
.201	23.56	5.32	6.51	5.135	6.950	1.67267	1.87365
.213	22.94	4.95	5.99	4.790	6.346	1.60054	1.79051
.239	22.31	4.36	5.46	4.435	5.737	1.47468	1.69772
.261	21.69	3.78	4.91	4.066	5.124	1.33019	1.59320
.308	21.07	3.11	4.36	3.682	4.507	1.13704	1.47257
.348	20.45	2.83	3.79	3.278	3.888	1.04195	1.33313
.401	19.83	2.42	3.25	2.852	3.267	.88735	1.18006
.467	19.21	1.90	2.79	2.396	2.646	.64512	1.02891
.592	18.58	1.44	2.14	1.904	2.024	.36583	.76135
.896	17.96	1.02	2.39	1.367	1.402	.02822	.87331

```
    XBAR= .1714E+01      YBAR= .1448E+01
    A=-.695486E+00  B= .1250E+01  CORR= .9861E+00
    SXX= .4314E+01       SXY= .5395E+01     SYY= .6938E+01
```

GASV	SOLP	DELPS	REC	DIFF	STAT		ACC		FRI	
28.53	.147	.120	6.80	-17.8	.0958	79.3	.0198	16.4	.0050	4.1
27.91	.147	.125	6.80	-14.9	.1014	81.1	.0183	14.6	.0052	4.1
27.29	.157	.129	6.36	-17.2	.1076	82.8	.0168	12.9	.0054	4.1
26.67	.154	.135	6.49	-11.8	.1147	84.5	.0153	11.2	.0056	4.1
26.04	.157	.142	6.36	-9.3	.1227	86.2	.0138	9.7	.0057	4.0
25.42	.167	.150	5.98	-9.9	.1320	87.8	.0123	8.2	.0059	3.9
24.80	.172	.159	5.81	-7.0	.1428	89.4	.0109	6.8	.0060	3.7
24.18	.182	.171	5.49	-5.7	.1560	90.9	.0095	5.5	.0060	3.5
23.56	.201	.185	4.97	-7.7	.1711	92.3	.0081	4.3	.0060	3.2
22.94	.213	.202	4.69	-4.8	.1898	93.6	.0068	3.3	.0060	2.9
22.31	.239	.224	4.18	-5.9	.2131	94.8	.0055	2.4	.0059	2.6
21.69	.261	.253	3.83	-2.7	.2434	95.9	.0044	1.7	.0058	2.2
21.07	.308	.291	3.24	-5.3	.2824	96.9	.0033	1.1	.0055	1.9
20.45	.348	.344	2.87	-1.0	.3364	97.7	.0024	.6	.0052	1.5
19.83	.401	.414	2.49	3.3	.4077	98.4	.0015	.3	.0049	1.1
19.21	.467	.498	2.14	6.8	.4934	98.9	.0009	.1	.0045	.9
18.58	.592	.691	1.68	16.8	.6874	99.3	.0004	.0	.0038	.5
17.96	.896	.603	1.11	-32.6	.5987	99.2	.0001	.0	.0041	.6

RUN GROUP NO.= 3 FEED RATE= .2560E+01 N=18
XBAR= .2325E+02 YBAR= .5395E+01
A=-.119748E+02 B= .7470E+00 CORR= .9978E+00
SXX= .1872E+03 SXY= .1398E+03 SYY= .1049E+03
INTERCEPT=-A/B= .1602E+02

SOLP	GASV	Y(I)	VPBAR	V1	V2	LN(Y)	LNV
.191	28.53	9.12	10.80	7.964	12.082	2.21126	2.38024
.190	27.91	8.63	10.35	7.671	11.525	2.15632	2.33731
.196	27.29	8.21	9.89	7.373	10.964	2.10629	2.29179
.207	26.67	8.18	9.42	7.072	10.396	2.10271	2.24354
.216	26.04	7.66	8.95	6.765	9.823	2.03638	2.19202
.224	25.42	7.23	8.47	6.454	9.245	1.97959	2.13665
.230	24.80	6.77	7.98	6.136	8.660	1.91350	2.07731
.244	24.18	5.99	7.48	5.811	8.070	1.79125	2.01308
.263	23.56	5.71	6.97	5.479	7.474	1.74368	1.94296
.282	22.94	5.10	6.46	5.138	6.872	1.63027	1.86653
.308	22.31	4.84	5.94	4.787	6.266	1.57806	1.78179
.334	21.69	4.28	5.40	4.424	5.654	1.45564	1.68705
.376	21.07	3.80	4.85	4.048	5.040	1.33679	1.58045
.418	20.45	3.15	4.29	3.656	4.422	1.14885	1.45816
.498	19.83	2.64	3.72	3.244	3.802	.97319	1.31515
.560	19.21	2.36	3.14	2.808	3.181	.85905	1.14572
.685	18.58	1.99	2.72	2.342	2.559	.69277	1.00110
.918	17.96	1.34	2.22	1.840	1.938	.29941	.79758

XBAR= .1791E+01 YBAR= .1556E+01
A=-.530396E+00 B= .1164E+01 CORR= .9976E+00
SXX= .3961E+01 SXY= .4613E+01 SYY= .5399E+01

GASV	SOLP	DELPS	REC	DIFF	STAT		ACC		FRI	
28.53	.191	.163	5.23	-14.4	.1287	78.8	.0257	15.7	.0088	5.4
27.91	.190	.168	5.26	-11.5	.1352	80.5	.0239	14.2	.0088	5.2
27.29	.196	.173	5.10	-11.4	.1426	82.1	.0221	12.7	.0088	5.1
26.67	.207	.180	4.83	-12.9	.1509	83.8	.0203	11.2	.0088	4.9
26.04	.216	.187	4.62	-13.1	.1602	85.4	.0185	9.8	.0087	4.6
25.42	.224	.196	4.46	-12.3	.1708	87.0	.0167	8.5	.0087	4.4
24.80	.230	.206	4.34	-10.1	.1831	88.5	.0150	7.2	.0086	4.1
24.18	.244	.219	4.09	-10.1	.1974	90.0	.0132	6.0	.0084	3.8
23.56	.263	.234	3.80	-10.9	.2143	91.4	.0116	4.9	.0083	3.5
22.94	.282	.252	3.54	-10.5	.2341	92.8	.0099	3.9	.0081	3.2
22.31	.308	.274	3.24	-10.8	.2582	94.0	.0083	3.0	.0078	2.8
21.69	.334	.302	2.99	-9.2	.2885	95.2	.0068	2.2	.0075	2.4
21.07	.376	.339	2.65	-9.6	.3269	96.2	.0054	1.6	.0072	2.1
20.45	.418	.388	2.39	-7.1	.3771	97.1	.0041	1.0	.0067	1.7
19.83	.498	.454	2.00	-8.7	.4451	97.9	.0029	.6	.0062	1.3
19.21	.560	.549	1.78	-1.8	.5422	98.6	.0019	.3	.0057	1.0
18.58	.685	.647	1.45	-5.5	.6409	99.0	.0010	.1	.0052	.8
17.96	.918	.816	1.08	-11.0	.8119	99.3	.0004	.0	.0045	.5

RUN GROUP NO.= 4 FEED RATE= .3250E+01 N=18
XBAR= .2325E+02 YBAR= .5530E+01
A=-.125472E+02 B= .7774E+00 CORR= .9963E+00
SXX= .1872E+03 SXY= .1455E+03 SYY= .1140E+03
INTERCEPT=-A/B= .1613E+02

SOLP	GASV	Y(I)	VPBAR	V1	V2	LN(Y)	LNV
.226	28.53	9.36	10.71	7.893	11.977	2.23743	2.37151
.232	27.91	9.00	10.25	7.600	11.421	2.19808	2.32812
.239	27.29	8.65	9.79	7.303	10.859	2.15852	2.28230
.252	26.67	8.71	9.33	7.001	10.291	2.16536	2.23352
.263	26.04	7.86	8.85	6.695	9.718	2.06228	2.18130
.273	25.42	7.01	8.37	6.384	9.139	1.94825	2.12563
.287	24.80	7.07	7.88	6.066	8.554	1.95587	2.06532
.299	24.18	6.08	7.39	5.741	7.963	1.80586	2.00029
.323	23.56	6.00	6.88	5.408	7.367	1.79276	1.92926
.344	22.94	5.01	6.36	5.067	6.765	1.61177	1.85135
.374	22.31	4.47	5.84	4.715	6.158	1.49808	1.76473
.402	21.69	4.37	5.30	4.351	5.546	1.47609	1.66861
.442	21.07	3.90	4.75	3.974	4.931	1.36123	1.55993
.499	20.45	3.34	4.20	3.579	4.313	1.20606	1.43560
.581	19.83	2.83	3.62	3.164	3.693	1.04258	1.28886
.677	19.21	2.47	3.04	2.725	3.072	.90588	1.11510
.823	18.58	1.90	2.70	2.255	2.450	.64380	.99597
1.143	17.96	1.43	2.37	1.745	1.828	.36067	.86343

XBAR= .1781E+01 YBAR= .1579E+01
A=-.517551E+00 B= .1177E+01 CORR= .9949E+00
SXX= .3863E+01 SXY= .4549E+01 SYY= .5410E+01

GASV	SOLP	DELPS	REC	DIFF	STAT		ACC		FRI	
28.53	.226	.200	4.42	-11.4	.1580	78.9	.0341	17.0	.0079	3.9
27.91	.232	.206	4.31	-11.1	.1663	80.6	.0316	15.3	.0081	3.9
27.29	.239	.213	4.18	-10.7	.1756	82.3	.0292	13.7	.0083	3.9
26.67	.252	.221	3.96	-12.2	.1858	84.0	.0268	12.1	.0085	3.8
26.04	.263	.230	3.80	-12.2	.1977	85.6	.0244	10.5	.0086	3.7
25.42	.273	.242	3.66	-11.3	.2111	87.2	.0220	9.1	.0087	3.6
24.80	.287	.255	3.48	-11.0	.2267	88.8	.0196	7.7	.0088	3.4
24.18	.299	.270	3.34	-9.4	.2445	90.3	.0173	6.4	.0088	3.2
23.56	.323	.289	3.09	-10.2	.2659	91.7	.0151	5.2	.0088	3.0
22.94	.344	.313	2.90	-8.8	.2917	93.0	.0129	4.1	.0087	2.7
22.31	.374	.342	2.67	-8.5	.3225	94.3	.0108	3.1	.0086	2.5
21.69	.402	.378	2.48	-5.7	.3616	95.4	.0088	2.3	.0083	2.2
21.07	.442	.426	2.26	-3.5	.4113	96.4	.0069	1.6	.0081	1.8
20.45	.499	.488	2.00	-2.1	.4755	97.3	.0052	1.0	.0077	1.5
19.83	.581	.577	1.72	-.6	.5663	98.1	.0036	.6	.0072	1.2
19.21	.677	.704	1.47	4.0	.6956	98.7	.0023	.3	.0066	.9
18.58	.823	.807	1.21	-1.9	.7998	99.0	.0012	.1	.0062	.7
17.96	1.143	.938	.87	-17.8	.9324	99.3	.0005	.0	.0057	.6

RUN GROUP NO.= 5 FEED RATE= .1140E+01 N=18
XBAR= .2698E+02 YBAR= .4070E+01
A=-.135740E+02 B= .6539E+00 CORR= .9923E+00
SXX= .1872E+03 SXY= .1224E+03 SYY= .8131E+02
INTERCEPT=-A/B= .2075E+02

SOLP	GASV	Y(I)	VPBAR	V1	V2	LN(Y)	LNV
.103	32.26	7.76	9.54	6.798	10.909	2.05025	2.25599
.103	31.64	7.72	9.12	6.537	10.378	2.04481	2.21090
.104	31.02	6.50	8.69	6.271	9.840	1.87285	2.16295
.108	30.40	6.43	8.26	6.001	9.296	1.86105	2.11158
.113	29.77	5.79	7.81	5.725	8.743	1.75740	2.05645
.117	29.15	5.45	7.36	5.442	8.183	1.69664	1.99674
.131	28.53	4.82	6.90	5.153	7.615	1.57359	1.93204
.136	27.91	4.42	6.43	4.856	7.039	1.48799	1.86115
.148	27.29	3.76	5.94	4.549	6.454	1.32650	1.78307
.162	26.67	4.01	5.45	4.232	5.861	1.39093	1.69582
.181	26.04	3.32	4.94	3.903	5.261	1.20140	1.59771
.202	25.42	2.76	4.41	3.560	4.654	1.01698	1.48543
.222	24.80	2.46	3.87	3.199	4.041	.90408	1.35568
.250	24.18	2.50	3.32	2.816	3.424	.91839	1.20256
.317	23.56	1.88	2.74	2.407	2.804	.63335	1.01074
.391	22.94	1.46	2.21	1.963	2.183	.38504	.79520
.473	22.31	1.29	1.71	1.474	1.561	.25958	.53827
.703	21.69	.82	1.66	.925	.939	-.19441	.51071

XBAR= .1586E+01 YBAR= .1232E+01
A=-.555326E+00 B= .1126E+01 CORR= .9884E+00
SXX= .5505E+01 SXY= .6203E+01 SYY= .7153E+01

GASV	SOLP	DELPS	REC	DIFF	STAT		ACC		FRI	
32.26	.103	.090	9.70	-12.5	.0739	82.1	.0097	10.8	.0063	7.0
31.64	.103	.093	9.70	-9.6	.0778	83.6	.0090	9.7	.0061	6.6
31.02	.104	.096	9.61	-7.2	.0821	85.1	.0083	8.6	.0059	6.1
30.40	.108	.100	9.25	-6.9	.0870	86.6	.0076	7.6	.0057	5.7
29.77	.113	.105	8.84	-6.8	.0926	88.0	.0069	6.6	.0055	5.3
29.15	.117	.110	8.54	-5.3	.0990	89.4	.0062	5.6	.0053	4.8
28.53	.131	.117	7.63	-10.4	.1065	90.8	.0055	4.7	.0051	4.3
27.91	.136	.125	7.35	-7.9	.1153	92.1	.0049	3.9	.0049	3.9
27.29	.148	.135	6.75	-8.7	.1261	93.4	.0042	3.1	.0046	3.4
26.67	.162	.146	6.17	-9.2	.1389	94.5	.0035	2.4	.0043	2.9
26.04	.181	.162	5.52	-10.3	.1552	95.6	.0029	1.8	.0041	2.5
25.42	.202	.182	4.95	-9.6	.1764	96.6	.0023	1.2	.0037	2.0
24.80	.222	.209	4.50	-5.5	.2043	97.5	.0017	.8	.0034	1.6
24.18	.250	.247	4.00	-1.1	.2428	98.2	.0012	.5	.0030	1.2
23.56	.317	.304	3.15	-3.8	.3014	98.8	.0008	.2	.0026	.8
22.94	.391	.386	2.55	-1.0	.3840	99.3	.0004	.1	.0022	.5
22.31	.473	.514	2.11	8.8	.5126	99.6	.0001	.0	.0018	.3
21.69	.703	.531	1.42	-24.3	.5300	99.6	.0000	.0	.0017	.3

RUN GROUP NO.= 6 FEED RATE= .1880E+01 N=18
XBAR= .2698E+02 YBAR= .4402E+01
A=-.133954E+02 B= .6596E+00 CORR= .9972E+00
SXX= .1872E+03 SXY= .1235E+03 SYY= .8192E+02
INTERCEPT=-A/B= .2030E+02

SOLP	GASV	Y(I)	VPBAR	V1	V2	LN(Y)	LNV
.168	32.26	7.78	9.89	7.044	11.318	2.05174	2.29205
.167	31.64	7.74	9.47	6.783	10.789	2.04645	2.24876
.168	31.02	6.75	9.04	6.518	10.254	1.91054	2.20271
.176	30.40	6.72	8.61	6.248	9.711	1.90595	2.15357
.181	29.77	6.40	8.17	5.972	9.161	1.85735	2.10108
.189	29.15	5.72	7.72	5.691	8.604	1.74552	2.04449
.201	28.53	5.42	7.26	5.404	8.039	1.69097	1.98331
.214	27.91	5.33	6.79	5.109	7.466	1.67494	1.91677
.228	27.29	4.38	6.32	4.806	6.885	1.47803	1.84373
.252	26.67	4.23	5.82	4.494	6.296	1.44284	1.76292
.273	26.04	3.80	5.32	4.171	5.700	1.33503	1.67258
.307	25.42	3.28	4.80	3.834	5.096	1.18904	1.57066
.346	24.80	2.88	4.27	3.483	4.486	1.05971	1.45331
.398	24.18	2.55	3.73	3.113	3.871	.93823	1.31782
.472	23.56	1.99	3.17	2.720	3.253	.68991	1.15449
.545	22.94	1.92	2.61	2.298	2.632	.65507	.96005
.695	22.31	1.37	2.14	1.839	2.011	.31967	.76178
1.098	21.69	.89	1.92	1.332	1.389	-.10700	.65234

XBAR= .1671E+01 YBAR= .1326E+01
A=-.671616E+00 B= .1195E+01 CORR= .9926E+00
SXX= .4574E+01 SXY= .5468E+01 SYY= .6634E+01

GASV	SOLP	DELPS	REC	DIFF	STAT		ACC		FRI	
32.26	.168	.139	5.95	-16.6	.1123	80.2	.0184	13.1	.0091	6.5
31.64	.167	.144	5.98	-13.4	.1183	81.8	.0171	11.8	.0090	6.2
31.02	.168	.149	5.95	-10.7	.1251	83.4	.0158	10.5	.0089	5.9
30.40	.176	.155	5.68	-11.3	.1326	85.0	.0145	9.3	.0088	5.6
29.77	.181	.163	5.52	-9.8	.1411	86.5	.0132	8.1	.0086	5.3
29.15	.189	.171	5.29	-9.2	.1510	88.0	.0119	6.9	.0084	4.9
28.53	.201	.181	4.97	-9.6	.1625	89.5	.0107	5.8	.0082	4.5
27.91	.214	.193	4.67	-9.5	.1761	90.9	.0094	4.8	.0080	4.1
27.29	.228	.207	4.38	-8.8	.1918	92.3	.0082	3.9	.0077	3.7
26.67	.252	.226	3.96	-10.2	.2117	93.5	.0070	3.1	.0074	3.3
26.04	.273	.248	3.66	-8.8	.2357	94.7	.0058	2.3	.0071	2.8
25.42	.307	.278	3.25	-9.4	.2665	95.8	.0047	1.7	.0067	2.4
24.80	.346	.316	2.89	-8.5	.3065	96.8	.0036	1.1	.0063	1.9
24.18	.398	.368	2.51	-7.3	.3603	97.6	.0027	.7	.0058	1.5
23.56	.472	.444	2.11	-5.7	.4376	98.4	.0018	.4	.0052	1.1
22.94	.545	.557	1.83	2.3	.5521	98.9	.0011	.2	.0046	.8
22.31	.695	.704	1.43	1.3	.6999	99.3	.0005	.0	.0040	.5
21.69	1.098	.800	.91	-27.0	.7968	99.5	.0001	.0	.0037	.4

RUN GROUP NO.= 7 FEED RATE= .2560E+01 N= 18
XBAR= .2698E+02 YBAR= .4635E+01
A=-.128176E+02 B= .6468E+00 CORR= .9950E+00
SXX= .1872E+03 SXY= .1211E+03 SYY= .7913E+02
INTERCEPT=-A/B= .1981E+02

SOLP	GASV	Y(I)	VPBAR	V1	V2	LN(Y)	LNV
.212	32.26	7.67	10.28	7.319	11.768	2.03781	2.33047
.216	31.64	7.27	9.86	7.057	11.241	1.98504	2.28891
.227	31.02	7.07	9.43	6.791	10.707	1.95633	2.24481
.231	30.40	7.06	9.00	6.522	10.166	1.95501	2.19789
.241	29.77	6.58	8.56	6.247	9.619	1.88510	2.14793
.251	29.15	6.39	8.12	5.967	9.064	1.85509	2.09440
.265	28.53	5.88	7.66	5.681	8.502	1.77232	2.03674
.282	27.91	5.34	7.20	5.389	7.933	1.67631	1.97413
.296	27.29	4.83	6.72	5.089	7.355	1.57503	1.90608
.322	26.67	4.62	6.24	4.780	6.770	1.53103	1.83126
.350	26.04	4.33	5.74	4.462	6.178	1.46723	1.74840
.389	25.42	3.59	5.23	4.132	5.578	1.27990	1.65564
.424	24.80	3.14	4.71	3.789	4.972	1.14472	1.55042
.478	24.18	2.83	4.17	3.430	4.360	1.04323	1.42900
.572	23.56	2.22	3.62	3.051	3.743	.80073	1.28813
.685	22.94	1.96	3.05	2.649	3.124	.67678	1.11731
.885	22.31	1.51	2.48	2.216	2.503	.41343	.90845
1.208	21.69	1.06	2.23	1.744	1.881	.05955	.80512

XBAR= .1753E+01 YBAR= .1395E+01
A=-.762026E+00 B= .1230E+01 CORR= .9948E+00
SXX= .3879E+01 SXY= .4773E+01 SYY= .5935E+01

GASV	SOLP	DELPS	REC	DIFF	STAT		ACC		FRI	
32.26	.212	.187	4.71	-11.6	.1474	78.7	.0268	14.3	.0130	6.9
31.64	.216	.193	4.62	-10.6	.1551	80.3	.0249	12.9	.0129	6.7
31.02	.227	.199	4.40	-11.9	.1639	81.9	.0231	11.5	.0128	6.4
30.40	.231	.207	4.32	-10.1	.1735	83.6	.0212	10.2	.0127	6.1
29.77	.241	.216	4.14	-10.0	.1846	85.2	.0194	8.9	.0125	5.8
29.15	.251	.227	3.98	-9.5	.1970	86.7	.0176	7.7	.0124	5.4
28.53	.265	.239	3.77	-9.5	.2116	88.2	.0158	6.6	.0121	5.0
27.91	.282	.254	3.54	-9.7	.2284	89.7	.0141	5.5	.0119	4.6
27.29	.296	.272	3.37	-7.8	.2486	91.1	.0123	4.5	.0116	4.2
26.67	.322	.294	3.10	-8.5	.2723	92.5	.0106	3.6	.0112	3.8
26.04	.350	.321	2.85	-8.0	.3018	93.8	.0090	2.8	.0108	3.3
25.42	.389	.356	2.57	-8.4	.3384	94.9	.0074	2.0	.0103	2.9
24.80	.424	.400	2.35	-5.4	.3849	96.0	.0059	1.4	.0098	2.4
24.18	.478	.460	2.09	-3.5	.4471	97.0	.0045	.9	.0091	1.9
23.56	.572	.543	1.74	-4.9	.5321	97.8	.0032	.6	.0084	1.5
22.94	.685	.666	1.45	-2.6	.6569	98.5	.0021	.3	.0075	1.1
22.31	.885	.855	1.12	-3.3	.8473	99.0	.0012	.1	.0065	.7
21.69	1.208	.972	.82	-19.5	.9656	99.3	.0005	.0	.0061	.6

RUN GROUP NO.= 8 FEED RATE= .3250E+01 N=18

XBAR= .2698E+02 YBAR= .4828E+01

A=-.131866E+02 B= .6676E+00 CORR= .9986E+00

SXX= .1872E+03 SXY= .1250E+03 SYY= .8371E+02

INTERCEPT=-A/B= .1974E+02

SOLP	GASV	Y(I)	VPBAR	V1	V2	LN(Y)	LNV
.265	32.26	8.17	10.33	7.356	11.829	2.10056	2.33560
.264	31.64	7.94	9.91	7.094	11.301	2.07240	2.29415
.269	31.02	7.51	9.49	6.829	10.768	2.01724	2.25027
.274	30.40	7.12	9.05	6.559	10.227	1.96321	2.20374
.288	29.77	6.71	8.62	6.284	9.680	1.90498	2.15415
.296	29.15	6.16	8.17	6.004	9.126	1.81852	2.10093
.320	28.53	5.76	7.71	5.718	8.564	1.75249	2.04357
.333	27.91	5.54	7.25	5.426	7.995	1.71377	1.98172
.356	27.29	5.27	6.78	5.127	7.418	1.66238	1.91416
.382	26.67	4.85	6.29	4.819	6.834	1.57925	1.84007
.413	26.04	4.30	5.80	4.501	6.242	1.46027	1.75812
.453	25.42	3.87	5.29	4.172	5.643	1.35548	1.66648
.510	24.80	3.36	4.77	3.830	5.037	1.21233	1.56259
.575	24.18	2.82	4.23	3.472	4.425	1.03729	1.44348
.663	23.56	2.51	3.68	3.095	3.809	.92159	1.30449
.782	22.94	2.10	3.11	2.695	3.190	.74344	1.13603
.990	22.31	1.66	2.55	2.265	2.569	.50906	.93648
1.311	21.69	1.19	2.23	1.798	1.947	.17496	.80216

XBAR= .1762E+01 YBAR= .1444E+01

A=-.661067E+00 B= .1194E+01 CORR= .9974E+00

SXX= .3825E+01 SXY= .4569E+01 SYY= .5486E+01

GASV	SOLP	DELPS	REC	DIFF	STAT		ACC		FRI	
32.26	.265	.232	3.77	-12.3	.1829	78.7	.0339	14.6	.0154	6.6
31.64	.264	.239	3.78	-9.4	.1921	80.3	.0316	13.2	.0152	6.3
31.02	.269	.246	3.71	-8.2	.2023	81.9	.0293	11.8	.0151	6.1
30.40	.274	.256	3.64	-6.4	.2141	83.5	.0271	10.5	.0149	5.8
29.77	.288	.266	3.47	-7.4	.2270	85.1	.0248	9.3	.0147	5.5
29.15	.296	.279	3.37	-5.6	.2420	86.6	.0226	8.0	.0145	5.2
28.53	.320	.293	3.12	-8.1	.2593	88.2	.0203	6.9	.0142	4.8
27.91	.333	.311	3.00	-6.5	.2791	89.6	.0181	5.8	.0139	4.4
27.29	.356	.331	2.80	-6.7	.3023	91.0	.0160	4.8	.0135	4.0
26.67	.382	.357	2.61	-6.3	.3307	92.4	.0138	3.8	.0131	3.6
26.04	.413	.388	2.42	-5.8	.3643	93.7	.0118	3.0	.0126	3.2
25.42	.453	.428	2.20	-5.4	.4066	94.9	.0098	2.2	.0120	2.8
24.80	.510	.479	1.96	-5.9	.4601	95.9	.0078	1.6	.0113	2.3
24.18	.575	.547	1.73	-4.7	.5311	96.9	.0060	1.1	.0106	1.9
23.56	.663	.641	1.50	-3.2	.6272	97.7	.0044	.6	.0097	1.5
22.94	.782	.778	1.27	-.4	.7668	98.4	.0029	.3	.0088	1.1
22.31	.990	.981	1.01	-.8	.9719	99.0	.0017	.1	.0077	.7
21.69	1.311	1.148	.76	-12.3	1.1407	99.3	.0008	.0	.0070	.6

RUN GROUP NO.= 9 FEED RATE= .1140E+01 N=21
XBAR= .3226E+02 YBAR= .3476E+01
A=-.129903E+02 B= .5103E+00 CORR= .9899E+00
SXX= .2976E+03 SXY= .1518E+03 SYY= .7909E+02
INTERCEPT=-A/B= .2545E+02

SOLP	GASV	Y(I)	VPBAR	V1	V2	LN(Y)	LNV
.108	38.48	6.74	9.99	6.826	11.806	1.90912	2.30245
.098	37.86	5.86	9.62	6.602	11.323	1.76886	2.26460
.108	37.23	6.25	9.25	6.374	10.834	1.83258	2.22463
.118	36.61	5.06	8.86	6.142	10.338	1.62143	2.18232
.120	35.99	5.54	8.47	5.906	9.835	1.71285	2.13731
.129	35.37	5.50	8.07	5.666	9.324	1.70587	2.08926
.139	34.75	5.05	7.67	5.420	8.804	1.62072	2.03783
.153	34.13	4.16	7.25	5.169	8.276	1.42770	1.98235
.161	33.50	4.26	6.83	4.911	7.738	1.45018	1.92220
.170	32.88	4.37	6.40	4.647	7.191	1.47502	1.85656
.185	32.26	3.50	5.95	4.374	6.634	1.25508	1.78436
.198	31.64	3.04	5.49	4.092	6.066	1.11345	1.70443
.216	31.02	2.61	5.02	3.799	5.487	.95967	1.61445
.244	30.40	2.48	4.53	3.493	4.898	.90999	1.51245
.278	29.77	2.07	4.03	3.172	4.300	.73017	1.39454
.318	29.15	1.78	3.50	2.832	3.692	.58107	1.25560
.379	28.53	1.43	2.96	2.469	3.078	.36240	1.08706
.458	27.91	1.14	2.41	2.076	2.459	.13712	.88084
.563	27.29	.94	1.88	1.643	1.838	-.05979	.63376
.734	26.67	.72	1.55	1.154	1.216	-.32538	.44253
1.246	26.04	.41	1.44	.591	.595	-.87856	.36964

XBAR= .1603E+01 YBAR= .1014E+01
A=-.103134E+01 B= .1275E+01 CORR= .9912E+00
SXX= .7480E+01 SXY= .9543E+01 SYY= .1239E+02

GASV	SOLP	DELPS	REC	DIFF	STAT		ACC		FRI	
38.48	.108	.101	9.25	-6.4	.0802	79.4	.0116	11.5	.0091	9.0
37.86	.098	.104	10.20	6.2	.0842	80.8	.0109	10.4	.0089	8.6
37.23	.108	.107	9.25	-.4	.0885	82.3	.0101	9.4	.0088	8.2
36.61	.118	.111	8.47	-5.3	.0935	83.7	.0094	8.4	.0086	7.7
35.99	.120	.116	8.33	-3.1	.0990	85.1	.0087	7.5	.0084	7.2
35.37	.129	.121	7.75	-5.7	.1053	86.6	.0080	6.6	.0082	6.7
34.75	.139	.127	7.19	-8.0	.1123	87.9	.0073	5.7	.0080	6.2
34.13	.153	.135	6.53	-11.6	.1207	89.3	.0066	4.9	.0077	5.7
33.50	.161	.143	6.21	-10.7	.1303	90.6	.0059	4.1	.0075	5.2
32.88	.170	.154	5.88	-9.3	.1415	91.8	.0052	3.4	.0072	4.6
32.26	.185	.166	5.40	-9.8	.1553	93.1	.0045	2.7	.0069	4.1
31.64	.198	.182	5.05	-7.7	.1721	94.2	.0039	2.1	.0065	3.6
31.02	.216	.202	4.62	-6.2	.1929	95.3	.0032	1.6	.0062	3.0
30.40	.244	.228	4.09	-6.3	.2199	96.3	.0026	1.1	.0058	2.5
29.77	.278	.262	3.59	-5.4	.2553	97.1	.0020	.7	.0053	2.0
29.15	.318	.311	3.14	-1.8	.3056	97.9	.0015	.4	.0048	1.5
28.53	.379	.383	2.63	1.2	.3784	98.6	.0010	.2	.0042	1.1
27.91	.458	.496	2.18	8.3	.4918	99.1	.0006	.1	.0036	.7
27.29	.563	.678	1.77	20.4	.6750	99.5	.0002	.0	.0030	.4
26.67	.734	.866	1.36	17.9	.8633	99.6	.0000	.0	.0025	.2
26.04	1.246	.950	.80	-23.6	.9483	99.7	.0000	.0	.0024	.2

RUN GROUP NO.= 10 FEED RATE= .1880E+01 N=20
XBAR= .3257E+02 YBAR= .4116E+01
A=-.141979E+02 B= .5621E+00 CORR= .9858E+00
SXX= .2570E+03 SXY= .1444E+03 SYY= .8358E+02
INTERCEPT=-A/B= .2525E+02

SOLP	GASV	Y(I)	VPBAR	V1	V2	LN(Y)	LNV
.166	38.48	8.17	10.13	6.920	11.975	2.10129	2.31632
.160	37.86	6.64	9.76	6.695	11.493	1.89343	2.27906
.176	37.23	6.97	9.39	6.468	11.005	1.94268	2.23968
.184	36.61	5.32	9.00	6.236	10.510	1.67221	2.19815
.194	35.99	6.44	8.61	6.000	10.008	1.86391	2.15394
.207	35.37	5.76	8.22	5.760	9.498	1.75237	2.10684
.217	34.75	5.39	7.81	5.516	8.980	1.68590	2.05643
.236	34.13	5.24	7.40	5.265	8.453	1.65648	2.00222
.252	33.50	4.57	6.98	5.009	7.917	1.52150	1.94365
.259	32.88	4.22	6.55	4.746	7.372	1.44032	1.87979
.282	32.26	3.80	6.10	4.474	6.817	1.33600	1.80972
.301	31.64	3.73	5.65	4.194	6.251	1.31676	1.73221
.323	31.02	3.04	5.18	3.904	5.675	1.11422	1.64576
.354	30.40	2.70	4.70	3.601	5.089	.99482	1.54765
.406	29.77	2.44	4.19	3.284	4.493	.89502	1.43504
.456	29.15	2.18	3.68	2.949	3.888	.78246	1.30315
.527	28.53	1.84	3.14	2.593	3.275	.61413	1.14544
.645	27.91	1.57	2.58	2.209	2.657	.45349	.95148
.771	27.29	1.31	2.03	1.789	2.037	.27119	.70943
1.016	26.67	.89	1.43	1.319	1.415	-.11507	.35954

XBAR= .1690E+01 YBAR= .1259E+01
A=-.599748E+00 B= .1099E+01 CORR= .9917E+00
SXX= .5847E+01 SXY= .6430E+01 SYY= .7189E+01

GASV	SOLP	DELPS	REC	DIFF	STAT		ACC		FRI	
38.48	.166	.158	6.02	-4.3	.1269	79.9	.0174	11.0	.0144	9.0
37.86	.160	.162	6.25	1.7	.1322	81.2	.0165	10.1	.0139	8.6
37.23	.176	.167	5.68	-5.0	.1379	82.5	.0155	9.3	.0135	8.1
36.61	.184	.172	5.43	-6.3	.1445	83.8	.0146	8.4	.0131	7.6
35.99	.194	.178	5.15	-8.2	.1517	85.2	.0136	7.6	.0126	7.1
35.37	.207	.184	4.83	-10.8	.1596	86.5	.0126	6.8	.0122	6.6
34.75	.217	.192	4.60	-11.3	.1689	87.8	.0116	6.0	.0117	6.1
34.13	.236	.201	4.23	-14.7	.1792	89.0	.0106	5.3	.0112	5.5
33.50	.252	.211	3.96	-16.0	.1911	90.3	.0096	4.5	.0107	5.0
32.88	.259	.223	3.86	-13.5	.2049	91.5	.0086	3.8	.0101	4.5
32.26	.282	.238	3.54	-15.2	.2216	92.7	.0077	3.2	.0096	4.0
31.64	.301	.256	3.32	-14.6	.2410	93.8	.0067	2.6	.0090	3.5
31.02	.323	.279	3.09	-13.4	.2652	94.9	.0057	2.0	.0084	3.0
30.40	.354	.307	2.82	-13.0	.2951	95.9	.0047	1.5	.0077	2.5
29.77	.406	.345	2.46	-14.8	.3348	96.8	.0038	1.1	.0070	2.0
29.15	.456	.395	2.19	-13.2	.3862	97.6	.0029	.7	.0063	1.6
28.53	.527	.467	1.89	-11.2	.4598	98.3	.0021	.4	.0055	1.1
27.91	.645	.576	1.55	-10.5	.5705	98.9	.0013	.2	.0047	.8
27.29	.771	.747	1.29	-3.0	.7426	99.3	.0007	.0	.0038	.5
26.67	1.016	1.094	.98	7.7	1.0913	99.7	.0002	.0	.0028	.2

RUN GROUP NO.= 11 FEED RATE= .2560E+01 N=19

XBAR= .3288E+02 YBAR= .4450E+01

A=-.137972E+02 B= .5548E+00 CORR= .9918E+00

SXX= .2203E+03 SXY= .1222E+03 SYY= .6893E+02

INTERCEPT=-A/B= .2486E+02

SOLP	GASV	Y(I)	VPBAR	V1	V2	LN(Y)	LNV
.209	38.48	6.98	10.41	7.104	12.305	1.94403	2.34297
.216	37.86	7.59	10.04	6.880	11.825	2.02684	2.30680
.229	37.23	6.82	9.66	6.652	11.338	1.92072	2.26864
.239	36.61	6.73	9.28	6.421	10.845	1.90759	2.22841
.248	35.99	6.05	8.89	6.186	10.345	1.80143	2.18571
.259	35.37	5.61	8.50	5.947	9.838	1.72456	2.14040
.277	34.75	6.01	8.10	5.703	9.322	1.79388	2.09197
.298	34.13	5.36	7.69	5.454	8.799	1.67999	2.04006
.316	33.50	4.67	7.27	5.200	8.266	1.54177	1.98414
.333	32.88	4.32	6.84	4.939	7.725	1.46425	1.92352
.352	32.26	3.89	6.40	4.670	7.174	1.35843	1.85718
.385	31.64	3.73	5.95	4.394	6.613	1.31793	1.78444
.412	31.02	3.72	5.49	4.108	6.042	1.31630	1.70357
.452	30.40	2.99	5.01	3.811	5.460	1.09829	1.61272
.509	29.77	2.65	4.52	3.501	4.869	.97716	1.50947
.569	29.15	2.27	4.01	3.175	4.268	.81984	1.38978
.647	28.53	2.10	3.48	2.830	3.659	.74628	1.24899
.763	27.91	1.64	2.94	2.462	3.044	.49871	1.07964
.938	27.29	1.33	2.37	2.063	2.424	.28576	.86496

XBAR= .1819E+01 YBAR= .1380E+01

A=-.779555E+00 B= .1187E+01 CORR= .9956E+00

SXX= .3401E+01 SXY= .4038E+01 SYY= .4837E+01

GASV	SOLP	DELPS	REC	DIFF	STAT		ACC		FRI	
38.48	.209	.209	4.78	.1	.1633	78.0	.0270	12.9	.0188	9.0
37.86	.216	.214	4.62	-.6	.1705	79.4	.0255	11.9	.0184	8.6
37.23	.229	.220	4.36	-3.6	.1785	80.9	.0240	10.8	.0180	8.1
36.61	.239	.227	4.18	-4.8	.1872	82.3	.0225	9.8	.0176	7.7
35.99	.248	.235	4.03	-5.1	.1970	83.7	.0209	8.9	.0172	7.3
35.37	.259	.244	3.86	-5.7	.2078	85.1	.0194	7.9	.0167	6.8
34.75	.277	.254	3.61	-8.1	.2200	86.5	.0179	7.0	.0163	6.4
34.13	.298	.266	3.35	-10.6	.2340	87.8	.0164	6.1	.0157	5.9
33.50	.316	.280	3.16	-11.2	.2501	89.2	.0148	5.3	.0152	5.4
32.88	.333	.296	3.00	-10.8	.2689	90.5	.0133	4.5	.0146	4.9
32.26	.352	.316	2.84	-9.9	.2910	91.8	.0118	3.7	.0140	4.4
31.64	.385	.341	2.59	-11.3	.3173	93.0	.0103	3.0	.0133	3.9
31.02	.412	.370	2.42	-10.0	.3491	94.1	.0089	2.4	.0126	3.4
30.40	.452	.408	2.21	-9.6	.3891	95.2	.0074	1.8	.0119	2.9
29.77	.509	.456	1.96	-10.2	.4397	96.2	.0060	1.3	.0110	2.4
29.15	.569	.521	1.75	-8.2	.5069	97.1	.0047	.9	.0101	1.9
28.53	.647	.612	1.54	-5.3	.5998	97.9	.0035	.5	.0091	1.4
27.91	.763	.743	1.31	-2.5	.7327	98.5	.0023	.3	.0080	1.0
27.29	.938	.954	1.06	1.7	.9463	99.1	.0014	.1	.0068	.7

RUN GROUP NO.= 12 FEED RATE= .3250E+01 N= 18

XBAR= .3319E+02 YBAR= .4848E+01

A=-.150322E+02 B= .5988E+00 CORR= .9963E+00

SXX= .1872E+03 SXY= .1121E+03 SYY= .6764E+02

INTERCEPT=-A/B= .2510E+02

SOLP	GASV	Y(I)	VPBAR	V1	V2	LN(Y)	LNV
.264	38.48	8.27	10.24	6.992	12.105	2.11270	2.32690
.259	37.86	7.27	9.87	6.768	11.624	1.98483	2.29003
.271	37.23	7.28	9.49	6.540	11.136	1.98627	2.25125
.287	36.61	7.04	9.11	6.309	10.642	1.95171	2.21013
.297	35.99	6.39	8.72	6.074	10.141	1.85624	2.16660
.308	35.37	6.17	8.33	5.834	9.632	1.82034	2.12019
.322	34.75	5.60	7.92	5.589	9.115	1.72283	2.07062
.345	34.13	5.33	7.51	5.340	8.590	1.67439	2.01739
.367	33.50	5.08	7.09	5.084	8.055	1.62594	1.95976
.392	32.88	4.71	6.66	4.822	7.512	1.55099	1.89731
.414	32.26	4.41	6.22	4.552	6.958	1.48518	1.82883
.449	31.64	3.90	5.77	4.273	6.394	1.36257	1.75320
.482	31.02	3.64	5.30	3.985	5.820	1.29312	1.66895
.524	30.40	3.23	4.82	3.684	5.236	1.17546	1.57389
.591	29.77	2.98	4.32	3.370	4.642	1.09343	1.46540
.655	29.15	2.62	3.81	3.039	4.038	.96535	1.33871
.754	28.53	1.82	3.28	2.688	3.427	.60051	1.18829
.886	27.91	1.44	2.72	2.310	2.810	.37132	1.00258

XBAR= .1840E+01 YBAR= .1479E+01

A=-.788347E+00 B= .1232E+01 CORR= .9955E+00

SXX= .2658E+01 SXY= .3275E+01 SYY= .4072E+01

GASV	SOLP	DELPS	REC	DIFF	STAT		ACC		FRI	
38.48	.264	.248	3.78	-5.9	.1921	77.3	.0383	15.4	.0179	7.2
37.86	.259	.254	3.86	-1.5	.2010	78.8	.0360	14.1	.0177	6.9
37.23	.271	.262	3.69	-3.1	.2110	80.3	.0338	12.8	.0176	6.7
36.61	.287	.270	3.48	-5.5	.2219	81.9	.0315	11.6	.0174	6.4
35.99	.297	.280	3.36	-5.4	.2342	83.4	.0293	10.4	.0172	6.1
35.37	.308	.291	3.24	-5.2	.2477	84.8	.0271	9.2	.0169	5.8
34.75	.322	.305	3.10	-5.2	.2636	86.3	.0248	8.1	.0166	5.4
34.13	.345	.320	2.89	-7.0	.2815	87.8	.0226	7.0	.0163	5.1
33.50	.367	.338	2.72	-7.7	.3022	89.2	.0204	6.0	.0159	4.7
32.88	.392	.360	2.55	-8.1	.3264	90.6	.0182	5.0	.0155	4.3
32.26	.414	.386	2.41	-6.7	.3551	91.9	.0160	4.1	.0150	3.9
31.64	.449	.417	2.22	-6.9	.3895	93.1	.0138	3.3	.0145	3.4
31.02	.482	.458	2.07	-4.9	.4325	94.3	.0117	2.5	.0139	3.0
30.40	.524	.509	1.90	-2.8	.4861	95.4	.0097	1.9	.0132	2.5
29.77	.591	.576	1.69	-2.4	.5564	96.4	.0078	1.3	.0124	2.1
29.15	.655	.667	1.52	1.8	.6495	97.3	.0059	.8	.0114	1.7
28.53	.754	.795	1.32	5.5	.7812	98.1	.0042	.5	.0104	1.3
27.91	.886	.995	1.12	12.3	.9838	98.7	.0027	.2	.0092	.9

RUN GROUP NO.= 13 FEED RATE= .3150E+01 N=14
XBAR= .4687E+02 YBAR= .2095E+01
A=-.124209E+02 B= .3096E+00 CORR= .9809E+00
SXX= .8792E+02 SXY= .2722E+02 SYY= .8762E+01
INTERCEPT=-A/B= .4010E+02

SOLP	GASV	Y(I)	VPBAR	V1	V2	LN(Y)	LNV
.462	50.91	3.58	7.60	4.982	9.266	1.27760	2.02866
.490	50.29	2.82	7.28	4.796	8.834	1.03693	1.98551
.512	49.67	3.10	6.95	4.606	8.393	1.13310	1.93941
.571	49.05	2.98	6.61	4.411	7.943	1.09306	1.88991
.609	48.43	2.61	6.27	4.211	7.482	.96042	1.83636
.679	47.80	2.18	5.91	4.005	7.010	.78009	1.77812
.721	47.18	2.15	5.55	3.793	6.525	.76841	1.71439
.792	46.56	1.85	5.17	3.572	6.028	.61837	1.64389
.860	45.94	1.74	4.78	3.343	5.516	.55571	1.56518
.955	45.32	1.58	4.37	3.103	4.989	.45962	1.47618
1.060	44.70	1.40	3.95	2.851	4.445	.33949	1.37395
1.161	44.07	1.23	3.50	2.584	3.883	.21423	1.25427
1.349	43.45	1.06	3.03	2.299	3.305	.06248	1.11056
1.428	42.83	.99	2.53	1.990	2.709	-.00180	.93184

XBAR= .1609E+01 YBAR= .6641E+00
A=-.124638E+01 B= .1187E+01 CORR= .9823E+00
SXX= .1506E+01 SXY= .1788E+01 SYY= .2200E+01

GASV	SOLP	DELPS	REC	DIFF	STAT		ACC		FRI	
50.91	.462	.515	2.16	11.6	.4657	90.2	.0162	3.1	.0339	6.5
50.29	.490	.537	2.04	9.7	.4901	91.1	.0151	2.8	.0326	6.0
49.67	.512	.563	1.95	10.0	.5178	91.9	.0140	2.5	.0313	5.5
49.05	.571	.592	1.75	3.8	.5496	92.7	.0130	2.1	.0300	5.0
48.43	.609	.625	1.64	2.7	.5852	93.5	.0119	1.9	.0287	4.5
47.80	.679	.665	1.47	-1.9	.6277	94.2	.0108	1.6	.0272	4.0
47.18	.721	.711	1.38	-1.2	.6763	95.0	.0097	1.3	.0257	3.6
46.56	.792	.768	1.26	-2.9	.7358	95.7	.0086	1.1	.0242	3.1
45.94	.860	.837	1.16	-2.5	.8075	96.4	.0075	.8	.0226	2.7
45.32	.955	.925	1.04	-3.0	.8983	97.0	.0064	.6	.0208	2.2
44.70	1.060	1.037	.94	-2.1	1.0127	97.6	.0053	.5	.0191	1.8
44.07	1.161	1.190	.86	2.5	1.1691	98.2	.0042	.3	.0171	1.4
43.45	1.349	1.405	.74	4.2	1.3874	98.6	.0032	.2	.0150	1.0
42.83	1.428	1.733	.70	21.4	1.7185	99.1	.0022	.1	.0128	.7

RUN GROUP NO.= 14 FEED RATE= .5050E+01 N=14

XBAR= .4687E+02 YBAR= .2700E+01

A=-.163763E+02 B= .4069E+00 CORR= .9759E+00

SXX= .8792E+02 SXY= .3578E+02 SYY= .1529E+02

INTERCEPT=-A/B= .4024E+02

SOLP	GASV	Y(I)	VPBAR	V1	V2	LN(Y)	LNV
.596	50.91	4.71	7.52	4.936	9.170	1.55150	2.01877
.624	50.29	4.51	7.20	4.750	8.736	1.50763	1.97510
.677	49.67	3.58	6.87	4.559	8.294	1.27551	1.92833
.736	49.05	3.56	6.54	4.364	7.842	1.27189	1.87804
.772	48.43	3.01	6.19	4.163	7.379	1.10488	1.82364
.823	47.80	2.83	5.83	3.956	6.905	1.04079	1.76435
.907	47.18	2.70	5.46	3.742	6.419	.99374	1.69927
.983	46.56	2.52	5.09	3.520	5.919	.92512	1.62730
1.097	45.94	2.06	4.69	3.289	5.404	.72398	1.54667
1.192	45.32	2.10	4.28	3.048	4.874	.74525	1.45517
1.346	44.70	1.82	3.85	2.793	4.327	.60028	1.34977
1.449	44.07	1.62	3.40	2.523	3.762	.48350	1.22577
1.678	43.45	1.39	2.93	2.234	3.180	.32934	1.07566
1.937	42.83	1.34	2.42	1.919	2.582	.29714	.88776

XBAR= .1589E+01 YBAR= .9179E+00

A=-.875217E+00 B= .1127E+01 CORR= .9725E+00

SXX= .1596E+01 SXY= .1800E+01 SYY= .2147E+01

GASV	SOLP	DELPS	REC	DIFF	STAT		ACC		FRI	
50.91	.596	.663	1.67	11.2	.5887	88.8	.0313	4.7	.0428	6.4
50.29	.624	.689	1.60	10.4	.6183	89.7	.0293	4.2	.0412	5.9
49.67	.677	.718	1.47	6.2	.6519	90.6	.0273	3.8	.0396	5.5
49.05	.736	.752	1.35	2.2	.6891	91.5	.0253	3.3	.0380	5.0
48.43	.772	.792	1.29	2.6	.7332	92.4	.0232	2.9	.0362	4.5
47.80	.823	.840	1.21	2.0	.7844	93.3	.0211	2.5	.0344	4.0
47.18	.907	.896	1.10	-1.1	.8445	94.2	.0190	2.1	.0325	3.6
46.56	.983	.961	1.01	-2.1	.9140	95.0	.0169	1.7	.0306	3.1
45.94	1.097	1.045	.91	-4.6	1.0024	95.8	.0147	1.4	.0285	2.7
45.32	1.192	1.150	.83	-3.5	1.1112	96.6	.0125	1.0	.0263	2.2
44.70	1.346	1.286	.74	-4.4	1.2521	97.3	.0104	.8	.0240	1.8
44.07	1.449	1.470	.69	1.4	1.4404	97.9	.0083	.5	.0215	1.4
43.45	1.678	1.728	.59	3.0	1.7033	98.5	.0062	.3	.0188	1.0
42.83	1.937	2.133	.51	10.1	2.1130	99.0	.0042	.1	.0159	.7

RUN GROUP NO.= 15 FEED RATE= .6910E+01 N=13

XBAR= .4656E+02 YBAR= .2941E+01

A=-.191420E+02 B= .4742E+00 CORR= .9782E+00

SXX= .7034E+02 SXY= .3336E+02 SYY= .1653E+02

INTERCEPT=-A/B= .4036E+02

SOLP	GASV	Y(I)	VPBAR	V1	V2	LN(Y)	LNV
.763	50.29	4.74	7.13	4.707	8.644	1.55672	1.96522
.838	49.67	4.29	6.80	4.516	8.201	1.45638	1.91782
.897	49.05	4.64	6.46	4.319	7.747	1.53682	1.86681
.956	48.43	3.63	6.11	4.118	7.283	1.28943	1.81153
1.027	47.80	3.43	5.76	3.910	6.807	1.23503	1.75123
1.102	47.18	3.35	5.39	3.695	6.318	1.21010	1.68493
1.179	46.56	2.90	5.00	3.472	5.816	1.06681	1.61140
1.305	45.94	2.53	4.61	3.239	5.299	.92904	1.52889
1.412	45.32	2.16	4.19	2.995	4.766	.77016	1.43501
1.600	44.70	1.65	3.76	2.738	4.216	.50676	1.32634
1.684	44.07	1.75	3.31	2.465	3.648	.56520	1.19803
1.896	43.45	1.57	2.83	2.172	3.063	.45628	1.04169
2.128	42.83	1.53	2.32	1.852	2.462	.42867	.84427

XBAR= .1537E+01 YBAR= .1000E+01

A=-.759460E+00 B= .1144E+01 CORR= .9600E+00

SXX= .1480E+01 SXY= .1695E+01 SYY= .2106E+01

GASV	SOLP	DELPS	REC	DIFF	STAT		ACC		FRI	
50.29	.763	.829	1.31	8.6	.7369	88.8	.0466	5.6	.0456	5.5
49.67	.838	.865	1.19	3.2	.7780	89.8	.0434	5.0	.0440	5.0
49.05	.897	.907	1.11	1.1	.8250	90.9	.0400	4.4	.0423	4.6
48.43	.956	.956	1.04	.0	.8793	91.9	.0366	3.8	.0405	4.2
47.80	1.027	1.012	.97	-1.3	.9407	92.8	.0332	3.2	.0387	3.8
47.18	1.102	1.081	.90	-1.8	1.0149	93.8	.0298	2.7	.0367	3.3
46.56	1.179	1.167	.84	-1.0	1.1060	94.7	.0263	2.2	.0346	2.9
45.94	1.305	1.269	.76	-2.7	1.2136	95.6	.0229	1.8	.0324	2.5
45.32	1.412	1.403	.70	-.6	1.3538	96.4	.0194	1.3	.0300	2.1
44.70	1.600	1.575	.62	-1.5	1.5323	97.2	.0159	1.0	.0275	1.7
44.07	1.684	1.810	.59	7.5	1.7729	97.9	.0125	.6	.0248	1.3
43.45	1.896	2.152	.52	13.5	2.1209	98.5	.0092	.4	.0218	1.0
42.83	2.128	2.686	.46	26.2	2.6623	99.0	.0061	.2	.0184	.6

APPENDIX 3.1 Description of the materials used for the fixed bed and transport reduction of N_1O with H_2O

(1) Preparation of the N_1O

The starting material used was fine, pure nickel monoxide supplied by the Mond Nickel Company. The fine powder was mixed with sufficient water to form small pellets and these pellets were then fired in an electric furnace in a special ceramic crucible ('Silliminite') at 1350°C for approximately four hours. The resulting hardened pellets were screened into three size ranges, viz. 35/42#, 42/48# and 48/60# (Tyler mesh). The sintered material was positively identified as N_1O (Bunsenite) by X-ray diffraction analysis and no impurities were detected.

(2) Gas specifications

The gases used were supplied in high pressure cylinders by Commonwealth Industrial Gases (Aust.) Pty. Ltd.,

(a) Oxygen free nitrogen

99.9% N_2

Water vapour <0.02 g/cu.m. full cylinder

.1% rare gases

O_2 < 10 vol. per 106

carbon and carbon compounds <10 vol. per 10^6

(b) Hydrogen (Industrial)

99.5% H_2

Water vapour < 0.02 g/cu.m full cylinder

.4% N_2

.1% oxygen

CO_2 approx. 100 vol. per 10^6

CO approx. 100 vol. per 10^6

APPENDIX 3.2 Chemical equilibrium and heat of reaction for the reduction of N_1O with hydrogen

A3.2.1 Chemical equilibrium

Theory: (HOUGEN et al (77))

For a reaction

$$bB + cC + \ldots = rR + sS + \ldots$$

the equilibrium constant K is defined by

$$K = \left[\frac{a^r_R \cdot a^s_S \cdots}{a^b_B \cdot a^c_C \cdots} \right] = \exp\left[\frac{-\Delta G^o_R}{RT} \right]$$

where K = the equilibrium constant,

a^x_X = activity of species X at equilibrium,

and ΔG^o = standard free energy change for the reactor, where G^o = f (temp., pressure, and composition) p.984

The standard free energy change for a reaction at 25°C may be written:

$$\left[\Delta G^o_R = \Sigma\Delta G^o_{f(products)} - \Sigma\Delta G^o_{f(reactants)} \right]_{25^oC}$$

where ΔG^o_f refers to the standard free energy of formation of a compound from its elements. If values of ΔG^o_f are available for a range of temperatures the equation may be written:

$$\left[\Delta G^{o}_{R} = \Sigma\Delta G^{o}_{f(products)} - \Sigma\Delta G^{o}_{f(reactants)} \right]_{T}$$

A.3.3.2 The equilibrium constant for gaseous reactions (Ref. Hougen, Watson, and Ragatz, Vol. 2, p. 1016).

In the equation

$$K = \left[\frac{a^{r}_{R} \cdot a^{s}_{S} \cdots\cdots}{a^{b}_{B} \cdot a^{c}_{C} \cdots\cdots} \right]$$

the activities ('a') may be represented in terms of mole fractions and fugacity coefficients:

$$a_B = (N_B \cdot \Pi) \quad \nu_{B\Pi}$$

where N_B = mole fraction B ,

Π = total pressure,

and $\nu_{B\Pi}$ = fugacity coefficient for B at total pressure.

If we assume that at 1.0 atm. the fugacity coefficients of the gases are equal to unity, then the expression for K becomes:

$$K = \left[\frac{N^{r}_{R} \cdot N^{s}_{S} \cdots\cdots}{N^{b}_{B} \cdot N^{c}_{C} \cdots\cdots} \right] \Pi^{r+s \cdots\cdots -b -c}$$

which in terms of the number of moles of a species present (η) is:

$$K = \left[\frac{\eta^{r}_{R} \cdot \eta^{s}_{S} \cdots}{\eta^{b}_{B} \cdot \eta^{c}_{C} \cdots}\right] \cdot \left[\frac{\Pi}{\eta_B + \eta_C \cdots + \eta_R + \eta_S \cdots + \eta_I}\right]^{(r+s+\ldots)-(b+c+\ldots)}$$

where η_I is the number of moles of inert gases present. In the case of a heterogeneous gas-solid reaction the activity of the solid may be taken as unity provided that the total pressure on the system does not differ much from the standard states.

Hence for the reaction:

$$NiO_{(s)} + H_{2(g)} = Ni_{(s)} + H_2O_{(g)}$$

$$K = \left[\frac{\eta H_2O}{\eta H_2}\right]\left[\frac{\Pi}{\eta H_2 + \eta H_2O}\right]^{1-1} = \frac{\eta H_2O}{\eta H_2}$$

Hence if the extent of the reaction at equilibrium is measured by the conversion of hydrogen to water:

$K = \left[\frac{x}{1-x}\right]$ where x is the degree of conversion

and $x = \frac{K}{1+K}$

Values of ΔG^o_f for NiO and H_2O are tabulated by ELLIOTT and GLEISER (1). These values are reproduced in TABLE A3.2.1, together with calculated values of ΔG^o_R, K and x.

TABLE A3.2.1 Summary of equilibrium data for the N_1O-H_2 reaction

Temp. °K	Free energies of formation		ΔG^o_R	K	x- Degree of Conversion of H_2 at eq.m
	$\Delta G^o_f N_1O_{(s)}$	$\Delta G^o_f H_2O_{(g)}$			
	cal/ g-mole	cal/ g-mole	cal/g-mole $N_1O_{(s)}$	per g-mole $N_1O_{(s)}$	
298	-50,570	-54,635	-4,065	963	.9999
400	-48,360	-53,520	-5,160	665	.9985
500	-46,200	-52,360	-6,160	493	.9980
600	-44,100	-51,150	-7,050	372	.9973
700	-42,060	-49,910	-7,850	284	.9965
800	-39,970	-48,640	-8,670	235	.9958
900	-37,940	-47,350	-9,410	193	.9949
1000	-35,910	-46,030	-10,120	162	.9939

NOTE: $K = \exp\left(- \frac{\Delta G^o_R}{RT} \right)$

T = absolute temp. °K,

ΔG^o_R = standard heat of reaction at T°K,

and R = gas constant, 1.987 cal/g-mole per °K.

A3.2.3 Heat of reaction

In this section the heat of reaction for the reaction $N_1O_{(s)} + H_{2(g)} = N_{1(s)} + H_2O_{(g)}$ is calculated as a function of temperature. "The standard heat of reaction is defined as the change in enthalpy resulting from the procedure of the reaction under a pressure of 1.0 atm., starting and ending with all materials at a constant temperature of 25°C."

"The heat of formation of a chemical compound is a special case of the standard heat of a chemical reaction wherein the reactants are the necessary elements and the compound in question is the only product formed. The molal heat of formation of a compound represents (unless otherwise stated) the heat of reaction, ΔH_f, when 1 mole of the compound is formed from the elements at 25°C and 1.0 atm. pressure with the reacting elements originally in the states of aggregation which are stable at these conditions of temperature and pressure." (HOUGEN et al (77)).

The standard heat of reaction may be calculated from the standard heats of formation using the following equation:

$$\left[\Delta H^o_R = \Sigma \Delta H^o_{f(products)} - \Sigma \Delta H^o_{f(reactants)} \right]_{25^oC}$$

where ΔH_R^o = standard heat of reaction

and ΔH_f^o = standard heat of formation

This analysis can be extended to calculate the heat of reaction at any temperature T since:

$$(\Delta H_f^o)_T = (\Delta H_f^o)_{298^oK} + \int_{298}^{T} (\Delta C_p)_f \, dT$$

hence $\left[\Delta H_R^o = \Sigma\Delta H^o_{f(products)} - \Sigma\Delta H^o_{f(reactants)}\right]_T$

For the reaction:

$$N_1O_{(s)} + H_{2(g)} = N_{1(s)} + H_2O_{(g)}$$

the values of ΔH_f for hydrogen and nickel are zero, hence the heat of reaction at temperature T^oK is

$$(\Delta H_R^o)_T = (\Delta H^o_{f(H_2O)})_T - (\Delta H^o_{f(N_1O)})_T$$

Values of $(\Delta H_f^o)_T$ for H_2O and N_1O are tabulated by ELLIOTT and GLEISER (1). These data are reproduced in TABLE A3.2.2 together with $(\Delta H_R)_T$ for a range of temperatures from 298 to 1000^oK.

TABLE A3.2.2 Heats of formation of H_2O and N_iO and heats of reaction for the reaction $N_iO_{(s)} + H_{2(g)} = N_{i(s)} + H_2O_{(g)}$ from a range of temperatures from 298-1,000°K.

Temp.		Heats of formation		Heats of reaction
°C	°K	ΔH_f^o $H_2O_{(g)}$ cal/g-mole	ΔH_f^o $N_iO_{(s)}$ cal/g-mole	ΔH_R^o $N_iO_{(s)} + H_{2(g)} = N_{i(s)} + H_2O_{(s)}$ cal/g-mole $N_iO_{(s)}$
25	298	-57,798	-57,300	-498
127	400	-58,040	-57,150	-890
227	500	-58,270	-56,830	-1440
327	600	-58,490	-56,600	-1890
427	700	-58,700	-56,460	-2240
527	800	-58,880	-56,310	-2570
627	900	-59,060	-56,180	-2880
727	1000	-59,210	-56,070	-3140

APPENDIX 3.3 The analysis of the reduction model of BANDROWSKI et al (6)

BANDROWSKI et al (6) proposed the following rate equation to describe the fixed bed reduction of N_1O:

$$r = r_1 + r_2 = k_1(1-\theta)p^{0.43} + k_2(1-\theta)(\theta)p^{0.05} \quad \ldots\ldots (A.3.1)$$

where r = overall reaction rate, g mole H_2O/g mole initial N_1O per min.

θ = total g moles of N_1O reduced per g mole N_1O charged,

k_1, k_2 = rate constants, and

p = partial pressure of H_2 charged, atm.

At 1.0 atm. pressure this equation reduces to:

$$r = k_1(1-\theta) + k_2(1-\theta)(\theta) \quad \ldots\ldots (A.3.2)$$

and the constants k_1 and k_2 can be evaluated by plotting $(\frac{r}{1-\theta})$ vs. θ and carrying out a linear regression since:

$$(\frac{r}{1-\theta}) = k_1 + k_2\theta \quad \ldots\ldots (A.3.3)$$

BANDROWSKI et al (6) published experimental results for a run at 295°C, 1.0 atm. pressure (Run 6A) but did not evaluate the constants for this run or compare their experimental results with their model. These constants are evaluated in this APPENDIX and the model predictions are compared with the experimental results.

Integration of the rate equation

Equation A.3.2 may be written:

$$r = \frac{d\theta}{dt} = k_1 + (k_2 - k_1)\theta - k_2\theta^2 \qquad \text{..... A.3.4}$$

therefore to solve for θ as a function of time:

$$\int \frac{d\theta}{k_1 + (k_2 - k_1)\theta - k_2\theta^2} = \int dt + \text{const.} \qquad \text{..... A.3.5}$$

where t = time, min. Let $k_1 = a$, $(k_2 - k_1) = b$ and $c = -k_2$, then we can write the L.H.S. of the equation

$$I = \int \frac{d\theta}{a + b\theta + c\theta^2}$$

which if $q = \sqrt{b^2 - 4ac}$ is equal to

$$I = \frac{1}{q} \ln \left[\frac{2c\theta + b - q}{2c\theta + b + q} \right], \text{ provided that } b^2 - 4ac > 0.$$

The solution of equation A.3.4 then becomes:

$$\frac{1}{q} \ln \left[\frac{2c\theta + b - q}{2c\theta + b + q} \right] = t + \text{const.} \qquad \text{...... (A.3.6)}$$

Now the only boundary conditions available are:

$t=0, \ \theta=0$

which means the equation becomes

$$\frac{1}{q} \ln \left[\frac{2c\theta + b - q}{2c\theta + b + q} \right] = t + \frac{1}{q} \ln \left[\frac{b-q}{b+q} \right] \qquad \text{..... (A.3.7)}$$

i.e.

$$\ln \left[\frac{2c\theta + b - q}{2c\theta + b + q} \cdot \frac{(b+q)}{(b-q)} \right] = qt \qquad \text{..... (A.3.8.)}$$

The form of equation A.3.8 is important as it avoids the possibility of negative logarithms which can occur in form A.3.7.

This equation can be solved for θ:

$$\theta = \frac{(b+q)(b-q)(\exp(qt)-1)}{2(c)\left[(b+q)-(b-q)\exp(qt)\right]} \qquad \text{..... (A.3.9)}$$

From this value of θ the rate time t can be determined from equation A.3.2

$$r = k_1(1-\theta) + k_2(1-\theta)(\theta) \qquad \text{..... (A.3.2)}$$

The boundary conditions $t=0$, $\theta=0$ are outside the range

$0.05 < \theta < .95$ claimed for the validity of the model. This may cause the model to give erroneous results for rate vs. time and fractional reduction vs. time.

A comparison between the experimental results of BANDROWSKI et al (6) ($295^{o}C$, 1.0 atm., Run 6A) and their model is shown in TABLE A.3.1. The constants k_1 and k_2 are obtained for a linear regression between $(\frac{r}{1-\theta})$ vs. θ for $0.05 < \theta < .95$; this gave $k_1 = .1303$ and $k_2 = 0.5808$. A similar comparison is made in TABLE A.3.2 between these data of BANDROWSKI et al (6) for $.05 < \theta < .95$ and the adsorption model proposed by the writer - see section 2.1.2 equations (3.8) and (3.9).

TABLE A.3.1 Comparison of experimental (Run 6A, 295°C, 1.0 atm.) and model results, BANDROWSKI et al (6), $.05 < \theta_e < .95$, $k_1 = .1303$ and $k_2 = .5808$.

Time	Experimental fractional reduction θ_e	Model fractional reduction θ Eqn. (I)	Experimental reduction rate r_e	Model reduction rate r Eqn. (B)	$(\theta - \theta_e)^2$	$(r - r_e)^2$
1.5	.1068	.2589	.1423	.2081	.02313	.00433
2.0	.1963	.3659	.2069	.2174	.02876	.000105
2.5	.3024	.4741	.2161	.2133	.02948	.00000784
3.0	.4145	.5772	.2196	.1968	.02647	.000520
4.0	.6232	.7481	.1933	.1422	.01560	.00261
4.5	.7162	.8119	.1630	.1132	.009159	.00248
5.0	.7916	.8618	.1216	.08716	.004928	.00119
5.5	.8457	.8998	.09768	.06542	.002927	.00104
6.0	.9996	.9280	.07260	.04817	.001552	.000597
6.5	.9192	.9486	.05479	.03497	.000864	.000393
7.0	.9414	.9635	.03619	.02513	.000488	.000122
min	g mole H_2O/ g mole initial N_1O		g mole H_2O/ g mole initial N_1O per min		R.M.S. .1015	R.M.S. .0349

TABLE A.3.2 Comparison of experimental results (BANDROWSKI et al (6) Run 6A, 295°C, 1.0 atm.) and model proposed in section 2.1.2 for $0.05 < \theta_e < .95$, A=.2804

Time	Experimental fractional reduction θ_e	Model fractional reduction y Eqn. (3.8)	Experimental reduction rate r_e	Model reduction rate $\frac{dy}{dt}$ Eqn. (3.9)	$(y - \theta_e)^2$	$(\frac{dy}{dt} - r_e)^2$
1.5	.1068	.1988	.1423	.2058	.00846	.00403
2.0	.1963	.3046	.2069	.2142	.01173	.000053
2.5	.3024	.4104	.2161	.2071	.01167	.000008
3.0	.4145	.6000	.2196	.1904	.03441	.00085
4.0	.6232	.6785	.1933	.1451	.00306	.00232
4.5	.7162	.7451	.1630	.1218	.0008092	.00170
5.0	.7916	.8006	.1216	.1002	.000081	.00046
5.5	.8457	.8457	.09768	.0809	.000000	.0002816
6.0	.8886	.8819	.07260	.0644	.0000005	.0000672
6.5	.9192	.9106	.05479	.0505	-	.0000184
7.0	.9414	.9329	.03619	.0391	.0000723	.00000847
Min	g mole H_2O/ g mole initial N_1O		g mole H_2O/g mole initial N_1O per min		SSD = .07029 RMS = .0799	SSD = .009797 RMS = .02984

APPENDIX 3.4 Analysis of variance and multiple regression for the values of the parameter A.

A.4.1 The regression equation

This analysis utilizes the technique of multiple linear regression (15). The dependent variate for this analysis is $\log_{10}A$; the independent variates are $\frac{10^3}{T}$ and $\log_{10}(\bar{d})$, where $\bar{d}$ is the mean particle diameter. These data for the eighteen runs are taken from TABLE 3.9 and are tabulated in TABLE A.4.1.

For the analysis:*

(i) $\log_{10}A = y$,

(ii) $\frac{10^3}{T} = x$,

and(iii) $\log_{10}(\bar{d}) = z$.

A linear relation is calculated such that:

$$Y = a + bx + cz \qquad .....(A.4.1)$$

where Y is a predicted value of y.

The values of the coefficients a, b, c are calculated such that:

---

*NOTE: It is assumed that there is no interaction between the effect of temperature and particle size.

$$Q = \Sigma(y - Y)^2 \text{ is a minimum.}$$

$$Q = \Sigma(y - Y)^2 = \Sigma(y_1 - a - bx_1 - cz_1)^2 \quad \text{..... (A.4.2)}$$

We have the following results from partial differentiation:

$$\frac{1}{2}\frac{\partial Q}{\partial a} = 0 = \Sigma - (y - a - bx - cz) \quad \text{..... (A.4.3)}$$

$$\frac{1}{2}\frac{\partial Q}{\partial b} = 0 = \Sigma - x(y - a - bx - cz) \quad \text{..... (A.4.4)}$$

$$\frac{1}{2}\frac{\partial Q}{\partial c} = 0 = \Sigma - z(y - a - bx - cz) \quad \text{..... (A.4.5)}$$

and points $\bar{y}$, $\bar{x}$, $\bar{z}$ must be on the line, therefore:

$$-a = -\bar{y} + b\bar{x} + c\bar{z} \quad \text{..... (A.4.6)}$$

Hence we can write the normal equations:

$$b\ \Sigma x(x-\bar{x}) + c\Sigma\ x(z-\bar{z}) = \Sigma x(y-\bar{y}) \quad \text{..... (A.4.7)}$$

$$\text{and } b\ \Sigma z(x-\bar{x}) + c\ \Sigma z(z-\bar{z}) = \Sigma\ z(y-\bar{y}) \quad \text{..... (A.4.8)}$$

These equations can be rewritten:

$$b(\Sigma x^2 - \Sigma x\bar{x}) + c(\Sigma\ xz - \Sigma\ x\bar{z}) = (\Sigma\ xy - \Sigma x\bar{y}) \quad \text{..... (A.4.9)}$$

and $b(\Sigma zx - \Sigma z\bar{x}) + c(\Sigma z^2 - \Sigma z\bar{z}) = (\Sigma zy - \Sigma z\bar{y})$

$$\ldots\ldots (A.4.10)$$

Since $\bar{x} = \frac{\Sigma x}{n}$, $\bar{y} = \frac{\Sigma y}{n}$, $\bar{z} = \frac{\Sigma z}{n}$, the equations become:

$$b\left(\Sigma x^2 - \frac{(\Sigma x)^2}{n}\right) + c\left(\Sigma xz - \frac{\Sigma x \, \Sigma z}{n}\right) = \Sigma xy - \frac{\Sigma x \Sigma y}{n} \quad \ldots\ldots (A.4.11)$$

and $$b\left(\Sigma xz - \frac{\Sigma z \, \Sigma x}{n}\right) + c\left(\Sigma z^2 - \frac{(\Sigma z)^2}{n}\right)$$

$$= \Sigma zy - \frac{\Sigma z \, \Sigma y}{n} \quad \ldots\ldots (A.4.12)$$

These equations (A.4.11) and (A.4.12) may be solved for b and c by the determinant method, using the data shown below; the numerical values on the right hand side are calculated from the data in TABLE A.4.1, n = 18.

$$\Sigma x^2 - \frac{(\Sigma x)^2}{n} = (1) = 0.204376$$

$$\Sigma xz - \frac{\Sigma x \, \Sigma z}{n} = (5) = -0.00018901$$

$$\Sigma xy - \frac{\Sigma x \, \Sigma y}{n} = (4) = -1.23920857$$

$$\Sigma z^2 - \frac{(\Sigma z)^2}{n} = (3) = 0.05748854$$

$$\Sigma yz - \frac{\Sigma y \Sigma z}{n} = (6) = 0.021630225$$

also we calculate the total variance of y, $\Sigma (y-\bar{y})^2$

$$= \Sigma y^2 - \frac{(\Sigma y)^2}{n} = (2) = 7.674276444$$

If we rewrite equations (A.4.11) and (A.4.12) respectively using these data, they become:

$$b(1) + c(5) = (4) \qquad \ldots\ldots (A.4.13)$$

$$b(5) + c(3) = (6) \qquad \ldots\ldots (A.4.14)$$

and the determinant solutions of these equations are:

$$b = \frac{\begin{vmatrix} (4) & (5) \\ (6) & (3) \end{vmatrix}}{\begin{vmatrix} (1) & (5) \\ (5) & (3) \end{vmatrix}} \quad \text{and } c = \frac{\begin{vmatrix} (1) & (4) \\ (5) & (6) \end{vmatrix}}{\begin{vmatrix} (1) & (5) \\ (5) & (3) \end{vmatrix}}$$

Evaluating these determinants yields:

(i) $b = -6.063046648$*

(ii) $c = 0.3563188167$, and

(iii) $a = \bar{y} - b\bar{x} - c\bar{z} = 8.946929169$

The regression equation then becomes:

* Note: A large number of figures is maintained for computation of the significance of a, b, c and the regression.

$$\log_{10}A = 8.947 - 6.063\left(\frac{10^3}{T}\right) + 0.3563\log_{10}(\bar{d})$$

..... (A.4.15)

A.4.2 The significance of the regression

The sum of the squares of the deviations of y, $\Sigma(y-\bar{y})^2$, is equal to the residual sum of squares plus the regression sum of squares:

$$\Sigma(y-\bar{y})^2 = \Sigma(y-Y)^2 + \Sigma(Y-\bar{y})^2$$ ..... (A.4.16)

SSy	SS Resid.	SS Regr.
17 df	15 df	2 df (two slope estimates are made)

Since $\Sigma(Y-\bar{y})^2 = (4)b + (6)c = 7.52108662$

and $\Sigma(y-\bar{y})^2 = 7.67427644$

by difference

SS Resid. = .15318982

Mean squares are therefore:

(1) $s^2 = \frac{\text{SS Resid.}}{15} = 0.01021266,$

and (ii) $\frac{\text{SS Regr.}}{2} = 3.7605433$

This gives a variance ratio of $F^2_{15} = \frac{3.7605433}{0.01021266} = 368.224$, which means that the regression is very highly significant.

A.4.3 The significance of the regression coefficients

It can be shown (15) that:

$$V(b) = s^2 \ \Sigma\,(z-\bar{z})^2/\Delta \qquad \ldots\ldots (A.4.17)$$

and $$V(c) = s^2 \ \Sigma\,(x-\bar{x})^2/\Delta \qquad \ldots\ldots (A.4.18)$$

where

$$\Delta = \begin{vmatrix} (1) & (5) \\ (5) & (3) \end{vmatrix}$$ and s^2 = residual mean square,
$= \frac{\text{SS Resid.}}{15} = 0.01021266$

Since $\Sigma\,(x-\bar{x})^2 = \Sigma\,x(x-\bar{x}) = \Sigma\,x^2 - \frac{(\Sigma\,x)^2}{n} = (1)$

and $\Sigma\,(z-\bar{z})^2 = \Sigma\,z(z-\bar{z}) = \Sigma\,z^2 - \frac{(\Sigma\,z)^2}{n} = (3)$

Evaluation of the Δ determinant gives $\Delta = 0.01174924$

$\therefore$ (i) $V(b) = 0.0499701$

$SE_b = .22354$ (standard error estimate) and (ii) $V(c) = 0.177647$

$$SE_c = .42155 \text{ (standard error estimate)}$$

By applying the t-test to the ratios:

$$\frac{b}{SE_b} = 27.123 \text{ and } \frac{c}{SE_c} = 0.8454$$

it is evident that the coefficient b is highly significant and that the coefficient c has a 60% chance of coming from a population whose true value is zero. Hence it is concluded that the coefficient c is not significant. From this it may be concluded that the particle size factor is not significant in this analysis.

A.4.4 The regression equation without the size factor

The regression equation becomes

$$y = a + bx \qquad \ldots\ldots \text{(A.4.19)}$$

$$\text{where } b = \frac{\Sigma xy - \frac{\Sigma x \Sigma y}{n}}{\Sigma x^2 - \frac{(\Sigma x)^2}{n}} = \frac{(4)}{(1)} = -6.06337618$$

and $a = \bar{y} - bx = 8.2716716$

Again the sum of the squares of the deviations of y is equal to the residual sum of squares plus the regression sum of squares:

$$\Sigma(y-\bar{y})^2 = \Sigma(y-Y)^2 + \Sigma(Y-\bar{y})^2$$

SSy	SS Resid.	SS Regr.
17 df	16 df	1 df

By difference

(i) $s^2 = \frac{\text{SS Resid.}}{16} = 0.010030545$ and

(ii) $\frac{\text{SS Regr.}}{1} = 7.5137877$

This gives a variance ratio of $F^1_{16} = 749$ which is extremely significant.

The final equation in terms of $\log_{10}A$ and $\frac{10^3}{T}$ therefore takes the form:

$$\log_{10}A = (8.2717 - \frac{6.0634 \times 10^3}{T}) \qquad \text{..... (A.4.20)}$$

with $SE_{\log_{10}A} = 0.1002$.

TABLE A.4.1 Data tabulation for analysis of variance on the experimentally determined values of the parameter A

Run No.	A Model Parameter	$\log_{10}A$ y	$\frac{10^3}{T}$ x	$\bar{d}$	$\log_{10}\bar{d}$ z
1	.00404	-2.39362	1.745	0.0151	-1.82102
2	.0175	-1.75696	1.672	"	"
3	.0459	-1.33819	1.605	"	"
4	.0996	-1.00174	1.543	"	"
5	.154	-0.81248	1.486	"	"
6	.00359	-2.44491	1.745	0.0127	-1.89620
7	.0152	-1.81816	1.672	"	"
8	.0512	-1.29073	1.605	"	"
9	.0905	-1.04335	1.543	"	"
10	.130	-0.88606	1.486	"	"
16	.395	-0.40340	1.433	"	"
17	.439	-0.35754	1.433	"	"
18	.313	-0.50446	1.433	"	"
11	.00491	-2.30892	1.745	0.01065	-1.97266
12	.0102	-1.99140	1.672	"	
13	.0385	-1.41454	1.605	"	
14	.0942	-1.02595	1.543	"	
15	.147	-0.83268	1.486	"	
		$\bar{y}$ = -1.312505	$\bar{x}$ = 1.5806		$\bar{z}$ = -1.8965

APPENDIX 4.1 Experimental results for the transport reduction of N_1O with hydrogen

The results which follow are tabulated for each run group designated in TABLE 4.1; each page corresponds to a run group.

TRANSPORT REDUCTION OF N_1O - Experimental results for 48/60# N_1O

Run group No. 1

Nominal Temp. = 500°C

Run No.	MASS BALANCE DATA			RESIDENCE TIME DATA		
	Feed wgt. (g) (N_1O)	Product wgt. (g) ($N_1O + N_1$)	Hydrogen make up, cub.ft. at 7.0 in. water and 72°F	Flowrator setting	Solids feed rate (g/sec)	Solids pressure drop - chart scale (approx. in H_2O
1-1	20.124	20.477	.0241	6.0	.3870	.071
1-2	19.982	19.187	.0468	5.5	.3996	.078
1-3	19.960	18.554	.0594	5.0	.4158	.090
1-4	20.040	18.718	.0664	4.5	.4008	.141
1-5	20.097	18.192	.0748	4.0	.3865	.220
1-6	29.779	26.269	.1428	3.5	.4025	.340
	Total H_2O adsorbed for run group = 13.590 g					

Run No.	TEMPERATURE DATA				
	Reactor exit gas °C	Reactor exit wall °C	Reactor inlet gas °C	Reactor inlet wall °C	Reactor cooler top °C
1-1	504	408	494	390	83
1-2	511	420	511	393	78
1-3	516	423	506	385	76
1-4	508	420	504	383	71
1-5	506	420	494	385	68
1-6	508	420	493	385	64

TRANSPORT REDUCTION OF NiO - Experimental results for 48/60 # NiO

Run group No. 2

Nominal Temp. = 550°C

Run No.	MASS BALANCE DATA			RESIDENCE TIME DATA		
	Feed wgt. (g) (NiO)	Product wgt. (g) (NiO + Ni)	Hydrogen make up. cub.ft. at 7.0 in. water and 75°F	Flowrator setting	Solids feed rate (g/sec)	Solids pressure drop - chart scale (approx. in H_2O)
2-1	10.030	9.968	.0504	6.0	.3960	.070
2-2	10.105	9.440	.0574	5.5	.3980	.072
2-3	9.997	8.894	.0660	5.0	.3951	.077
2-4	20.032	16.731	.1410	4.5	.3998	.078
2-5	19.952	16.689	.1414	4.0	.3951	.096
2-6	29.882	25.808	.2464	3.0	.4011	.230
	Total H_2O adsorbed for run group = 17.755 g					

	TEMPERATURE DATA				
	Reactor exit gas °C	Reactor exit wall °C	Reactor inlet gas °C	Reactor inlet wall °C	Reactor cooler top °C
2-1	558	460	557	418	100
2-2	555	460	554	420	93
2-3	558	460	553	415	86
2-4	562	460	558	420	81
2-5	554	455	553	415	76
2-6	555	455	555	415	64

TRANSPORT REDUCTION OF N_1O - Experimental results for 48/60 N_1O

Run group No. 3

Nominal Temp. = 600°C

Run No.	MASS BALANCE DATA			RESIDENCE TIME DATA		
	Feed wgt. (g) (N_1O)	Product wgt. (g) ($N_1O + N_1$)	Hydrogen make up. cub.ft. at 7.0 in. water and 71°F	Flowrator setting	Solids feed rate (g/sec)	Solids pressure drop - chart scale (approx. in H2O)
3-1	10.021	9.069	.0872	5.0	.3782	.082
3-2	10.005	8.381	.0872	4.5	.4002	.086
3-3	10.011	8.455	.0910	4.0	.4004	.083
3-4	20.000	15.868	.1960	3.0	.4032	.134
3-5	20.001	15.628	.1970	2.5	.4124	.168
3-6	30.006	21.244	.3098	2.0	.4055	.243
	Total H_2O adsorbed for run group = 18.362 g					

Run No.	TEMPERATURE DATA				
	Reactor exit gas °C	Reactor exit wall °C	Reactor inlet gas °C	Reactor inlet wall °C	Reactor cooler top °C
3-1	609	488	583	445	94
3-2	607	490	608	455	88
3-3	609	493	595	450	83
3-4	614	490	590	445	69
3-5	607	488	612	447	57
3-6	607	485	604	440	42

TRANSPORT REDUCTION OF N_1O - Experimental results for $^{48}/_{60}$# N_1O

Run group No. 4

Nominal Temp. = 700°C

Run No.	MASS BALANCE DATA			RESIDENCE TIME DATA		
	Feed wgt. (g) (N_1O)	Product wgt. (g) ($N_1O + N_1$)	Hydrogen make up, cub.ft. at 7.0 in. water and 73°F	Flowrator setting	Solids feed rate (g/sec)	Solids pressure drop - chart scale (approx. in H_2O)
4-1	9.994	8.740	.1060	3.5	.3919	.078
4-2	10.038	8.233	.1054	3.0	.3937	.077
4-3	10.111	8.069	.1084	2.5	.4178	.081
4-4	19.993	16.240	.2180	2.0	.3920	.110
4-5	20.045	14.534	.2212	1.5	.4133	.151
4-6	29.960	21.840	.3253	1.0	.4104	.283
4-7	20.037	16.055	.2148	4.0	.4200	.073
	Total H_2O adsorbed for run group = 22.405 g					

Run No.	TEMPERATURE DATA				
	Reactor exit gas °C	Reactor exit wall °C	Reactor inlet gas °C	Reactor inlet wall °C	Reactor cooler top °C
4-1	713	565	692	525	95
4-2	709	570	692	510	88
4-3	709	570	690	517	83
4-4	709	563	697	510	59
4-5	709	560	708	510	49
4-6	709	553	699	495	62
4-7	711	570	692	510	86

TRANSPORT REDUCTION OF N_1O - Experimental results for $^{42}/_{48}$ # N_1O

Run group No. 5

Nominal Temp. = 500°C

Run No.	MASS BALANCE DATA			RESIDENCE TIME DATA		
	Feed wgt. (g) (N_1O)	Product wgt. (g) ($N_1O + N_1$)	Hydrogen make up, cub.ft. at 7.0 in. water and 65°F	Flowrator setting	Solids feed rate (g/sec)	Solids pressure drop - chart scale (approx. in H_2O)
5-1	20.014	19.424	.0302	7.5	.4068	.117
5-2	19.904	18.698	.0355	7.0	.4121	.232
5-3	20.049	18.872	.0636	6.5	.4050	.420
5-4	20.084	19.935	.0273	8.0	.4099	.261
5-5	20.052	16.839	.0863	6.0	.3994	1.052
5-6	29.995	25.674	.1001	6.5	.4042	1.038
5-7	19.941	20.009	.0140	8.5	.4154	.211
	Total H_2O adsorbed for run group = 11.345 g					

Run No.	TEMPERATURE DATA				
	Reactor exit gas °C	Reactor exit wall °C	Reactor inlet gas °C	Reactor inlet wall °C	Reactor cooler top °C
5-1	504	395	505	390	67
5-2	506	397	501	385	54
5-3	511	395	504	385	52
5-4	508	375	507	373	80
5-5	505	387	502	378	52
5-6	504	380	511	372	57
5-7	501	373	497	365	57

Note: A nitrogen leak into the apparatus was discovered during this group of runs.

TRANSPORT REDUCTION OF N_1O - Experimental results for $^{42}/_{48}$ # N_1O

Run group No. 6

Nominal Temp. = 550°C

Run No.	MASS BALANCE DATA: Feed wgt. (g) (N_1O)	MASS BALANCE DATA: Product wgt. (g) ($N_1O + N_1$)	MASS BALANCE DATA: Hydrogen make up, cub.ft. at 7.0 in. water and 72°F	RESIDENCE TIME DATA: Flowrator setting	RESIDENCE TIME DATA: Solids feed rate (g/sec)	RESIDENCE TIME DATA: Solids pressure drop - chart scale (approx. in H_2O)
6-1	9.896	9.528	.0314	8.5	.3990	.071
6-2	10.010	9.172	.0385	8.0	.4004	.081
6-3	10.055	8.897	.0464	7.5	.4054	.099
6-4	20.032	17.551	.1070	7.0	.4088	.190
6-5	19.985	17.044	.1225	6.5	.3957	.278
6-6	29.991	24.806	.1968	6.0	.4026	.786
	Total H_2O adsorbed for run group = 12.195 g.					

Run No.	TEMPERATURE DATA: Reactor exit gas °C	Reactor exit wall °C	Reactor inlet gas °C	Reactor inlet wall °C	Reactor cooler top °C
6-1	553	435	546	420	59
6-2	553	435	543	415	52
6-3	558	430	562	415	49
6-4	560	425	559	403	48
6-5	558	418	546	400	52
6-6	558	410	555	400	57

TRANSPORT REDUCTION OF N_1O - Experimental results for $^{42}/_{48}$# N_1O

Run group No. 7

Nominal Temp. = 600°C

Run No.	MASS BALANCE DATA			RESIDENCE TIME DATA		
	Feed wgt. (g) (N_1O)	Product wgt. (g) ($N_1O + N_1$)	Hydrogen make up, cub.ft. at 7.0 in. water and 70°F	Flowrator setting	Solids feed rate (g/sec)	Solids pressure drop - chart scale (approx. in H_2O)
7-1	10.011	11.689	.0781	7.5	.3973	.073
7-2	9.998	8.419	.0830	7.0	.3921	.078
7-3	9.959	8.509	.0865	6.5	.3801	.079
7-4	20.079	16.147	.1775	6.0	.4089	.090
7-5	20.063	16.678	.1829	5.5	.3934	.086
7-6	30.006	24.227	.2922	4.5	.3798	.160
7-7	19.985	15.974	.1952	5.0	.3843	.094
	Total H_2O adsorbed for run group = 18.835 g					

Run No.	TEMPERATURE DATA				
	Reactor exit gas °C	Reactor exit wall °C	Reactor inlet gas °C	Reactor inlet wall °C	Reactor cooler top °C
7-1	612	479	593	460	107
7-2	604	493	595	464	102
7-3	602	495	607	459	98
7-4	602	495	600	450	95
7-5	614	492	590	455	91
7-6	607	491	602	445	76
7-7	607	490	607	450	83

TRANSPORT REDUCTION OF N_1O - Experimental results for $^{42}/_{48}$ # N_1O

Run group No. 8

Nominal Temp. = 700°C

Run No.	MASS BALANCE DATA			RESIDENCE TIME DATA		
	Feed wgt. (g) (N_1O)	Product wgt. (g) ($N_1O + N_1$)	Hydrogen make up, cub.ft. at 7.0 in. water and 71°F	Flowrator setting	Solids feed rate (g/sec)	Solids pressure drop - chart scale (approx. in H_2O)
8-1	9.982	8.494	.1026	5.0	.3961	.075
8-2	10.041	7.931	.1052	4.5	.3862	.076
8-3	9.982	8.284	.1034	4.0	.3810	.082
8-4	19.962	15.730	.2136	3.5	.4033	.090
8-5	19.940	14.750	.2150	2.5	.3949	.152
8-6	30.028	23.537	.3240	2.0	.3925	.245
8-7	20.935	16.046	.2158	3.0	.4042	.137
	Total H_2O adsorbed for run group = 22.974 g					

Run No.	TEMPERATURE DATA				
	Reactor exit gas °C	Reactor exit wall °C	Reactor inlet gas °C	Reactor inlet wall °C	Reactor cooler top °C
8-1	704	555	699	540	100
8-2	713	568	692	535	94
8-3	704	570	697	520	86
8-4	713	570	707	528	68
8-5	697	565	696	510	44
8-6	705	555	697	505	61
8-7	711	563	697	510	66

TRANSPORT REDUCTION OF N_1O - Experimental results for $^{35}/_{42}$ # N_1O

Run group No. 9

Nominal Temp. = 500°C

Run No.	MASS BALANCE DATA			RESIDENCE TIME DATA		
	Feed wgt. (g) (N_1O)	Product wgt. (g) ($N_1O + N_1$)	Hydrogen make up, cub.ft. at 7.0 in. water and 67°F	Flowrator setting	Solids feed rate (g/sec)	Solids pressure drop - chart scale (approx. in H_2O)
9-1	10.079	10.366	.0080	10.0	.4032	.090
9-2	9.946	9.852	.0170	9.5	.3916	.101
9-3	10.004	9.576	.0188	9.0	.4002	.132
9-4	20.063	18.671	.0556	8.5	.4180	.212
9-5	19.930	18.601	.0684	8.5	.4170	.194
9-6	30.039	26.687	.1253	7.5	.4048	.438
9-7	20.152	18.684	.0676	8.0	.3991	.336
	Total H_2O adsorbed for run group = 12.102 g					

	TEMPERATURE DATA				
	Reactor exit gas °C	Reactor exit wall °C	Reactor inlet gas °C	Reactor inlet wall °C	Reactor cooler top °C
9-1	505	408	503	388	76
9-2	506	413	509	390	86
9-3	501	410	497	383	70
9-4	503	410	500	385	70
9-5	503	410	503	385	69
9-6	498	410	497	380	68
9-7	506	407	498	375	66

TRANSPORT REDUCTION OF N_1O - Experimental results for $^{35}/_{42}$ N_1O

Run group No. 10

Nominal Temp. = 550°C

Run No.	MASS BALANCE DATA			RESIDENCE TIME DATA		
	Feed wgt. (g) (N_1O)	Product wgt. (g) ($N_1O + N_1$)	Hydrogen make up. cub.ft. at 7.0 in. water and 65°F	Flowrator setting	Solids feed rate (g/sec)	Solids pressure drop - chart scale (approx. in H_2O)
10-1	10.640	9.356	.0354	9.5	.4239	.110
10-2	10.073	9.385	.0484	9.0	.4111	.161
10-3	9.989	8.810	.0562	8.5	.3842	.273
10-4	20.005	16.976	.1457	8.0	.3885	.454
10-5	19.976	16.272	.1522	7.5	.3902	.823
10-6	30.033	26.770	.1901	8.0	.3941	.978
10-7	10.029	9.626	.0303	10.0	.3933	.235
	Total H_2O adsorbed for run group = 15.442 g					

Run No.	TEMPERATURE DATA				
	Reactor exit gas °C	Reactor exit wall °C	Reactor inlet gas °C	Reactor inlet wall °C	Reactor cooler top °C
10-1	553	425	555	420	61
10-2	555	430	553	418	58
10-3	555	428	560	414	55
10-4	554	419	550	408	58
10-5	555	412	546	398	55
10-6	558	407	558	400	67
10-7	554	400	560	398	66

TRANSPORT REDUCTION OF N_1O - Experimental results for 35/42# N_1O

Run group No. 11

Nominal Temp. = 600°C

Run No.	MASS BALANCE DATA			RESIDENCE TIME DATA		
	Feed wgt. (g) (N_1O)	Product wgt. (g) ($N_1O + N_1$)	Hydrogen make up, cub.ft. at 7.0 in. water and 71°F	Flowrator setting	Solids feed rate (g/sec)	Solids pressure drop - chart scale (approx. in H_2O)
11-1	10.008	8.615	.0747	8.5	.4170	.091
11-2	9.918	8.432	.0827	8.0	.4700	.105
11-3	10.060	7.967	.0906	7.5	.4209	.129
11-4	9.986	8.230	.0927	7.0	.4027	.161
11-5	9.982	7.792	.0937	6.5	.4125	.206
11-6	20.103	15.987	.2113	6.0	.4085	.289
11-7	20.007	15.620	.1932	6.5	.3962	.248
11-8	20.086	16.041		7.0	.3900	.190
	Total H_2O adsorbed for run group = 19.271 g					

Run No.	TEMPERATURE DATA				
	Reactor exit gas °C	Reactor exit wall °C	Reactor inlet gas °C	Reactor inlet wall °C	Reactor cooler top °C
11-1	621	475	600	450	103
11-2	606	483	594	445	68
11-3	608	480	604	445	62
11-4	603	480	609	435	56
11-5	602	475	607	440	54
11-6	608	473	608	438	36
11-7	604	473	600	437	44
11-8	606	473	602	445	49

TRANSPORT REDUCTION OF N_1O - Experimental results for 35/42 # N_1O

Run group No. 12

Nominal Temp. = 700°C

Run No.	MASS BALANCE DATA			RESIDENCE TIME DATA*		
	Feed wgt. (g) (N_1O)	Product wgt. (g) ($N_1O + N_1$)	Hydrogen make up, cub.ft. at 7.0 in. water and 63°F	Flowrator setting	Solids feed rate (g/sec)	Solids pressure drop - chart scale (approx. in H_2O)
12-1	9.956	7.360	.1015	6.0		
12-2	10.054	7.561	.1056	5.0		
12-3	9.957	6.300	.1015	4.0		
12-4	9.979	8.289	.1048	5.5		
12-5	10.157	7.869	.1022	6.5		
12-6	10.025	8.148	.1003	7.0		
	Total H_2O adsorbed for run group = 14.752 g					

* Note: The last two columns of data are not presented as the manometer lines became blocked during this run group

Run No.	TEMPERATURE DATA				
	Reactor exit gas °C	Reactor exit wall °C	Reactor inlet gas °C	Reactor inlet wall °C	Reactor cooler top °C
12-1	701	523	685	515	81
12-2	703	520	696	505	47
12-3	702	505	697	485	53
12-4	706	498	701	485	48
12-5	700	498	699	495	59
12-6	703	510	698	500	64

APPENDIX 4.2 Results of the analysis for the degree of reduction, mass balance, temperature correction and pressure drop data

The data in this appendix are the results of an analysis of the data in APPENDIX 4.1 made with the aid of an I.B.M. 1620 computer. The results are presented separately for each run group. No analysis of the data from run group 12 was made as during this series of runs the manometer lines became blocked. The data for run group 5 were included but no further analysis of these data was made as the nitrogen leaked into the apparatus during this set of experiments.

The headings used for the presentation of the data are summarized below:

Heading	Description	Units
N	No. of runs in group	-
FEED	wgt. of N_iO feed	g
PRODUCT	reduced product wgt. (N_iO + Ni)	g
HYDROGEN	wgt. of hydrogen consumed by reaction $N_iO + H_2 = N_i + H_2O$	g
RED	fractional reduction of the N_iO	g oxygen removed
TBAR	mean corrected hydrogen temp. for run	^oC

(continued)

Heading	Description	Units
GASV	mean corrected hydrogen velocity for run	ft/sec
DELPS	solids pressure drop	in H_2O
REC	$^1/_{DELPS}$	in^{-1} H_2O
MASS BALANCE	summary of mass balance data	g

RESULTS OF MASS BALANCE, GAS VELOCITY AND TEMPERATURE CORRECTIONS FOR HYDROGEN REDUCTION OF N_iO IN TRANSPORT

```
RUN GROUP    1    N=  6   NOMINAL TEMP.= 500.
RUN NO. FEED   PRODUCT HYDROGEN RED   TBAR  GASV   DELPS REC
  1   1 20.124 20.477      .0576  .106  503. 40.17    .071 14.078
  1   2 19.982 19.187      .1119  .207  515. 38.79    .078 12.808
  1   3 19.960 18.554      .1420  .263  516. 36.76    .090 11.092
  1   4 20.040 18.718      .1588  .293  510. 34.50    .141  7.056
  1   5 20.097 18.192      .1788  .329  504. 32.22    .222  4.499
  1   6 29.779 26.269      .3415  .424  505. 30.25    .346  2.888
MASS BALANCE
 INFLOW
     TOTAL FEED WGT.     =  129.982
     TOTAL HYDROGEN WGT.=    .9908
 OUTFLOW
     TOTAL NIO+NI   WGT.=  121.397
     TOTAL WATER   WGT. =  13.590
 RESIDUAL=INFLOW-OUTFLOW= -4.014
RUN GROUP    2    N=  6   NOMINAL TEMP.= 550.
RUN NO. FEED   PRODUCT HYDROGEN RED   TBAR  GASV   DELPS REC
  2   1 10.030  9.968      .1198  .442  563. 43.29    .070 14.280
  2   2 10.105  9.440      .1365  .500  560. 40.98    .072 13.881
  2   3  9.997  8.894      .1569  .581  561. 38.89    .077 12.975
  2   4 20.032 16.731      .3353  .620  566. 36.95    .078 12.808
  2   5 19.952 16.689      .3362  .624  560. 34.52    .096 10.394
  2   6 29.882 25.808      .5860  .726  561. 30.29    .232  4.300
MASS BALANCE
 INFLOW
     TOTAL FEED WGT.     =   99.998
     TOTAL HYDROGEN WGT.=  1.6709
 OUTFLOW
     TOTAL NIO+NI   WGT.=   87.530
     TOTAL WATER   WGT. =  17.755
 RESIDUAL=INFLOW-OUTFLOW= -3.616
RUN GROUP    3    N=  6   NOMINAL TEMP.= 600.
RUN NO. FEED   PRODUCT HYDROGEN RED   TBAR  GASV   DELPS REC
  3   1 10.021  9.069      .2089  .772  603. 40.84    .082 12.180
  3   2 10.005  8.381      .2089  .773  615. 39.12    .086 11.611
  3   3 10.011  8.455      .2180  .806  610. 36.59    .083 12.033
  3   4 20.000 15.868      .4696  .870  610. 32.06    .134  7.428
  3   5 20.001 15.628      .4720  .874  618. 30.07    .169  5.912
  3   6 30.006 21.244      .7423  .916  615. 27.65    .245  4.067
MASS BALANCE
 INFLOW
     TOTAL FEED WGT.     =  100.044
     TOTAL HYDROGEN WGT.=  2.3199
 OUTFLOW
     TOTAL NIO+NI   WGT.=   78.645
     TOTAL WATER   WGT. =  18.362
 RESIDUAL=INFLOW-OUTFLOW=  5.356
```

RUN GROUP 4 N= 7 NOMINAL TEMP.= 700.

RUN	NO.	FEED	PRODUCT	HYDROGEN	RED	TBAR	GASV	DELPS	REC
4	1	9.994	8.740	.2530	.938	715.	38.40	.078	12.808
4	2	10.038	8.233	.2516	.928	713.	35.79	.077	12.975
4	3	10.111	8.069	.2587	.948	712.	33.22	.081	12.331
4	4	19.993	16.240	.5204	.964	717.	30.82	.110	9.063
4	5	20.045	14.534	.5280	.975	723.	28.46	.151	6.584
4	6	29.960	21.840	.7765	.960	719.	25.79	.287	3.483
4	7	20.037	16.055	.5127	.948	714.	40.90	.073	13.690

MASS BALANCE

INFLOW

TOTAL FEED WGT. = 120.178

TOTAL HYDROGEN WGT.= 3.1012

OUTFLOW

TOTAL NIO+NI WGT.= 93.711

TOTAL WATER WGT. = 22.405

RESIDUAL=INFLOW-OUTFLOW= 7.163

RUN GROUP 5 N= 7 NOMINAL TEMP.= 500.

RUN	NO.	FEED	PRODUCT	HYDROGEN	RED	TBAR	GASV	DELPS	REC
5	1	20.014	19.424	.0731	.135	509.	46.52	.117	8.517
5	2	19.904	18.698	.0860	.160	508.	44.45	.234	4.263
5	3	20.049	18.872	.1541	.284	512.	42.67	.429	2.326
5	4	20.084	19.935	.0661	.122	512.	48.76	.264	3.782
5	5	20.052	16.839	.2091	.386	508.	40.45	1.120	.892
5	6	29.995	25.674	.2425	.299	513.	42.70	1.104	.905
5	7	19.941	20.009	.0339	.063	504.	50.22	.213	4.694

MASS BALANCE

INFLOW

TOTAL FEED WGT. = 150.039

TOTAL HYDROGEN WGT.= .8852

OUTFLOW

TOTAL NIO+NI WGT.= 139.451

TOTAL WATER WGT. = 11.345

RESIDUAL=INFLOW-OUTFLOW= .108

RUN GROUP 6 N= 6 NOMINAL TEMP.= 550.

RUN	NO.	FEED	PRODUCT	HYDROGEN	RED	TBAR	GASV	DELPS	REC
6	1	9.896	9.528	.0750	.281	555.	53.52	.071	14.078
6	2	10.010	9.172	.0920	.340	553.	51.30	.081	12.331
6	3	10.055	8.897	.1109	.408	566.	49.93	.099	10.077
6	4	20.032	17.551	.2559	.473	566.	47.76	.191	5.219
6	5	19.985	17.044	.2929	.543	558.	45.19	.281	3.547
6	6	29.991	24.806	.4706	.581	563.	43.30	.823	1.214

MASS BALANCE

INFLOW

TOTAL FEED WGT. = 99.969

TOTAL HYDROGEN WGT.= 1.2977

OUTFLOW

TOTAL NIO+NI WGT.= 86.998

TOTAL WATER WGT. = 12.195

RESIDUAL=INFLOW-OUTFLOW= 2.073

```
RUN GROUP   7   N=  7   NOMINAL TEMP.= 600.
RUN NO. FEED   PRODUCT HYDROGEN RED   TBAR  GASV   DELPS REC
  7   1 10.011 11.689      .1874  .693  609. 52.50   .073 13.690
  7   2  9.998  8.419      .1992  .738  606. 50.03   .078 12.808
  7   3  9.959  8.509      .2076  .772  611. 48.06   .079 12.645
  7   4 20.079 16.147      .4261  .786  608. 45.61   .090 11.092
  7   5 20.063 16.678      .4390  .810  609. 43.39   .086 11.611
  7   6 30.006 24.227      .7014  .866  612. 38.99   .161  6.210
  7   7 19.985 15.974      .4686  .868  615. 41.38   .094 10.617
MASS BALANCE
 INFLOW
     TOTAL FEED WGT.     =  120.101
     TOTAL HYDROGEN WGT.=  2.6297
 OUTFLOW
     TOTAL NIO+NI   WGT.=  101.643
     TOTAL WATER   WGT. =  18.835
 RESIDUAL=INFLOW-OUTFLOW=  2.252
RUN GROUP   8   N=  7   NOMINAL TEMP.= 700.
RUN NO. FEED   PRODUCT HYDROGEN RED   TBAR  GASV   DELPS REC
  8   1  9.982  8.494      .2458  .912  713. 45.95   .075 13.323
  8   2 10.041  7.931      .2520  .930  714. 43.45   .076 13.147
  8   3  9.982  8.284      .2477  .919  712. 40.84   .082 12.180
  8   4 19.962 15.730      .5118  .949  723. 38.71   .090 11.092
  8   5 19.940 14.750      .5151  .957  709. 33.12   .152  6.541
  8   6 30.028 23.537      .7763  .957  715. 30.77   .247  4.033
  8   7 20.935 16.046      .5170  .915  717. 35.94   .137  7.264
MASS BALANCE
 INFLOW
     TOTAL FEED WGT.     =  120.870
     TOTAL HYDROGEN WGT.=  3.0661
 OUTFLOW
     TOTAL NIO+NI   WGT.=   94.772
     TOTAL WATER   WGT. =  22.974
 RESIDUAL=INFLOW-OUTFLOW=  6.190
RUN GROUP   9   N=  7   NOMINAL TEMP.= 500.
RUN NO. FEED   PRODUCT HYDROGEN RED   TBAR  GASV   DELPS REC
  9   1 10.079 10.366      .0193  .071  508. 56.52   .090 11.092
  9   2  9.946  9.852      .0410  .152  511. 54.76   .101  9.876
  9   3 10.004  9.576      .0453  .168  503. 52.16   .132  7.542
  9   4 20.063 18.671      .1342  .247  505. 50.33   .214  4.671
  9   5 19.930 18.601      .1651  .306  507. 50.43   .195  5.111
  9   6 30.039 26.687      .3025  .373  501. 46.08   .448  2.228
  9   7 20.152 18.684      .1632  .300  506. 48.37   .341  2.923
MASS BALANCE
 INFLOW
     TOTAL FEED WGT.     =  120.213
     TOTAL HYDROGEN WGT.=   .8708
 OUTFLOW
     TOTAL NIO+NI   WGT.=  112.437
     TOTAL WATER   WGT. =  12.102
 RESIDUAL=INFLOW-OUTFLOW= -3.455
```

RUN GROUP 10 N= 7 NOMINAL TEMP.= 550.

RUN	NO.	FEED	PRODUCT	HYDROGEN	RED	TBAR	GASV	DELPS	REC
10	1	10.640	9.356	.0857	.298	560.	58.12	.110	9.063
10	2	10.073	9.385	.1173	.431	560.	55.98	.162	6.171
10	3	9.989	8.810	.1362	.505	563.	54.08	.225	4.437
10	4	20.005	16.976	.3531	.653	558.	51.59	.465	2.147
10	5	19.976	16.272	.3688	.684	557.	49.37	.864	1.157
10	6	30.033	26.770	.4607	.568	565.	52.00	1.036	.964
10	7	10.029	9.626	.0734	.271	563.	60.55	.237	4.208

MASS BALANCE
INFLOW
TOTAL FEED WGT. = 110.745
TOTAL HYDROGEN WGT.= 1.5954
OUTFLOW
TOTAL NIO+NI WGT.= 97.195
TOTAL WATER WGT. = 15.442
RESIDUAL=INFLOW-OUTFLOW= -.296

RUN GROUP 11 N= 8 NOMINAL TEMP.= 600.

RUN	NO.	FEED	PRODUCT	HYDROGEN	RED	TBAR	GASV	DELPS	REC
11	1	10.008	8.615	.1786	.661	618.	57.61	.091	10.969
11	2	9.918	8.432	.1977	.738	607.	54.62	.105	9.498
11	3	10.060	7.967	.2166	.798	613.	52.74	.129	7.718
11	4	9.986	8.230	.2217	.822	614.	50.48	.162	6.171
11	5	9.982	7.792	.2241	.831	612.	48.11	.207	4.809
11	6	20.103	15.987	.5053	.931	616.	46.03	.293	3.409
11	7	20.007	15.620	.4620	.855	610.	47.97	.250	3.984
11	8	20.086	16.041	.4615	.851	612.	50.35	.191	5.219

MASS BALANCE
INFLOW
TOTAL FEED WGT. = 110.150
TOTAL HYDROGEN WGT.= 2.4679
OUTFLOW
TOTAL NIO+NI WGT.= 88.684
TOTAL WATER WGT. = 19.271
RESIDUAL=INFLOW-OUTFLOW= 4.662

NO ANALYSIS FOR RUN 12

APPENDIX 4.3 Summary of the particle residence time estimates

The calculation of the data contained in this appendix is described in detail in section 4.8.4. The estimates of the residence time for runs 6-6, 10-5 and 10-6 were inadmissable, presumably due to the occurrence of unstable 'slug' flow or the partial blockage of a manometer line.

```
RUN NO.  1  1   RESIDENCE TIME= .2905E+01
RUN NO.  1  2   RESIDENCE TIME= .3102E+01
RUN NO.  1  3   RESIDENCE TIME= .3449E+01
RUN NO.  1  4   RESIDENCE TIME= .5592E+01
RUN NO.  1  5   RESIDENCE TIME= .9024E+01
RUN NO.  1  6   RESIDENCE TIME= .1308E+02
RUN NO.  2  1   RESIDENCE TIME= .2740E+01
RUN NO.  2  2   RESIDENCE TIME= .2833E+01
RUN NO.  2  3   RESIDENCE TIME= .3075E+01
RUN NO.  2  4   RESIDENCE TIME= .3096E+01
RUN NO.  2  5   RESIDENCE TIME= .3859E+01
RUN NO.  2  6   RESIDENCE TIME= .8974E+01
RUN NO.  3  1   RESIDENCE TIME= .3318E+01
RUN NO.  3  2   RESIDENCE TIME= .3311E+01
RUN NO.  3  3   RESIDENCE TIME= .3222E+01
RUN NO.  3  4   RESIDENCE TIME= .5237E+01
RUN NO.  3  5   RESIDENCE TIME= .6446E+01
RUN NO.  3  6   RESIDENCE TIME= .9369E+01
RUN NO.  4  1   RESIDENCE TIME= .3044E+01
RUN NO.  4  2   RESIDENCE TIME= .3024E+01
RUN NO.  4  3   RESIDENCE TIME= .3027E+01
RUN NO.  4  4   RESIDENCE TIME= .4401E+01
RUN NO.  4  5   RESIDENCE TIME= .5712E+01
RUN NO.  4  6   RESIDENCE TIME= .1069E+02
RUN NO.  4  7   RESIDENCE TIME= .2618E+01
RUN NO.  6  1   RESIDENCE TIME= .2928E+01
RUN NO.  6  2   RESIDENCE TIME= .3327E+01
RUN NO.  6  3   RESIDENCE TIME= .4001E+01
RUN NO.  6  4   RESIDENCE TIME= .7594E+01
RUN NO.  6  5   RESIDENCE TIME= .1127E+02
RUN NO.  6  6   RESIDENCE TIME= .3074E+02 SLUG FLOW
```

```
RUN NO.  7  1   RESIDENCE TIME= .2878E+01
RUN NO.  7  2   RESIDENCE TIME= .3146E+01
RUN NO.  7  3   RESIDENCE TIME= .3310E+01
RUN NO.  7  4   RESIDENCE TIME= .3529E+01
RUN NO.  7  5   RESIDENCE TIME= .3522E+01
RUN NO.  7  6   RESIDENCE TIME= .6797E+01
RUN NO.  7  7   RESIDENCE TIME= .3944E+01
RUN NO.  8  1   RESIDENCE TIME= .2912E+01
RUN NO.  8  2   RESIDENCE TIME= .3061E+01
RUN NO.  8  3   RESIDENCE TIME= .3383E+01
RUN NO.  8  4   RESIDENCE TIME= .3530E+01
RUN NO.  8  5   RESIDENCE TIME= .6095E+01
RUN NO.  8  6   RESIDENCE TIME= .9785E+01
RUN NO.  8  7   RESIDENCE TIME= .5396E+01
RUN NO.  9  1   RESIDENCE TIME= .3646E+01
RUN NO.  9  2   RESIDENCE TIME= .4222E+01
RUN NO.  9  3   RESIDENCE TIME= .5406E+01
RUN NO.  9  4   RESIDENCE TIME= .8384E+01
RUN NO.  9  5   RESIDENCE TIME= .7656E+01
RUN NO.  9  6   RESIDENCE TIME= .1750E+02
RUN NO.  9  7   RESIDENCE TIME= .1389E+02
RUN NO. 10  1   RESIDENCE TIME= .4292E+01
RUN NO. 10  2   RESIDENCE TIME= .6478E+01
RUN NO. 10  3   RESIDENCE TIME= .9527E+01
RUN NO. 10  4   RESIDENCE TIME= .1864E+02
RUN NO. 10  5   RESIDENCE TIME= .6166E-98 SLUG FLOW
RUN NO. 10  6   RESIDENCE TIME= .4150E+02 SLUG FLOW
RUN NO. 10  7   RESIDENCE TIME= .1002E+02
RUN NO. 11  1   RESIDENCE TIME= .3526E+01
RUN NO. 11  2   RESIDENCE TIME= .3635E+01
RUN NO. 11  3   RESIDENCE TIME= .5005E+01
RUN NO. 11  4   RESIDENCE TIME= .6586E+01
RUN NO. 11  5   RESIDENCE TIME= .8190E+01
RUN NO. 11  6   RESIDENCE TIME= .1159E+02
RUN NO. 11  7   RESIDENCE TIME= .1031E+02
RUN NO. 11  8   RESIDENCE TIME= .8033E+01
```

APPENDIX 4.4 Tabulation of transformed residence time and conversion data for the transport reactor results for substitution in the fixed bed rate equation.

The calculation and use of the tabulated data is described in section 4.8.5. Two sets of data are presented for each run group listed, viz. corresponding values of:

$$\text{(i)} \quad FT = \{ (t+1.0) [\ln(t+1.0)-1.0] + 1.0 \} \qquad \ldots\ldots (3.12)$$

and

$$\text{(ii)} \quad FY = -\ln(1-y_e)$$

where y_e = observed degree of reduction,

and t = estimated particle residence time (min.)

RUN GROUP NO. 1 N= 6

FT	FY
.11575E-02	.11204E+00
.13123E-02	.23193E+00
.16223E-02	.30516E+00
.42112E-02	.34672E+00
.10772E-01	.39898E+00
.22267E-01	.55164E+00

RUN GROUP NO. 2 N= 6

FT	FY
.10272E-02	.58339E+00
.10953E-02	.69314E+00
.12955E-02	.86988E+00
.13123E-02	.96758E+00
.20263E-02	.97816E+00
.10656E-01	.12946E+01

RUN GROUP NO. 3 N= 6

FT	FY
.15034E-02	.14784E+01
.14944E-02	.14828E+01
.14149E-02	.16398E+01
.37071E-02	.20402E+01
.55816E-02	.20714E+01
.11604E-01	.24769E+01

RUN GROUP NO. 4 N= 7

FT	FY
.12624E-02	.27806E+01
.12460E-02	.26310E+01
.12542E-02	.29565E+01
.26255E-02	.33242E+01
.43911E-02	.36888E+01
.15032E-01	.32188E+01
.93980E-03	.29565E+01

RUN GROUP NO. 6 N= 5

FT	FY
.11734E-02	.32989E+00
.15123E-02	.41551E+00
.21744E-02	.52424E+00
.76835E-02	.64055E+00
.16715E-01	.78307E+00

RUN GROUP NO. 7 N= 7

FT	FY
.11340E-02	.11809E+01
.13546E-02	.13394E+01
.14944E-02	.14784E+01
.16977E-02	.15417E+01
.16881E-02	.16607E+01
.61924E-02	.20099E+01
.21104E-02	.20249E+01

RUN GROUP NO. 8 N= 7

FT	FY
.11575E-02	.24304E+01
.12789E-02	.26592E+01
.15577E-02	.25133E+01
.16977E-02	.29759E+01
.50013E-02	.31465E+01
.12641E-01	.31465E+01
.39336E-02	.24651E+01

RUN GROUP NO. 9 N= 7

FT	FY
.18139E-02	.73646E-01
.24173E-02	.16487E+00
.39481E-02	.18392E+00
.93286E-02	.28369E+00
.78232E-02	.36528E+00
.38913E-01	.46680E+00
.24973E-01	.35667E+00

RUN GROUP NO. 10 N= 5

FT	FY
.24973E-02	.35382E+00
.56326E-02	.56387E+00
.11994E-01	.70319E+00
.43735E-01	.10584E+01
.13175E-01	.37979E+00

RUN GROUP NO. 11 N= 8

FT	FY
.16977E-02	.10817E+01
.18041E-02	.13394E+01
.33930E-02	.15994E+01
.58223E-02	.17259E+01
.89190E-02	.17778E+01
.17588E-01	.26736E+01
.13957E-01	.19310E+01
.85809E-02	.19038E+01